The Multifocal Visual Evoked Cortical Potential in Visual Field Mapping: A Methodological Study.

by

Jennifer Anne Macfarlane

Thesis submitted to the University of Glasgow for the degree of Doctor of Philosophy

This research was conducted in the Department of Clinical Physics and Bioengineering, North Glasgow University Hospitals NHS Trust and the University of Glasgow.

June 2008

Abstract

The application of multifocal techniques to the visual evoked cortical potential permits objective electrophysiological mapping of the visual field.

The multifocal visual evoked cortical potential (mfVECP) presents several technical challenges. Signals are small, are influenced by a number of sources of noise and waveforms vary both across the visual field and between subjects due to the complex geometry of the visual cortex. Together these factors hamper the ability to distinguish between a mfVECP response from the healthy visual pathway, and a response that is reduced or absent and is therefore representative of pathology.

This thesis presents a series of methodological investigations with the aim of maximising the information available in the recorded electrophysiological response and thereby improve the performance of the mfVECP.

A novel method of calculating the signal to noise ratio (SNR) of mfVECP waveform responses is introduced. A noise estimate unrelated to the response of the visual cortex to the visual stimulus is created. This is achieved by cross-correlating m-sequences which is created when the orthogonal set of m-sequences are created but are not used to control a stimulus region, with the physiological record. This metric is compared to the approach of defining noise within a delayed time window and shows good correlation. ROC analysis indicates a small improvement in the ability to distinguish between physiological waveform responses and noise. Defining the signal window as 45-250ms is recommended.

Signal quality is improved by post-acquisition bandwidth filtering. A wide range of bandwidths are compared and the greatest gains are seen with a bandpass of 3 to 20Hz applied after cross-correlation.

Responses evoked when stimulation is delivered using a cathode ray tube (CRT) and a liquid crystal display (LCD) projector system are compared. The mode of stimulus delivery affects the waveshape of responses. A significantly higher SNR is seen in waveforms is shown in waveforms evoked by an m=16 bit m-sequence delivered by a CRT monitor. Differences for shorter m-sequences were not statistically significant.

The area of the visual field which can usefully be tested is investigated by increasing the field of view of stimulation from 20° to 40° of radius in 10° increments. A field of

view of 30° of radius is shown to provide stimulation of as much of the visual field as possible without losing signal quality.

Stimulation rates of 12.5 to 75Hz are compared. Slowing the stimulation rate produced increases waveform amplitudes, latencies and SNR values. The best performance was achieved with 25Hz stimulation. It is shown that a six-minute recording stimulated at 25Hz is superior to an eight-minute, 75Hz acquisition.

An electrophysiology system capable of providing multifocal stimulation, synchronising with the acquisition of data from a large number of electrodes and performing cross-correlation has been created. This is a powerful system which permits the interrogation of the dipoles evoked within the complex geometry of the visual cortex from a very large number of orientations, which will improve detection ability.

The system has been used to compare the performance of 16 monopolar recording channels in detecting responses to stimulation throughout the visual field. A selection of four electrodes which maximise the available information throughout the visual field has been made. It is shown that a several combinations of four electrodes provide good responses throughout the visual field, but that it is important to have them distributed on either hemisphere and above and below O_z.

A series of investigations have indicated methods of maximising the available information in mfVECP recordings and progress the technique towards becoming a robust clinical tool. A powerful multichannel multifocal electrophysiology system has been created, with the ability to simultaneously acquire data from a very large number of bipolar recording channels and thereby detect many small dipole responses to stimulation of many small areas of the visual field. This will be an invaluable tool in future investigations.

Performance has been shown to improve when the presence or absence of a waveform is determined by a novel SNR metric, when data is filtered post-acquisition through a 3-20Hz bandpass after cross-correlation and when a CRT is used to deliver the stimulus. The field of view of stimulation can usefully be extended to a radius of 30° when a 60-region dartboard pattern is employed. Performance can be enhanced at the same time as acquisition time is reduced by 25%, by the use of a 25Hz rate of stimulation instead of the frequently employed rate of 75Hz.

List of Contents

		Page
Title ……..		1
Abstract ……		2
List of Contents ……		5
List of Figures ……..		6
List of Tables ……...		17
Acknowledgements ……..		19
Author's Declaration ……...		20
Glossary ……...		21
Chapter 1	The Visual System.….....	22
Chapter 2	Conventional Visual Electrophysiology ……..	34
Chapter 3	Multifocal Electrophysiology …….. ……...	42
Chapter 4	Quantifying Multifocal Signal Quality ……...…….	67
Chapter 5	Filtering Bandwidth ……. ……...	106
Chapter 6	Stimulus Delivery ……... ……	154
Chapter 7	Rate of mfVECP Stimulus Presentation ……..……	186
Chapter 8	Creating A Multichannel Multifocal Electrophysiology System ..……	228
Chapter 9	Conclusions and Further Work …… ……...	283
Reference List …..……		294

List of Figures

Chapter 1

Page

1.1 Axial section of the human eye …….. 24

1.2 The cellular layers of the retina …….. 25

1.3 Variation of rod and cone density with eccentricity …….. 26

1.4 Fundus image of the human retina ……. 26

1.5 The image pathway from the retina to the visual cortex. ……... 28

Chapter 2

2.1 A normal pattern reversal VECP response. Taken from Odom *et al* 2004 …… 37

Chapter 3

Page

3.1 A snapshot of the multifocal ERG stimulus is shown on the left hand side with 103 regions. 103 corresponding waveform responses are shown on the right. …….. 44

3.2 Primitive polynomial x^4+x+1 has tap positions at x^4 and x. The LFSR can be filled with any non-zero seed pattern. **1010** has been chosen here. The XOR operation creates a new bit, **0**, which is fed into the rightmost register. The original bits are shifted left, pushing the leftmost **1** out. This bit is the first step of the m-sequence. The process is repeated to generate the full 15-bit sequence. ……. 47

3.3 Decimation of the 4-bit m-sequence generated in Figure 3.2. ……. 48

3.4 Illustrating the control of a pattern reversal by the m-sequence. ……. 49

3.5 Cross-correlation of a first order response in the mfERG can be described as the addition of all responses to a flash stimulus minus the sum of all the responses to a dark stimulus element. ……. 49

3.6 The second order response of the mfERG is the addition of all responses to a change in luminance minus the sum of all responses where there is no change in luminance. ……... 51

3.7 The mfVECP Dartboard Stimulus ……... 53

3.8 The hardware required for a multifocal electrophysiology system. … 55

Chapter 4

Page

4.1 A cross-correlated mfERG trace array using (a) the original program and (b) the same data analysed using the modified program. (c) shows the difference between the two, shown on a higher resolution amplitude scale…… 81

4.2 Graph showing DeadM-SNR values plotted against DTW SNR values…… 83

4.3 The median SNR values for the two SNR calculation approaches are compared……... 85

4.4 Distribution of SNR for signals and noise estimations using the DTW-SNR and DeadM-SNR calculation methods…….. 87

4.5 ROC curves for the DeadM-SNR and DTW-SNR values…… 86

4.6 Normalised histogram showing the distribution of SNR values for mfERG waveforms acquired using gold foil and DTL electrodes…... 92

4.7 Normalised histogram showing the distribution of SNR values for noise estimations acquired using gold foil and DTL electrodes……... 93

4.8 Data plotted in Figures 4.6 and 4.7 is presented simultaneously to illustrate the separation of signal and noise SNR values…….. 95

4.9 ROC curves for Gold Foil and DTL electrodes…… 94

4.10 mfVECPs from a single subject recorded with increasing m-sequence length……. 100

Page

4.11 Central waveform from the lower right quadrant of the trace arrays shown in Figure 3.13 …… 101

4.12 Plot of observed and theoretical median SNR against m-sequence length for mfVECP records…… 102

Chapter 5

		Page
5.1	High and low-pass filtering circuits……..	109
5.2	The frequency response of unfiltered and filtered data……	118
5.3	(a&b) A waveform array, filtered through eight different bandpasses	119-120
5.4	Effect of the eight bandpasses on a single waveform……...	121
5.5	Median SNR values are presented for data filtered through eight bandpasses……	123
5.6	ROC curves for data filtered through eight different bandpasses…….	124
5.7	Waveform trace array before any filtering was applied……...	128
5.8	a,b,c & d. Filtered waveform arrays …….	129-132
5.9	Unfiltered waveform. ……...	133
5.10	The waveform evoked by region 48 of the dartboard stimulus is shown after filtering through each of the 20 bandwidths ……	134
5.11	Unfiltered data are shown on the left. The right shows data filtered through bandpasses with a highpass setting of 10Hz. …….	135
5.12	Median SNR values for signals within the waveform array are plotted for each filter bandwidth……...	137
5.13	SNR value distribution of noise estimates. ……..	138

Page

5.14 ROC curves for 20 bandpass filters…..……... 140

5.15 Frequency content of waveforms containing physiological signal and waveforms created by the cross-correlation of the raw data with unused m-sequences. ……... 142

5.16 ROC curves for the same data filtered through a 0.1 to 100Hz and a 1 to 100Hz filter …….. 144

5.17 Data filtered before and after cross-correlation is compared ……... 145

5.18 Examples of Wavelet and Smart Filtering. …….. 149

5.19 SNR values are plotted for data from a single waveform array. Each of the 60 waveforms has a SNR value calculated after filtering with the 3-30Hz bandpass, the Wavelet filtering and the Moderate Smart Filter. …… 150

5.20 ROC curves for unfiltered data, data filtered through a 3-30Hz bandpass, a wavelet filter and a Moderate Smart Filter. …….. 151

Chapter 6

		Page
6.1	Cathode Ray Tube…….	158
6.2	Concentric ring analysis of the inserted full field flash response from the CRT and LCD stimulus……...	160
6.3	Horizontal luminance profiles for LCD and CRT screens……	164
6.4	Vertical luminance profiles for LCD and CRT screens……	165
6.5	mfVECP trace arrays from Channel 0. Data in the left hand column was acquired when the stimulus was presented via CRT, with responses to LCD stimulation on the left……..	170-171
6.6	The number of detectable waveforms achieved with LCD vs. CRT stimulation is plotted. ……...	172
6.7	An example of the changes seen in the trace array as the radius of the FOV was increased from 10° to 40°. ……...	177
6.8	The number of detectable waveforms in the whole trace array is plotted against the field of view of acquisition. ……	179
6.9	Reproducibility of waveforms……...	181

Chapter 7

		Page
7.1	**a** Responses to stimulation at five different frequencies from a single subject. Data was acquired by Channel A10 and an m=13 bit m-sequence was used in each case. Acquisition times are noted……..	194
	b Three pairs of trace arrays are shown. In each pair, the recording time was the same, but there was a difference in the stimulation rate and m-sequence length. Data was acquired from a single subject by Channel A10…….	195-196
7.2	ROC curves are presented for each of the recordings A-H ……	197-198
7.3	**a** Region 58 of the mfVECP stimulus …….	199
	b Waveforms evoked by stimulating region 58 are shown for each recording A-H. …….	200-202
7.4	ROC Curves for eight recordings. …..……..	204
7.5	Pairs of recordings with the same recording time are compared via ROC curves. …….	206
7.6	The difference in test performance between test C, which was found to be the best performer and test H, which uses the most commonly used combination of stimulation rate and m-sequence length (75Hz & m=13), is shown ……..	207
7.7	SNR is plotted against stimulation rate for the waveform response to stimulation by region 56 …….	209
7.8	SNR is plotted against stimulation rate for the waveform response to stimulation by region 58. …….	210

		Page
7.9	Median SNR values are plotted against stimulation rate for the four central waveforms. ……...	211
7.10	Waveform detection rate is plotted against stimulation rate. ……..	213
7.11	Schematic showing how frequently waveforms in each area of the waveform trace array reach the detection threshold when a 25Hz stimulation rate was used. ……	215
7.12	As for Figure 7.11this maps the detection rate of waveforms within the mfVECP trace array, but is based on a 75Hz stimulation rate. …	216
7.13	The relationship between detection rate and eccentricity is plotted for recordings with 25Hz and 75Hz stimulation rates. ……	217
7.14	Detectable waveforms within the mfVECP trace array are mapped. ..	218-219
7.15	Trace arrays from subject CC. A detectable waveform was found in all 60 locations of the waveform array from at least one of the 16 recording electrodes …….	221-222

Chapter 8

		Page
8.1	An Active Electrode ……	235
8.2	Trigger signal as illustrated by a screenshot from the BioSemi System software. ……..	237
8.3	A schematic illustration of the different structures of .mf and .edf file formats. ……	239
8.4	The functional steps of the file conversion software are shown……..	240
8.5	The experimental set up used to test the multichannel acquisition system with a photodiode is shown. ……	243
8.6	BioSemi diagram showing how the CMS & DRL work. ……	244
8.7	Data recorded from the photodiode. ……	245
8.8	An ECG signal shown on two different temporal scales……..	246
8.9	An example ECG waveform ……	246
8.10	The photodiode response to the beginning of two different 30-second segments of multifocal stimulation. …….	251
8.11	A photodiode response recorded by BioSemi ActiveOne electrodes, converted and successfully cross-correlated. The stimulus was a single hexagonal element. ……	252
8.12	Photodiode response recorded by BioSemi ActiveOne electrodes. Data was successfully cross-correlated. The stimulus was a seven hexagonal region mfERG stimulus. ……	252

		Page
8.13	A mfERG response to a single hexagonal flash stimulus recorded using the BioSemi ActiveOne system. ……	253
8.14	A mfVECP response to stimulation with a square stimulus with 9 regions. Each region contained a 4x4 checkerboard pattern……	254
8.15	Locations of 16 active electrodes. ……..	259
8.16	A mfVECP recorded from a normal volunteer from the BioSemi ActiveTwo System. ……..	261
8.17	mfVECP data acquired from 16 recording channels. ……..	262-263
8.18	The detection efficiency of each of the 16 recording electrodes. ……	268
8.19	Schematic showing how frequently each of the 16 recording electrodes acquires a mfVECP response that exceeds the detection threshold……..	269-271
8.20	The top row (a) shows bipolar data derived from the BioSemi Multifocal Multichannel Acquisition system. The bottom row (b&c) is data acquired from the same subject with the EDIU Multifocal system and Ag/AgCl electrodes……	273
8.21	Showing the locations of the 4 electrodes which provided the best detection performance …….	276
8.22	The pattern of detection of waveforms in the trace array with the worst performing combination of four electrodes and the best. ……..	277
8.23	The first 12 best combinations of electrodes. ……..	280

List of Tables

Page

Chapter 3

3.1 Amplifier specifications…….. 58

Chapter 4

4.1 The correlation coefficient between the SNR calculated via the Delayed Time Window and Dead M-sequence noise estimation techniques…… 82

Chapter 5

5.1 Filter bandpasses used in recent mfVECP publications…….. 105

Chapter 6

6.1 The relative merits of two locally available modes of multifocal stimulus delivery…… 157

6.2 The range of fields of view used to stimulate mfVECPs…… 162

6.3 The number of detectable waveforms in the trace arrays acquired with increasing field of view (FOV) is shown for a single subject…….. 178

Page

Chapter 7

7.1 Table showing the combination of stimulation frequency, m-sequence length and the recording time for eight mfVECP recordings, A-H…….. 189

7.2 Active Electrode positions ……. 190

Chapter 8

8.1 Summarised Technical Details of the Recording Systems used in Developing the Multichannel Multifocal VECP……. 234

8.2 Data showing that file conversion software correctly identified the trigger points…….. 238

8.3 Active Electrode positions ……. 258

.

Acknowledgements

The author wishes to than the following people:

Dr D Keating, supervisor (Department of Clinical Physics and Bioengineering, Ophthalmology) for his contributions, advice and role in the initial formulation of this research project.

Dr S Parks (Department of Ophthalmology) for his contributions, advice, role in the project formulation, programming lessons and practical assistance.

Professor D Wyper, advisor of studies (Department of Clinical Physics and Bioengineering) for persistent encouragement and advice.

Dr A L Evans (Department of Clinical Physics and Bioengineering, Electronics Section) for his help and advice.

Professor A T Elliott, Department of Clinical Physics and Bioengineering, Greater Glasgow and Clyde NHS Trust, University of Glasgow for providing the facilities of the department.

Colleagues and friends who acted as volunteer test subjects.

Finally, the author wishes to thank her husband, parents, parents-in-law and brother for invaluable child-care, proof-reading services, patience and moral support, without which this thesis could not have reached completion.

Author's Declaration

The material presented in this thesis is the author's own work with the following exceptions:

Dr D Keating proposed the method of signal to noise ratio calculation introduced in Chapter 4.

Dr A L Evans wrote the Delphi program to filter raw multifocal data described in Chapter 5.

Dr S W Parks created the EDIU Multifocal System, created the Multifocal Image 3 software and made the modifications to the EDIU Multifocal System Software described in Chapter 8.

Material contained in this thesis has been disseminated at national and international meetings, including the following presentations:

Chisholm JA, S Parks, D Keating, AL Evans
A Multi-channel Multifocal VECP System Invest. Ophthalmol. Vis. Sci. 2002 43: E-Abstract 4741.
Association of Research in Vision and Ophthalmology, May 2002, Fort Lauderdale, USA.

Chisholm JA, S. Parks, D. Keating, A. L. Evans
A Multi-channel Multifocal VECP System.
Scottish NHS Research Day, September 2002, Aberdeen, UK.

Chisholm JA, S. Parks, D. Keating, A. L. Evans.
A Multi-channel Multifocal VECP System
IPEM Visual Electrophysiology Meeting, June 2002, York, UK.

Chisholm JA, Evans AL, Keating D, Parks S
The effect of filter bandwidth on the multifocal visual evoked cortical potential.
British Chapter of the International Society of Clinical Electrophysiology of Vision, August 2003, Nottingham, UK.

Chisholm JA, Keating D, Parks S
CRT vs LCD stimulus display during mfVECP recordings
British Chapter of the International Society of Clinical Electrophysiology of Vision, August 2005, Glasgow, Scotland, UK.

Chisholm JA, Parks S, Keating D.
Variation in the mfVECP response with stimulation rate, a 16-channel mfVECP experiment.
International Society of Clinical Electrophysiology of Vision, August 2005, Glasgow, Scotland, UK.

Glossary

Abbreviation or Term	Definition or Meaning
ADC	Analogue to Digital Converter
ASCII	American Standard Code for Information Interchange
CMS	Common Mode Sense
CRT	Cathode Ray Tube
CT	Computed Tomography
cVECP	conventional VECP
DeadM	This refers to the Dead M-sequence method of signal to noise ratio calculation defined in Chapter 4
DRL	Driven Right Leg
DTL	Dawson, Trick and Litzkow, the inventors of the DTL electrode.
DTW	Delayed Time Window. This refers to a method of signal to noise ratio calculation defined in Chapter 4.
ECG	Electrocardiogram
EDIU	ElectroDiagnostic Imaging Unit
EEG	Electroencephalogram
EOG	Electro-oculogram
ERG	Electroretinogram
fMRI	Functional Magnetic Resonance Imaging
FOV	Field of View
LCD	Liquid Crystal Display
LED	Light Emitting Diode
LFSR	Linear Feedback Shift Register
LGN	Lateral Geniculate Nucleus
MEG	Magnetoencephalogram
mfERG	Multifocal electroretinogram
mfVECP	Multifocal VECP
MRI	Magnetic Resonance Imaging
PET	Positron Emission Tomography
PRBS	Pseudorandom Binary Sequence
RMS	Root Mean Square
ROC	Receiver Operating Curve
RPE	Retinal Pigment Epithelium

SLO	Scanning Laser Ophthalmoscope
SNR	Signal to Noise Ratio
SPECT	Single Photon Emission Computed Tomography
SQUIDS	Super Conducting Quantum Interference Devices
V1,V2, V3, V4, V5	Volumes of the Visual Cortex
VECP	Visual Evoked Cortical Potential
VEP	Visual Evoked Potential

Chapter 1

The Visual System

Contents

1.0 Introduction …… 23

1.1 The Visual System……... 23

1.1.1 The Fibrous Layer ……. 24

1.1.2 The Vascular Pigmented Layer ……. 24

1.1.3 The Retina……..... 25

1.1.4 Optic Nerve ……... 27

1.1.5 The Optic Chiasm ……. 27

1.1.6 The Lateral Geniculate Nucleus …… 28

1.1.7 Visual Cortex …… 28

1.1.7.1 Primary Visual Cortex …… 28

1.1.7.2 Secondary Visual Cortex …… 30

1.2 Assessing Visual Function …….. 31

1.2.1 The Visual Field …… 31

1.2.2 Perimetry…….... …… 31

1.2.2.1 Kinetic Examination Strategies …….. 31

1.2.2.2 Static Examination Strategies ……. 32

1.3 Summary …… 33

1.0 Introduction

Visual electrophysiology measures the electrical activity of the visual system and allows an objective assessment of function. Light in the form of flashes or patterns is used to stimulate the retina, evoking a response which is communicated to the visual cortex where the brain interprets the visual input. The evoked response can be measured as an electroretinogram (ERG) from the retina, using corneal electrodes and as the visually evoked cortical potential (VECP) from the visual cortex using scalp electrodes.

Recent research and improving technology has expanded the capability of visual electrophysiology. This thesis investigates the multifocal visual evoked cortical potential in human subjects.

This chapter comprises brief descriptions of the anatomy of the visual system and visual field measurement.

1.1. The Visual System

The visual system is part of the nervous system which detects light and interprets it as a visual image. It comprises the eye, the optic nerve, optic chiasm, optic tract, lateral geniculate nucleus, optic radiation and the visual cortex.

Light enters the eye through the transparent cornea and passes through the pupil, the opening in the iris. The light converges as it passes through the lens, it continues through the aqueous humour and in the healthy eye, a clear, focused and inverted image is incident upon the retina. The retina converts the light into electrical signals which are transmitted via the optic nerve to the occipital lobe of the brain.

The eye itself is composed of three layers; the fibrous layer which provides structure and protection, the vascular pigmented layer which provides blood supply, secretes aqueous humour and controls the amount of light entering the eye and the nervous layer or retina. The centre of the eye is filled with jelly-like vitreous humour. An axial section of the eye is shown in Figure 1.1.

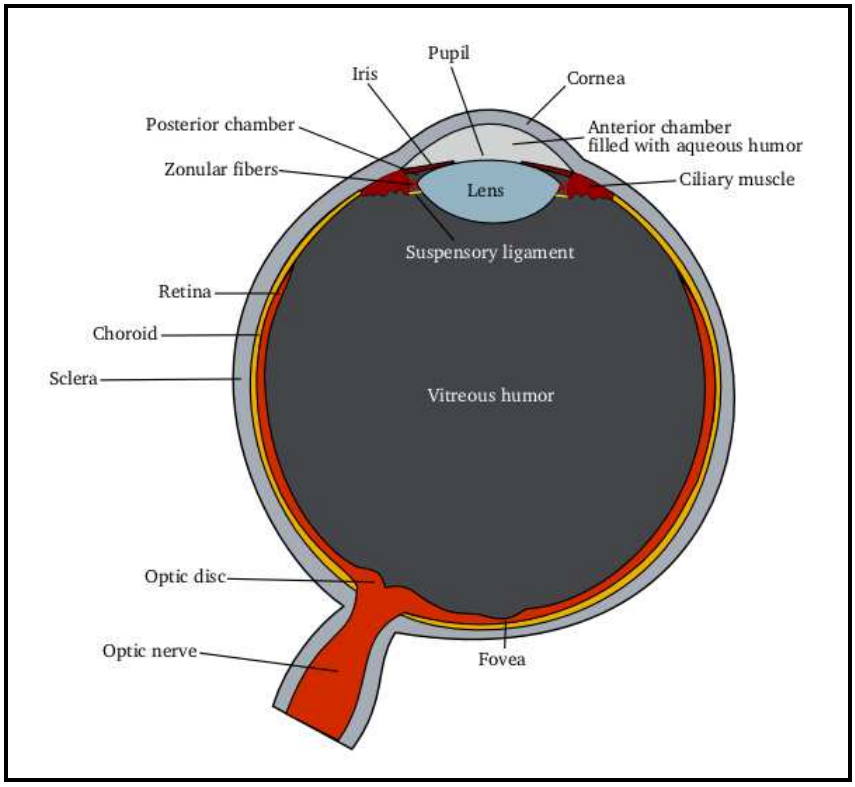

Figure 1.1 *Axial section of the human eye.*
http://en.wikipedia.org/wiki/Sclera

1.1.1. The Fibrous Layer

The sclera and cornea make up the fibrous layer which, when filled with internal fluid, gives shape to the eye and protection to the internal structures.

The cornea is the most powerful optical lens in the eye. Its anterior surface meets the air. Posteriorly, it meets liquid aqueous humour and its coronal circumference is continuous with the sclera at the corneo-scleral limbus.

The sclera is the white outer coating of the eye and has a posterior opening for the optic nerve fibres and retinal vessels. It is made of dense, fibrous tissue making it strong enough to withstand the intraocular pressure and to provide protection.

1.1.2. The Vascular Pigmented Layer

The middle vascular pigmented layer is also known as the uvea and has three distinct regions. The choroid is a highly vascular, pigmented layer whose blood vessels supply nutrients and oxygen to the whole eye. Its pigmentation helps to absorb light, and prevent its scattering within the eye. The ciliary body completely encircles the lens and secretes aqueous humour. Ciliary muscles control lens shape. Suspensory ligaments hold the lens in place. The iris incompletely covers the anterior portion of

the lens, forming an adjustable opening called the pupil, which allows light to enter the eye.

1.1.3. The Retina

The innermost layer of the eyeball is the retina which is a thin sheet of neural tissue. This is the image plane on to which the optical system projects. It is here that incident photons are converted to neural impulses to be transmitted to the brain for analysis and interpretation.

The outer surface of the sensory retina is apposed to the retinal pigment epithelium and the inner surface is next to the vitreous.

The retina contains three principal groups of neurons. Anteriorly are the ganglion cells, followed by the bipolar cells with the photoreceptors arranged posteriorly. Light passes through the ganglion and bipolar cells and is detected by the photoreceptors. The impulses are transmitted anteriorly through the layers. The retina also contains other neurons; the horizontal and amacrine cells and supporting Muller cells.

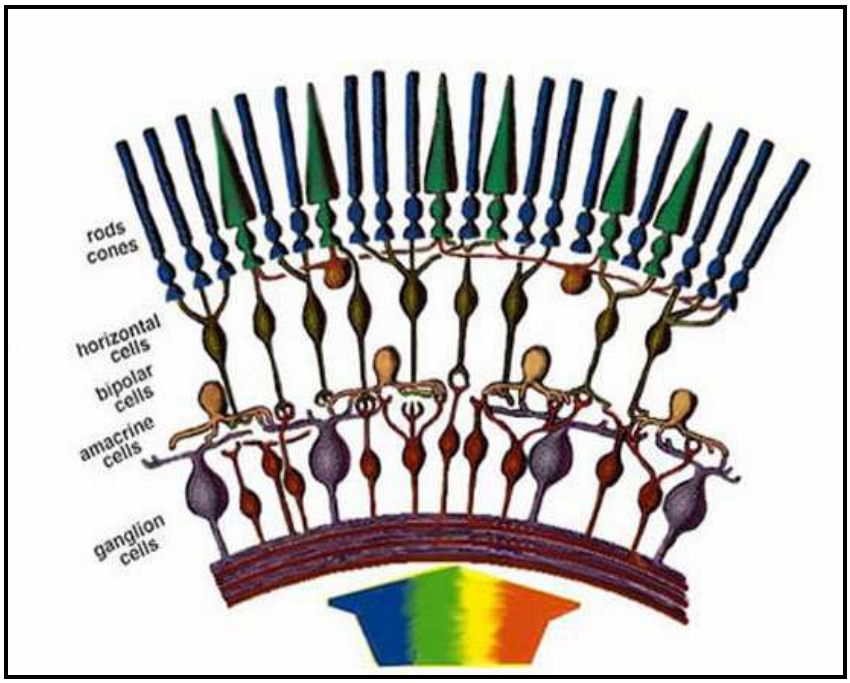

Figure 1.2 *The cellular layers of the retina*

There are two types of photoreceptor cells, rods and cones. Rods are specialised for vision in dim light. They discriminate between areas of light and dark and allow the determination of shape and motion. Cones are specialised for colour vision and high

visual acuity and are most densely concentrated within the central one degree of vision, an area called the fovea. Rod density reaches a maximum at approximately 18 degrees from the fovea. Figure 1.3 below shows the relationship of cone and rod density with eccentricity.

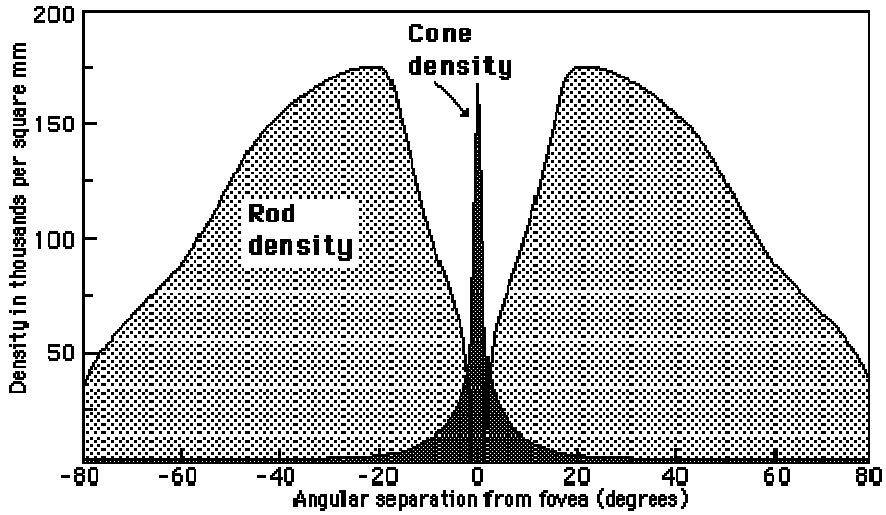

Figure 1.3 *Variation of rod and cone density with eccentricity.*

(taken from http://hyperphysics.phy-astr.gsu.edu/hbase/vision/rodcone.html)

Many rods connect with one bipolar neuron, and many of these bipolar neurons connect with a single ganglion cell. This greatly reduces visual acuity but the summation effect permits a ganglion cell to be stimulated. A ganglion cell connected to a single cone would not be stimulated by the same level of light as the ganglion cell connected to several rods. Synaptic connections therefore contribute greatly to differences in visual acuity and light sensitivity.

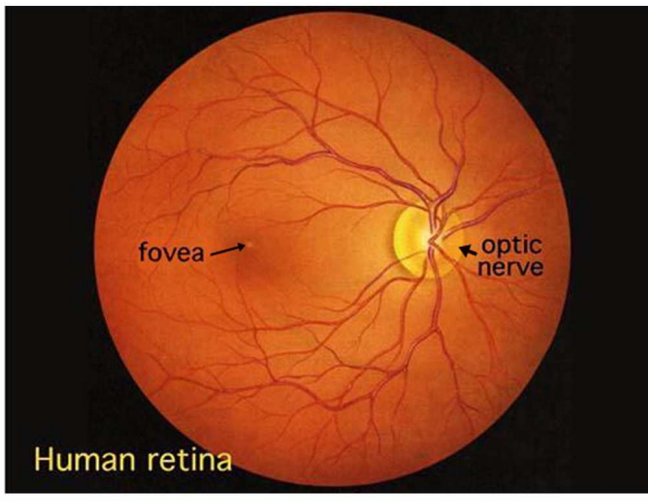

Figure 1.4 *Fundus image of the human retina*

Bipolar cells are primarily responsible for transmitting information between photoreceptors and ganglion cells. In the fovea where acuity is highest there is a 1:1:1 ratio of photoreceptors : bipolar : ganglion cells. In the peripheral retina where acuity is lower, bipolar cells can receive inputs from up to 100 rods. Acuity reduces with eccentricity and this is reflected in the ratio of photoreceptors to bipolar cells.

Posteriorly, bipolar cells also interact with horizontal cells to enhance the edges present in an image and increase the contrast of the retinal image.

Anteriorly they interact with amacrine cells to adjust the brightness of the retinal image and integrate sequential activation of neurons to detect motion.

Ganglion cells receive input from bipolar, amacrine and horizontal cells. Their axons extend posteriorly to a small area of the retina called the optic disc where they exit the eyeball as the optic nerve. They terminate in the lateral geniculate nucleus. The optic nerve head is located 17° nasally to the central fovea. It has no photoreceptors. It cannot therefore detect light and is known as the blind spot.

1.1.4. Optic Nerve

The optic nerve contains approximately 1 000 000 nerve fibres, each one arising from a single retinal ganglion cell. The optic nerve connects the eyeball to the optic chiasm and leaves the orbit via the superior orbital fissure. When the ganglion cell axons enter the optic nerve they are distributed according to their retinal origin. The axonal density is highest in the inferior temporal quadrant where the majority of the papillomacular bundle enters the nerve. As the ganglion cell axons progress down the nerve, they redistribute themselves.

1.1.5. The Optic Chiasm

The two optic nerves join together at the chiasm and the fibres from the nasal retinae cross over (decussate) and join the fibres from the temporal retina of the contralateral eye. This decussation results in all information presented to each half of the visual field being processed by the contralateral visual cortex.

Within the chiasm the fibres are arranged in a systematic manner. The macular fibres lie centrally, those from the upper portions of the retinae lie dorsally and those from the lower quadrants lie in its ventral or nasal part.

1.1.6. The Lateral Geniculate Nucleus

From the optic chiasm, the fibres progress through the optic tracts to the lateral geniculate nuclei (LGN), which act as a relay station from which fibres fan out, finally reaching the visual or striate cortex within the occipital lobe of the brain. The LGN are composed of six layers of cells separated by white bands of optic nerve fibres. The striation of the lateral geniculate bodies is organised in such a way that no cell receives input from both eyes and each layer contains only right or left eye cells. The two ventral layers contain large cells (magnocellular) which process information relatively quickly. The remaining four dorsal layers contain smaller cells (parvocellular) which take longer to process more detailed information.

1.1.7. Visual Cortex

The final stages of visual processing occur in the visual cortex. It can be subcategorised as the primary visual area (V1, Brodmann's area 17) and the secondary visual areas which include V2, V3, V4 and V5 and are encompassed by Brodmann's areas 18 and 19.

1.1.7.1. Primary Visual Cortex

The functionally defined primary visual cortex is approximately the same volume of brain as that described anatomically as striate cortex. The term 'striate' is used because myelinated nerve fibres create white stripes within the grey matter.

The primary visual cortex occupies the walls of the deep calcarine sulcus on the medial surface of each hemisphere and extends on to the cortex above and below the sulcus. It extends posteriorly as far as the occipital pole and a small portion extends on to the posterolateral aspect of the pole. Anteriorly, the area extends forwards above the calcarine sulcus as far as the parietal-occipital sulcus; below the calcarine sulcus it extends forward a little further.

V1 has a topographic map of the visual field. There is a 'neural image' which retains the spatial layout of the pattern of light incident in the retina. This mapping is referred to as retinotopy. Information presented in the left half of the visual field is detected by the nasal half of the left retina and the temporal half of the right retina. Fibres from these retinal areas project on to the right cerebral hemisphere and vice versa. (Figure 1.5)

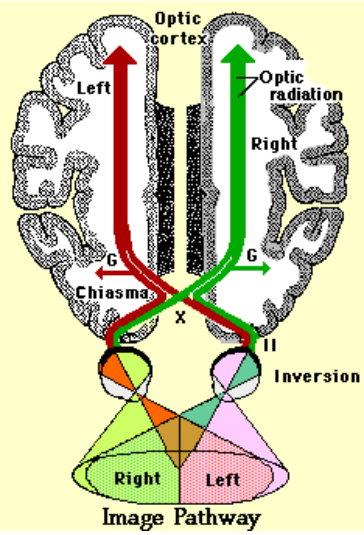

Figure 1.5 *The image pathway from the retina to the visual cortex.*

(Taken from http://gwis2.circ.gwu.edu/~atkins/Neuroweb/visualpath.html#chiasma)

Input from the upper visual field is incident on the inferior retinal quadrants which project on to the lower lip of the calcarine sulcus. The inferior visual field is represented on the calcarine sulcus' upper lip.

The cortical representation of the macula was investigated by Holmes and Lister in 1916 (1). They mapped the visual field defects of soldiers of the First World War who had sustained bullet or shell fragment wounds to the occipital cortex.

More recently, retinotopic mapping has been investigated using functional Magnetic Resonance Imaging (fMRI) (2-4), Positron Emission Tomography (PET) (5-7), magnetoencephalography (MEG) (8-11) and the multifocal visual evoked cortical potential (mfVECP) (12-17).

Mapping is non-linear. Information presented to the central visual field is processed by a greater number of neurons and hence a much larger volume of visual cortex than information presented to more peripheral regions. This phenomenon is described as cortical magnification, and corresponds to the superior visual performance of the central visual field.

There is a significant variation in the positions of gyri, sulci and different regions of the primary visual cortex with respect to outward structures such as the inion (18;19). There is significant variation in how V1 maps around the calcarine sulcus (20).

1.1.7.2. Secondary Visual Cortex

The secondary visual cortex does not exhibit white stripes within grey matter and is referred to as the extrastriate visual cortex. It is thought to be responsible for higher order visual information processing It surrounds V1 (area 17) on the medial and lateral sides of the cortex and are important to the integration and processing of visual data.

V2 is directly adjacent to V1 and V3 occupies the posterior parietal and temporal lobes of the lateral surface of the hemisphere. Each V2 projects to the contralateral V2 and ipsilateral V1 & V3 and responds to simple properties such as orientation, spatial frequency and colour. V3 processes global motion information (21) and receives input from both V1 and V2. V4 cells exhibit length, width, orientation, direction of motion and spatial frequency selectivity (22) and shows strong attentional modulation (23). V5 is also known as visual are MT (middle temporal) and is thought to be tuned to the speed and direction of motion.

1.2. Assessing Visual Function

Assessment of visual function can be performed by a combination of subjective tests by the optometrist or ophthalmologist and objective functional tests in the electrophysiology clinic.

Sub-categories of visual function include: acuity, contrast sensitivity, colour perception, stereoacuity (depth perception), fixation stability and visual field.

1.2.1. The Visual Field

The visual field can be defined as the area of space that one eye can see at any given instant. The sensitivity of the eye is not constant across the whole visual field. It varies with eccentricity, adaptation level and the nature of the test stimulus. The normal monocular extent of the visual field for a bright stimulus is 60° superiorly, 75° inferiorly, 100° temporally and 60° nasally (24), although this can be affected by facial contours. The binocular field increases the horizontal extent of this field to approximately 200°. The clinical recording of visual fields is called perimetry.

1.2.2. Perimetry

Perimetry was introduced into clinical medicine in 1856 when von Graefe mapped scotomas, visual field constrictions and blind spots using a chalk board. This developed to include the use of an arc-shaped arm which allowed the full limits of the visual field to be investigated rather than just the central vision.

The boundaries of the visual field can be crudely assessed using confrontational field testing. More detailed information can be obtained using perimetry. Perimetry is the measurement of differential light sensitivity in the visual field using the detection of test targets. The two most commonly used forms are kinetic and static examination strategies.

1.2.2.1. Kinetic Examination Strategies

Kinetic perimetry involves a perimetrist who moves a source of fixed size and luminance from outside the visual field towards the centre and plots the point of detection, to create an isoptre. The involvement of a perimetrist brings the advantage

of allowing the test to be tailored to pay particular attention to a specific region and/or to adapt the direction and speed of the stimulus to suit the patient. The disadvantage is that the test is not standardised and can result in operator-dependent, between-test differences. The Goldmann perimeter is the most commonly used type of kinetic examination strategy and employs a bowl of uniform background luminance upon which the moving stimulus is presented.

1.2.2.2. Static Examination Strategies

Static perimetry presents test stimuli of differing area and luminance at a series of locations on a grid. The luminance is gradually increased to identify the threshold of visibility. This process is carried out in an automated fashion and it therefore less sensitive to operator variability than kinetic techniques. Static perimetry is used to screen the visual field rapidly.

The most commonly used method is the Humphrey 24-2 or 30-2 standard automated threshold test.

In kinetic and static approaches to perimetry, subject co-operation and input is required to achieve an accurate visual field map.

The techniques of perimetry are well-refined and established in the assessment of the visual field. This assessment is a crucial tool in diagnosing the presence and monitoring the progress of many diseases and conditions such as glaucoma, macular degenerations and lesions within the visual system.

1.3. Summary

The visual system, the visual field and perimetric testing have been described. The merits of perimetry have been discussed; however perimetric testing requires the full co-operation of the patient and at best can only reflect an abnormality from a non-specific part of the visual pathway. For objective evaluation of some forms of visual dysfunction it is necessary to perform clinical electrophysiology.

In a review of perimetric developments, Wall (25) concluded that while modifications in perimetric technology and statistical analysis have provided improvements in standard differential light sensitivity perimetry, it remains relatively insensitive and plagued with high test-retest variability in damaged fields. He reported that new developments appear to be improving on both these counts and the multifocal visual evoked cortical potential (mfVECP) is cited as one of the new approaches to perimetry.

Chapter 2

Conventional Visual Electrophysiology

Contents

		Page
2.0 Conventional Visual Electrophysiology ……..		35
2.1	Electroretinogram …….....	35
2.2	Visual Evoked Cortical Potential …….....	36
	2.2.1 Different Types of VECP …….....	38
	2.2.1.1 Pattern Reversal ……..	38
	2.2.1.2 Pattern Onset/Offset ……...	39
	2.2.1.3 Flash ……..	39
	2.2.2 The Limitations of the Conventional VECP ……	400
2.3	Summary …….	41

2.0 Conventional Visual Electrophysiology

Electrodiagnostic testing complements the information obtained by subjective measures of visual function. In general, electrophysiology gives global information on a particular level or layer of the visual pathway.

Investigations fall into three main categories; the electrooculogram (EOG) is a test of the retinal pigment epithelium (RPE), the electroretinogram (ERG) gives functional information on a number of retinal cells such as the photoreceptors, bipolar cells, muller cells, and the RPE and finally, the visual evoked cortical potential (VECP) which indicates the integrity and speed with which signals travel from the eye to the cortex.

This chapter aims to review the ERG in brief and the VECP in more depth. The ERG is introduced because of its pivotal involvement in the development of multifocal electrophysiology. The VECP is the precursor to the multifocal VECP, the focus of this body of research.

2.1 Electroretinogram

The ERG is an extracellular response which arises during neuronal activity because localised regions of cell membrane become depolarized or hyperpolarized and thus become sinks or sources of current.

An ERG signal is created when the eye is presented with a visual stimulus, commonly a flash. The signal acquired is of a characteristic shape. The amplitude and latency of different components of this waveform can be used to determine if the ERG response is normal or abnormal.

The degree of influence of specific cells on the components in the response can be varied by means of stimulus illumination, background illumination and frequency of stimulation. Thus, while the response to a flash of light under a steady background illumination (photopic response) will yield information predominantly from the outer and mid-retinal cone pathways, a dim flash of light under dark adapted conditions (scotopic response) will yield information from the outer and mid-retinal rod pathways.

The clinical ERG is a summation of massed discharge of large numbers of receptors. The standard ERG records the response of the whole of the retina and does not therefore detect small focal lesions.

2.2 Visual Evoked Cortical Potential

Human visual evoked potentials were discovered soon after human electroencephalography (EEG). Visual evoked cortical potentials (referred to as VEPs or VECPs) generated in the occipital cortex represent the end of the basic visual processing elicited by appropriate stimulation of the retina. Surface electrodes placed over the occipital cortex can be used to detect small electrical signals when the eye is presented with a flash of light or other visual stimulus. The International Society for the Clinical Electrophysiology of Vision (ISCEV) published a standard for the measurement of VECP recordings in 1996 (26) which was revised by Odom *et al* in 2004 (27).

Visual evoked cortical potentials are very small signals (3-25μV) and a record of a single VECP response is frequently obscured by superimposed electrical noise. Filtering can eliminate some but not all of this noise. Time locked signal averaging is used to improve the signal quality. Data acquisition is synchronised with the repeated presentation of the visual stimulus and the recorded signals are averaged. Sources of noise such as muscle artefact and extraneous background electrical noise which are not related to the rate of stimulus presentation are averaged out while the VECP is reinforced. The ISCEV standard requires that the recorded signal is sampled at a minimum of 500Hz and that the number of signal averages should be at least 64.

The first VECP studies were performed using a flash stimulus. It was observed that there was a large inter-subject variability in the waveforms produced. Investigation of other types of stimulus revealed that a reversing checkerboard removed the flash component of the VECP, since the overall luminance of the stimulus does not change, making it a response to contrast changes. This improves the intra-subject and inter-subject variability.

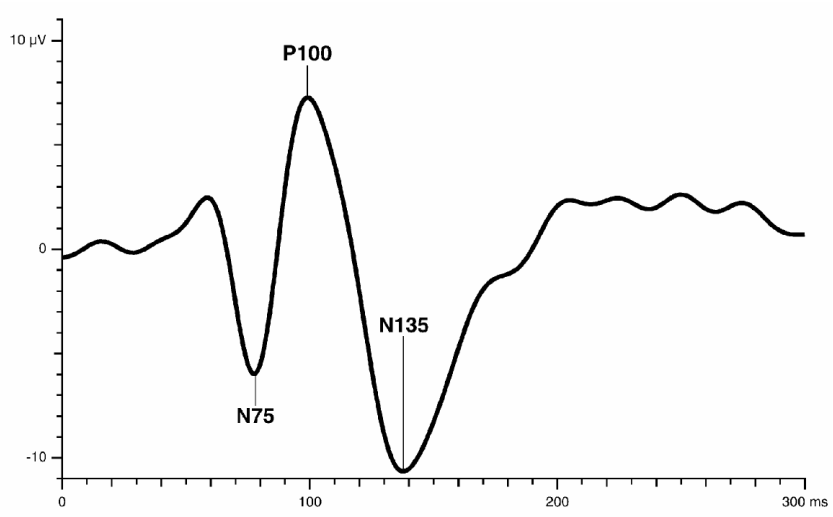

Figure 2.1 *A normal pattern reversal VECP response. Taken from Odom et al 2004(27)*

Early microelectrode studies of the cellular formation of the visual cortex showed that while a diffuse white light will stimulate cells within the retina and the lateral geniculate nucleus, it will not stimulate all the cells within the visual cortex. When a more visually complex stimulus is used, a greater number of cells will be stimulated, thus producing a greater measurable potential difference between the recording electrodes.

The normal pattern reversal response shown in Figure 2.1 comprises a negative peak at 75ms (N75), a positive peak at 100ms (P100) and a negative peak at 135ms (N135). The P100 exhibits the least variability and is therefore the most useful parameter.

A further advantage of the checkerboard reversal pattern is a correlation between the amplitude of the evoked potentials and visual acuity (28;29). When a checkerboard pattern of a spatial resolution that cannot be resolved by the patient is reversed, they are unaware of any change in the stimulus and no potential is evoked in the visual cortex. By gradually increasing the size of the checks, the point at which the patient's visual system can respond to the stimulus can be identified and used as a measure of their visual acuity.

2.2.1 Different Types of VECP

The VECP is commonly defined by the visual content of the stimulus and the rate and mode of presentation used to elicit a response (30). Diffuse light can be used either as a flash or a sine wave modulation of light intensity. Patterned stimuli include checkerboard patterns and sine wave gratings. In all cases, VECPs can be transient or steady state. The transient VECP allows the cortical response to return to baseline after stimulation and consists of a sequence of peaks that occur with a constant latency after each stimulus. Steady state recordings stimulate the visual system at higher frequency and the cortical response does not return to baseline. The record consists of a rhythm of uniform peaks occurring as the same frequency as the stimulus or its harmonics.

Three of the more commonly used VECP techniques are the pattern reversal, pattern onset and flash.

2.2.1.1 Pattern Reversal

Pattern reversal uses a stimulus of black and white checks or gratings with an equal number of black and white checks to ensure constant luminance. It is the preferred procedure in most clinical circumstances due to its relatively low variability of waveform and latency both within a subject and throughout the normal population. The pattern reversal VECP has negative peaks at 75 and 135 msec, and a positive peak at 100 msec. The latency of the P100 component shows relatively small variation between subjects and also shows a very small interocular range (27). Pattern reversal is used most commonly in assessment of the integrity of the optic nerve and the objective assessment of visual acuity. The Pattern VECP has proven to be a useful indicator of the state of retino-geniculo-cortical pathways. Amplitude decrease and increased latency have been reported in many pathological conditions involving the impairment of conductivity along the optic nerve.

2.2.1.2 Pattern Onset/Offset

The pattern onset/offset VECP uses the same pattern stimulus as pattern reversal, but it is abruptly appears from an equiluminant diffuse background.

The response has three main components. These are positive components at 75 and 150msec, and a negative component at 125msec.

It is difficult to deliberately de-focus a transient pattern on-set/offset stimulus, making it useful in patients with nystagmus and in cases of potential malingering (27;31;32).

Both pattern VECPs preferentially stimulate the central visual field. If there is a problem with the central retina, the optic nerve may not be stimulated sufficiently to produce a detectable VECP signal. In such cases, a flash can stimulate a wider area including the peripheral retina, testing whether any information is transmitted through the optic nerve.

2.2.1.3 Flash

The VECP response to flash stimulation consists of a complex series of negative and positive waves beginning around 30msec and terminating around 300msec. The most common components are the N2 and P2 components around 90 and 120 msec (27). Flash VECP latency is age dependent.

The clinical usefulness of the transient flash VECP is limited to conditions in which pattern VECPs cannot be obtained, such as the presence of opacities in the media which obscure pattern stimulation or when a patient is unable or unwilling to focus or fixate. Variation in the waveform in and between subjects precludes its wider use (30). Responses to flash stimuli are variable across subjects but show high inter-ocular symmetry (27).

The diagnostic process commonly uses complementary information from the electro-oculaogram (EOG), ERG and VECP to locate and identify dysfunction in the visual pathway.

2.2.2 The Limitations of the Conventional VECP

Conventional electrophysiology is objective, less dependent on patient co-operation than perimetry and can identify the site of dysfunction (i.e. outer, mid, inner retina and visual cortex). However, all of the tests described so far result in a global response to stimulation of a large proportion of the visual field which limits their ability to detect subtle or local pathology.

The VECP technique is limited to obtaining responses to stimulation in only a few field locations within a single session (33).

In an attempt to reveal local visual function within the visual field, researchers have suggested that a smaller stimulus be used to evoke a cortical response (34).

The type of stimulus has varied – small stimulus fields (34;35), half fields (36-40), quadrants (37;41;42), octants (43) and central/peripheral fields (44;45).

As spatial resolution is improved the stimulated volume of the visual cortex is reduced and the recorded signal is correspondingly decreased. A higher number of signal averages is therefore required in order to detect a reliable signal over the various sources of noise (environmental, muscular and cortical).

When different areas of the visual field are stimulated sequentially, the achievable resolution and signal to noise ratios are limited by the time available to make the recording. This in turn is dependent on the co-operation, ability and alertness of the subject. When considering a test to be applied to elderly, very young or unwell patients there is an upper limit to testing time, beyond which reliable results cannot be anticipated.

In addition, sequential stimulation is open to systematic error in spatial registration if there is an unnoticed movement by the subject.

A method which successfully overcomes these limitations is that of multifocal nonlinear analysis. In 1992 Sutter and Tran published a technique of multi-input systems analysis to explore the field topography of ERG responses to local luminance modulation (46). Using a special class of pseudorandom binary m-sequences, a large number of local areas of the visual field are simultaneously stimulated. Cross-correlating the recorded electrophysiological response with the m-sequence selects the response of the visual system to each region. As a result, localised areas of reduced

function can be determined. The multifocal technique has improved spatial resolution and sensitivity over standard electrophysiology techniques.

The application of multifocal techniques to the ERG (the multifocal ERG or mfERG) has successfully resulted in clinically useful information about local retinal defects in conditions including retinitis pigmentosa (47;48), retinal vein occlusions (49-53), glaucoma (54;55), diabetes (56;57), Stargardt's (58;59), retinal toxicity (60-62) and has been extensively incorporated into clinical practice (63;64).

In 1994 Baseler et al (12) applied multifocal techniques to the VECP allowing an electrophysiological map of the visual field to be obtained, by using a stimulus containing multiple checkerboard patterns.

Since then clinical uses of the mfVECP have expanded and include the study of glaucoma (14;19;65-82), optic neuritis and multiple sclerosis (15;73;83-86) and amblyopia (87).

The development from full-field to multifocal VECP mirrors the advance from full-field to multifocal ERG, but is more technically challenging. mfVECP signals are smaller than mfERGs, the sources of noise are more complex and more difficult to separate from the physiological signal of interest and the geometry of the visual cortex is considerably more convoluted than that of the retina. These factors combine to make the waveforms within a trace array more heterogeneous and the between subject variability far greater than that seen in the mfERG. As a result, there remains necessity for optimising the recording parameters during data acquisition and the analysis mfVECP data.

2.3 Summary

Conventional electrophysiology has been introduced with emphasis on the VECP. The advantages and limitations of the VECP have been discussed and the mfVECP has been introduced as a means of overcoming some of its drawbacks.

Chapter 3

Multifocal Electrophysiology

Contents

	Page
3.0 Introduction ……..	44
3.1 Multifocal Electrophysiology ……...	44
3.1.1 How the Multifocal Technique Works ……...	45
3.1.1.1 Binary m-sequences …….....	45
3.1.1.2 Generation of m-sequences ……	46
3.1.1.3 Creating Orthogonal M-sequences or ‘Sequence Decimation’ ……	48
3.1.1.4 Stimulus Control ……	49
3.1.1.5 Cross-correlation ……	49
3.1.1.6 First and Second Order Responses …….	50
3.1.1.7 Linear and Non-linear Systems ……..	51
3.2 The Multifocal Visual Evoked Cortical Potential ……	52
3.2.1 Flash/Checkerboard …….....	52
3.2.2 Cortical Scaling ……..	52
3.2.3 The Dartboard Stimulus …….	53
3.3 Multifocal Electrophysiology Recording Systems ……...	54
3.3.1 System Hardware and Software …….	55
3.3.2 Computing Hardware and Software ……...	55
3.3.3 Stimulus Display …….....	55
3.3.3.1 CRT Monitor ……..	56
3.3.3.2 LCD Projection System …….…….	56
3.3.4 Stimulus …….…….	56
3.3.5 Electrodes ……..……	57
3.3.6 Amplifiers ……..……	58
3.3.7 Analogue to Digital Converter (ADC) ……..……	58
3.3.8 Subject Preparation ……...……	59
3.3.9 Signal Analysis ……..……	59

Page

3.4 Summary of Investigations to Date ……...…….... 60

3.4.1 Investigations of Recording Parameters …… 60

3.4.1.1 Electrode Positions ……. 60

3.4.1.2 Dichoptic Stimulation …… 60

3.4.1.3 Investigations of Stimulus Parameters… 61

3.4.1.4 Stimulation Rate and Mode of Stimulation ……. 61

3.4.1.5 Check Size …….. 62

3.4.1.6 Effect of Defocus ……..... 63

3.4.2 Approaches to Data Analysis …… 63

3.4.2.1 Summation of Signals …… 63

3.4.2.2 Interocular Comparison …….. 63

3.4.2.3 Normalisation to EEG …… 64

3.4.3 Dipole Source Localisation and Magnetoencephalography ……..... 64

3.5 Summary ……... 66

3.0. Introduction

This chapter describes multifocal electrophysiology, discusses the requirements for its acquisition and reviews the application of multifocal techniques to the visual evoked cortical potential.

3.1. Multifocal Electrophysiology

Conventional electrophysiology records a global response from the retina or visual cortex in the case of the electroretinogram (ERG) or visually evoked cortical potential (VECP), respectively. Multifocal electrophysiology simultaneously stimulates many small areas.

Stimuli with as many as 241 regions have been used (46), but the most commonly used stimulus uses 61 regions, obtaining 61 local responses. A snapshot of the stimulus with 103 regions is shown on the left hand side of Figure 3.1. Each region stimulates a small, local area of the retina, evoking its own response. The array of waveform responses is shown on the right hand side of Figure 3.1.

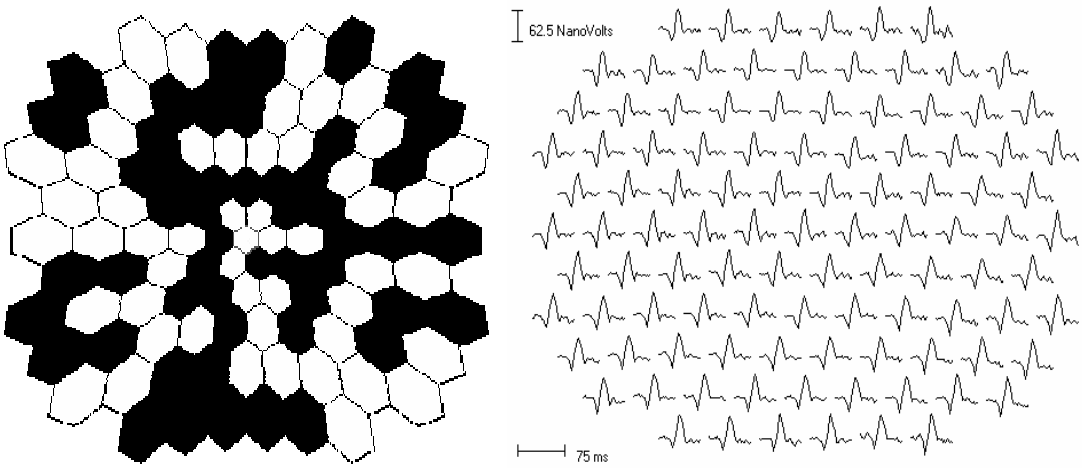

Figure 3.1 *A snapshot of the multifocal ERG stimulus is shown on the left hand side with 103 regions. 103 corresponding waveform responses are shown on the right.*

3.1.1. How the Multifocal Technique Works

The multifocal technique employs a stimulus with multiple regions, each of which flashes or goes through a pattern reversal in order to stimulate small, local areas of the visual field. The behaviour of each region is controlled by a binary m-sequence (46). Binary m-sequence inputs are white-noise inputs with a binary amplitude distribution. Each region is controlled by the same sequence which is shifted in time. This shift is 1/*k*th of a stimulation cycle, where *k* is the power of 2 nearest to, but larger than, the number of stimulating regions. The time shift renders the shifted and original m-sequences orthogonal.

Linear systems can be completely described by their response to an impulse function. The visual system however, is non-linear. Binary m-sequences are a special class of pseudo-random binary sequences and their properties make them useful for the analysis of non-linear systems. When properly generated, a set of m-sequences are orthogonal and this property allows the selection of a response to an individual region of the stimulus to be selected from the recorded signal. Careful selection of the m-sequence means that the presence of nonlinearities can be found in between first order responses. Appropriate selection of m-sequences has been addressed by Ireland *et al* (88).

3.1.1.1. Binary m-sequences

Binary m-sequences have the following characteristics (88;89):-

- The period of the sequence is 2^{m-1}, where m is the order of the polynomial.
- Each m-sequence contains one more 1 than 0.
- An m-sequence can be 'decimated' into 2^n columns ($n \in \mathbf{Z}$). Each column then contains a shifted version of the initial sequence. This shift acts as a time delay which renders the focal response uncorrelated. 'Sequence decimation' is a term used in a specific sense in multifocal techniques and is defined in Section 3.1.1.3.
- Shift and add property: the sum of any two distinct shifts of an m-sequence is a third shift.
- An m-sequence has the 'window property': any *m*-bit word appears once and only once.

3.1.1.2. Generation of m-sequences

A primitive polynomial of order *m* will produce an m-sequence of length 2^m-1 (90). A linear-feedback shift register (LFSR) can be used for sequence generation. The feedback or 'tap' positions are determined by the terms of the polynomial. The bits present in the tap positions are combined using exclusive OR (XOR) logic or modulo 2 addition. This operation creates a new bit which is shifted into the left hand side of the register. The bit that was previously in the *m*th position (right-most position) is shifted out and forms the first term of the m-sequence. The generation of an *m*=4 m-sequence of length 2^4-1 = 15 using the primitive polynomial x^4+x+1 is shown in Figure 3.2.

Practical m-sequences are formed using higher degree polynomials. Commonly 15-bit m-sequences are employed using a primitive polynomial such as $x^{15}+x^{13}+x^{12}+x^{11}+x^6+x^3+x+1$. This creates an *m*-sequence of length 2^{15}-1 = 32767 steps.

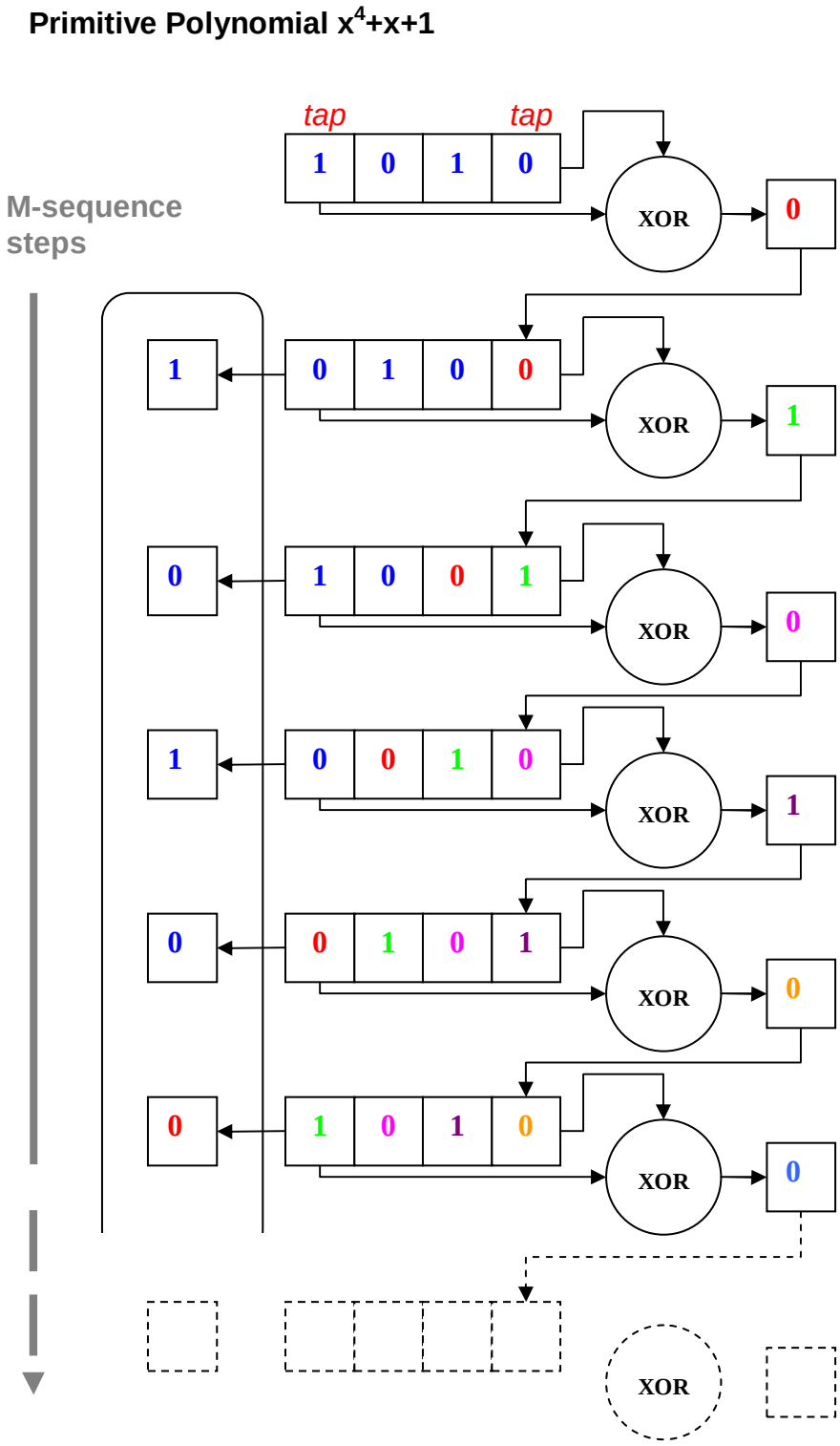

Figure 3.2 *Primitive polynomial x^4+x+1 has tap positions at x^4 and x. The LFSR can be filled with any non-zero seed pattern.* ***1010*** *has been chosen here. The XOR operation creates a new bit,* ***0****, which is fed into the rightmost register. The original bits are shifted left, pushing the leftmost* ***1*** *out. This bit is the first step of the m-sequence. The process is repeated to generate the full 15-bit sequence.*

3.1.1.3. Creating Orthogonal M-sequences or 'Sequence Decimation'.

The multifocal stimulus requires a set of orthogonal sequences to control the behaviour of its multiple regions. This is generated by process called decimation. The original *m*-sequence is used to fill the rows of 2^n columns, where $n \in \mathbf{Z}$ and $n>0$. This procedure is repeated until each column is of length 2^m-1. Each column contains the same sequence with a different starting point. The 2^n new, shifted m-sequences create an orthogonal set and can be used to control up to 2^n regions of a stimulus independently. This is illustrated in Figure 3.3.

Sequence 101011001000111

Col1	Col2	Col3	Col4
1	0	1	0
1	1	0	0
1	0	0	0
1	1	1	

Col1	Col2	Col3	Col4
1	0	1	0
1	1	0	0
1	0	0	0
1	1	1	1
0	1	0	1
1	0	0	1
0	0	0	1
1	1	1	0
1	0	1	1
0	0	1	0
0	0	1	1
1	1	0	1
0	1	1	0
0	1	0	0
0	1	1	1

Figure 3.3 *Decimation of the 4-bit m-sequence generated in Figure 3.2, 101011001000111. The sequence is used to fill the rows from left to right as shown on the left hand side. Once the sequence has run out, the process is repeated. The red 1 indicates the beginning of the sequence. This process is repeated until each of the four columns contains 15 entries. Each column now contains an orthogonal m-sequence.*

Throughout this thesis, the word 'decimation' and its derivatives will be used in relation to the process described above rather than its conventional meaning.

3.1.1.4. Stimulus Control

An example of the stimulus used in the mfERG is shown in Figure 3.1 above. Each hexagonal region alternates between black and white. The alternation of each hexagon is controlled by one of the set of orthogonal m-sequences. When the sequence is a 0, the hexagon appears black. When it is a 1, the hexagon appears white.

During the recording of multifocal pattern ERGs (55) and mfVECPs, instead of controlling the luminance of a region, the m-sequence can be used to control a pattern reversal. A 0 in the sequence indicates one state of the pattern or checkerboard and a 1 is its reversal, as illustrated in Figure 3.4

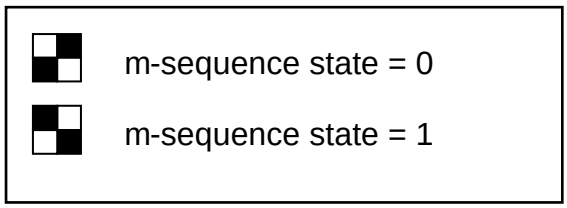

Figure 3.4 *Illustrating the control of a pattern reversal by the m-sequence.*

Commonly the rate of stimulation is 75Hz, as determined by the frame rate of the cathode ray tube. In this case, the m-sequence advances through each step every 13.3ms.

3.1.1.5. Cross-correlation

The visual system is simultaneously stimulated by the different regions of the multifocal stimulus and the electrophysiological data acquired from the visual system is a composite of responses to all these regions. Cross-correlation of the recorded data with each of the orthogonal m-sequences is the process by which responses to individual regions are calculated.

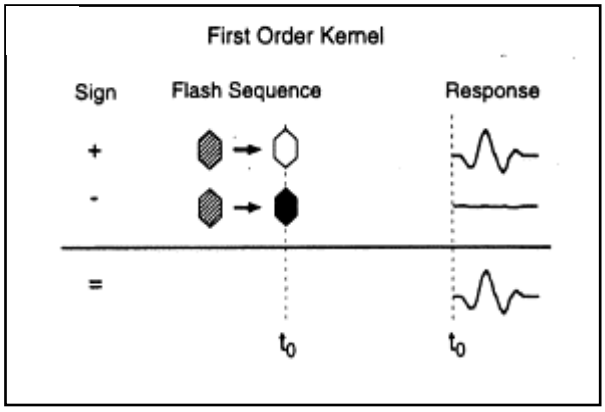

Figure 3.5 *Cross-correlation of a first order response in the mfERG can be described as the addition of all responses to a flash stimulus minus the sum of all the responses to a dark stimulus region.*

The process of cross-correlation is illustrated by the first order schematic diagram in Figure 3.5. The hexagonal regions used in the mfERG are used for illustration.
The first order kernel is the sum of all responses to a flash minus the sum of all responses to a black stimulus region. When each flash occurs a fixed length of the recorded data, starting at the beginning of the flash, is added to a memory buffer. At the beginning of each off-state, or black hexagon, the same duration of data are subtracted from the memory buffer.

In contrast to conventional electrophysiology, the duration of the added data segment is longer than the inter-stimulus interval.

Computational effort required to perform the cross-correlation can be significantly decreased by the use of a Fast Walsh Transform (91).

3.1.1.6. First and Second Order Responses

The multifocal technique can calculate the correlation coefficient not only between a response and a single flash or pattern reversal, but also between the response and pattern of stimulus behaviour over a longer period, by measuring higher order kernels. The order *n* of the response indicates the number of steps or base periods in the stimulus pattern. The response to a particular stimulus pattern is called a kernel slice.

The first order kernel of the system is the best linear prediction of all the different impulse responses produced by the system (i.e. the closest match to the linear impulse response).

The second order kernel is the sum of all responses to a change (black to white and white to black), minus the sum of all responses when no change in the stimulus region occurs (black to black and white to white), as shown in Figure 3.6.

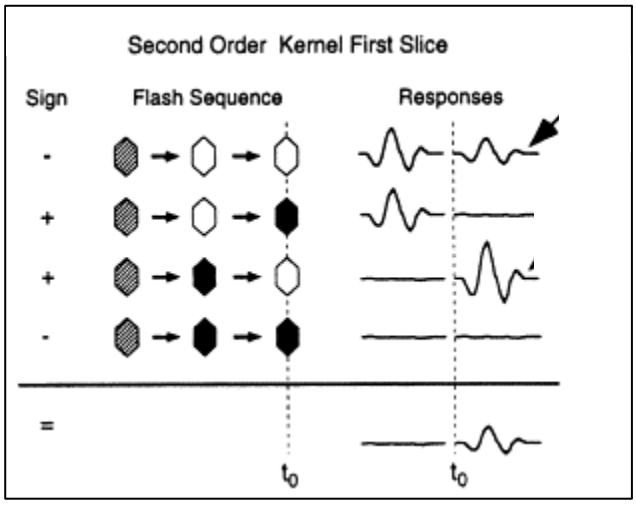

Figure 3.6 *The second order response of the mfERG is the addition of all responses to a change in luminance minus the sum of all responses where there is no change in luminance.*

The second order kernels can be thought of as a measure of how the multifocal response is influenced by the adaptation to successive flashes. A more mathematical description of kernels is given by Sutter (92;93).

The first slice of the second-order kernel measures the effect of an immediately preceding flash, while the second slice of a second-order kernel measures the effect of a flash two frames away, and so on.

When the stimulus regions are checkerboard patterns, the luminance in each region is constant and the response of the visual cortex is evoked by contrast reversals of the pattern. The occurrence of a reversal is dependent on the checkerboard pattern in two frames and it is therefore necessary to look at the second order kernel in order to retrieve the visual evoked cortical response.

3.1.1.7. Linear and Non-linear Systems

If a system is linear, its response to a series of events is the same as the superposition of the responses to individual events occurring in isolation. The visual system is, however, non-linear. The response to a stimulus event is, therefore, dependent on the events immediately preceding it. For example, an mfERG response to a flash depends on whether the base periods immediately preceding it were 0s or 1s. A series of 1s will depress the response. The non-linearities of the visual system can be investigated by cross-correlating higher order kernels of the multifocal response.

3.2. The Multifocal Visual Evoked Cortical Potential

The application of multifocal techniques to the visual evoked potential was first performed as a means of monitoring the direction of gaze in the severely handicapped, rather than as a means of detecting local variations in VECP topography (94).

Pseudorandom binary sequences (PRBS) have been used to drive high frequency (500Hz) flash stimuli to improve the sensitivity of the flash VECP. These were found to have the same morphology as conventional flash VECPs and suggested that the PRBS VECP is more sensitive than the pattern VECP and less sensitive than the flash VECP (95).

In 1994 Baseler and Sutter focussed on the multifocal VECP as a diagnostic tool. Since then the use of mfVECP as a means of detecting local variations in VECP topography has been developed.

There are several major differences between the mfERG and the mfVECP, which include the type of stimulus used and the kernel of data which reveals the most diagnostically useful information.

3.2.1. Flash/checkerboard

As discussed in section 2.2.1 on the standard VECP, a flash of white light is not the optimum stimulus to use to evoke a response from the visual cortex. Instead, a checkerboard pattern is used. For this reason the mfERG stimulus which uses a series of flashes, is not appropriate when attempting to record a mfVECP. Instead, the checkerboard pattern is commonly incorporated into a series of independent regions of a circular checkerboard pattern.

3.2.2. Cortical Scaling

The size of the hexagons in the mfERG stimulus varies with eccentricity in order to achieve signals of similar amplitude and signal to noise ratio in response to the stimulus presented by each hexagon. The size of the hexagons is scaled to match the density of photoreceptor cells across the visual field.

Similar scaling is necessary in the mfVECP stimulus, however, instead of scaling to photoreceptor density, cortical magnification is used. The magnification in humans has been studied by Horton and Hoyt (96).

They correlated structural magnetic resonance scans from patients with clearly defined occipital lobe lesions and homonymous field defects. This allowed them to create a map of the human striate cortex indicating sections which respond to stimuli in a given part of the visual field. It was confirmed that the central retina, which is more densely cellular and specialised for best visual acuity, has a relatively expanded representation in the striate cortex.

They determined the linear magnification factor, M_{linear}, or number of millimetres of cortex representing 1° of the visual field at any given eccentricity. M_{linear} has units of millimetre per degree, has been found to be inversely proportional to eccentricity, E, and is given by Equation 2.1.

$$M_{linear} = \frac{17.3}{E + 0.75} \qquad \text{Equation 2.1}$$

The use of cortical scaling in the mfVECP stimulus was first introduced used by Baseler and Sutter (12).

3.2.3. The Dartboard Stimulus

Figure 3.7 shows the dartboard stimulus.

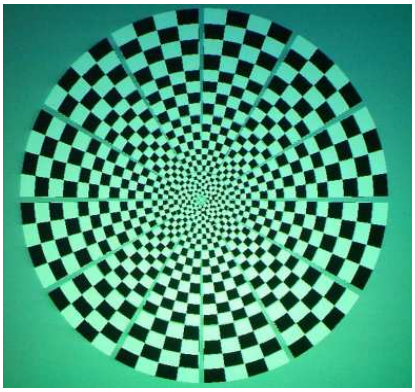

Figure 3.7 *The mfVECP Dartboard Stimulus.*

It has been observed that the waveforms obtained immediately above and below the horizontal meridian differ significantly and are commonly inverted. A region

straddling the horizontal midline would evoke responses of both polarities and result in signal cancellation, which could be confused with an absence of signal. Therefore, there are no stimulus regions which straddle the horizontal meridian.

Each region contains a 4 x 4 checkerboard pattern which reverses according to a binary m-sequence. Each region has a probability of 0.5 of reversing during each frame.

During a pattern reversal of a checkerboard, there is no change in the mean luminance. As a result, there is no first order kernel response to a change in luminance.

The change in stimulus does, however, give rise to a second order component. This is recorded in the multifocal VECP to pattern reversal stimulation.

3.3. Multifocal Electrophysiology Recording Systems

As multifocal electrophysiology has developed, a number of recording systems have become available. The first commercially available system was VERIS, developed by Sutter and colleagues, which has been used in many laboratories and clinics around the world. Subsequently other systems have come on to the market.

The ElectroDiagnostic Imaging Unit in Glasgow has a custom built system. This has been used extensively for both clinical and research purposes (64;97-101). It will be referred to as the EDIU Multifocal System throughout this thesis.

This thesis employed both the EDIU Multifocal System and a modification of it which used active electrodes (BioSemi, Amsterdam, Netherlands) for acquisition. A description of the EDIU Multifocal System is given here. Data presented in Chapters 3, 4 and 5 were recorded using the original EDIU Multifocal System. A detailed description of the modification process can be found in Chapter 8. Data presented in Chapter 7 was acquired with the modified system.

3.3.1. System Hardware and Software

There are many similarities between the recording of multifocal and conventional electrophysiology. Basic requirements common to both are electrodes, amplifiers, filters, stimulus display and a computer. Figure 3.8 shows a block diagram of the necessary components.

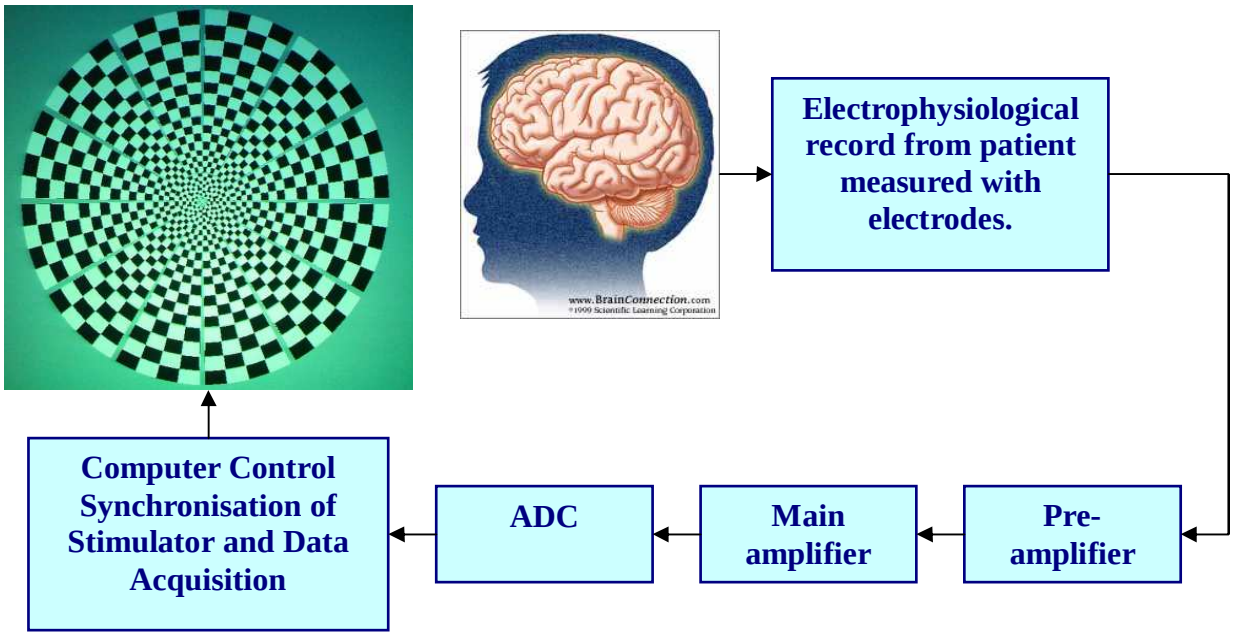

Figure 3.8 *The hardware required for a multifocal electrophysiology system. Adapted from (90).*

3.3.2. Computing Hardware and Software

The EDIU Multifocal System can run on any modern desktop computer running a Windows operating system. The software is written in Delphi (Borland, USA) and basic assembly programming. In order to create the stimulus, a graphics card (VSG - Cambridge Research Systems, UK) is used.

3.3.3. Stimulus Display

In the experiments described in this thesis, the stimulus is displayed on either a cathode ray tube (CRT) monitor or back-projected on to a screen using an LCD projector. Other modes of stimulation have been employed in multifocal electrophysiology including LEDs (102), scanning laser ophthalmoscopes (98) and virtual reality shutter goggles (17;103-108). Different modes of stimulus display are discussed in more depth in Chapter 6.

Unless stated otherwise, the stimulus was presented at a frequency of 75Hz. A steady background luminance filled the periphery of the display and a central cross was used to maintain fixation. The stimulus subtended a hemifield angle of 41°, and the subject's eye was at a distance of 30cm from the screen.

3.3.3.1. CRT monitor

A high luminance CRT monitor was used (Richardson Electronics, UK).

3.3.3.2. LCD Projection system

A Sharp XG NV4SE LCD projector was used.

The stimulus is displayed by back-projection on to a screen containing micro light diffusing optical lenses. This screen achieves a more even illumination than standard back projection techniques. The maximum illumination of the screen was 1500cd.m^{-2}.

3.3.4. Stimulus

The stimulus used was a dartboard pattern scaled for cortical magnification and is shown in Figure 3.7. Each region contained a checkerboard pattern. The checkerboard pattern in each region reverses according to a binary m-sequence. A central cross was used to maintain fixation. The recording period comprised intervals of 30-seconds. When a 15-bit m-sequence is used, this results in a total recording time of 8 minutes. Between each 30-second interval, the subject is allowed to rest for a few seconds, allowing better fixation during the recording time. The m-sequence is guaranteed to be orthogonal up to the third order kernel for 512 samples or 427ms.

The dartboard stimulus used throughout this thesis has 6 rings, with radii of 0.40, 1.20, 2.90, 5.20, 8.70 and 13.75 cm when the whole stimulus subtends 27.5 cm. For a FOV of 20° this translates to rings subtending 0.6°, 1.8°, 4.4°, 7.84°, 13.0° and 20.0° of eccentricity.

3.3.5. Electrodes

The original EDIU Multifocal System was designed to use standard Ag/AgCl electrodes.

Ag/AgCl electrodes require skin preparation via mild abrasion and are fixed in place with conductive paste.

The modified EDIU Multifocal System used active electrodes (BioSemi, Amsterdam, Netherlands). These were held in place with a headcap with locators in the 10-20 locations. Each electrode contained an amplifier. The amplified signal was then communicated to the acquisition computer via an optical cable. This is designed to reduce noise and signal loss. It obviates the need for skin preparation which allows the application of a higher number of recording electrodes in a timescale acceptable to the volunteer.

3.3.6. Amplifiers

In the original EDIU Multifocal System a preamplifier is used to provide an initial amplification of 100. This reducethe extraneous noise from environmental sources and provides electrical isolation of the patient by the use of an opto-isolator chip. This has the additional benefit of improving signal to noise ratio by interrupting ground loops and eliminating capacitance problems.

The original EDIU Multifocal System's amplifiers were designed and built by the Department of Clinical Physics and Bioengineering's Electronics Section. Specifications are given In Table 3.1.

Common mode rejection ratio (CMRR) – balanced	125dB (pre-amp + amp), 170dB (main amplifier)
CMRR unbalanced	85dB (pre-amp + amp), 160dB (main amplifier)
Noise	1μV peak to peak (0.1Hz -100Hz)
Bandwidth	DC-700Hz (IA296@ 1kHz = signal 1kHz filter)
DC restoration	±500mV
Calibration Pulse	15.25μV

Table 3.1 *Amplifier specifications.*

A gain of 100,000 was used during recordings.

3.3.7. Analogue to Digital Converter (ADC)

Analogue signals are digitized using a 12-bit ADC contained on a National Instruments NB-MIO-16 board. A sampling rate of 1200Hz was used. This satisfies the following requirements; the stimulation rate must be sparse in comparison to the sampling rate (93); that an integral number of samples are acquired during each base period in order to avoid aliasing problems (93) and sampling rate must be at least twice that of the highest frequency component expected from the input signal.

The maximum operating range for the NB-MIO-16 is ±5V.

3.3.8. Subject Preparation

Prior to recording mfVECPs, the nature of the test and its purpose was explained. Subjects were asked to fixate on the central cross and to endeavour to avoid blinking while the stimulus was running. Subjects were reassured that small blinks would not render the recording un-useable, in order that they remained relaxed. Subjects were seated comfortably in front of the screen with the centre of the screen level with their eyes. All subjects were refracted optimally using their own spectacles. Pupils were undilated. Each run was split into 30-second overlapping intervals. Subjects were encouraged to use the time between recording intervals to blink and relax their eyes. All recordings were monocular. The eye which was not under test was covered with a patch.

3.3.9. Signal analysis

The EDIU Multifocal System software was used to cross-correlate the first slice of the second order response of all mfVECP recordings.

Manipulation of data formats and data analysis was performed in custom-written Delphi programs and Microsoft Excel and is described in later sections.

3.4. Summary of Investigations to Date

Initial investigations into the multifocal visual evoked cortical potential resulted in pessimistic conclusions. In 1994, Baseler *et al* concluded that variability among normal subjects would make the mfVECP unsuitable for clinical field testing (12).

The relative contribution from different visual areas to the full-field VECP is dependent on the individual cortical anatomy as well as the particular stimulus characteristics and electrode positions (109). The anatomy of the primary visual cortex exhibits wide intersubject variability (110). Furthermore, extrastriate areas also contribute to the VECP. It is therefore not surprising that there is wide variation in VECP results.

Despite this, development has continued, with more encouraging results.

3.4.1. Investigations of Recording Parameters

3.4.1.1. Electrode Positions

In 1998 Klistorner, Graham and co-workers turned their attention to the electrode placement used to record the mfVECP. They found that the conventional occipito-frontal electrode placements, recommended by ISCEV for VECP recordings, favour the lower field response (111). This is most likely due to the complicated anatomy of the retino-cortical projections and the convoluted structure of the visual cortex.

Several other electrode placements have been suggested to balance the difference in upper and lower hemifield waveform amplitudes (16). However, variations in the visual cortex result in a large variation in the waveforms obtained from different individuals, regardless of electrode placement. It can therefore be difficult to distinguish between small normal responses and an abnormal response.

3.4.1.2. Dichoptic Stimulation.

The majority of mfVECP investigations record responses monocularly, in keeping with the approach taken for the full-field VECP, however dichoptic stimulation (presenting different images to each eye) has been investigated.

Arvind *et al* (103) found that the amplitude of responses to dichoptic stimulation was suppressed compared to monocular stimulation but that this suppression was minimised by increasing the sparseness of stimulation. James *et al* (104) found that the level of suppression compared to monocular stimulation was greatest when a contrast reversal stimulus was used rather than either a slow or rapid pattern pulse or temporally sparse stimulus.

3.4.1.3. Investigations of Stimulus Parameters

The multifocal VECP remains a relatively new technique for the objective assessment of the visual field. Currently there is no ISCEV standard for the mfVECP recording. A cortically scaled multifocal dartboard is commonly (12;14;33;70;71;79;83;85;109;112;113), but not exclusively (11;17;114;115) used. The dartboard regions increase in size from centre to periphery according to human cortical magnification, with the aim of maintaining uniformly sized responses throughout the tested field (12).

3.4.1.4. Stimulation Rate and Mode of Stimulation

Fortune *et al* have shown that significantly slowing stimulation rate increases both amplitude and latency of mfVECP responses (109). Martins' (116) and Balachandran's (117) work suggest an increase in response amplitude with decreasing stimulation rate.

The Pattern Pulse stimulation was introduced by James *et al* (17). It consists of a cortically scaled checkerboard pattern in which regions are either active or inactive. When inactive, a region is the mean luminance of a checkerboard and when active, a region has a pattern present for one frame (1/75th second) and is considered an impulse of contrast against a zero-contrast baseline. Stimulus onset intervals were pseudorandomly distributed between 0.4 and 0.6 seconds. This was compared to a

'conventional' multifocal visual evoked cortical potential using contrast reversal. A significant increase in response amplitude was achieved, while response topography was maintained. It is argued that the response to contrast adapts as a function of the preceding stimulation and that the zero-contrast interval lasting on average 0.5 seconds allows the system to recover its maximal contrast sensitivity. Longer inter-stimulus intervals were tested but no further amplitude increases were seen beyond 500ms. Increases in amplitude were approx 15-fold, however the signal to noise ratio (SNR) was not improved to the same extent. The SNR for the same duration of recording with Pattern Pulse stimulation compared to contrast reversal increased by a factor of 1.94. This reflects the larger number of stimulus presentations with the contrast reversal pattern and the correspondingly lower standard error in the responses (17;103-108).

The use of contrast-reversal stimuli is an established standard for clinical evaluation of the integrity of the visual pathway (118;119).

In a comparison of the effects of pattern-onset and pattern-reversal stimulation, Hoffman *et al* (120) hypothesised that the former would stimulate extra-striate cortex in addition to striate and would therefore have a different response topography to pattern-reversal stimulation which is thought to excite striate cortex alone. This was not borne out by their experiments. They did however discover a difference in the dependence of the SNR of responses on eccentricity. The central visual field had a greater SNR response to the pattern-onset stimulus, with the pattern reversal stimulation eliciting a greater SNR response peripherally.

3.4.1.5. Check Size

Baseler and Sutter have investigated the effect of check size on the mfVECP. The number of checks per patch was varied from 4x4, to 2x2 and 1. Tests were carried out under low (13%) and high (95%) contrast conditions. In both cases, the amplitude response of the waveform improved when 4 or 16 checks were used, over 1 check. No further distinction was made as to whether 4 or 16 checks were better. This proves that a checkerboard pattern is an improvement over the uniform region colour (13).

Martins *et al* (116) varied check sizes in blue-yellow mfVECPs and found no impact on response latencies. Subtle differences in amplitude were seen at central field locations.

3.4.1.6. Effect of Defocus

Central responses are affected by defocus to a greater extent than peripheral regions. Since the central stimulating regions have a higher spatial frequency, they are more susceptible to blurring effects. This means that the mfVECP is affected by defocus to a greater extent than the mfERG, which has lower spatial frequency and has been shown to be invariant over a range of optical defocus of -3.0D to +6.0D (121;122).

3.4.2. Approaches to Data Analysis

3.4.2.1. Summation of Signals

In order to increase the signal to noise ratio (SNR) of responses when individual responses are noisy or too small to distinguish details of interest, it is common to sum local groups of waveforms. In the case of the mfERG, grouping is commonly performed according to eccentricity. Klistorner & Graham (79) proposed grouping mfVECP waveforms in sectors. It is important to make sure that summation only occurs over locations which contain similar waveforms. This is straightforward with mfERG records where the normal response contains uniform waveforms throughout. Where traces are markedly different, cancellation can occur and information will be lost rather than revealed.

While increases in SNR are advantageous, the pay-off is a loss of spatial resolution.

3.4.2.2. Interocular Comparison

As mentioned previously, individual differences in cortical anatomy contribute to a wide variation in mfVECP responses. Furthermore, inspection of the mfVECP response shows variation in amplitude, latency and waveform throughout the trace array. Comparison of responses to left and right eye stimulation, however, shows a

similarity between corresponding signals. This suggests that underlying cortical convolution plays a significant role in the variation in waveforms seen within a trace array and between healthy individuals (71). Although points in the visual field are incident upon different hemi-retinas of the two eyes, they project to cortical locations that are within a few hundred microns of one another. Therefore, the mfVECP should be the same from both eyes when the optics, retinae and pathways are functioning equally well.

In 2000 Graham *et al* (71) and Hood *et al* (33) introduced the idea of interocular comparison. This has successfully been used to overcome the restrictions imposed by intersubject variability and has improved the sensitivity of the mfVECP in detecting monocular visual field defects. The disadvantage of this approach is that it will be incapable of detecting bilateral visual field defects and cannot therefore be used in isolation. However, early signs of conditions such as localised ganglion cell or optic pathway damage are unlikely to be identical in the temporal retina of one eye and the nasal retina of the other.

3.4.2.3. Normalisation to EEG

Klistorner and colleagues observed a correlation between electroencephalogram (EEG) activity and the amplitude of the mfVECP response (123). EEG signals were quantified in the frequency domain after ECG and high alpha rhythm contributions were removed and used to scale the mfVECP response. This resulted in a decrease in the interindividual variability of response amplitudes and effectively removed the systematic difference seen between male and female mfVECP responses.

3.4.2.4. Dipole Source Localisation and Magnetoencephalography

The multifocal technique has been applied to the acquisition of visual evoked magnetic fields. When the brain is stimulated, ionic currents flow in the dendrites of neurons as a result of synaptic transmission. In accordance with Maxwell's equations, any electrical current will produce an orthogonal magnetic field. These magnetic fields are measured in magnetoencephalography or MEG. The detectors are SQUIDS or Superconducting Quantum Interference Devices which measure the magnetic fields at the surface of the scalp.

In both MEG and multichannel electroencephalogram (EEG) recordings, advanced signal processing techniques are used to estimate the location of the activity's source from data recorded from a large number of locations (typically 32-156). Unfortunately there is no unique solution to dipole localisation and the analytical methods used are themselves a subject of research that cannot be fully addressed in this thesis. One approach is to use prior knowledge of the sources of brain activity. Another is the use of independent component analysis. Generally, localisation algorithms operate by successive refinement. The system is initialized with a first approximation. A loop is then entered, in which a forward model is used to generate the magnetic field that would result from the current approximation, and the approximation then adjusted to reduce the difference between this estimated field and the measured field. This process it iterated until convergence is achieved.

Dipole source localisation has been performed on multifocal VECP data (124) and the findings were in keeping with classical models of visual cortex organisation.

Wang *et al* (11) were the first to report the acquisition of multifocal visual evoked magnetic field recording (mfVEFs) in 2001. They carried out a comparison of mfVEFs and mfVECPs from a square, 64-region stimulus and investigated the maximum eccentricity at which they could be recorded. The mfVEF was recordable at greater eccentricity with larger checksizes, increasing the amplitude of eccentric responses.

Tabuchi *et al* 2002 (10) use the VERIS system to create a dartboard stimulus with four independent quadrants. 16 of their MEG system's 160 channels were used for data acquisition and cross-correlation. They compared equivalent current dipoles determined by MEG source localisation with the location suggested by the cortical magnification equation proposed by Horton & Hoyt (96) and the cruciform model and found good agreement.

Nishiyama *et al* 2004 (8) used a higher resolution stimulus with 48 independent regions. Once again, good agreement with the cruciform model was observed.

Owaki *et al* 2004 (9) investigated human stereoscopic vision. The stimulus consisted of four random dot patterns. The results were not as the authors expected, but the study indicates the successful initial application of multifocal visual stimulation to MEG recordings.

When compared to other functional neuroimaging techniques, MEG and VECP can provide temporal resolution that is superior to functional magnetic resonance imaging (fMRI), positron emission tomography (PET) and single photon emission computed tomography (SPECT). The disadvantages of MEG include its comparative scarcity and expense and the fact that its algorithms are less widely accepted than those of the aforementioned techniques. In comparison with EEG, MEG signals are relatively undistorted. When compared to the type of electrophysiology system used throughout this project, MEG recordings are performed on a more complex, costly scale. They provide additional information about the source of activity which is not directly considered in mfVECP recordings.

3.5. Summary

Improvements in the spatial resolution of visual electrophysiology are achievable using multifocal techniques. The theory behind the application of multifocal techniques has been discussed, the more commonly used methods of stimulation have been described and the technical requirements for acquisition have been detailed. The merits of the mfVECP are compared with those of functional neuroimaging and magnetoencephalography.

Recent areas of technical development in the mfVECP have been reviewed. However, in light of the very small signals involved and the complexity of the visual cortex from which they are measured, there remains a necessity to optimise the methods of mfVECP stimulation, their detection and the manner in which recorded data are assessed.

Chapter 4

Quantifying Multifocal Signal Quality

Contents

			Page
4.0 Introduction ……..			69
4.1.Why is the Signal to Noise Ratio Important?…….....			69
	4.1.1.	Peak to Trough ……...	71
	4.1.2.	mfERG Scalar Product ……...	71
	4.1.3.	Latencies and Amplitudes ……..	71
	4.1.4.	RMS ……...	72
	4.1.5.	SNR ……	73
	4.1.6.	Interocular Comparisons ……	75
	4.1.7.	Other Approaches ……...	75
	4.1.8.	“Dead M-sequences” ……..	76
	4.1.9.	Terminology ……...	77
4.2.Validation of the Dead-M SNR Against the DTW SNR			78
	4.2.1.	Aims ……...	78
	4.2.2.	Methods ……..	78
		4.2.2.1. Software Modifications ……..	78
		4.2.2.2. Dead-M vs DTW SNR Values ……...	78
	4.2.3.	Results ……	80
		4.2.3.1. Software Modifications …….....	80
		4.2.3.2. Dead-M vs DTW SNR Values ……...	82
		4.2.3.3. Distribution of Noise Estimations ……..	85
		4.2.3.4. Discrimination Between Signal and Noise – DTW vs Dead M .....…	86
	4.2.4.	Discussion ……..	88
	4.2.5.	Conclusion ……..	88

Page

4.3.Quantifying Signal Quality in Robust mfERG Signals Using the Dead-M SNR ……..... 89

4.3.1. Aim…….. 89

4.3.2. Introduction …… 89

4.3.3. Method ……... 89

4.3.4. Results …… 91

4.3.4.1. Distribution of Signal SNR Values …… 91

4.3.4.2. Distribution of Noise SNR Values …… 91

4.3.4.3. Separation of Signal and Noise …….. 94

4.3.5. Discussion ……. 96

4.3.6. Conclusion ……. 96

4.4.Assessing SNR in the mfERG with Increasing m-sequence Length using the Dead-M SNR Parameter …….. 97

4.4.1. Aim ……..…… 97

4.4.2. Introduction…… 97

4.4.3. Methods ……. 97

4.4.4. Results …… 99

4.4.5. Discussion …….. 103

4.4.6. Conclusion …….. 103

4.5.Quantifying Multifocal Signal Quality - Conclusion …..…… 104

4.0 Introduction

This chapter discusses common approaches to quantifying signal quality and introduces a new approach which makes use of orthogonal m-sequences that are unused by the stimulus. It aims to:

- Validate the new approach against the commonly used method of using a delayed time window in the cross-correlated mfVECP signal as an estimation of noise.
- Demonstrate the utility of the new metric is useful with both robust mfERG and smaller, noisier mfVECP signals by using it
    - to compare mfERG signal quality between acquisitions made with DTL and gold foil electrodes and
    - to compare improvements in mfVECP SNR with increasing m-sequence length against the theoretical improvement of a factor of $\sqrt{2}$ for each increment.

4.1 Why is the Signal to Noise Ratio Important?

The perfect recorded signal would be a true representation of retinal or cortical response to the visual stimulus alone. In reality there are a number of unwanted contributions to the signal. Common to both the mfERG and mfVECP are the presence of electrical noise from the environment and muscle activity. The mfVECP also contains contributions from cortical activity such as alpha waves that are unrelated to visual processing. The mfERG contains noise due to eye movements and blinks.

During a standard ERG or VECP recording, data are acquired for a time period longer than the physiological response. Once the response is complete, the record provides a good representation of noise.

This is not the case for a waveform produced by the cross-correlation of the raw electrophysiological signal with an m-sequence. Cross-correlated responses are typically displayed over 100-200ms, while the base period of stimulation is commonly 13.3ms.

For a second order response, the response is a summation of all responses to a pattern reversal minus the sum of all responses when there is no pattern reversal.

This is achieved by selecting data epochs of 256 or 512 samples (213 or 427msec) in length, beginning from the start of each base period. Within this sample there will be 16 (or 32) frames. With the exception of the first two of the 16 (32) frames, the remaining pairs of frames may or may not provide a pattern reversal, at random.

Data are selected for addition or subtraction based on whether there is, or is not, a pattern reversal at the beginning of the data interval. The behaviour of the stimulus in the remaining 14 (or 30) frames will vary, but will be balanced.

To illustrate: The cross-correlation process requires the addition of all epochs beginning with a pattern reversal and the subtraction of all epochs that begin without a pattern reversal. Let us consider these epochs to fall into category A or B, respectively. If we consider a later base period, BP_{LATE} , within the epoch, in some cases this will be a pattern reversal and in others it will not be. The number of pattern reversals at frame BP_{LATE} that fall into category A will equal the number that fall into category B and their impact on the cross-correlated waveform will therefore cancel. The same is true of occasions where there is no change of state. Where an m-sequence is properly selected for the length of data epoch, this will be true for all frames beyond the first two.

In situations where the selection of m-sequence is not appropriate or sections of data are missing due to blinking or lack or subject co-operation, cancellation may be incomplete and will show waveforms reflecting the behaviour of the visual system after the first frame of the epoch. This is referred to as contamination of the signal and can appear superimposed on the signal window, or at a later time window within the cross-correlated response.

Just as signal averaging will reduce the noise contribution in a conventional electrophysiology recording, due to the random nature of noise, the process of cross-correlation will reduce the impact of any noise contribution that is uncorrelated with the m-sequence. As with conventional techniques, noise cannot be totally removed.

When testing patients there will be cases where there is a lack of response. It is important that the recording set up is sufficiently robust that we are confident that the

lack of a recognisable waveform is due to a lack of response rather than an excess of noise.

A number of different approaches to quantifying signal quality have been employed in multifocal electrophysiology. These are as follows:-

4.1.1 Peak to Trough.

Records with peak to trough values that are less than a criterion value could be rejected. However, when signal free mfVECP records are contaminated with alpha waves or high frequency noise, it is possible that the peak to trough value will exceed the criterion (125). Peak to trough measures are useful in mfERG recordings.

4.1.2 mfERG Scalar Product.

mfERG responses exhibit less inter subject variability than the mfVECP, and uniform waveforms throughout the trace array. This allows a scalar product measure to be used (46). A template is created by defining a time window (a,b) which contains the relevant response components and the template, t, is normalised over this window (Equation 4.1). The dot product of an individual waveform, $r_{k,}$ with an ideal response is calculated to give the scalar product, A_k (Equation 4.2). Increases in latency or reductions in amplitude result in a reduction in the scalar product value.

$$t = \frac{s}{\sqrt{s \bullet s}} = \frac{\{s_i\}}{\sqrt{\frac{1}{(b-a)}\sum_{i=a}^{b}(s_i)^2}} \qquad \textbf{Equation 4.1}$$

$$A_k = r_k \bullet t = \sum_{i=a}^{b}(r_k)_i t_i \qquad \textbf{Equation 4.2}$$

4.1.3 Latencies and Amplitudes

Latencies and amplitudes have been used to quantify mfVECP records (67;76;109;126;127). These are good where the waveform is constant throughout the trace array, however, this is not always the case. When dealing with large quantities of data, finding the appropriate waveform characteristic on which to define a latency or amplitude value can be impractically time consuming.

4.1.4 RMS

The root mean square of the record is an improvement on the peak to trough measurement because it does not rely on a particular feature of the response waveform. It is, however, still distorted by alpha wave or high frequency contamination. The RMS for each time window is calculated, as shown in Equation 4.3.

$$RMS = \sqrt{\frac{\sum_{t=t_1}^{t_2} \left(R_t - \mu_{t_1-t_2}\right)^2}{N}} \qquad \textbf{Equation 4.3}$$

where R_t = response amplitude at time t, μ is the average of the amplitudes from t_1 to t_2 and N is the number of samples in the time period.

4.1.5 SNR

An advantage of a signal to noise ratio (SNR) over an RMS or a peak to trough amplitude is that it can be defined independently of noise level. Biological and environmental noise varies from day to day, subject to subject and laboratory to laboratory. Removing the dependence of our description of signal quality on noise allows comparison of signal quality at different time points, between different subject and between labs.

A number of approaches to calculating SNR in mfVECP records have been suggested.

Zhang *et al* (125) created three new measures that are calculated as follows:-

The 'Two run signal to noise ratio' (2rSNR). In this calculation, the noise is estimated as the RMS of the difference between the waveforms acquired in two separate runs, A and B:-

$$2rSNR = \frac{RMS(RunA + RunB)}{RMS(RunA - RunB)} - 1 \qquad \textbf{Equation 4.4}$$

A later time window in the cross-correlated response is assumed to be a noise window. The 'individual noise window SNR' ($nwSNR_i$) for each waveform *i*, within the trace array is calculated using its own noise window:-

$$nwSNR_i = \frac{RMS(signalwindow)_i}{RMS(noisewindow)_i} - 1 \qquad \textbf{Equation 4.5}$$

The third approach is the average noise window SNR ($nwSNR_{average)}$ is a variation of the second. This time the denominator is the average RMS value of all the noise windows within the trace array.

$$nwSNR_{average} = \frac{RMS(signalwindow)_i}{RMS(noisewindow)_{average}} - 1 \qquad \textbf{Equation 4.6}$$

Zhang reports that the 2 run SNR showed the highest false-positive rate which he attributes to poor cancellation of alpha waves. A disadvantage of this approach is by requiring two runs, it does not take advantage of Sutter's advice (92) to the use the

longest m-sequence practicable instead of making multiple, shorter recordings and averaging the results, to prevent cross-contamination.

Of the nwSNR and $nwSNR_{average}$, approaches, the latter was found to have the lower false positive rate and is now used most widely (14;19;81;113;128).

The signal window is usually taken to be 45ms to 150ms and the noise window from 325 to 430ms and Equation 4.6 can be re-written as:-

$$SNR = \frac{RMS(45 to 150 m\sec)}{RMS_{average}(325 to 430 m\sec)} \qquad \textbf{Equation 4.7}$$

There is an inherent difficulty with the assumption that the later time window contains contributions from noise alone for two reasons:

Firstly, with a perfect mfVECP recording, cross-correlation will result in a complete cancellation of all physiological responses that occur after the second order response. However, small blinks or losses of data during a practical, clinical recording may mean that this cancellation is sub-optimal and it is possible that small physiological responses may appear later in the waveform, reducing its accuracy as an example of noise.

Secondly, there could be cross-contamination from another stimulus region. This contamination could be in the form of any order of kernel response. This is possible because the orthogonality of m-sequences holds for a finite period. The length of the period depends on the choice of m-sequence. Unless a manufacturer quotes that there is no cross-contamination by kernel overlap up to a given order (usually third) in a given time window, there is no way of knowing whether a contamination free window has been selected for time estimation.

Furthermore, Zhang *et al* (125) observe that the noise outside the signal window is poorly correlated with the noise in the signal window.

4.1.6 Interocular Comparisons

While there may be marked variation in waveform within a trace array, the symmetry of responses between the two eyes of control subjects has been observed (71), arising from the interleaving of the optic projections from the two eyes. This has been quantified using the relative asymmetry coefficient (RAC) (71), calculated as

$$RAC = \frac{\left(Amplitude_{OD} - Amplitude_{OS}\right)}{Amplitude_{OD} + Amplitude_{OS}} \qquad \textbf{Equation 4.9}$$

Or using an intraocular ratio (33)

$$InterocularRatio = \log_{10}\left(\frac{RMS_{OD}}{RMS_{OS}}\right). \qquad \textbf{Equation 4.10}$$

While this approach has the advantage of overcoming inter-individual variation, it cannot highlight bilateral damage.

4.1.7 Other Approaches

Klistorner and Graham (129) combine amplitude and SNR approaches. They divide the maximal peak to trough amplitude in the time window 60-250msec by the 'noise level', which they define as the RMS of the window 660-1100msec. This publication discusses data acquired with their OPERA^{TM} V1.3 system (ObjectiVision Pty Ltd, Sydney, Australia), which uses several runs of short, 512 step m-sequences. It is possible that with such short m-sequences, cross-contamination will be an issue (88).

4.1.8 "Dead M-sequences"

The orthogonal m-sequences which control the on-off or pattern reversal in the different regions of a mfERG or mfVECP stimulus, are created by 'decimating' the sequence as described in Chapter 3.

For a mfERG stimulus with 61 regions, or a mfVECP stimulus with 60 regions, the m-sequence must be decimated into a minimum of 64 columns. Custom software used in this department routinely decimates an m-sequence into 128 columns in order to allow the same process to be carried out for mfERG stimuli containing 61 or 103 regions. When controlling a 61 region mfERG stimulus there are therefore, 67 orthogonal m-sequences that are unused or 'dead'. When a 60-region dartboard mfVECP stimulus is shown 60 sequences are used and 68 are 'dead'.

Cross-correlating the recorded electrophysiological signal with a dead-sequence, results in a response which is unrelated to the response of the retina or visual cortex to any stimulus area and is therefore representative of the noise in the recording.

68 'dead' sequences permits 68 independent estimates of noise and provides a distribution of the noise contribution. Individually, they can be treated as truly absent waveforms, as they are known to be without a physiological response to a pattern reversal.

Averaging the waveforms containing only noise will result in cancellation. They can be quantified by their RMS value. The average RMS value is therefore more meaningful.

Zhang *et al* (125) approximated this method by covering up the outer regions of the stimulus. SNR were calculated for these locations to give a distribution of SNR in the absence of signal response.

This approach has been investigated with mfERG data by Hagan *et al* using m=9 m-sequences (130).

4.1.9 Terminology

For clarity and consistency throughout the rest of this thesis, the approach of using a delayed time window in the cross-correlated response as an indication of noise will be referred to as Delayed Time Window (DTW) noise characterisation. The alternative approach assessing the noise contribution by investigating the data resulting from the cross-correlation of the physiological record with the un-used m-sequences will be termed Dead M-Sequence (DeadM) noise characterisation.

4.2 Validation of the Dead-M SNR Against the DTW SNR

4.2.1 Aims

To adapt EDIU Multifocal System software to perform cross-correlation of the electrophysiological signal, with all 128 orthogonal m-sequences, rather than only those used to control the stimulus. To verify that the original cross-correlation process is not altered.

To compare Dead-M SNR values with DTW SNR values.

4.2.2 Methods

4.2.2.1 Software modifications

EDIU Multifocal System software was modified to perform 128 cross-correlations using orthogonal m-sequences using Delphi 4, the language in which it was originally written.

This resulted in an ASCII file containing all 128 cross-correlated waveforms. This was transposed using a short program also written in Delphi, in order that the file could be read into Microsoft Excel for further analysis. A macro was written to perform the SNR calculation.

To ensure that the modification of the program has not introduced bugs or systematic error to the cross-correlation process, the raw mfERG data from five subjects was processed using the original program and the modified version. The first order waveforms of all four recording channels were compared by visual inspection. The first order data from one channel, chosen at random, from each subject was compared by subtraction.

4.2.2.2 Dead-M vs DTW SNR Values

Dead-M and DTW SNR values were compared using a subset of mfVECP data recorded to compare responses to CRT and LCD projector delivered stimulation, described in Chapter 6.

mfVECP responses were recorded from four normal, healthy volunteers with no known ophthalmic or neurological conditions using the EDIU Multifocal System.

Subjects were optimally refracted using their own spectacles and their pupils were not dilated. Recordings were monocular.

Stimulation was provided by a 60-region dartboard pattern. Each region contained a 4x4 black and white checkerboard pattern and the size of the regions was scaled for cortical magnification. The stimulus was presented on a cathode ray tube (CRT) monitor and subtended a 20.5°radius of the visual field. The luminance of white areas varied across the screen from 735 cdm^{-2} to 960 cdm^{-2} and black areas varied from 6 cdm^{-2} to 162 cdm^{-2}. Contrast varied from 99% peripherally to 64% at the centre of the screen.

An m=15 bit m-sequence was used to drive the pattern reversal of the stimulus regions at a rate of 75Hz. Acquisition time was approximately eight minutes, divided into 30 second overlapping periods to allow the subject to blink and rest, in order to maintain good fixation.

Ag/AgCl electrodes were placed 4cm above the inion, 4cm left and right of the inion and 1cm below the inion on the midline. Acquired channels were Channel 0 = 4cm above the inion – 1cm below the inion, Channel 1 = 4cm left of the inion – 1cm below the inion, Channel 2 = 4cm right of the inion – 1cm below the inion and Channel 3 = 4cm left of the inion – 4cm right of the inion, similar to the montage employed by Hood *et al* (19). A reference electrode was placed at International 10-20 position F_Z and a ground electrode was placed on the temple. Electrode impedances were matched and below 5kΩ. The skin was prepared with abrasive gel and the electrodes affixed with conductive paste.

Signals were sampled at 1200Hz recorded with a 0.1 to 100Hz analogue filter and filtered through a 3-30Hz digital bandpass prior to cross-correlation.

The Delayed Time Window (DTW) SNR calculation was carried out using Equation 3.7. A minor modification to the standard time window of 325 to 430ms was necessary since our system cross-correlates a waveform of 426ms duration. The noise window was taken to be 321 to 426ms.

The signal window was taken as 45-150ms in both calculation methods.

Data was plotted in Microsoft Excel and analysed further in Minitab 13.32.

4.2.3 Results

4.2.3.1 Software modifications

The modified program was successfully used to perform 128 cross-correlations. Visual comparison of data showed no differences. The subtractions showed no non-zero values for all 5 datasets. An example is shown in Figure 4.1.

The results of the transposition program were plotted. Comparison with the EDIU Multifocal System trace arrays indicated a faithful row to column conversion.

128 waveforms were calculated. The Microsoft Excel macro was successfully created and tested allowing SNRs to be calculated using both the ‘dead m-sequence’ and delayed time window approach to characterising noise.

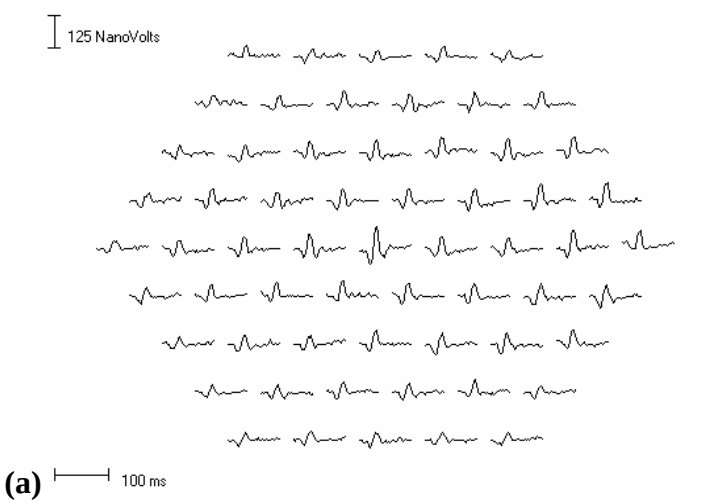

Original

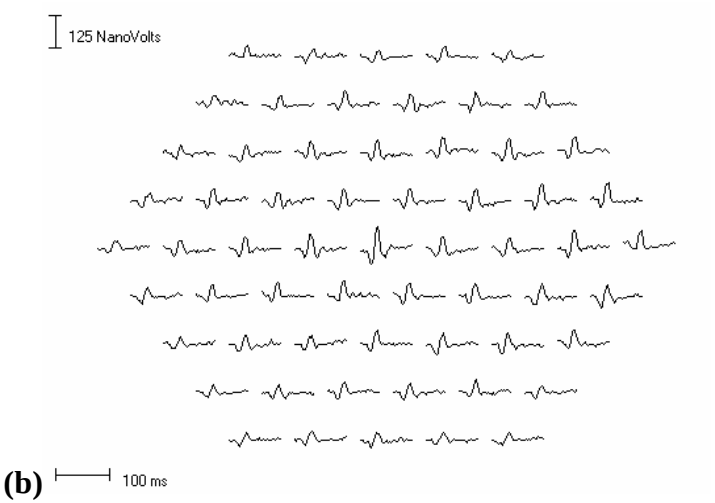

Modified Program

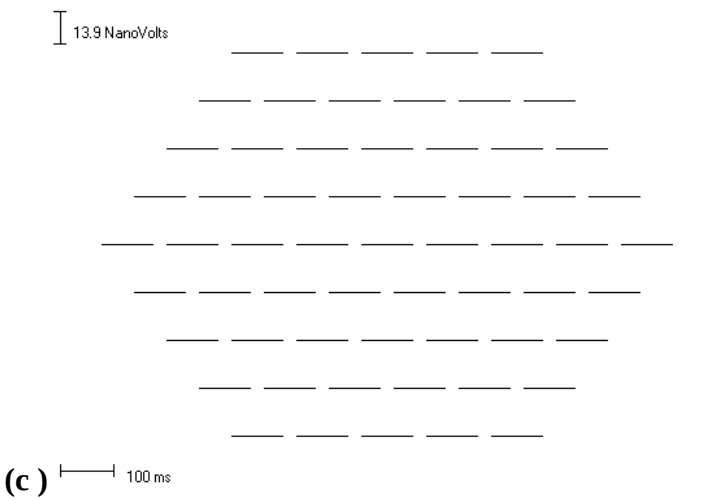

Figure 4.1 *A cross-correlated mfERG trace array using (a) the original program and (b) the same data analysed using the modified program. (c) shows the difference between the two, shown on a higher resolution amplitude scale. There is no difference between the analyses.*

4.2.3.2 Dead-M vs DTW SNR Values

Figure 4.2 shows the DeadM SNR plotted against the DTW SNR. Each plot contains data from the four recording channels. Each series contains 60 data points, representing the 60 waveforms in the trace array.

The plots indicate reasonable, although imperfect agreement between the two approaches.

It is reasonable to anticipate differences in the noise component in different recording channels in the same subject, due to small differences in resistance, wire geometry, background cortical activity and different locations. Similarly, the noise contribution will vary from person to person, with the additional variation of scalp, skull and cortical shape and conductivity.

As a result, statistical tests investigating the SNR values and distributions should be performed within subject and within channel.

The Pearson correlation coefficient was calculated (Minitab 13.32) for each channel and each subject. The null hypothesis is that there is no correlation between the datasets. In all 16 cases (4 subjects x 4 channels), the p value returned by Minitab was 0.000, confirming a statistically significant correlation.

The correlation coefficients are given in Table 4.1.

Subject	Channel 0	Channel 1	Channel 2	Channel 3
AM	0.62	0.58	0.86	0.62
DK	0.88	0.56	0.84	0.77
GA	0.89	0.87	0.92	0.79
JC	0.79	0.90	0.87	0.77

Table 4.1 *The correlation coefficient between the SNR calculated via the Delayed Time Window and Dead M-sequence noise estimation techniques*

.

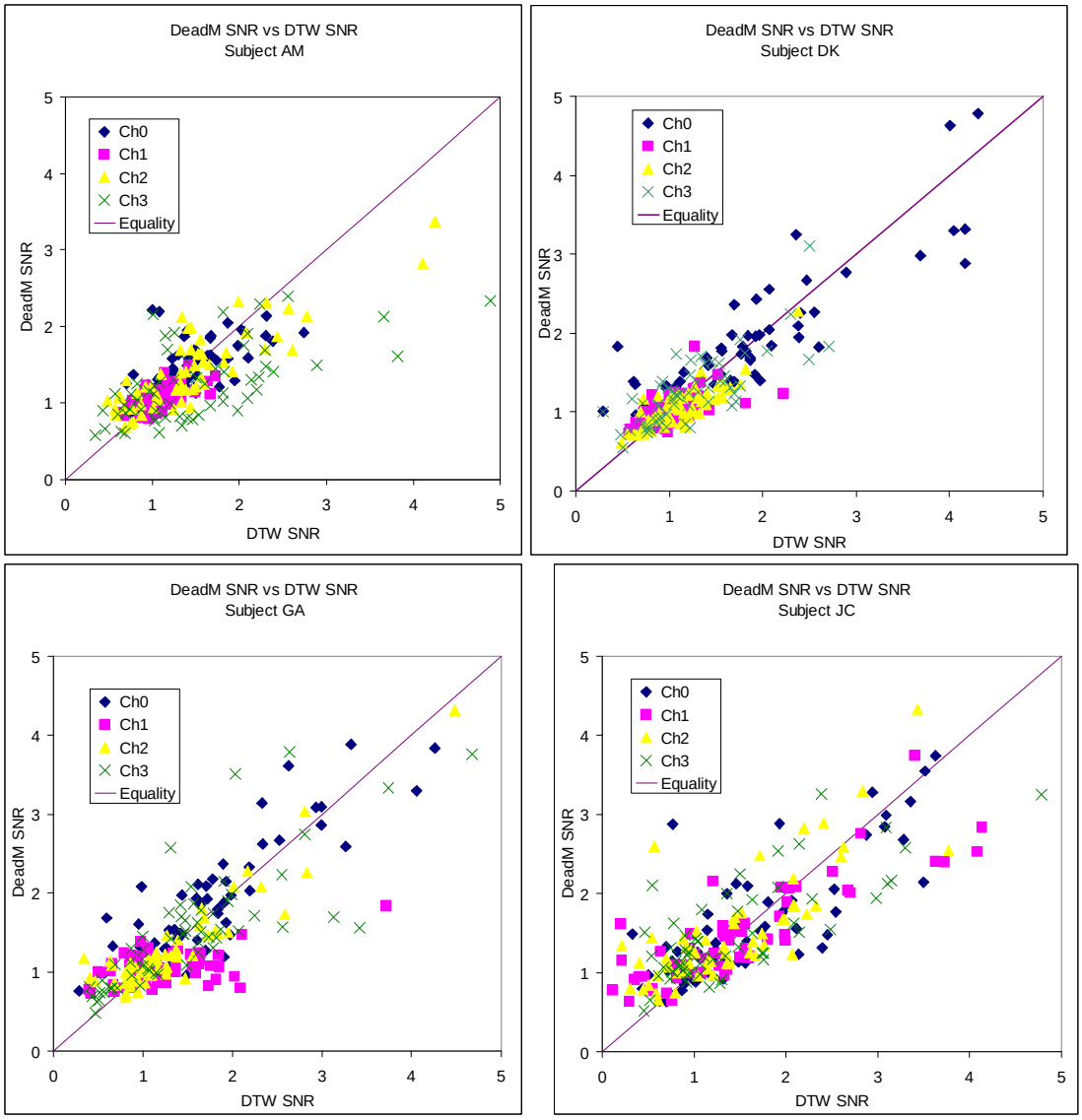

Figure 4.2 *Graph showing DeadM-SNR values plotted against DTW SNR values. mfVECP data recorded from 4 healthy volunteers is shown. Each plot shows data from a different subject. Each series shows data from a different channel.*

Using an Anderson-Darling Test for Normality, the SNR values calculated by both methods were shown to follow distributions other than the Normal Distribution ($p<0.001$). A non-parametric Wilcoxon Signed Rank Sum test was used to test the null hypothesis that there is no difference between the median SNR, as calculated by the DTW and DeadM methods. Again, this was performed for each channel and each subject. The majority of results could not reject the null hypothesis at the $p<0.05$

level, indicating that there is no significant difference between average value based on calculation method.

There were two exceptions:

Subject AM showed a significant difference in the Channel 3 trace. Reference to Figure 4.2 indicates that larger values were obtained via the DTW method.

Subject JC showed a significant difference in the Channel 2. This time, inspection of Figure 4.2 indicates that larger values were obtained via the DeadM method.

While these individual results appear real, when considered in context with the rest of the data here, they are not suggestive of a trend.

They could simply be observed due to multiple comparisons. A simple multiple comparisons correction can be applied by multiplying the p value by the number of statistical tests performed, which would increase it beyond p=0.05 in both cases.

4.2.3.3 Distribution of Noise Estimations

Calculations for the DTW approach used the same RMS noise value used for the stimulating m-sequences to calculate the SNR from the waveforms produced by cross-correlation of the physiological signal with the inactive m-sequences.

The DeadM-SNR distribution for the inactive m-sequences is centred about 1. This is because the denominator of the SNR is the average RMS value of the 68 noise estimations. There is no such restriction on the SNR values of the inactive m-sequences, using the DTW-SNR calculation.

The distribution of DeadM-SNR values for inactive m-sequences is narrower than that of the corresponding DTW-SNR values. Figure 4.3 shows the median SNR value for the noise estimated based on both methods of SNR calculation. Error bars show the 10^{th} and 90^{th} percentiles. In all cases the median SNR value for the DeadM method is greater than the DTW method, yet the range of values is greater for the DTW method. Figure 4.3 shows data recorded from Channel 0 for each of the four volunteers and is representative of findings from the other three channels.

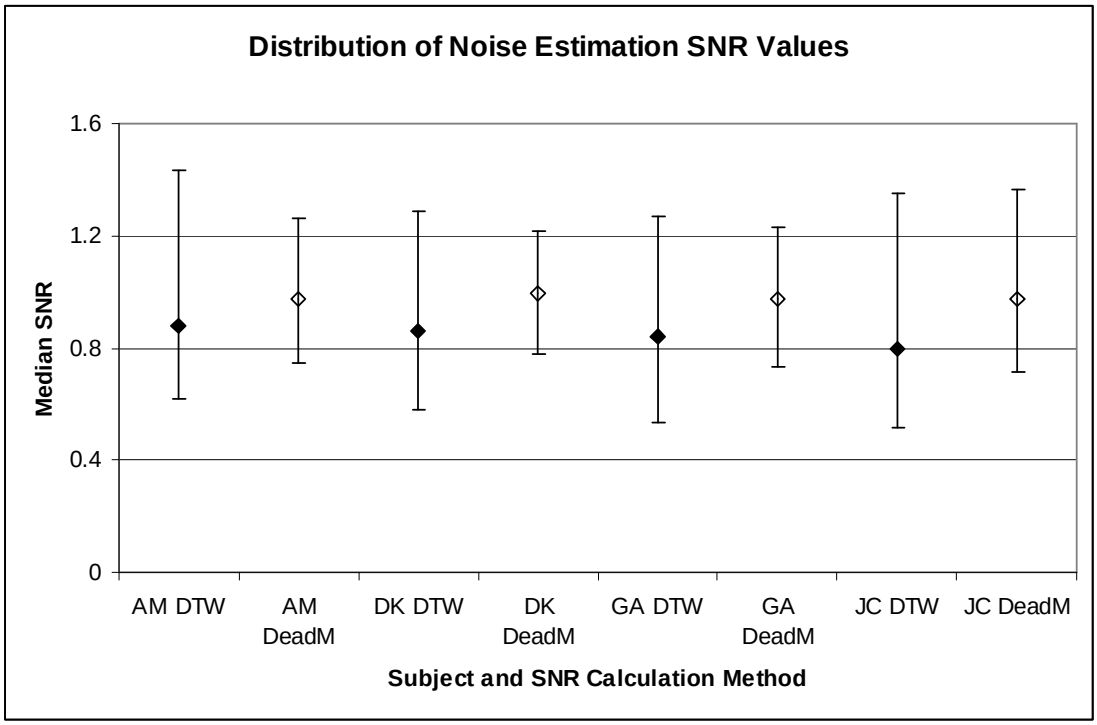

Figure 4.3 *The median SNR values for the two SNR calculation approaches are compared. Filled data points represent SNR values calculated by the Delayed Time Window Method. Unfilled data points represent the DeadM method. Error bars indicate the 10^{th} and 90^{th} percentiles of the distributions.*

4.2.3.4 Discrimination Between Signal and Noise – DTW vs DeadM

Figure 4.4 shows the distribution of SNR for the 60 waveforms and the 68 noise estimations. Data from four volunteers and four recording channels is presented.

The peaks of both the signal and noise estimation DeadM-SNR values appear at a higher numerical value than the corresponding DTW-SNR values. It is not clear from this plot whether either approach can improve on the separation of signal and noise.

An ROC plot was therefore created from the same data and is shown in Figure 4.5. ROC curves for the DeadM-SNR and DTW-SNR values. True positives were defined as the number of active m-sequence waveforms that reached a cut-off SNR value. False positives were defined as the number of inactive m-sequence waveforms that reached the same cut-off.

The area under the DeadM (solid) curve is greater than the area under the DTW (dotted) curve. This demonstrates an improvement in the separation of the signal and noise SNR values when calculated using the DeadM approach.

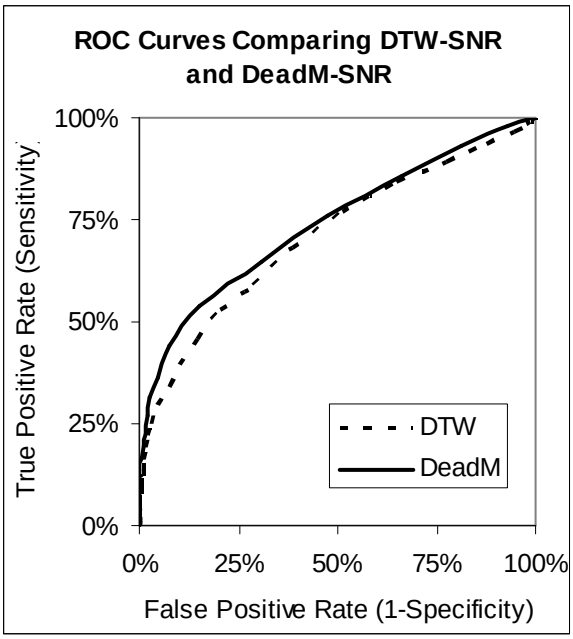

Figure 4.5 *ROC curves for the DeadM-SNR and DTW-SNR values. True positives were defined as the number of waveforms within the trace array that reached a cut-off SNR value. False positives were defined as the number of noise estimations that reached the same cut-off.*

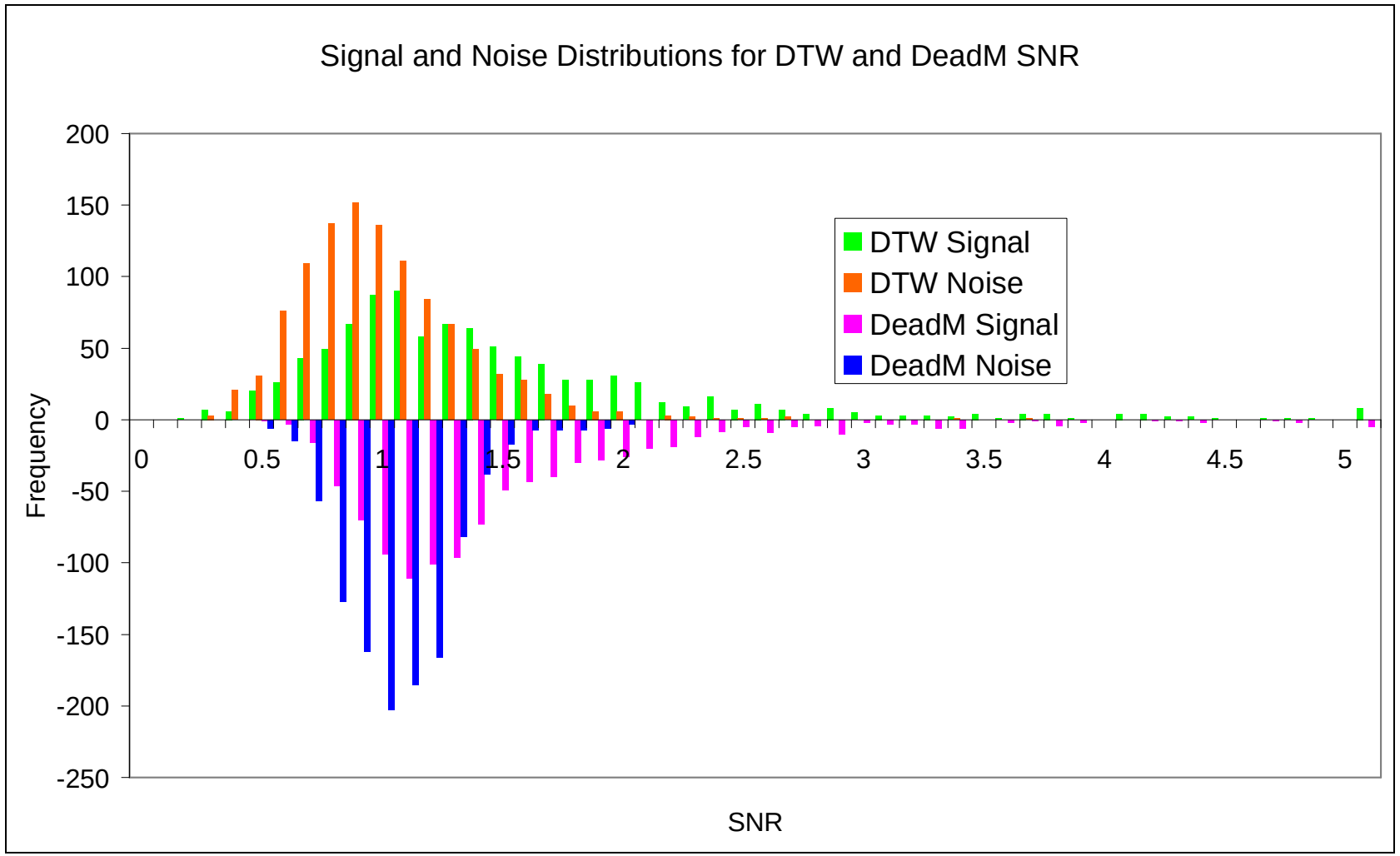

Figure 4.4 *Distribution of SNR for signals and noise estimations using the DTW-SNR and DeadM-SNR calculation methods. Values for the DeadM-SNR distributions have been multiplied by -1 in order to present them below the x-axis, for clarity.*

4.2.4 Discussion

The DeadM SNR calculation method does not return exactly the same value as the DTW method. This is unsurprising given the different approaches to characterising noise. There is however, a good correlation.

Visual inspection of the plots of Dead-M SNR vs. DTW-SNR indicates a positive linear relationship between the two parameters. This is to be expected since they are both descriptors of the same waveforms. There is a significant spread of data points which is reflected in the Pearson correlation coefficients.

There does not appear to be a significant systematic difference in the numerical value of the SNR.

The approach of cross-correlating the raw signal with unused m-sequences allows the creation of truly absent waveforms, which permits receiver operating characteristic (ROC) analysis to be performed. ROC analysis is a powerful tool in assessing differences in multifocal electrophysiology test performance under different acquisition or data processing conditions.

The DeadM-SNR approach shows an advantage in distinguishing known signals from noise, over the DTW-SNR calculation. This translates into an improvement in the performance of the mfVECP test when the DeadM-SNR approach is used to quantify signal quality.

4.2.5 Conclusion

The EDIU Multifocal System has successfully been adapted to allow 128 cross-correlations of data to be performed and permit calculation of the Dead-M SNR values. This has no detrimental effect on the original cross-correlation process.

The DeadM SNR value correlates well with the DTW SNR value but has advantageous characteristics that make it particularly useful when applied to mfVECP data.

4.3 Quantifying Signal Quality in Robust mfERG Signals Using the Dead-M SNR

4.3.1 Aim

Having shown the advantages of the Dead-M SNR metric in mfVECP data, the aim of this section is to demonstrate it utility with robust multifocal signals. In order to do this, an investigation of the impact of electrode choice on the signal quality of the mfERG is presented.

4.3.2 Introduction

Several different types of ERG electrode are used in clinical electrophysiology including the contact lens electrode, gold foil, DTL fibre and skin electrodes. Every electrode has its own inherent impedance and recording characteristics with unique associated artefacts.

There is no universally accepted ocular electrode for general use in ERG recordings and there are many to choose from (131;132). Consideration of ease of placement, subject comfort, electrode stability, the need for optical clarity and acceptable signal to noise ratio (SNR) should be made when selecting electrodes.

The following analysis tests whether robust mfERG signals recorded with Gold foil or DTL electrodes provide superior SNR responses.

4.3.3 Methods

mfERGs were recorded from 11 healthy volunteers using DTL and gold foil electrodes.

Testing was performed using the EDIU Multifocal System. The stimulus was the standard 61-region hexagonal pattern scaled for photoreceptor density, on a background with luminance equal to the mean luminance of the black and white hexagons. The stimulus was controlled by a 15-bit m-sequence, presented at a frame rate of 75 Hz, back-projected on to an LCD screen and presented to 90° diameter of the visual field. The luminance of white areas varied from 903cdm^{-2} to 1297cdm^{-2} and

that of black regions varied from 12cdm^{-2} to 309cdm^{-2}. Contrast varied from 98% peripherally to 48% centrally.

Subjects had a DTL electrode in the left eye and a gold foil electrode in the right. Skin electrodes placed at the temporal orbital rim were used as reference electrodes and a third skin electrode placed on the forehead served as a ground electrode. Skin was prepared with abrasive gel prior to affixing the skin electrodes and impedances were less than 5kΩ. Recordings from both eyes were made simultaneously.

Data was sampled at 1200Hz and filtered through two bandwidths 3-100Hz and 10-100Hz according to local protocol. Data acquired with a 10-100Hz bandpass filter was analysed.

Tropicamide (1%) was given 20 minutes prior to testing to dilate the pupils and subjects were allowed short breaks between 30-second segments of stimulation. Recording took approximately 8 minutes.

This data was acquired to provide control data for a study of retinal toxicity (133) involving serial mfERG recordings. There are therefore three repetitions of the above recordings.

SNR calculations were performed using the DeadM approach to noise characterisation, as described previously in this chapter. The signal window was taken to be the first 100ms of the waveform.

The separation of the values of SNR for signal responses and noise estimations is assessed. Since the mfERG used 61 stimulus regions there were 67 unused m-sequences and therefore 67 estimations of noise, per recording channel.

4.3.4 Results

4.3.4.1 Distribution of Signal SNR Values

A frequency histogram of the SNR values of signal responses is shown in Figure 4.6. Each dataset contains data from 61 waveforms acquired from 11 normal volunteers (giving 671 SNR values per electrode). The histogram is normalised.

Inspection of the histogram shows significant overlap of the distributions. Neither is normally distributed. There are, however subtle differences. The peak of the gold foil distribution appears at a higher SNR, but falls off more steeply with increasing SNR, than the DTL. The DTL distribution shows a larger number of high SNR outliers.

A Wilcoxon signed rank test was used to identify whether the median values ($median_{gold\ foil}$ = 3.10, $median_{DTL}$ = 2.80) of the distributions were the same. It indicated a significant difference, returning a p-value of <0.001.

This test was repeated on the other two repetitions of this data acquisition, with the same result.

4.3.4.2 Distribution of Noise SNR Values

For both electrodes, the noise SNR values have a mean of 1 (as required by the DeadM SNR measurement technique). The standard deviation of the noise SNR values is 0.271 and 0.269 for the gold foil and DTL electrodes, respectively.

A frequency histogram of the noise estimation SNR values is shown in Figure 4.7. Each dataset contains data from 67 unused m-sequences from 11 healthy volunteers giving 737 SNR values per electrode. Once again, the histogram is normalised.

Inspection of the histograms suggests that the distribution of values is not normal in either case.

A Wilcoxon signed rank test was therefore performed. In concordance with the appearance of the histogram, it indicated no significant difference between the median values of noise SNR.

This test was repeated on the other two repetitions of this data acquisition, with the same result.

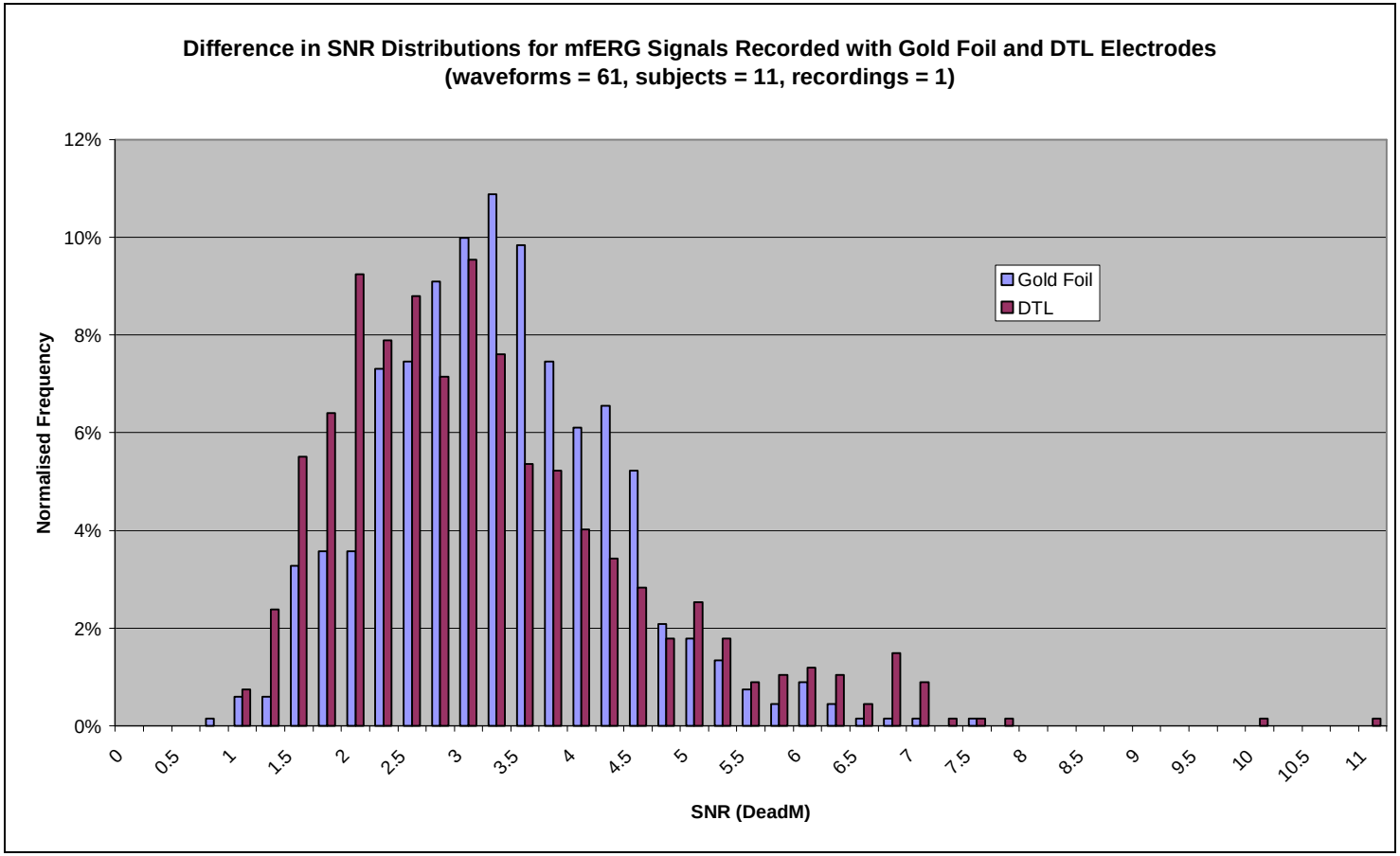

Figure 4.6 *Normalised histogram showing the distribution of SNR values for mfERG waveforms acquired using gold foil and DTL electrodes. SNR values were calculated using the DeadM method. The red series represents data acquired with a DTL electrode and the violet series represents gold foil electrode data.*

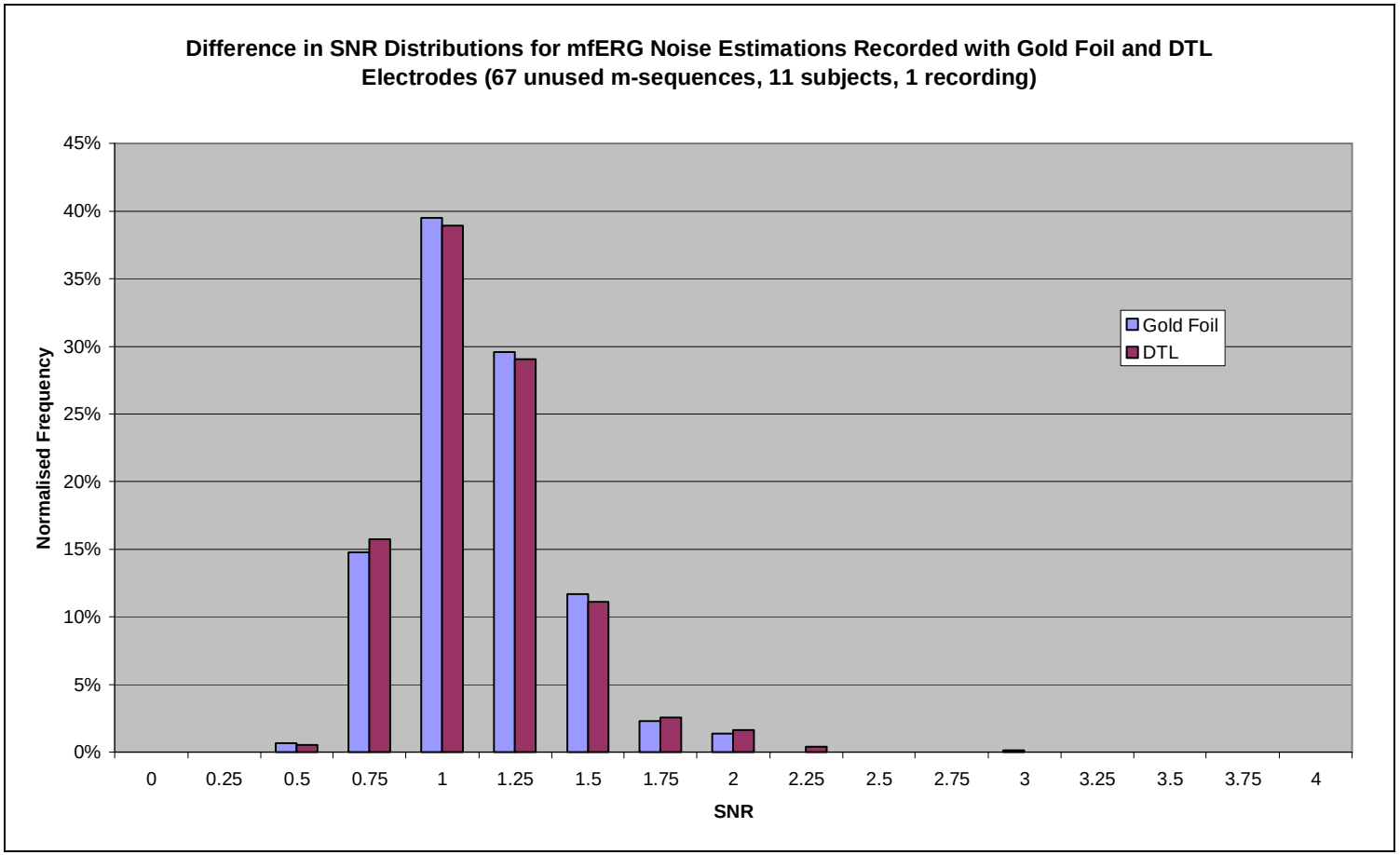

Figure 4.7 *Normalised histogram showing the distribution of SNR values for noise estimations acquired using gold foil and DTL electrodes. SNR values were calculated using the DeadM method. The red series represents data acquired with a DTL electrode and the violet series represents gold foil electrode data.*

4.3.4.3 Separation of Signal and Noise

Figure 4.8 (next page) summarises the data shown in the preceding two figures. Frequency data from the DTL electrode has been multiplied by -1 so that is plotted below the x-axis, for clarity. This gives the impression of improved separation of the noise and signal SNR values when the gold foil electrode is used.

That impression is confirmed by the ROC curve (Figure 4.9), which shows a greater area under the Gold Foil ROC curve (dotted line) than the DTL (solid line).

The true positive rate is defined as the percentage of waveforms in the mfERG trace array that exceed a given SNR. The false positive rate is defined as the percentage of noise estimations that also exceed the same SNR value.

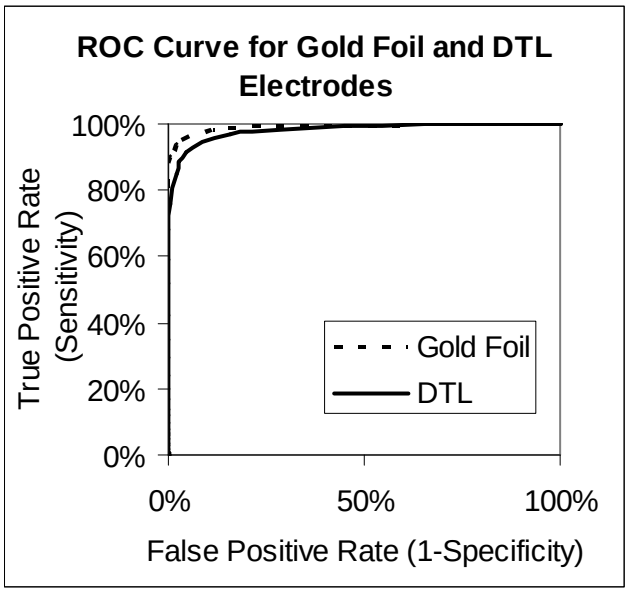

Figure 4.9 *ROC curves for Gold Foil and DTL electrodes.*

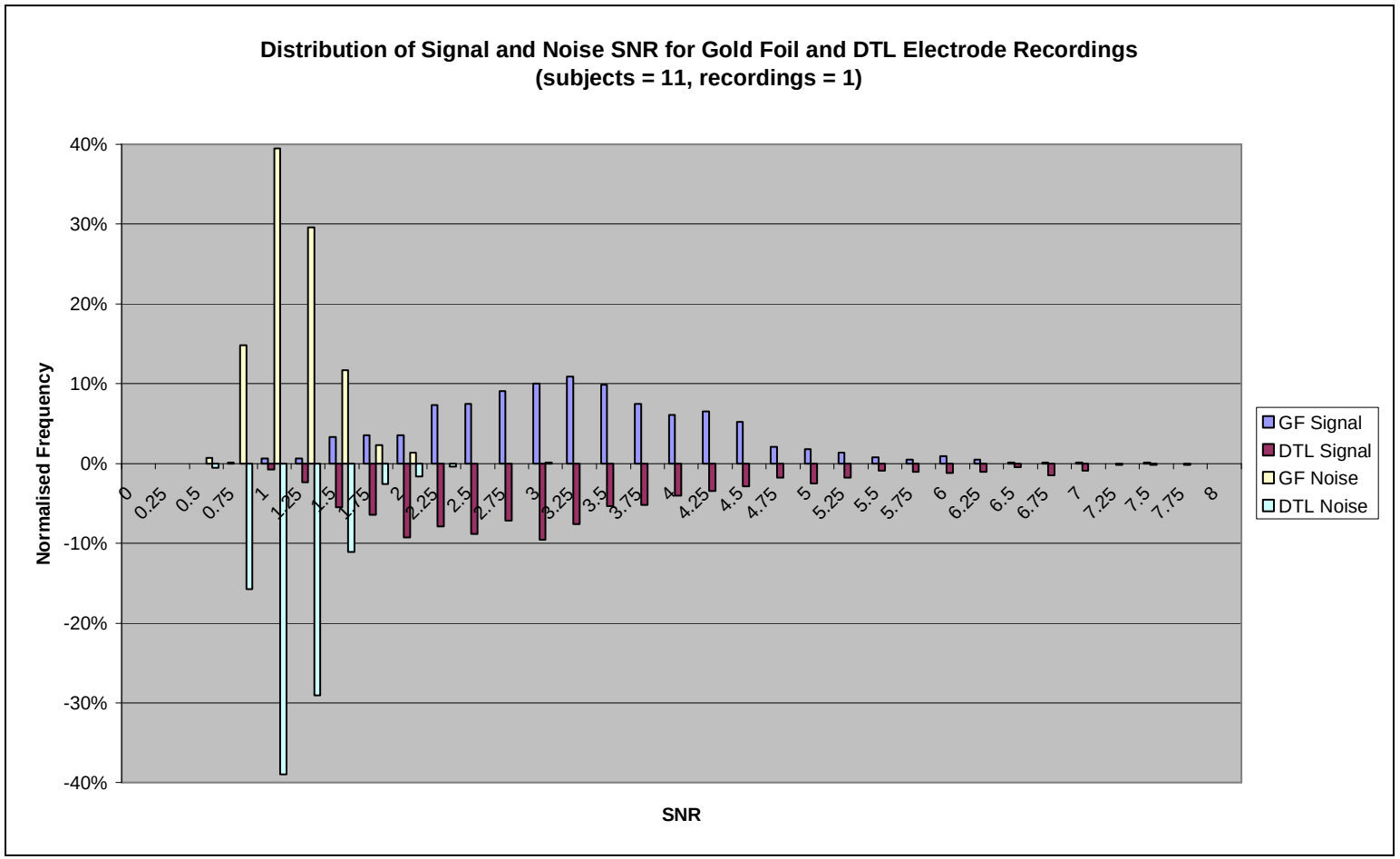

Figure 4.8 *Data plotted in Figures 4.6 and 4.7 is presented simultaneously to illustrate the separation of signal and noise SNR values. DTL Frequency data has been multiplied by -1 in order to display it beneath the x-axis, for clarity.*

4.3.5 Discussion

Gold foil and DTL electrodes are both routinely used in clinical mfERG recordings. By using a gold foil in one eye and a DTL electrode in the other during binocular acquisition of mfERG data from healthy volunteers, inter-subject variability and environmental variables were standardised to as great a degree as possible.

The results presented here indicate a small improvement in performance when gold foil electrodes are used. On a routine clinical basis, this advantage may well be over-shadowed by the increased patient comfort provided by DTL electrodes. However, in cases where signals are particularly small or the physiological record is especially noisy, gold foil electrodes may assist.

4.3.6 Conclusion

The Dead-M SNR has proved to be a useful parameter in distinguishing signal quality between two sets of robust mfERG data.

4.4 Assessing SNR in the mfVECP with Increasing m-sequence Length using the Dead-M SNR parameter.

4.4.1 Aim

To demonstrate the value of the Dead-M SNR parameter in assessing small mfVECP signals and to quantify the improvement in signal quality as the stimulating m-sequence length increases.

4.4.2 Introduction

The m-sequences that are chosen to run the multifocal stimuli are especially selected to ensure that the period of orthogonality is sufficiently long to prevent cross-contamination of the responses with (a) responses to other stimulus regions or (b) from higher-order responses(88;92).

As m-sequence length increases, the proportion of sequences which are orthogonal for a given time period increases (88).

Increasing the m-sequence length has the advantage of improving the SNR of the recorded data by virtue of increasing the number of data averages. This is accompanied by an increase in the testing time making the test more arduous for the patient and increasing the likelihood of loss of fixation and fatigue. Each increment in m-sequence doubles the testing duration, for a fixed stimulus presentation rate. Doubling the sampling should theoretically increase the signal to noise ratio by a factor of $\sqrt{2}$.

4.4.3 Methods

mfVECP responses were recorded from four normal, healthy volunteers using the EDIU Multifocal System. Subjects were optimally refracted using their own spectacles and their pupils were not dilated. Recordings were monocular. Stimulation was provided by a 60-region dartboard pattern. Each region contained a 4x4 black and white checkerboard pattern and the size of the regions was scaled for cortical magnification. The stimulus was presented on a cathode ray tube (CRT) monitor and

subtended a 20.5° of radius of the visual field. The luminance of white areas varied across the screen from 735 cdm^{-2} to 960 cdm^{-2} and black areas varied from 6 cdm^{-2} to 162 cdm^{-2}. Contrast varied from 99% peripherally to 64% at the centre of the screen.

m=12, 13, 14, 15 and 16 bit m-sequences were used to drive the pattern reversal of the stimulus regions at a rate of 75Hz. Acquisition time was approximately 1,2,4,8 and 16 minutes, depending on the m-sequence length. This was divided into 30 second overlapping periods to allow the subject to blink and rest, in order to maintain good fixation.

Ag/AgCl electrodes were placed 4cm above the inion, 4cm left and right of the inion and 1cm below the inion on the midline. Acquired channels were Channel 0 = 4cm above the inion – 1cm below the inion, Channel 1 = 4cm left of the inion – 1cm below the inion, Channel 2 = 4cm right of the inion – 1cm below the inion and Channel 3 = 4cm left of the inion – 4cm right of the inion, similar to the montage employed by Hood *et al* (19). A reference electrode was placed at International 10-20 position F_Z and a ground electrode was placed on the temple. Electrode impedances were matched and below 5kΩ. The skin was prepared with abrasive gel and the electrodes affixed with conductive paste.

Signals were sampled at 1200Hz and filtered through a 3-30Hz digital bandpass after cross-correlation.

SNR values were calculated for each waveform using the DeadM approach to noise characterisation, using a time window of 45 to 150ms.

Data from Channel 0 has been analysed. Datasets were checked for normality using the Anderson-Darling Normality test. The majority of datasets were not normally distributed at the p=0.05 level and so non-parametric statistics were used.

Confidence intervals for median SNR values were calculated using a method described by Bland (134). Data was sorted and the upper and lower confidence limits were defined as the j^{th} and k^{th} sample, where

$$j = nq - 1.96\sqrt{nq(1-q)} \qquad \textbf{Equation 4.11(a)}$$

and

$$k = nq + 1.96\sqrt{nq(1-q)} \qquad \textbf{Equation 4.11(b)}$$

Where n= the number of samples and q = the quartile (0.5 for the median).

The median SNR of the 60 waveforms in the trace array was compared with the theoretical increase of √2. 95% confidence intervals of the median values were calculated as described in section 3.6.4 and Equations 4.11(a) and (b).

The theoretical gain in SNR was calculated for each dataset. The median SNR for the mid m-sequence length of m=14 was used as a reference.

4.4.4 Results

A plot of the mfVECP trace arrays from Channel 0 can be seen for one subject, JC in Figure 4.10.

Successive increases in signal quality can be seen as the m-sequence length increases.

It can however be seen that the underlying waveforms are very reproducible in repeated recordings within a session, in terms of waveshape, amplitude and latency. This was apparent in recordings from all subjects from all recording channels.

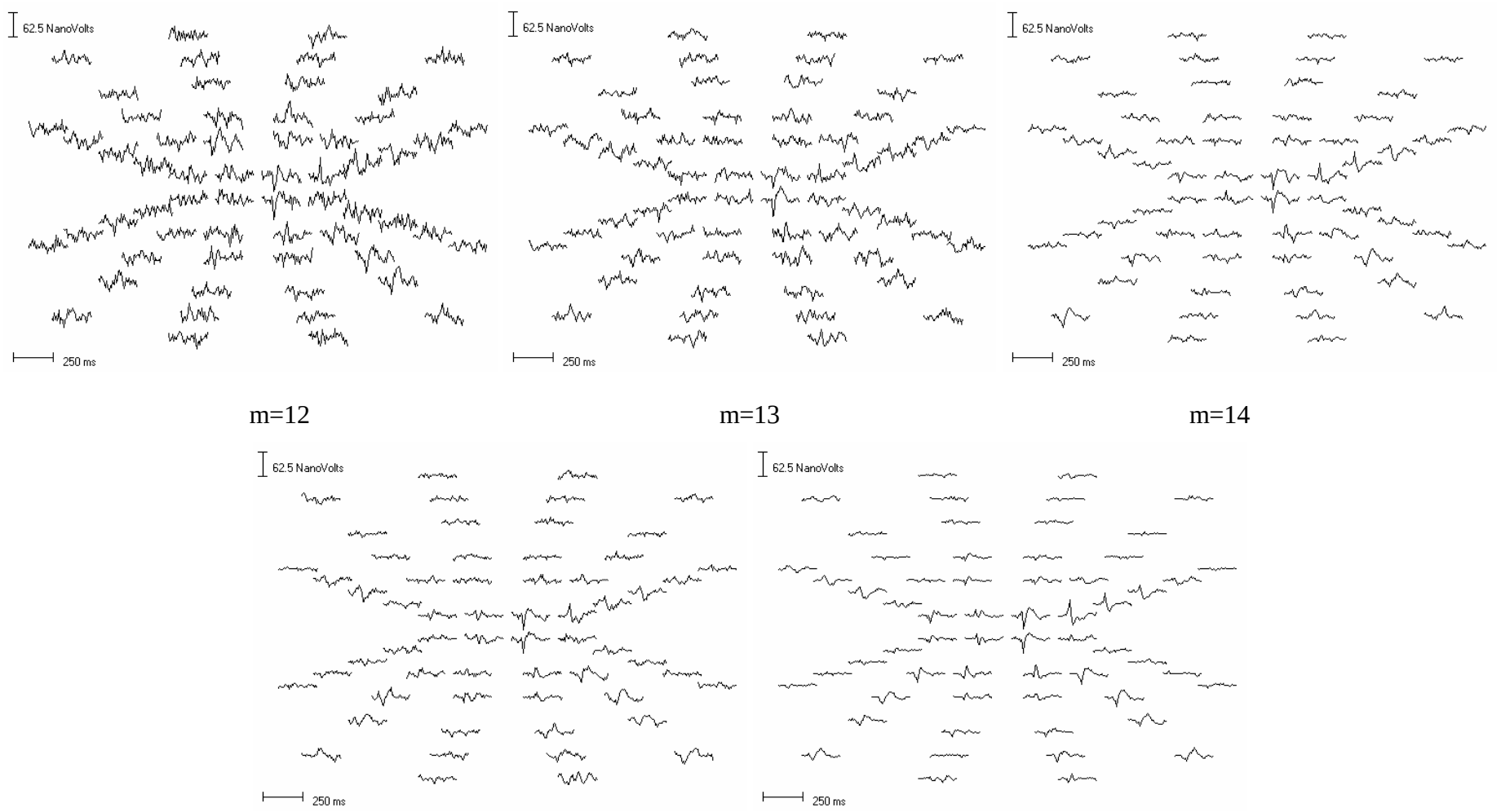

Figure 4.10 *mfVECPs from a single subject recorded with increasing m-sequence length.*

Figure 4.11 shows the improvement in signal quality in a central waveform from the right, lower quadrant as seen on the trace array. This example demonstrates both a decrease in noise and an increase in the amplitude of the trough at 100ms.

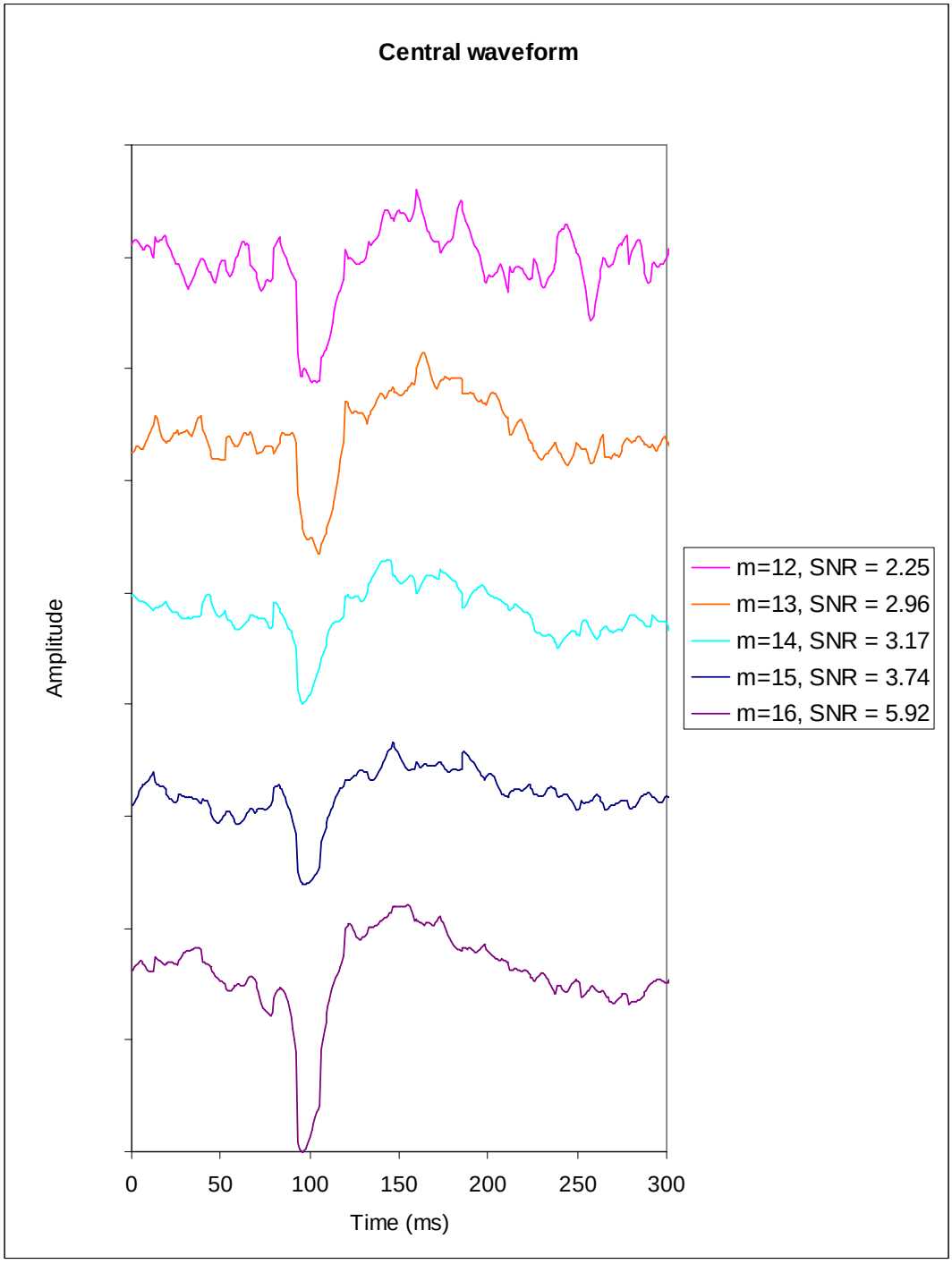

Figure 4.11 *Central waveform from the lower right quadrant of the trace arrays shown in Figure 4.13.*

Figure 4.12 shows the increase in SNR with m-sequence for each of the four healthy volunteers. Solid data points indicate observed measurements. Unfilled data points reflect the theoretical maximum in SNR improvement of a factor of √2 with each increment of m-sequence, normalised to the median SNR value achieved with an m=14 bit m-sequence. For every subject, we see an increase in the median SNR for each increment of m-sequence.

The increases in SNR fall short of a factor of √2 for each increment, although, in general they follow the trend of the predicted pattern reasonably well.

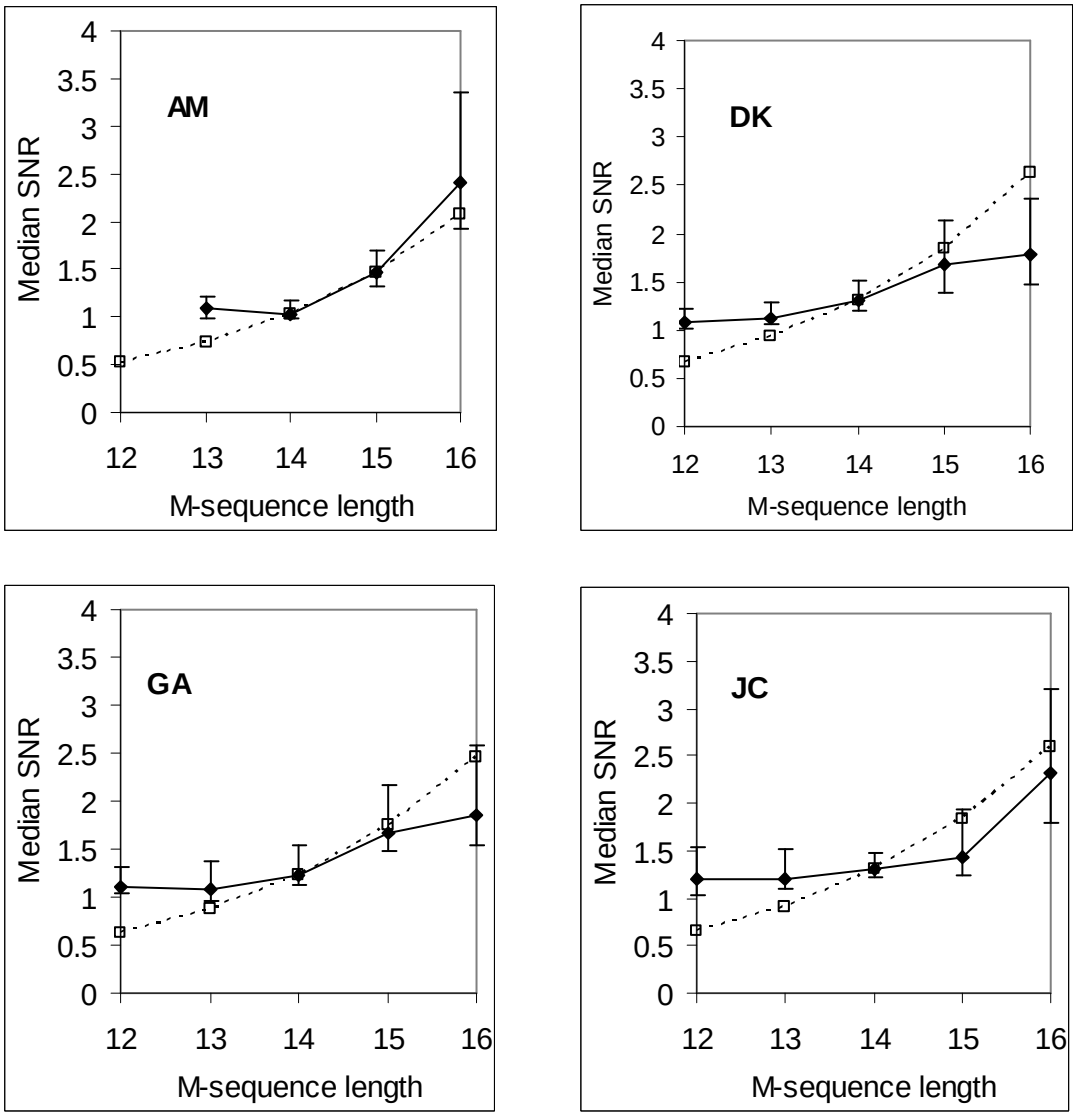

Figure 4.12 *Plot of observed (solid lines) and theoretical (dotted lines) median SNR against m-sequence length for mfVECP records. The four plots contain data from the four healthy volunteers. Error bars on the observed data indicate the 95% confidence interval of the median.*

4.4.5 Discussion

The gain of √2 in SNR is a theoretical maximum and does not account for loss of signal quality due to small losses of fixation due to subject fatigue. Fatigue could reasonably be expected to increase with the duration of recording.

It is possible that a low frequency adaptation process occurs which reduces signal quality as recording proceeds. This could be tested by performing mfVECPs of the same m-sequence length back to back and comparing the SNRs.

Less than an increase in √2 should be expected with mfVECP data since there will not necessarily be a waveform in each of the 60 locations.

With records from a single channel, it is not uncommon that stimulation with some regions of the dartboard does not result in a discernable waveform. Where this is due to cancellation of the signal, or due to a dipole orientation within the visual cortex which cannot be detected with surface electrodes, increasing the sampling time will not increase the SNR. An increase in the average SNR of less than √2 is therefore to be expected.

The signals in mfVECP recordings are significantly smaller than those seen in mfERG records. Coupled with the additional challenges of the variability in waveform appearance seen between normal subjects, all advantages in signal detection should be carefully considered. It is therefore likely that increasing the m-sequence from the clinical standard for m=15 for mfERG acquisition, to m=16 for mfVECP records will be clinically significant and allow a more robust determination of whether results are normal or abnormal.

4.4.6 Conclusion

The Dead-M SNR metric has been put to good use in assessing the improvement in mfVECP signal quality as m-sequence length increases. Deviations from a theoretical increase of √2 in SNR can be explained and are not a reflection on the performance of the Dead-M SNR metric.

4.5 Quantifying Multifocal Signal Quality - Conclusion

A novel method of calculating the signal to noise ratio in multifocal electrophysiology recordings has been presented which employs orthogonal m-sequences that are not used to control regions of the stimulus.

Software has been written to perform the necessary calculations accurately. The approach has been compared to one of the most widely used methods of mfVECP SNR calculation (Delayed Time Window, DTW) and found to give comparable results.

The cross-correlation of raw data with unused m-sequences produces waveforms known to contain no signal response. These are noise estimations which can be used as truly absent waveform responses and open up the possibility of receiver operating characteristic (ROC) curve analysis to compare the performance of a multifocal test under different conditions.

When the DeadM-SNR value is calculated for noise estimations, a tighter distribution of values is seen, compared to those produced using the DTW approach. This created a small improvement in the ability to distinguish between noise and signal. mfVECP test performance can therefore be improved, albeit slightly, by the use of the DeadM SNR value calculation method.

The Dead-M SNR parameter was shown to be useful with both robust mfERG signals and smaller, noisier mfVECP responses.

When applied to mfERG data it illustrated a small, statistically significant improvement in signal quality when data are acquired using gold foil electrodes compared to DTL electrodes.

Recording mfVECP responses from the same individuals with differing m-sequence lengths resulted in waveforms with different noise contributions, however the underlying waveforms were similar, indicating good reproducibility.

Improvements in signal quality of mfVECP data with increasing m-sequence length were investigated using the new SNR metric. SNR increased with each increment of the m-sequence, but failed to reach the maximum theoretical improvement. Given the size and complexity of mfVECP responses, the m=16 m-sequence is recommended for future clinical acquisition in order to make the test as robust as possible.

mfVECP responses remain small and their detection is hindered by the superposition of noise from a number of sources. Filtering the data has the potential to improve signal quality. The Dead-M SNR value is a robust and useful parameter which will be used to quantify enhancements brought about by filtering in the following chapter.

Chapter 5

Filtering Bandwidth

Contents

Page

5.0 Introduction…… 108

5.1 The Purpose of Filtering……. …… 108

5.2 Simple Hardware Filters ……. 109

5.3 Hardware vs. Software Filtering ……. 110

5.3.1 DSDP Filtering Options …… 111

5.3.2 EDIU Multifocal System software (Multifocal Imager 3) – Filtering Options …… 111

5.4 Current Standards for the Standard Visual Evoked Potential. ……. 112

5.5 Variation in Current mfVECP Recordings ……. 112

5.6 A Two-Stage Experiment ……... 114

5.7 Stage One …… 115

5.7.1 Aim …… 115

5.7.2 Methods – Filters ……... 115

5.7.3 Methods – Data ……. 115

5.7.4 Methods – Analysis ……... 116

5.7.5 Results ……... 118

5.7.5.1 Frequency Content of Raw and Filtered Data ……. 118

5.7.5.2 Filtered Waveform Arrays …….. 118

5.7.5.3 The Effect of Filtering on Individual Waveforms …….. 121

5.7.5.4 The Effect of Filtering on the Signal to Noise Ratio…… 122

5.7.5.5 ROC Analysis ……. 122

5.7.6 Stage One – Conclusion and Discussion ……... 123

Page

5.8 Stage Two ……... 127

5.8.1 Aim …… 127

5.8.2 Methods ……. 127

5.8.3 Results ……... 128

5.8.3.1 Filtered Waveform Arrays …….. 128

5.8.3.2 The Effect of Filtering on Individual Waveforms …….. 133

5.8.3.3 The Effect of Filtering on the Signal to Noise Ratio…… 136

5.8.3.4 ROC Analysis ……. 139

5.8.3.5 Stage Two –Conclusion & Discussion … 141

5.9 Comparison of Stage One and Stage Two Results ……. 144

5.10 Wavelet Filtering and Smart Filters …… 148

5.11 Conclusions and Discussion ……... 152

5.0 Introduction

Filters serve to exclude from the electrophysiological record those potential changes that have frequencies different from the frequencies represented in the response under study. This chapter systematically investigates a range of filter bandwidths in order to determine which one is the most appropriate for clinically acquired data.

5.1 The Purpose of Filtering

In an ideal world, recording electrodes would record cortical activity related to visual stimulation and nothing else. In reality, the recorded signal contains additional contributions from a number of sources. Some of these are environmental, such as noise due to the mains electrical supply or electromagnetic interference from CRT monitors, while others are physiological arising from muscle spasms or cortical EEG activity which is unrelated to the response of interest. Noise from all of these sources obscures the signal of interest. When the frequency spectra of the unwanted components differs from the VECP, it is possible to remove them using filtering.

High frequency artefacts in the form of background noise and/or muscle spasm are removed by a low pass filter.

Low frequency artefacts such as baseline drift can distort the recorded signal, particularly if they are continuous throughout the duration of a mfVECP recording. The high pass filter is used to eliminate this. The disadvantage is that the low frequency components of the physiological response may also be compromised.

Occasionally, a notch filter is used to remove the effect of mains noise. This is a filter at 50Hz in the UK, and 60Hz in the USA. The use of a notch filter is not recommended in the Standard VECP Guidelines (27).

There are cases where the noise source contains frequency components that are also in the mfVECP. To remove the noise completely would result in the removal of some of the mfVECP signal and could reduce its amplitude and/or distort the waveform of the recovered response.

It has been shown throughout this thesis that the SNR of mfVECP records is low. All assistance in removing unwanted components will therefore help us reach the goal of detecting as many real signals within the trace array as possible, and give us confidence in describing absent waveforms as exactly that.

5.2 Simple Hardware Filters

A simple, passive high or low-pass analogue filters consists of a single resistor capacitor (RC) network as illustrated in Figure 5.1.

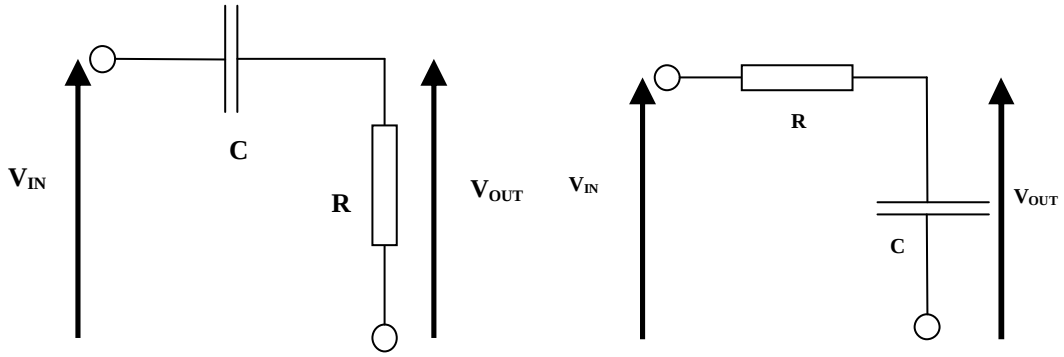

Figure 5.1 *High and low-pass filtering circuits are shown on the left and right, respectively.*

A bandpass can be constructed by cascading a high and low-pass filter.

Cascaded RC circuits can produce a steep falloff of the frequency response above or below the low or high pass settings, but the 'knee' of the curve of response versus frequency is not sharpened.

Sharper knees can be achieved with filters containing inductors, however inductors are often bulky, expensive and inefficient (135).

Improved performance is achieved by active filters, which make use of op-amps. Butterworth, Chebychev and Bessel filters are all examples of op-amp filters, designed to have different frequency and phase responses. Differential amplifiers are used to reduce the effect of common mode interference such as that due to mains electricity.

5.3 **Hardware and Software Filtering**

Analogue filters are applied with hardware circuitry, while digital filters are applied post acquisition via software. Digital filters have a number of advantages over their analogue counterparts:-

- Analogue filters distort the time relationship between some of the desired signal components passing through the filter, especially those near the cut-off frequencies.
- Digital filters have better response characteristics.
- In complex multi-stage filtering operations, digital filters have the potential to attain much better signal to noise ratios than analogue filters. At each intermediate stage the analogue filter adds noise to the signal whereas the digital filter performs noiseless mathematical operations.
- A digital filter can easily be changed without affecting circuitry. Analogue filters can only be changed by redesigning the filter circuit.
- The characteristics of analogue filter circuits are subject to drift and are dependent on temperature.
- Digital filters are more versatile in their ability to process signals. Some are capable of adapting to changes in the characteristics of the signal.
- Fast DSP (Digital Signal Processing) processors can handle complex combinations of filters in parallel or cascade (series), making the hardware requirements relatively simple and compact in comparison with the equivalent analogue circuitry.
- Relying on analogue filtering requires that the optimal filter is known prior to data acquisition. Digital filtering allows different filters to be applied after acquisition.

5.3.1 **DSDP Filtering Options**

This chapter uses filters designed using Digital Filter Design Package (DFDP) Version 1.1 (Atlanta Signal processors Inc.). The programme can be used to create the coefficients necessary to implement a recursive infinite impulse response (IIR) filter design, a Kaiser finite impulse response (FIR) filter or a Parks- McClellan Equiripple FIR filter.

FIR filters offer advantages over IIR filters. They have a constant group delay throughout the frequency spectrum and are stable at all frequencies regardless of the size of the filter. The disadvantages of an FIR filter are that the frequency response is not as easily defined as it is with IIR filters and a greater degree of complexity is required to meet a frequency specification than is required for IIR filters.

The Kaiser filter was chosen because the linear phase response will minimise distortion of the mfVECP waveforms.

5.3.2 EDIU Multifocal System software (Multifocal Imager 3) - Filtering Options

Multifocal Imager 3 is a new version of the EDIU Multifocal System software, which allows the user to filter cross-correlated data through three traditional types of filter – Butterworth, Chebychev and Bessel.

The Butterworth is a maximally flat filter with an optimally constant gain in the passband. The sharpness of cut-off is not as good as the Chebychev.

The Chebychev is maximally sharp in the transition from passband to stopband but the passband gain varies and is described as ‘equiripple’.

Bessel filters are neither optimally flat in the passband, nor do they have a sharp transition, but their advantage is a linear phase response. If different frequencies are delayed by different times then the output of the filter will not be a faithful version of the input. This lack of fidelity will be most clearly seen in the response to a step input, where overshoot and ringing may occur after filtering.

Bessel filters were used because they cause little distortion to the waveform.

5.4 **Current Standards for Standard Visual Evoked Potential**

The Visual Evoked Potentials Standard (2004) (27) recommends that "Analogue high and low pass filters should be set at 1Hz or less (corresponding to a time constant of 0.16s or more) and at 100Hz or more, respectively." It also states that "The use of notch or comb line frequency filters is not recommended."

It has been suggested by Hood *et al* (54) that 'the bandpass of the amplifier is not a major factor' , during mfERG acquisitions. However, the effect of filter bandwidth on the mfERG has been investigated by Keating *et al* (97) who observed that increasing the high-pass filter setting beyond 1Hz had little effect on the normal mfERG response, but significantly distorted abnormal signals.

5.5 **Variation in Current mfVECP Recordings**.

Throughout the mfVECP literature, variation exists in the filter bandwidths used. Hood *et al* employ 3-100Hz (33;73;85;128;136). Subsequently, his group has employed an additional low-pass filter with a sharp cut-off at 35Hz using a Fast Fourier Transform technique (14;113). More recent studies from the same group have employed the 3-100Hz bandwidth alone (137). Hood's review of 2003 (19) indicates that the use of their sharp cut-off software filter had relatively little effect on either amplitude or latency.

Klistorner & Graham in 2001 reduced their hardware low pass setting to 30Hz (123). They reported latencies increased by 2-3msec and unaltered amplitudes. In 2005, they reduced it further to 1-20Hz by digital filtering (129), but made no further comment on the effect on the waveforms.

Table 5.1 shows the range of filter bandpasses that have been used in recent publications and indicates where filtering was achieved during acquisition or by digital post-acquisition filtering.

Study	*Recording Filter*	***Post Recording Filter***
Visual evoked potential standards (2004) Odom, J.V. *et al* Documenta Ophthalmologica 2004 (27)	1Hz to 100Hz	-
Electroencephalogram-Based Scaling of Multifocal Visual Evoked Potentials: Effect on Intersubject Amplitude Variability Klistorner & Graham IOVS 2001 (123)	3 to 30Hz	-
The Pattern Pulse Multifocal Visual Evoked Potential James AC IOVS 2003 (17)	0.1 to 100Hz	1 to 45Hz
Multifocal VECP and ganglion cell damage: applications and limitations for the study of glaucoma Hood & Greenstein Prog Ret Eye Res 2003 (19)	Veris settings	3 to 35Hz
Quantifying the benefits of additional channels of multifocal VECP recording Hood *et al* Doc Ophth. 2002 (128)	3-100Hz	-
Effect of pupil size on multifocal pattern visual evoked potentials Martins *et al* Clin Exper Ophth 2003 (138)	1-20Hz	-
The detection of small simulated field defects using multifocal VECPs Chan *et al* Ophthal. Physiol. Opt. 2002 (139)	1-100Hz	-

Table 5.1 *Filter bandpasses used in recent mfVECP publications.*

5.6 A Two-Stage Experiment

Investigation of the optimal filter has been performed as two experiments for pragmatic rather than scientific reasons.

Stage one was performed in the early stages of the presented PhD work. It investigated eight bandwidths resulting from four high- and two low-pass settings. It used a piece of MS-DOS software (Digital Filter Design Package) originally created in 1987, to create filter coefficients. The coefficients were used by a Delphi program to filter the electrophysiological record prior to cross-correlation.

This data was presented at The British Chapter of ISCEV (Briscev) in 2003. Feedback suggested that investigation of a greater number of low-pass settings would make the investigation more useful. This is in keeping with the variation in the low-pass settings reported recently in the literature.

Stage two was performed in 2007. In the intervening time, filtering software has become more readily available and simpler to use. Indeed, locally, Dr Stuart Parks has written a new version of the EDIU Multifocal System software (Multifocal Imager 3) which integrates the ability to filter data with any selected bandpass, interactively. Multifocal Imager 3 filters the waveform array once cross-correlation has been performed.

The original EDIU Multifocal System made use of a VSG card (Cambridge Research Systems, Rochester, UK), production of which has ceased. The System has therefore been revised to remove its independence on the VSG card. During revision, the opportunity has been taken to introduce further utility.

The ease with which Multifocal Imager 3 can be used, coupled with difficulties in re-installing DFDP on a new desktop computer, resulted in the change in filtering software.

5.7 Stage One

5.7.1 Aim

To determine an appropriate bandpass for the post-acquisition filtering of mfVECP data, with the goal of achieving maximising the discrimination between noise and signal responses.

5.7.2 Methods – Filters

Eight post-acquisition filters were created and are listed below.

- 0.1to 30Hz
- 1 to 30Hz
- 3 to 30Hz
- 10 to 30Hz
- 0.1 to 100Hz
- 1 to 100Hz
- 3 to 100Hz
- 10 to 100Hz

Digital Filter Design Package (DFDP) Version 1.1 (Atlanta Signal processors Inc.) was used to calculate the coefficients necessary for filtering. A Kaiser Window Non Recursive (FIR) Filter Design was employed.

The coefficients were applied to raw data, prior to cross-correlation, in a filtering program that was written by Dr Aled Evans, in Delphi 4.0 (Borland, USA).

5.7.3 Methods – Data

A subset of the data that was acquired during an investigation of the optimal field of view of stimulus presentation (described in Chapter 6) was used to investigate the optimal bandwidth filter.

mfVECP responses were recorded from 9 normal, healthy volunteers with a mean age of 34.5 years (standard deviation 12.4 , range 23-52) using the EDIU Multifocal System. Subjects were optimally refracted using their own spectacles and their pupils were not dilated. Recordings were monocular and made from the right eye.

Stimulation was provided by a 60-region dartboard pattern. Each region contained a 4x4 black and white checkerboard pattern and the size of the regions was scaled for cortical magnification. The stimulus was back-projected onto a screen using an LCD

projector. The stimulus subtended a 20° of radius of the visual field. The luminance of white areas varied across the screen from 735 cdm^{-2} to 960 cdm^{-2} and black areas varied from 6 cdm^{-2} to 162 cdm^{-2}. Contrast varied from 99% peripherally to 64% at the centre of the screen.

An m=15 bit m-sequence was used to drive the pattern reversal of the stimulus regions at a rate of 75Hz. Acquisition time for each recording was approximately eight minutes, divided into 30 second overlapping periods to allow the subject to blink and rest, in order to maintain good fixation.

Data was recorded from midline bipolar channels as follows and incorporates a selection of electrode positions used by Hood *et al* (19) and Klistorner and Graham (16):

Channel 0 = 10% above the inion – 30% above the nasion, Fz.

Channel 1 = 2cm above the inion – 6cm below the inion,

Channel 2 = 2cm above the inion – 4.5cm below the inion,

Channel 3 = 4cm above the inion – the inion.

Ag/AgCl electrodes were used and impedances were matched and below 5kΩ. The skin was prepared with abrasive gel and the electrodes affixed with conductive paste. A reference electrode was placed at International 10-20 position F_Z and a ground electrode was placed on the temple.

Signals were sampled at 1200Hz recorded with a 0.1 to 100Hz analogue filter and filtered through a 3-30Hz digital bandpass prior to cross-correlation.

5.7.4 Methods - Analysis

A Fast Fourier Transform (FFT) of the raw data before and after filtering was calculated to allow inspection of the effect of filtering on the frequency spectra.

After filtering, data was cross-correlated to produce waveform arrays.

Signal to noise ratios were calculated as described in Chapter 4. A window of 45-250ms was used to calculate SNR. This is different from the 45-150ms time window used in the previous chapter and is based on an observation and subsequent analysis presented in Chapter 7.

The distribution of the SNR values was tested for normality using the Anderson Darling Test for Normality.

Median SNR values of data passed through each of the bandpasses are compared. A Wilcoxon Signed Rank Sum was used to test the null hypothesis that data filtered with a lowpass setting of 30Hz results in SNR values with the same distribution as that filtered with a lowpass of 100Hz.

Confidence intervals for median SNR values were calculated using a method described by Bland (134) and Equations 4.11(a) and (b).

Use was made of statistical software packages SPSS 15.0 for Windows and Minitab 13.0

Receiver Operating Characteristic (ROC) curves were plotted for each bandpass. In order to provide specificity data for ROC curves, cross-correlations of the raw data with orthogonal, but unused m-sequences were used to create waveforms that could not contain any physiological data and could therefore be considered to be True Negatives. SNR values were calculated for these waveforms in the same way as SNR calculations are performed for waveforms within the trace array which contain physiological data. The percentage of noise estimations that exceed a given SNR value was taken as the False Positive Rate or (1-specificity).

5.7.5 Results

5.7.5.1 Frequency Content of Raw and Filtered Data

Filters coefficients were successfully created and implemented in the filtering software.

FFTs of the raw data and filtered data are shown in Figure 5.2 and demonstrate that the designed filters were performing as intended. The example shown is for data from a single channel, from a single subject, but is representative.

This is the FFT of the raw multifocal file, prior to cross-correlation.

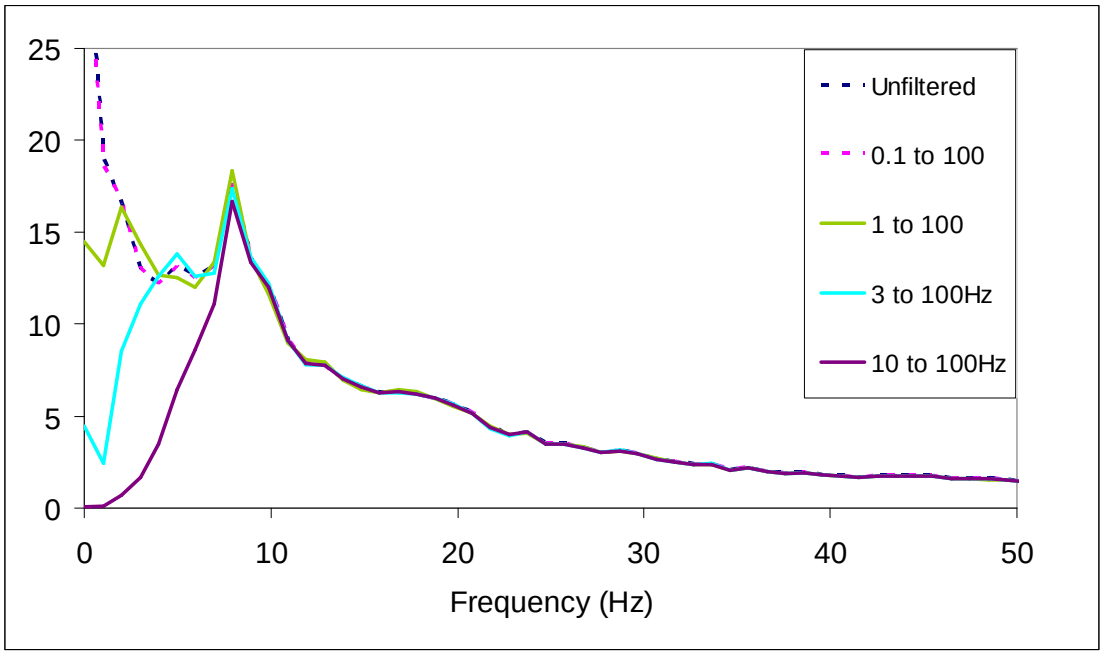

Figure 5.2 *The frequency response of unfiltered and filtered data.*

5.7.5.2 Filtered Waveform Arrays

Figure 5.3 (a&b) shows an example of a waveform array from a single subject that has been passed through each of the eight bandpasses.

0.1 to 100Hz

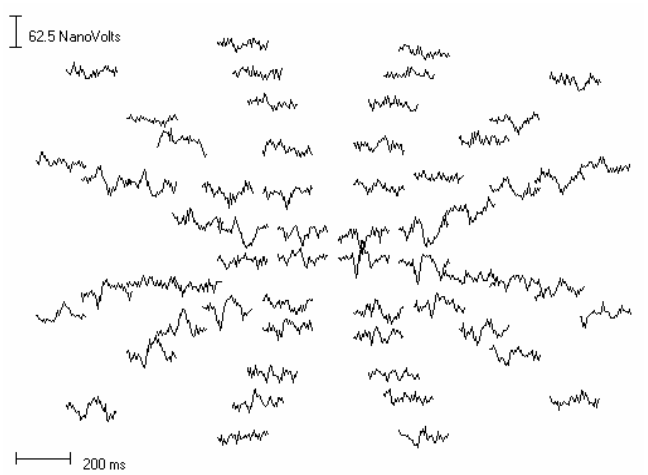

3 to 100Hz

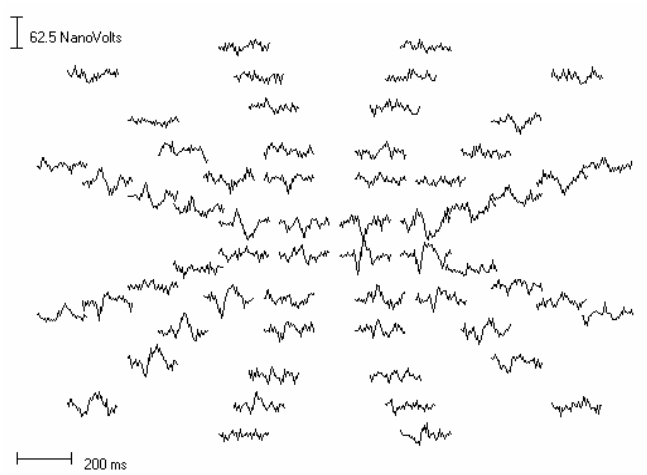

1 to 100Hz

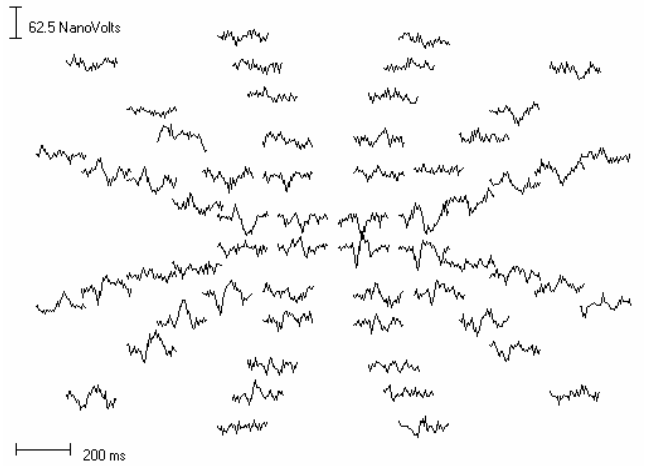

10 to 100Hz

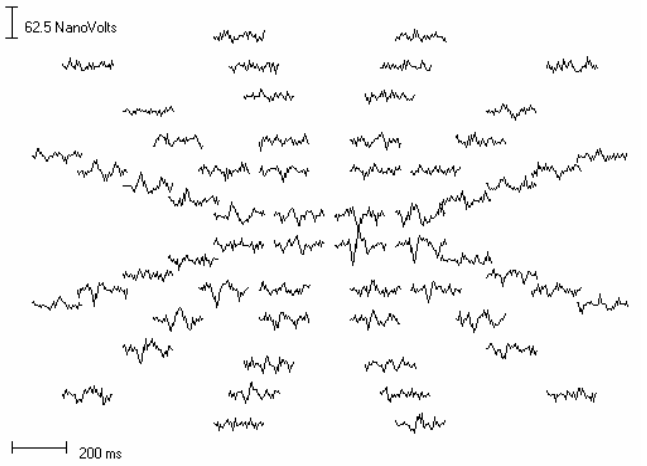

Figure 5.3a *A waveform array, filtered through eight different bandpasses*

0.1 to 30 Hz

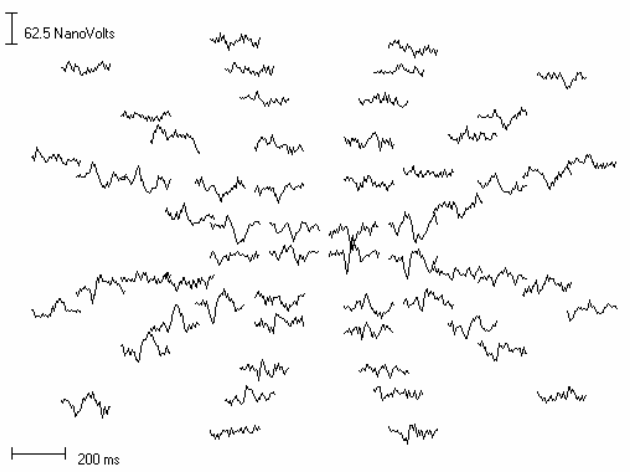

1 to 30Hz

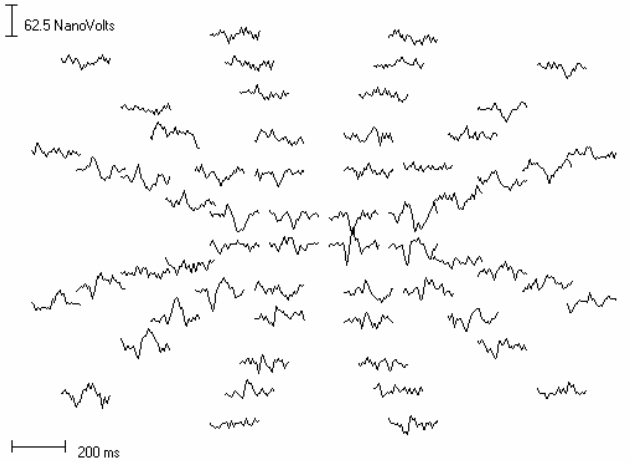

3 to 30Hz

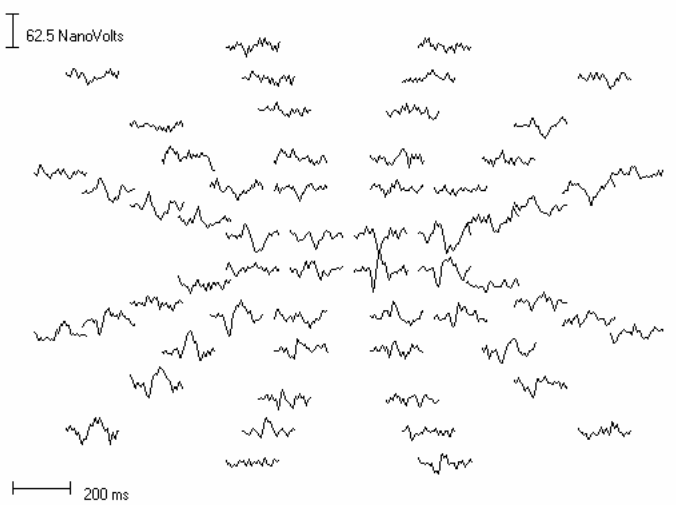

10 to 30Hz

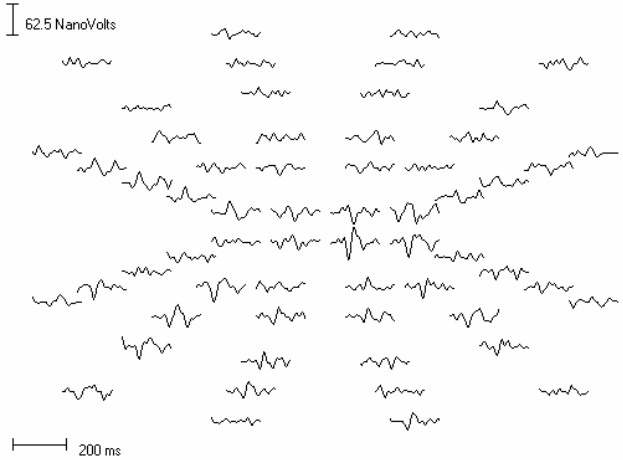

Figure 5.3b *A waveform array, filtered through eight different bandpasses.*

5.7.5.3 The Effect of Filtering on Individual Waveforms

Figure 5.4 shows the effect of each of the bandpasses on a single central waveform. The top trace in each column is the unfiltered data. Waveforms filtered with a 30Hz low pass setting are less noisy than their 100Hz lowpass counterparts. In both columns, the bottom-most trace has a highpass setting of 10Hz. In both cases, we begin to see a degree of distortion of the waveform. While the positive going peak that appears just after 100ms is relatively unaffected, the negative going peak at approximately 170ms is diminished.

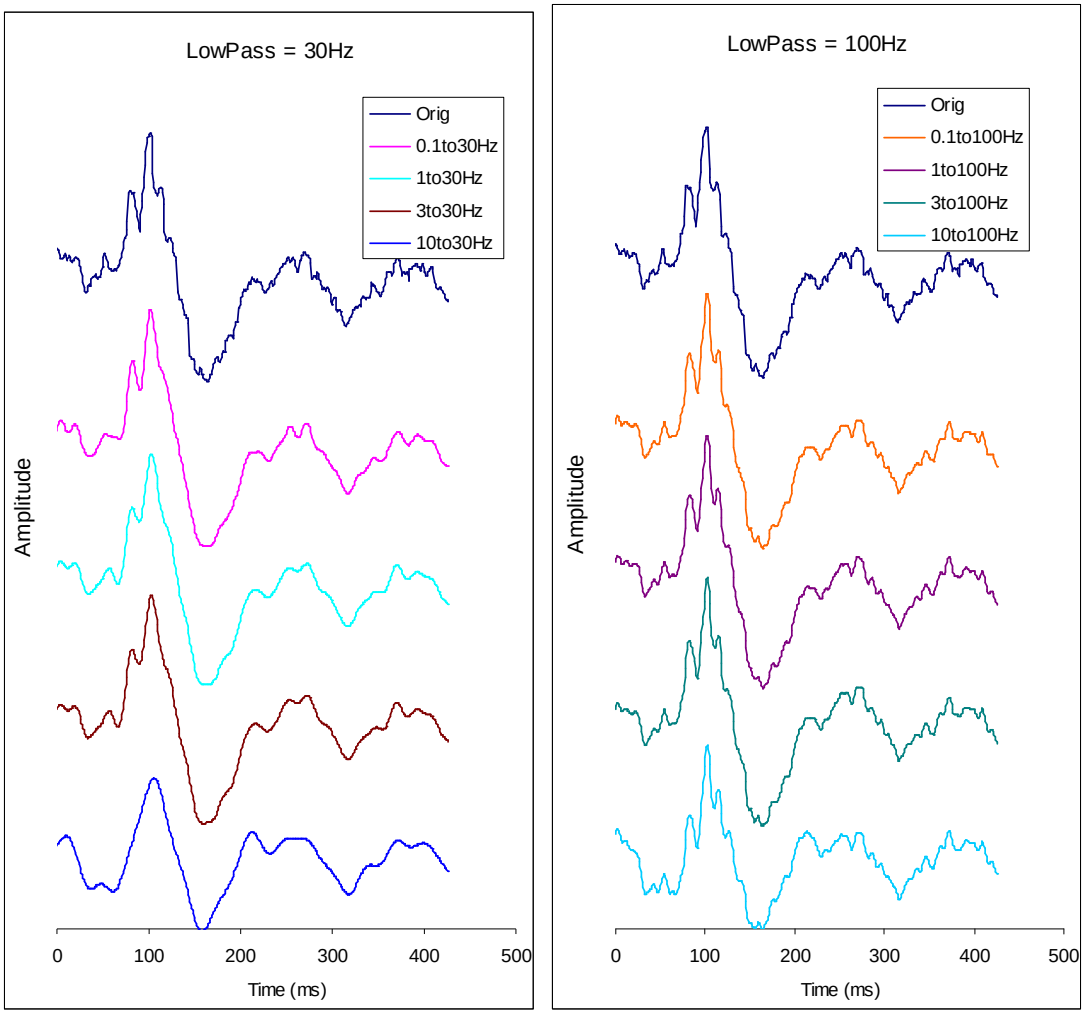

Figure 5.4 *Effect of the eight bandpasses on a single waveform. The left-hand plot shows bandpasses with a lowpass setting of 30Hz, and the right hand plots shows those with a lowpass of 100Hz. In both columns the uppermost trace is the original, unfiltered data. This waveform is the response to stimulation by a central region in the lower, right quadrant of the dartboard pattern.*

5.7.5.4 The Effect of Filtering on the Signal to Noise Ratio

Reducing the lowpass from 100Hz to 30Hz makes the signal clearer and does not exclude any useful data. A comparison of the SNR values calculated from the waveforms was performed.

The distribution of SNR values was tested for normality using the Anderson-Darling test for Normality, performed by Minitab. This returned a probability of less than 0.001, suggesting the values are not normally distributed. Comparisons of SNR distributions were therefore based on non-parametric tests and characterised by median rather than mean values.

SSPS 15.0 for Windows was used to perform a Wilcoxon Signed Rank Test. This was performed on data from a single channel for each subject, comparing the 30 and 100Hz low pass setting for each of the high pass settings. i.e.:

0.1to100Hz vs. 0.1to30Hz,

1to100Hz vs. 1to30Hz,

3to100Hz vs. 3to30Hz,

10to100Hz vs. 10to30Hz.

Each test included data from a single channel only, to ensure independence of samples. The test was repeated for each of the four channels. The Wilcoxon Signed Rank Test was therefore performed 16 times. In every case, the significance returned was $p<0.000$, suggesting that the null hypothesis that the SNR values come from the same distribution can be rejected i.e., there is a statistically significant increase in SNR when a 30Hz lowpass setting is used compared to a 100Hz lowpass.

Median values are plotted in Figure 5.5. The error bars indicate the 95% confidence interval of the median.

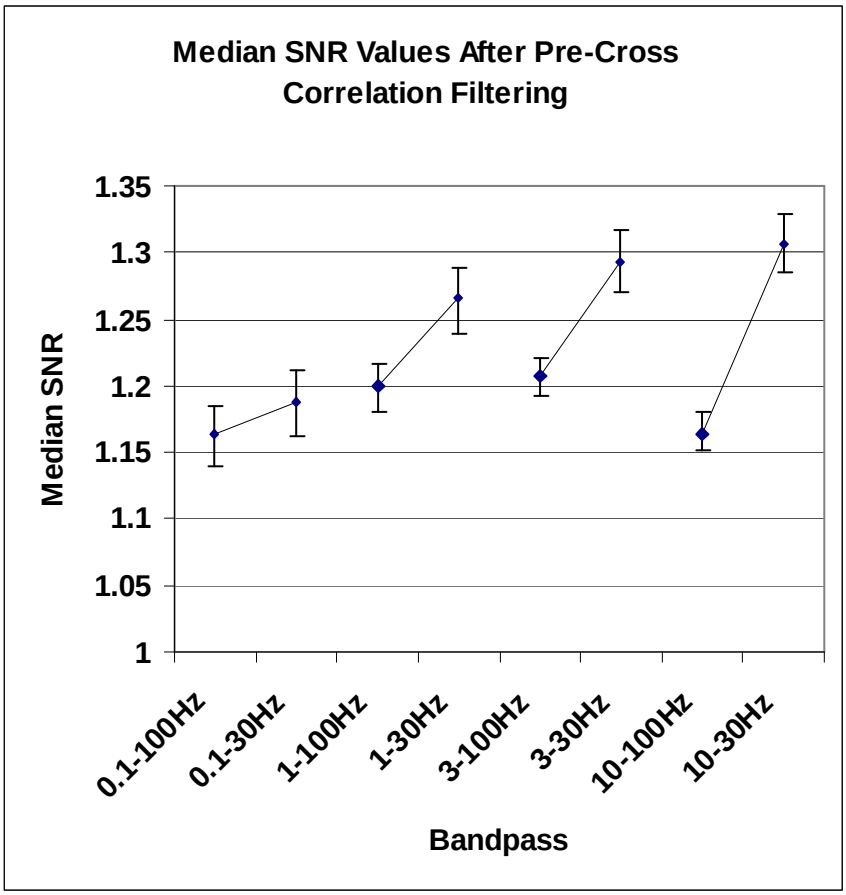

Figure 5.5 *Median SNR values are presented for data from four channels acquired from nine subjects, filtered through eight bandpasses. Error bars indicate the 95% confidence interval of the median. Datapoints with the same highpass value are joined to allow comparison of 100Hz and 30Hz lowpass settings.*

5.7.5.5 ROC Analysis

ROC curves are shown in Figure 5.6. The bandpass that allows the best performance in terms of both sensitivity and specificity will have the largest area under the ROC curve. Inspection of Figure 5.6 indicates that there are a number of filters that provide very similar performance. It is clear, however, that the 0.1 to 100Hz and 0.1 to 30Hz filters perform more poorly than the others. The greatest area under the curve is provided by SNR values calculated from data filtered through a 3 to 30Hz bandpass.

The data included in this analysis is from four recording channels acquired from nine subjects. There are therefore 2160 true signals and 2448 estimations of noise used in each curve.

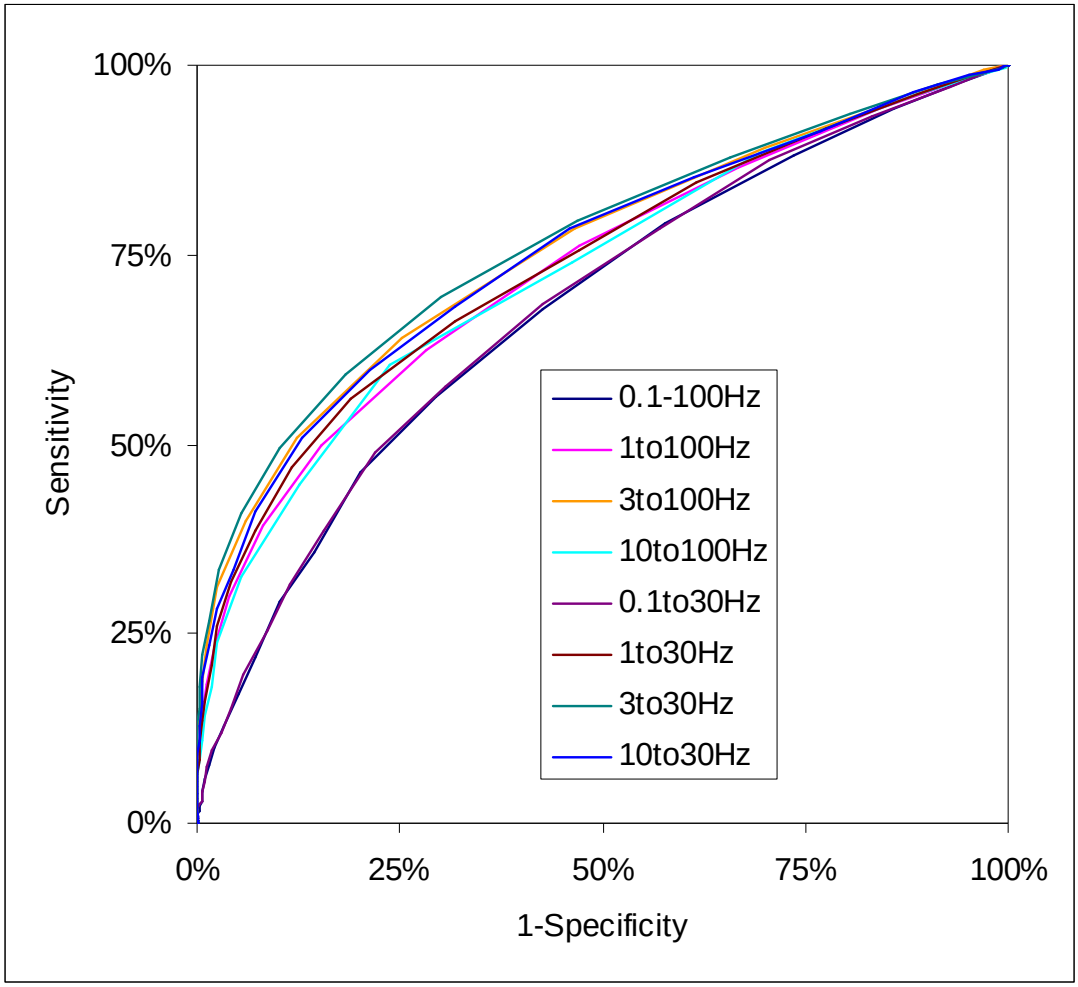

Figure 5.6 *ROC curves for data filtered through eight different bandpasses. Each curve is based on data from nine subjects and four recording channels (i.e. 2160 signal samples and 2448 noise samples).*

5.7.6 Stage One - Conclusion and Discussion

Filters were successfully created and applied to multifocal visual evoked cortical potential records, prior to cross-correlation.

Distortion of the waveform is introduced when a 10Hz highpass setting is used. This is not easily seen in Figure 5.3 due to the size of the waveform arrays, but is demonstrated clearly in Figure 5.4.

Waveform arrays show that the use of a 30Hz lowpass setting removes high frequency noise, making the waveforms appear ‘cleaner’. This is reflected in the median SNR values, which are consistently higher for direct comparisons of 30Hz and 100Hz lowpass settings.

10-30Hz filtering maximises the SNR value, but also introduces waveform distortion. 3-30Hz filtering does not sacrifice the SNR value to a great degree and does not introduce significant distortion.

Filtering affects both cross-correlations of the m-sequence that contain a signal and those that are not used to drive a region of the stimulus and therefore contain noise alone. Changes in the SNR of true signals will be accompanied by changes in the SNR value of the noise estimations. Genuine improvements in the performance of the mfVECP test require an ability to distinguish between real signal and the absence of signal. ROC analysis was therefore carried out to determine which filter bandwidth that allows the best performance of the mfVECP test.

Filters which have a 0.1Hz highpass setting show a smaller under the ROC curve than any of the other bandpasses suggesting a comparatively poor ability to distinguish between the presence and absence of a signal. The highpass of 0.1Hz possibly allows too much low frequency through, disturbing the baseline.

The remaining filters show subtle differences between the areas under their ROC curves, however the 3-30Hz ROC curve shows the greatest area.

In comparisons of 1-30Hz vs. 1-100Hz, 3-30Hz vs. 3-100Hz and 10-30Hz vs. 10-100Hz, the 30Hz lowpass resulted in a slightly larger area under the ROC curve. This is in keeping with the findings that a lowpass of 30Hz results in a statistically significant improvement in the SNR over 100Hz. This translates to a slight

improvement in the performance of the mfVECP test in terms of distinguishing between signal and noise.

Having shown statistically significant differences in the median SNR values after filtering data, it might have been reasonable to expect to see clearer differences in test performance reflected in the ROC curves. Differences are slight for two reasons:

Firstly, the relatively tight 95% confidence interval of the median values presented in Figure 5.5 result from the large number of samples (n=2160). The underlying distribution is wide and there is significant overlap between the distribution of noise and signal SNR values.

Secondly, filtering acts upon the estimations of noise in the same manner as the cross-correlations containing signal and has an impact on the true negative waveforms' SNR values. As the signal SNR values shift their distribution towards greater values, so do the noise SNR values, reducing the ability of a cut-off SNR value to distinguish between signal and noise.

Post-acquisition filtering has been shown to have a positive effect on mfVECP trace arrays and the performance of the mfVECP test. Of the eight bandpasses investigated, 3-30Hz is to be recommended.

5.8 Stage Two

5.8.1 Aim

To increase the number of low-pass settings investigated in Stage One of this experiment. Low pass setting of 20, 30, 40, 50 and 100Hz were applied in order to cover the range of settings reported in the literature, and the recommended ISCEV setting.

5.8.2 Methods

The same data was used as in Stage One. Filtering was performed by Multifocal Imager 3. A total of 20 filters were investigated and are listed below. Eight of these were those used in Stage One and are highlighted by a *.

- 0.1to 20Hz
- 1 to 20Hz
- 3 to 20Hz
- 10 to 20Hz
- 0.1to 30Hz*
- 1 to 30Hz*
- 3 to 30Hz*
- 10 to 30Hz*
- 0.1to 40Hz
- 1 to 40Hz
- 3 to 40Hz
- 10 to 40Hz
- 0.1 to 50Hz
- 1 to 50Hz
- 3 to 50Hz
- 10 to 50Hz
- 0.1 to 100Hz*
- 1 to 100Hz*
- 3 to 100Hz*
- 10 to 100Hz*

First order Bessel filters were used. Initial observations indicated that higher order filters could distort waveforms.

Data from four acquisition channels was filtered through the 20 filters for nine subjects' data.

In contrast to the approach of filtering raw data prior to cross-correlation described in Stage One, Multifocal Imager 3 is designed to perform filtering on the cross-correlated waveforms.

Signal to noise ratios were calculated as described in Chapter 4. A window of 45-250ms was used to calculate SNR. This is different from the 45-150ms time window used in the previous chapter and is based on an observation and subsequent analysis presented in Chapter 7 (section 7.3.4).

.

5.8.3 Results

5.8.3.1 Filtered Waveform Arrays

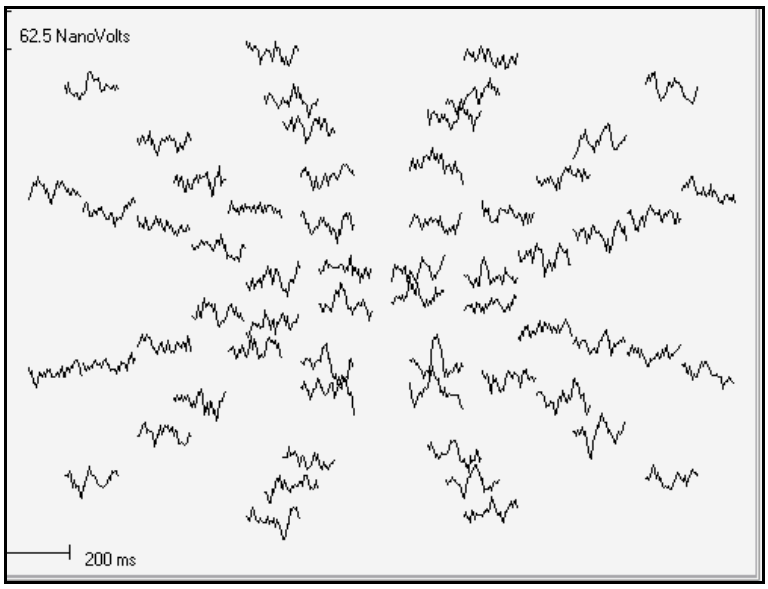

Figure 5.7 *Waveform trace array before any filtering was applied.*

Figure 5.7 shows unfiltered data. Figures 5.8a and b show the same data filtered through the 20 bandwidths listed in Section 5.8.2.

Inspection of the trace arrays shows

- Using a high pass of 10Hz introduces considerable distortion to the waveform.
- Reducing the low pass setting of the filter makes the waveforms increasingly clearer.

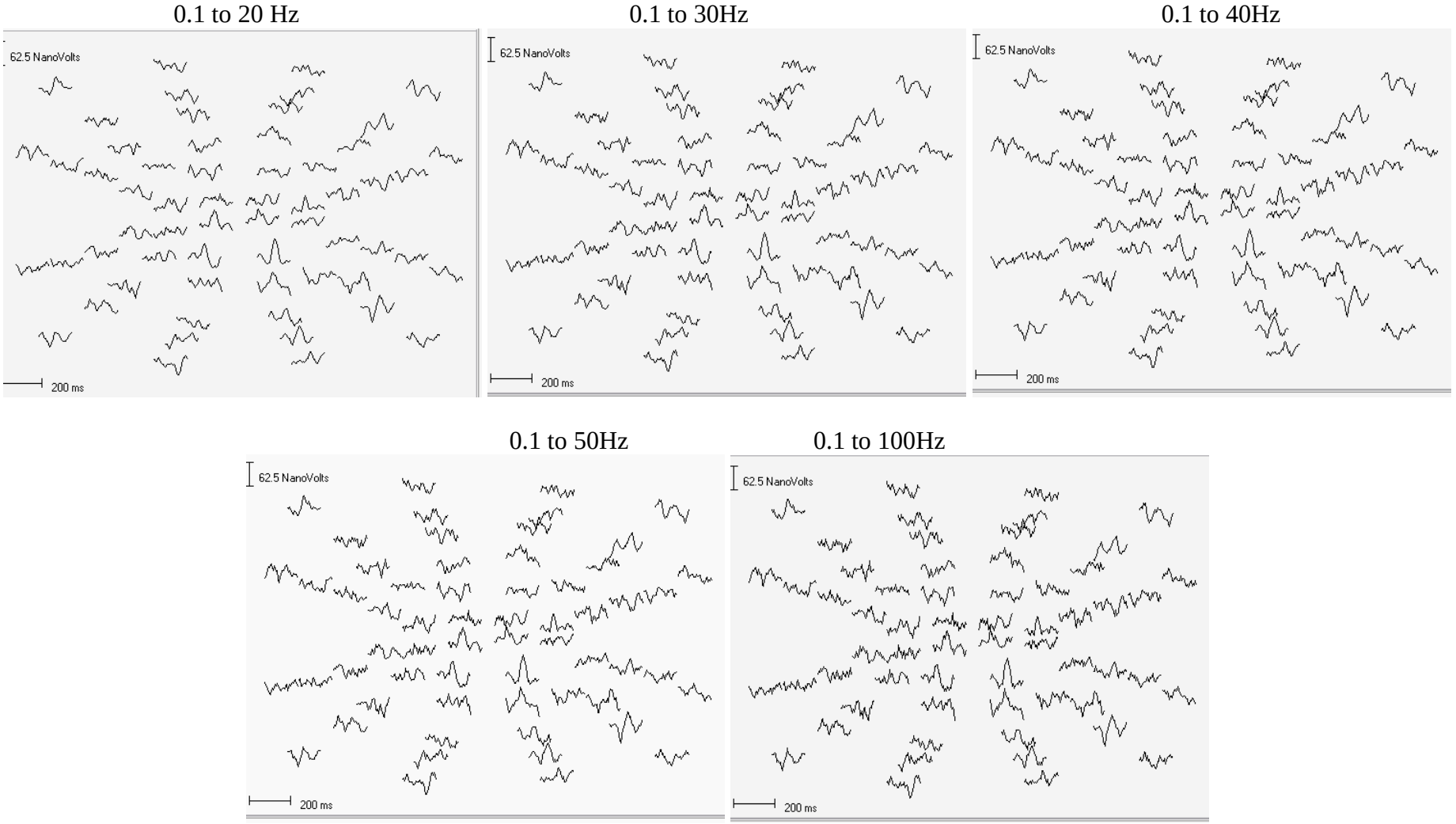

Figure 5.8a *Filtered waveform arrays*

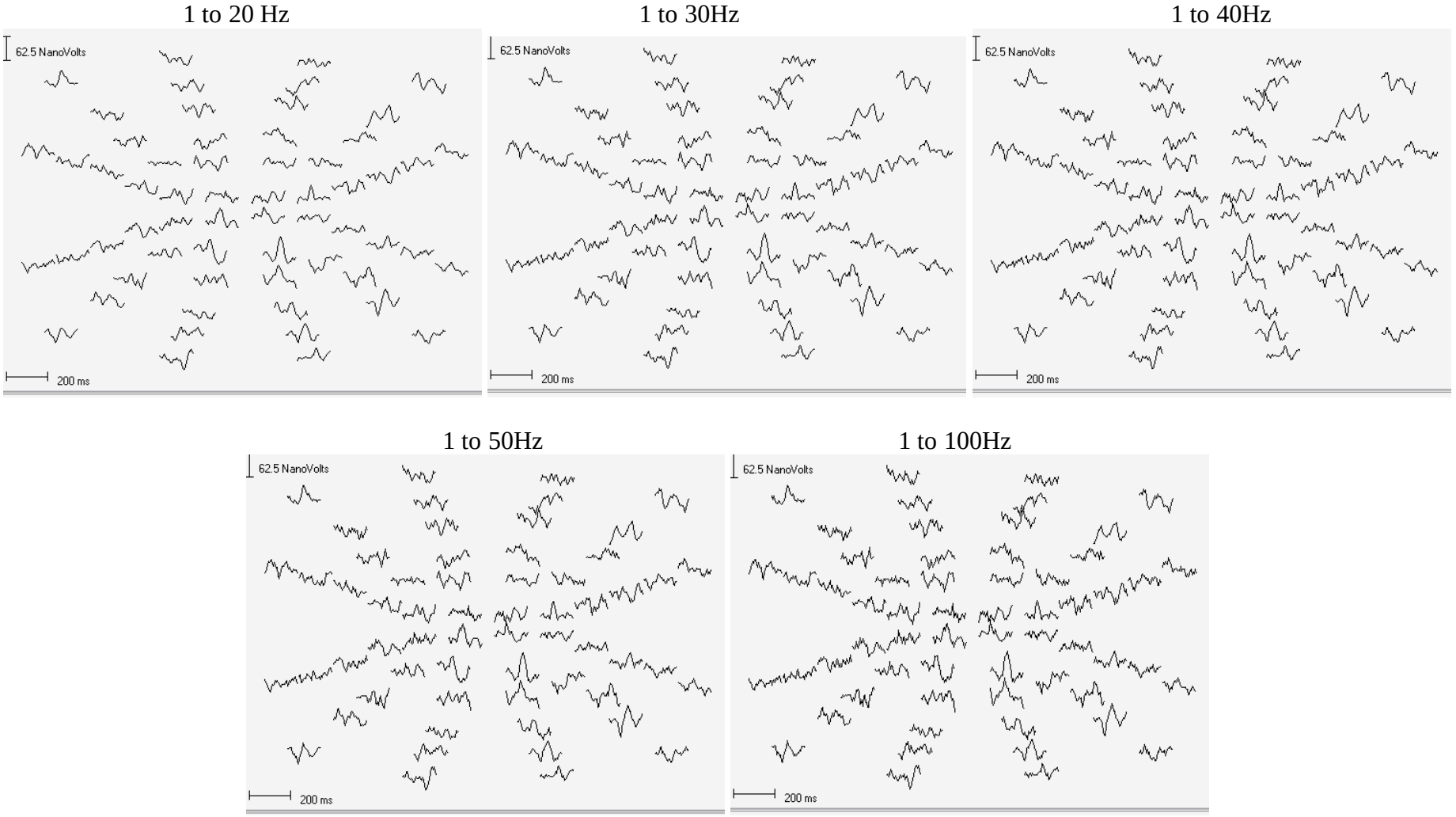

Figure 5.8b *Filtered waveform arrays*

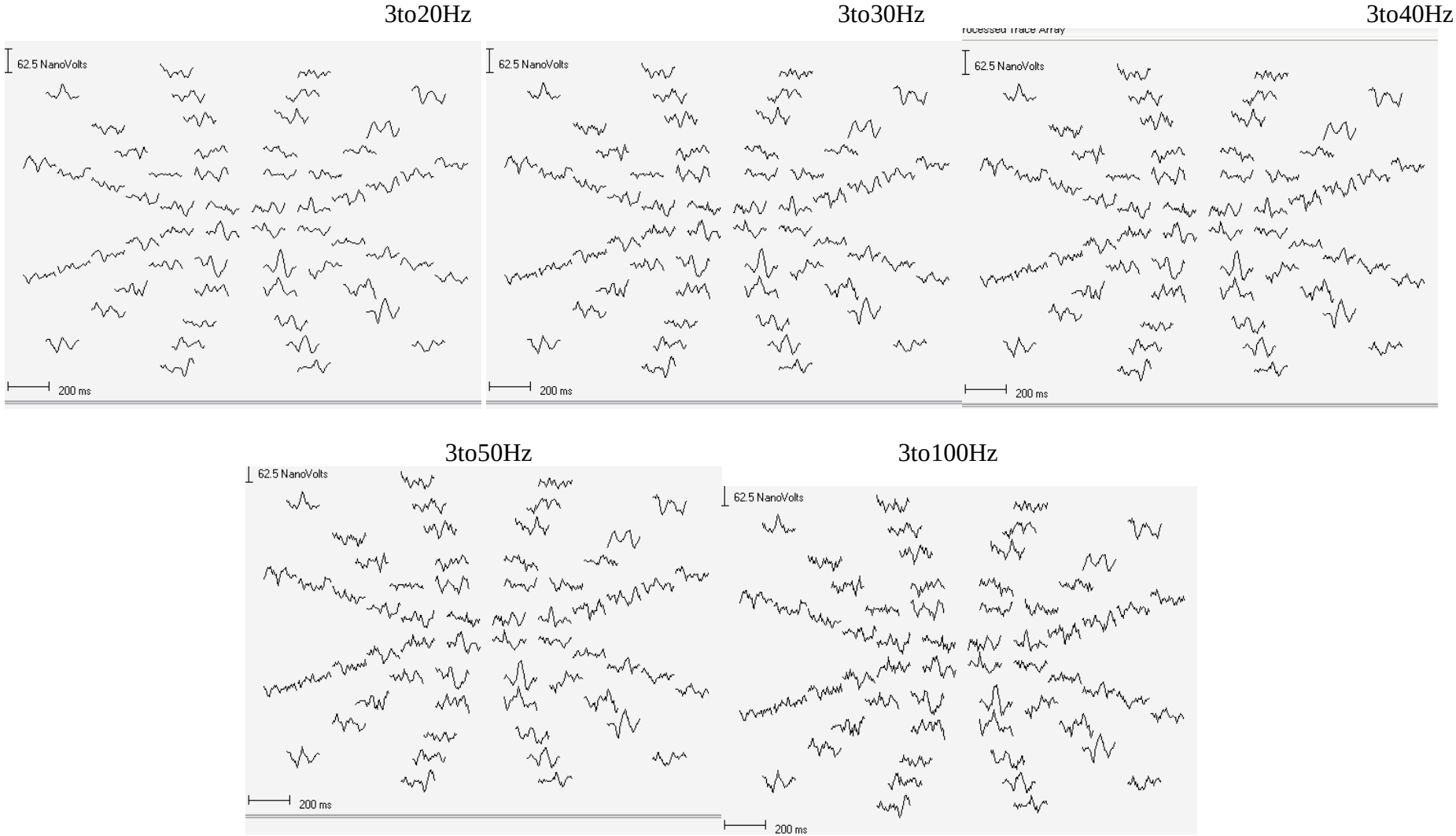

Figure 5.8c *Filtered waveform array*

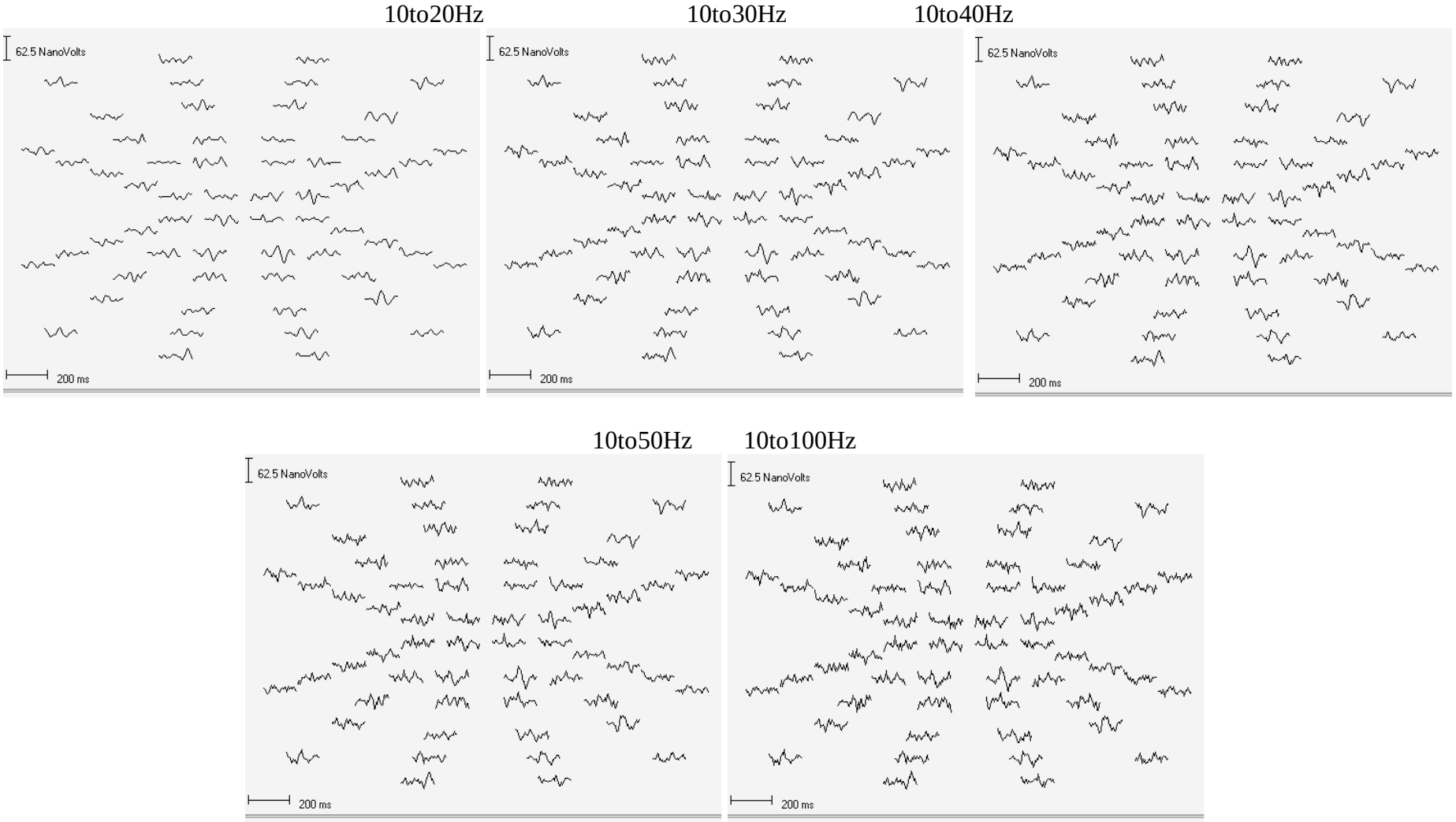

Figure 5.8d *Filtered waveform array*

5.8.3.2 The Effect of Filtering on Individual Waveforms

Figure 5.10 shows the effect of each of the filters on the waveform in Figure 5.9, below. This waveform is the response to stimulation by region 48 of the dartboard pattern. This is in the second ring in the upper right quadrant of the dartboard.

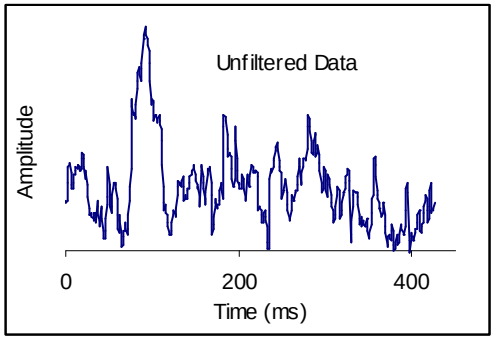

Figure 5.9 *Unfiltered waveform.*

Data are grouped by the highpass setting. Within each plot, the lowpass setting increases from 20Hz at the top to 100Hz at the bottom. In each of the four plots, a clear reduction in high frequency noise can be seen in the 20 and 30Hz lowpass filtered waveforms, compared to the 100Hz lowpass.

Differences between waveforms with a 0.1Hz and a 1Hz highpass setting are marginal. As the highpass is increased to 3Hz, we begin to see subtle changes in the waveshape in the form of an accentuation of the trough at approximately 170ms. Further distortion can be seen in the 10Hz lowpass filtered waveforms. Distortion with a 10Hz lowpass setting was encountered frequently. A further example is given in Figure 5.11.

In Figure 5.11, the original data shows a peak at approximately 100ms with troughs roughly symmetrically placed either side at ≈50ms and ≈150ms. Applying bandpasses with 10Hz highpass settings appears to remove the trough at 50ms and emphasis the one at 150ms, giving the waveform a very different waveshape.

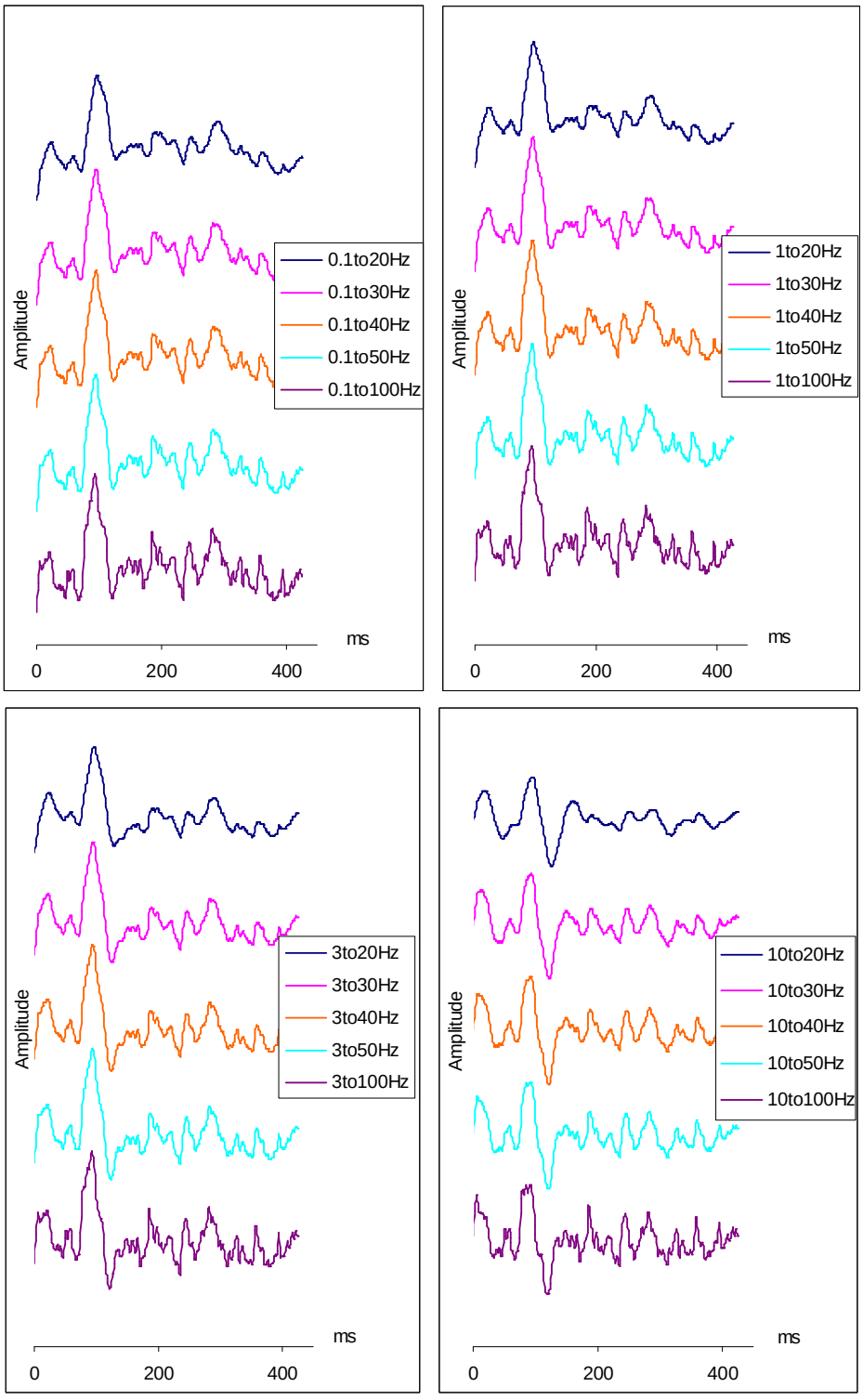

Figure 5.10 *The waveform evoked by region 48 of the dartboard stimulus is shown after filtering through each of the 20 bandwidths. Waveforms are grouped by the highpass setting of the bandwidth. Within each plot, the lowpass setting increases from 20 to 100Hz, from top to bottom. Region 48 is in the second ring and the lower right quadrant.*

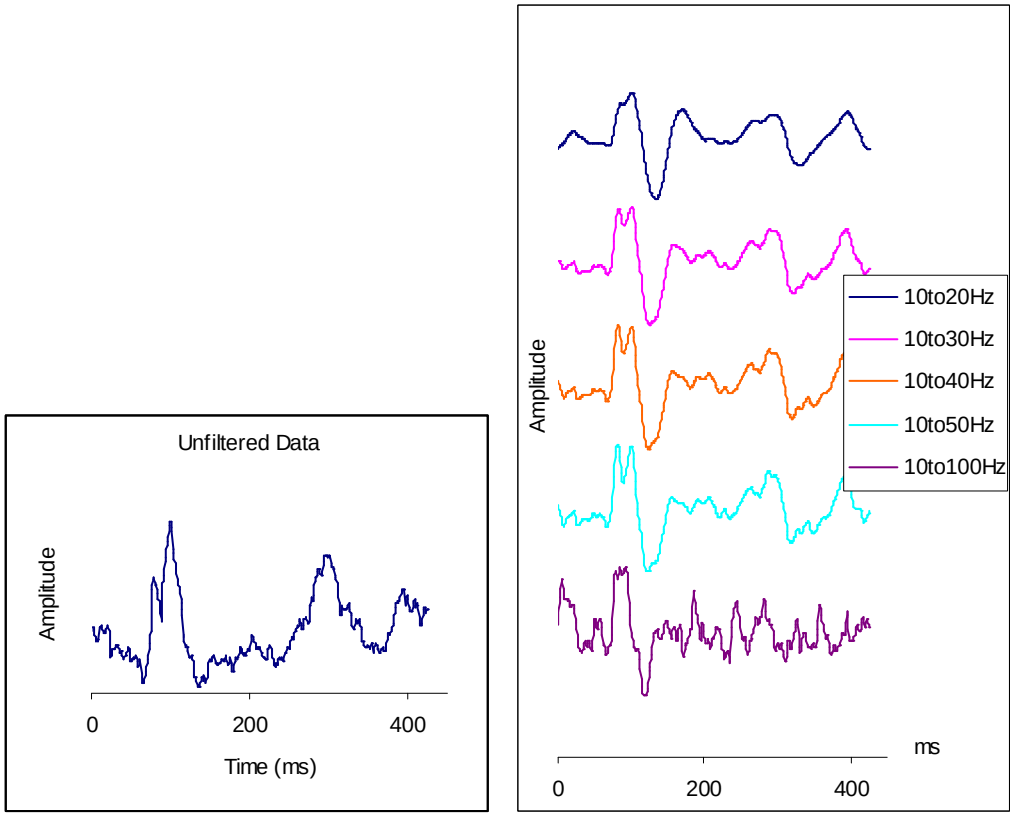

Figure 5.11 *Unfiltered data are shown on the left. The right shows data filtered through bandpasses with a highpass setting of 10Hz. Significant distortion of the waveform can be seen.*

5.8.3.3 The Effect of Filtering on the Signal to Noise Ratio

Using data from nine volunteers and four recording channels, median, 10^{th} and 90^{th} percentile SNR values were calculated and are plotted in Figure 5.12.

In this plot, the first vertical data series is for the original, unfiltered data (dark blue). All pink data series have a lowpass setting of 20Hz, yellow series represent a lowpass of 30Hz, aqua series represent 40Hz, purple represent 50Hz and brown represent 100Hz. Going from left to right, the series with squares have a highpass of 0.1Hz, circles are the next group, representing a highpass of 1Hz, triangles represent a highpass of 3Hz and the rightmost group of crosses represent a highpass of 10Hz.

For each highpass setting we see a consistent, monotonic trend of decreasing median SNR as the lowpass setting increases from 20Hz to 100Hz. The larger median value is accompanied by a larger range of SNR values. The range decreases as the lowpass setting increases from 20 to 100Hz.

This will have an impact on the ability to distinguish between signal and noise, particularly if filtering decreases the value of lower percentiles and brings it into greater overlap with the range of noise. Indeed, Figure 5.13 shows that filtering increases the range of SNR values of cross-correlated m-sequences that were not used to drive the mfVECP stimulus (i.e. the 68 representations of noise). The colour scheme used in this figure is the same as that used in Figure 5.12. The distribution of noise SNR values decreases as the lowpass setting is increased from 20Hz to 100Hz, a pattern that is consistent for all highpass settings.

It can be seen that filtering data can improve the median SNR value. Only the 10-100Hz filter reduces the median SNR when compared to unfiltered data.

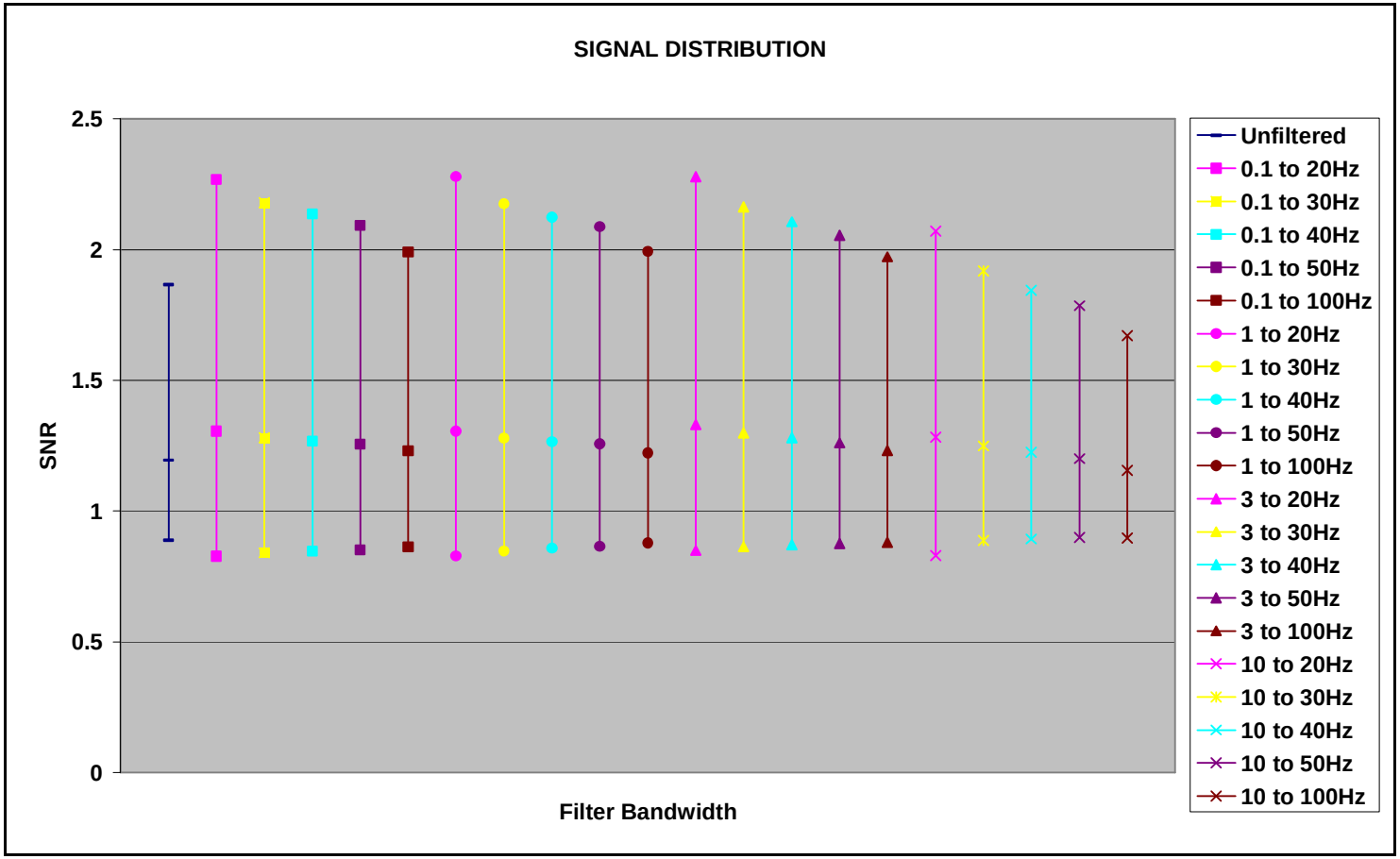

Figure 5.12 *Median SNR values for signals within the waveform array are plotted for each filter bandwidth. 10th and 90th percentiles are also shown. Unfiltered data are represented by the blue series. Each colour of series represents a different low pass (pink- 20Hz, yellow – 30Hz, aqua – 40Hz, purple – 50Hz and brown – 100Hz). Squares indicate a high pass of 0.1Hz, circles – 1Hz, triangles – 3Hz and crosses – 10Hz.*

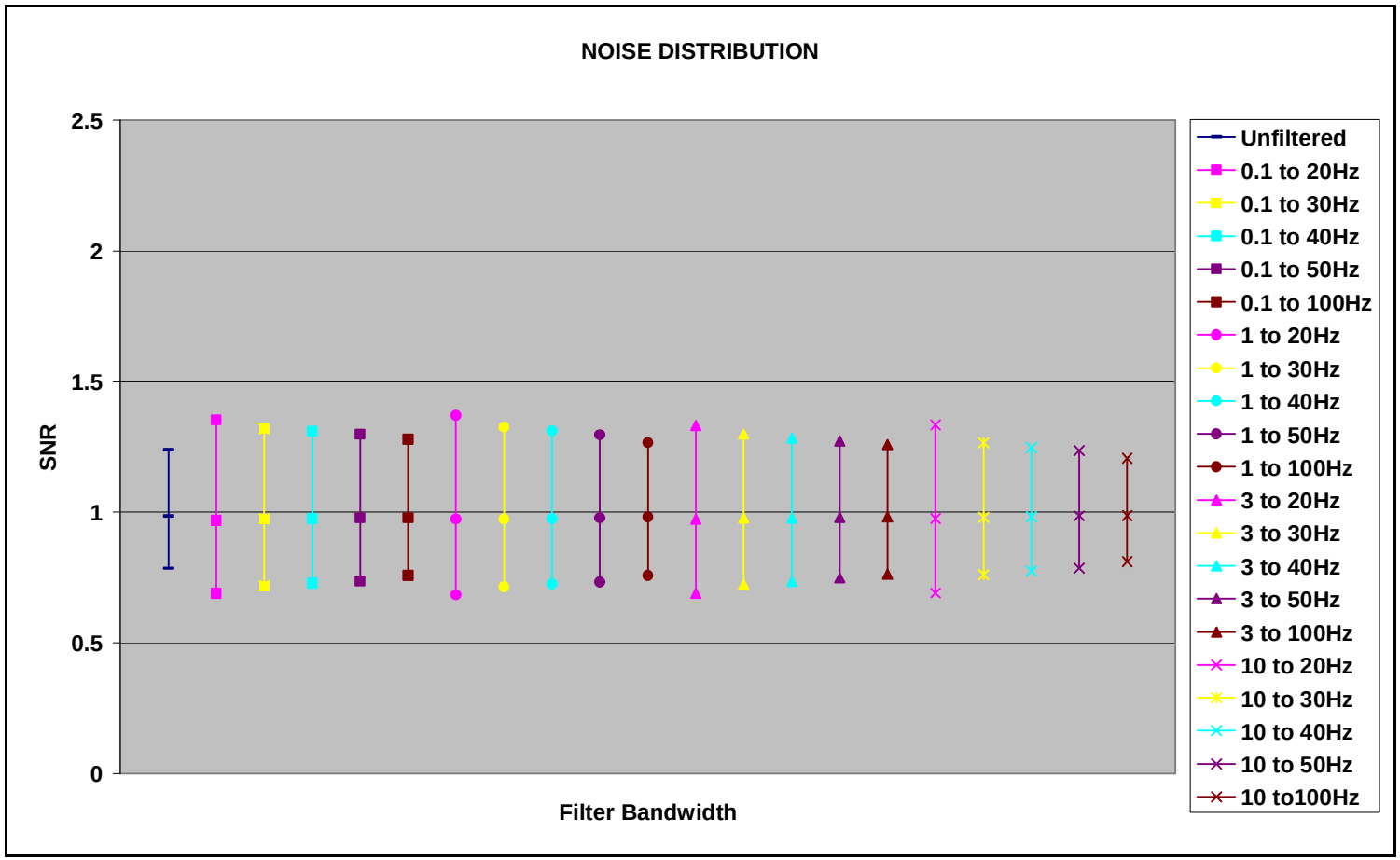

Figure 5.13 *SNR value distribution of noise estimates. The median SNR values are given, along with the 90th and 10th percentiles. The unfiltered data are represented by the blue series. Each colour of series represents a different low pass (pink- 20Hz, yellow – 30Hz, aqua – 40Hz, purple – 50Hz and brown – 100Hz.) Squares indicate a high pass of 0.1Hz, circles – 1Hz, triangles – 3Hz and crosses – 10Hz.*

5.8.3.4 ROC Analysis

ROC analysis was performed. Results have been grouped by the lowpass setting of the bandpass and are shown in Figure 5.14.

The areas under the ROC curves are very similar, suggesting that large improvements in signal detection will not be achieved by post cross correlation bandpass filtering. There are, however, subtle differences. In each of the five plots, the pale blue curve representing a highpass setting of 3Hz shows a small increase in the area under the curve, compared to all other highpass settings.

The bandpass of 10-100Hz (shown in the bottom plot, purple curve) shows a small but clear reduction in the area under the ROC curve, which is consistent the fact that it maintains a high degree of high frequency noise and that the 10Hz highpass setting introduces considerable waveform distortion.

ROC curves were grouped by the highpass setting of the bandpass (not shown) in order to highlight differences in performance based on the lowpass setting of the bandpass, but did not result in any noteworthy findings.

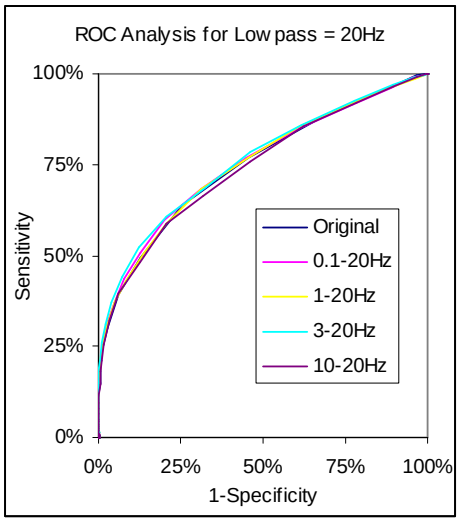

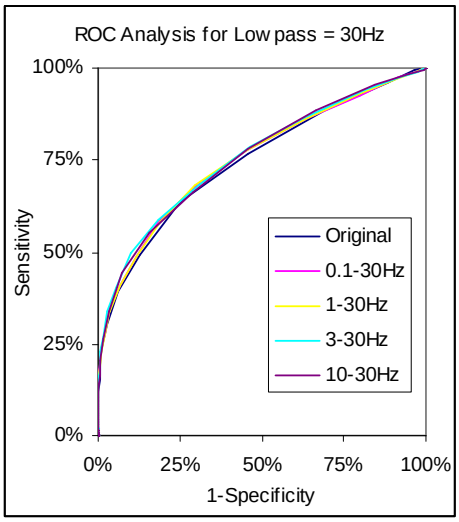

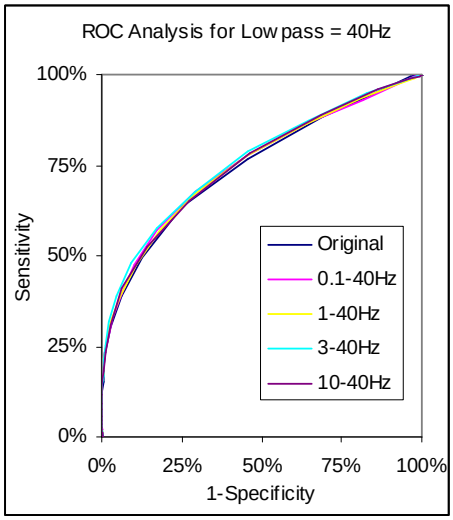

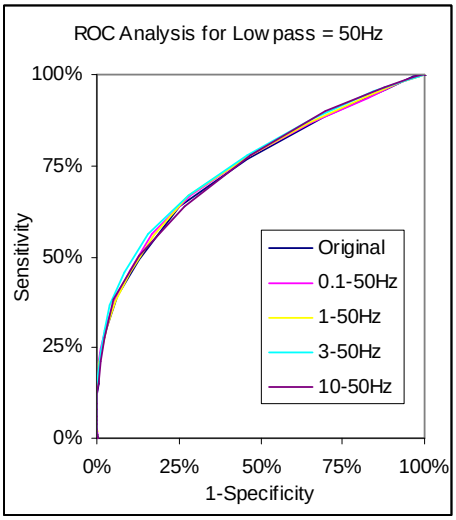

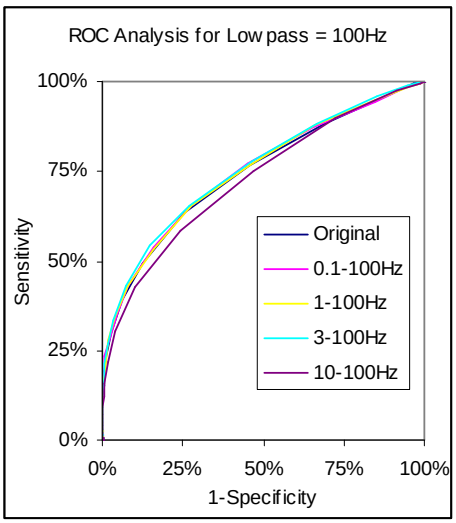

Figure 5.14 *ROC curves for all 20 filters. Data from nine subjects and four recording channels was used to create these ROC curves. Each curve represents 2160 signals and 2448 noise estimation.*

5.8.4 Stage Two - Conclusion & Discussion

On inspection of both waveform arrays and individual waveforms, decreasing the lowpass setting improves the appearance of the waveform and would ease the placement of cursors to quantify amplitude and latency values.

The use of a 10Hz highpass setting introduces significant distortion to the waveforms.

Applying filtering can increase the median SNR value, with the largest values being seen for a lowpass setting of 20Hz. This is, however, accompanied by an increase in the range of SNR values.

This analysis included all data acquired from four midline recording channels. There will be waveforms within the trace arrays which represent a volume of the visual cortex which may be oriented at such an angle that it is not possible for a channel to detect the evoked dipole. The resulting waveform is treated as containing a physiological signal. The downward trend of the 10^{th} percentile value as the lowpass setting is reduced could therefore be due to these waveforms where signal is not present.

If these waveforms could be clearly identified and removed from the analysis, we may see greater improvements in the ROC curves of 20Hz and 30Hz lowpass setting datasets. A simple automated means of making this identification is not immediately obvious and so inspection of all the waveforms would be required. This is not practicable with the volume of data involved here.

ROC analysis suggests that the use of a 3Hz highpass setting on the bandpass provides a small improvement in the ability to distinguish between signal and noise when compared to unfiltered data and data filtered through any other bandpass.

The ROC analysis does not inform the selection of a lowpass setting.

As with the data presented in Stage One, we see small improvements in SNR values. These do not translate into substantial differences in test performance, as defined by the ROC curves.

One explanation for this could be that the differences in the frequency content of cross-correlations containing physiological signal plus noise and those containing noise alone, are slight. This was investigated by taking a Fast Fourier Transform (FFT) of 6 waveform responses to stimulation (one from each ring of the waveform

array) and 6 waveforms representing noise (i.e. cross-correlations of unused m-sequences). Data was from a single subject and a single recording channel. The average FFTs are shown in Figure 5.15.

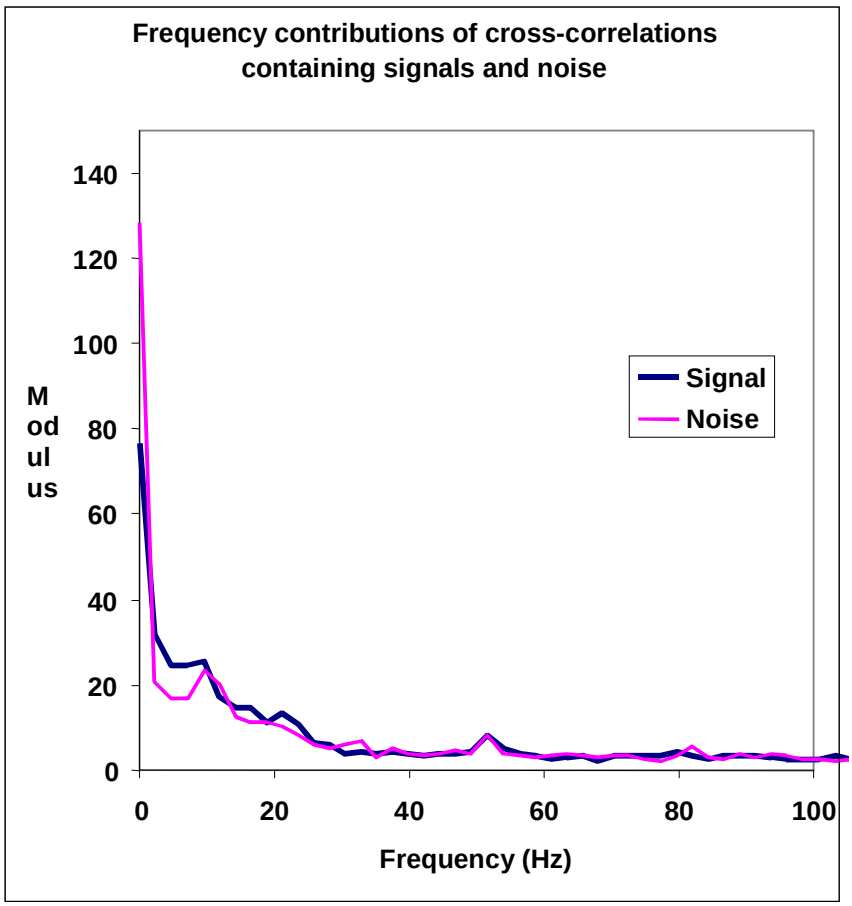

Figure 5.15 *Frequency content of waveforms containing physiological signal (Blue – Signal) and waveforms created by the cross-correlation of the raw data with unused m-sequences (Pink – Noise).*

The FFTs show a remarkable similarity in frequency content for frequencies greater than 40Hz. Differences are present at frequencies lower than 10Hz. Changing the lowpass settings of the filter bandwidths will therefore have the same impact on both cross-correlations of physiological signal plus noise and cross-correlations of noise

alone, and we should not therefore expect to see an improvement in the ability to distinguish between them.

Data presented in Stage Two suggests that a post cross-correlation filter bandwidth of 3 to 20Hz will improve the appearance of the waveform array, assist in the positioning of cursors for amplitude and latency determination, increase SNR values of physiological responses and allow a small improvement in the ability to distinguish between the presence and absence of a physiological response.

5.9 Comparison of Stage One and Stage Two Results

The analysis performed in Stage One and Stage Two of this investigation have resulted in very similar conclusions. There are, however, some differences of interest.

ROC analysis performed in Stage One showed a distinct disadvantage in the use of a 0.1Hz high pass setting (Figure 5.6), but this was not seen in the Stage Two study (Figure 5.14).

For the same nominal 0.1 to 100Hz filter, the application prior to cross-correlation results in poorer performance of the test than application after cross-correlation. This is not the case for higher highpass settings. This is demonstrated in Figure 5.16 Similar results are seen for a 30Hz lowpass setting (not shown).

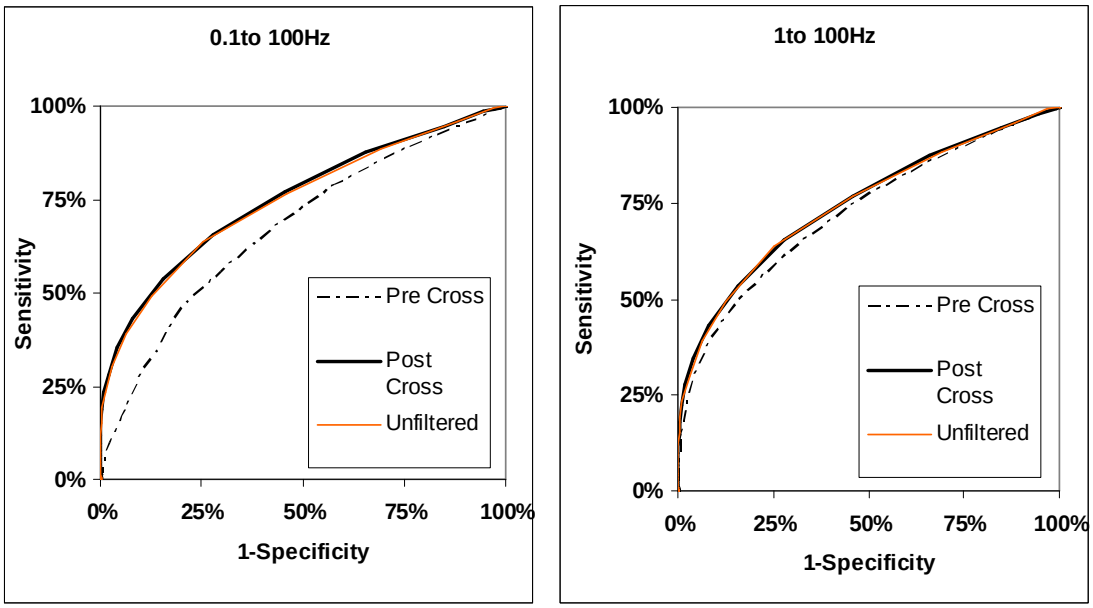

Figure 5.16 *ROC curves for the same data filtered through a 0.1 to 100Hz (left hand side) and a 1 to 100Hz (right hand side) filter. The solid curve is for data filtered after cross-correlation, and the broken line is data filtered prior to cross-correlation. The orange curve is unfiltered data.*

The median values of the SNR distributions for waveforms within the trace array were compared using data filtered before and after cross-correlation. The median values were found to be significantly greater ($p<0.05$) when filtering was applied after cross-correlation, for filters with a highpass setting of 0.1Hz. Significance was determined by the lack of overlap of the 95% confidence intervals of the median value.

No significant difference was seen in the median values when the highpass setting was 1Hz.

These findings were consistent when tested for lowpass settings of both 30 and 100Hz. These finding are illustrated in Figure 5.17.

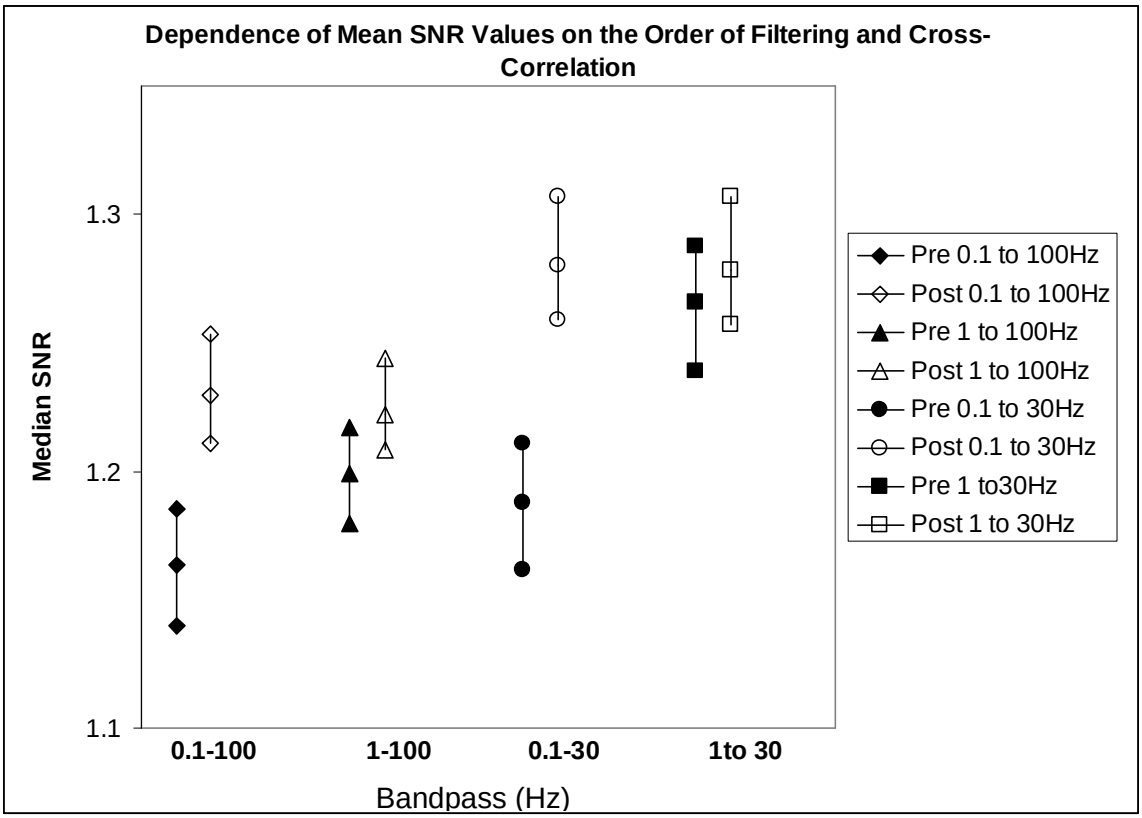

Figure 5.17 *Data filtered before and after cross-correlation is compared. Median SNR values and their 95% confidence intervals are plotted. Each pair of series represents the same filter, applied before (filled shapes) and after cross-correlation (unfilled shapes). From left to right, the pairs show data filtered through a 0.1-100Hz filter (diamonds), a 1-100Hz filter (triangles), a 0.1 to 30Hz filter (circles) and a 1 to 30Hz filter (squares).*

The power of the analysis was improved by performing a paired, non-parametric test. The Wilcoxon Signed Rank Sum Test returned a significant difference for all highpass settings at the $p<0.001$ level.

There are two major differences between the methodologies used in Stage One and Stage Two.

Firstly, a Kaiser filter was used in the first and a Bessel was used in the second. Both of these are linear phase filters and while their characteristics are not identical, it would seem unlikely that they would fully explain the discrepancy.

The second difference is the stage in the data processing at which filtering was applied. Stage One filtered the raw data, prior to cross-correlation, while Stage Two allowed filtering to be performed interactively on cross-correlated waveforms.

The process of cross-correlation can produce frequency components in the waveforms that were not present in the raw data. This arises because discrete windows of data are selected for addition or subtraction, based on the value of the m-sequence and the order and kernel of the cross-correlation. It is possible that when data are filtered before cross-correlation, the creation of the waveform array re-introduces unwanted frequency components which degrade the signal and reduce the performance of the mfVECP test.

By increasing the highpass setting from 0.1Hz to 1Hz, low frequency baseline fluctuations are removed. A wandering baseline could result in more discontinuous jumps as discrete sections of the raw data are added and subtracted during cross-correlation, which would introduce unwanted frequency components to the waveform response. This would happen to a lesser degree if the baseline was flatter, which explains why the 0.1Hz highpass setting performs more poorly than the other highpass setting for pre cross-correlation filtering.

Data filtered through a bandpass with a 0.1Hz highpass setting, prior to cross-correlation creates data with a poorer ROC curve than unfiltered data. This is at first counter-intuitive. One possible explanation lies in the similarity of the hardware acquisition and software filter settings, and their non-ideal performances. Data was acquired through a 0.1 to 100Hz hardware filter and was then passed through a software filter which also had a highpass setting of 0.1Hz. Neither filter will have a perfect frequency response curve. A sharp transition from stopband to passband between DC and 0.1Hz is a demanding requirement for a filter and it is possible that overshoot will appear at frequencies of close to 0.1Hz in one or both of the filters. The poor performance identified here could be the result of an interaction of the serial application of two non-ideal filters on frequencies close of 0.1Hz.

Filtering with a 1Hz highpass setting shows a very slight drop in the area under the ROC curve, when compared to unfiltered data, suggesting that the disadvantageous interaction of filters is lessened by separating their transition bands.

5.10 **Wavelet Filtering and Smart Filters**

Filtering is becoming more sophisticated than the use of simple bandpasses. Two examples of new techniques are wavelet filtering and smart filters.

Wavelet filtering is used to remove noise from the signal whilst minimising problems associated with high pass and low pass filters, such as degradation of the signal. Furthermore, using Discrete Wavelet Transforms, as opposed to Fast Fourier Transforms to analyse a signal, allows both the frequency and the temporal content of the input wave to be examined.

When using wavelet filtering, the time domain signal is passed through a series of high and low pass filters. At the first stage, the signal is split into two parts, using a high and low pass filter. Two versions of the signal then exist; one contains the low frequencies within the signal while the other contains the high frequencies. The above process is then carried out on the low pass portion of the signal, again resulting in two versions of the signal. This is continued until an adequate frequency resolution is achieved.

Different combinations of the generated frequency slices are combined, as governed by the wavelet order, to optimise the filtering process.

Wavelet filtering has been used to positive effect in 103-region mfERGs (140).

Smart filtering employs both wavelets and traditional bandpass filtering and is designed to assist in cursor placement.

The Multifocal Imager 3 software allows the application of wavelet filtering and Minimal, Mild, Moderate and Maximum Smart Filters. These were applied to a single subject's waveform array. The Minimal and Mild options appeared to have little or no effect on data, while the Maximum distorted data significantly. When judged by eye, the Moderate option appeared to remove noise without introducing distortion.

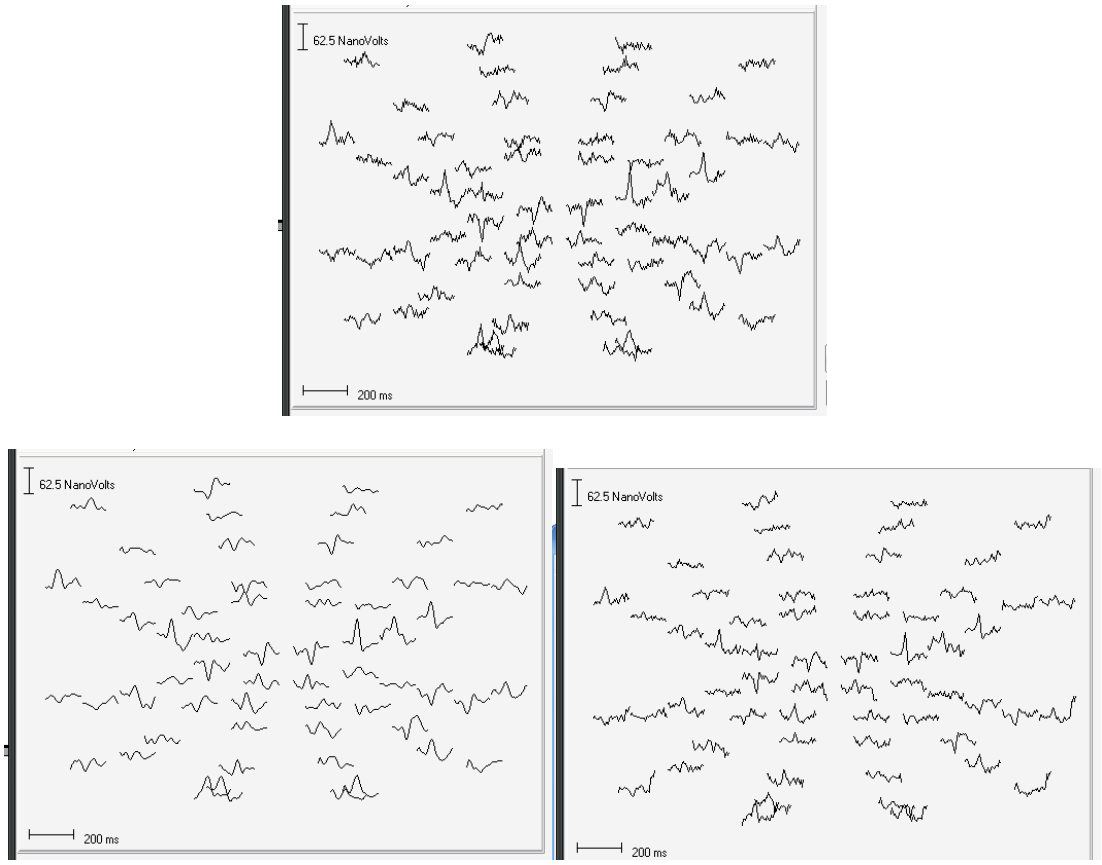

Figure 5.18 *Examples of Wavelet and Smart Filtering. The top trace array is unfiltered. The bottom left has been through a wavelet filter and the bottom right has had a Moderate Smart Filter applied.*

Data from a single recording channel (Channel 1) acquired from a single subject has been put through a Wavelet and a Moderate Smart Filter.

The effect on the waveform array can be seen in Figure 5.18. SNR values were calculated for both types of filtering and are compared with unfiltered data and data filtered through a traditional 3-30Hz bandpass, in Figure 5.19. Unfiltered data are represented by dark blue squares, data filtered through a 3-30Hz bandpass, post cross-correlation by pink squares, wavelet filtered data are shown by yellow triangles and smart filtered data by pale blue squares.

Wavelet filtering shows improvements in SNR values in several cases. The SNR values obtained after the application of the Moderate Smart Filter are poorest.

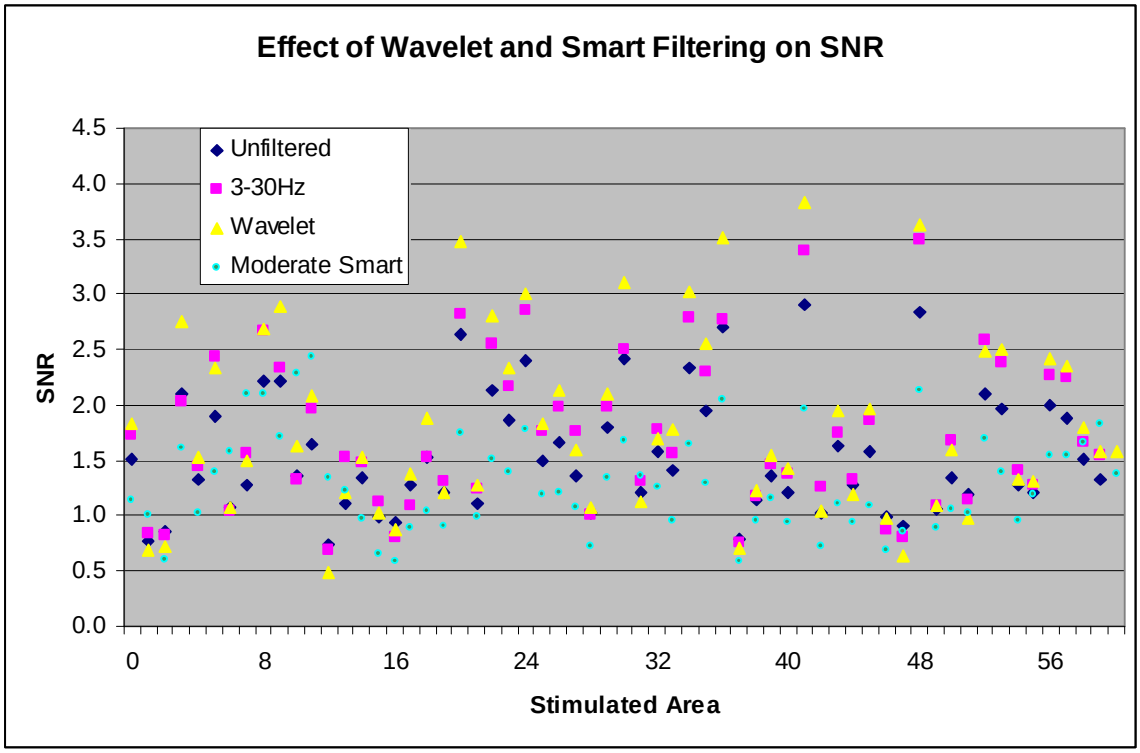

Figure 5.19 *SNR values are plotted for data from a single waveform array. Each of the 60 waveforms has a SNR value calculated after filtering with the 3-30Hz bandpass (pink squares), the Wavelet filtering (yellow triangles) and the Moderate Smart Filter (pale blue circles). The unfiltered data are represented by navy blue squares.*

ROC curves were plotted from this data and are shown in Figure 5.20. Please note that unlike all previous ROC curves presented in this chapter, these represent data from a single channel and subject and are therefore considerably noisier.

The ROC curves show that the ability to distinguish between noise and signal is not enhanced by the application of either the Wavelet or Moderate Smart Filtering, in this subject. In fact, the application of the Moderate Smart Filter appears to be detrimental. This could be because the Moderate Smart Filter has been optimised for mfERG data rather than mfVECP data.

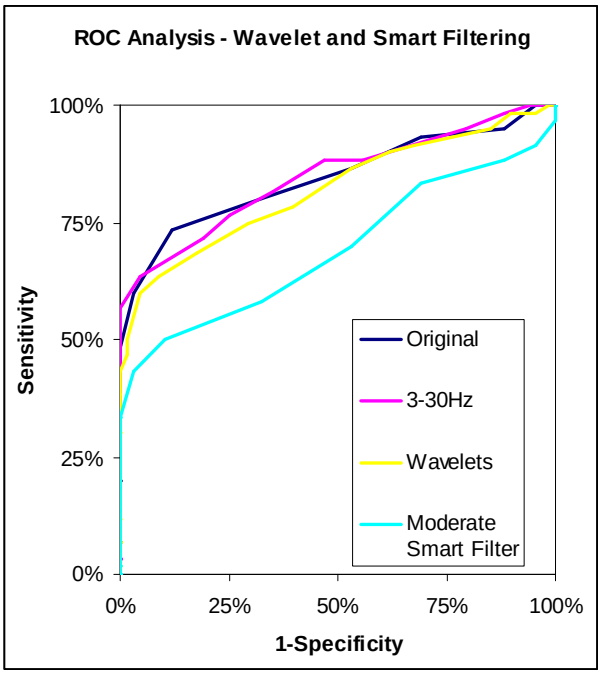

Figure 5.20 *ROC curves for unfiltered data (dark blue curve), data filtered through a 3-30Hz bandpass (pink curve) a wavelet filter (yellow curve) and a Moderate Smart Filter (pale blue curve).*

5.11 Conclusions and Discussion

In this chapter it has been shown that the best mfVECP signal quality and test performance are achieved when a 3-20Hz bandpass digital Bessel filter is applied after cross-correlation.

Post-acquisition filtering software is becoming more readily available, making the selection of acquisition filtering less important. If a wide bandpass is selected during acquisition then flexibility remains for selecting a narrower filter afterwards.

Improvements in the appearance of waveform responses and their SNR values can be brought about by appropriate filtering. This translates into subtle differences in the ability to distinguish between the presence and absence of a signal, as defined by ROC analysis. These differences were smaller than might be expected, which can be explained by a corresponding increase in the SNR values calculated from noise estimations.

Cross-correlation is a technique for improving signal to noise ratio and providing optimal signal detection. While the application of filtering can increase the numeric value of the SNR and make the waveform more pleasing to the eye, those improvements do not translate to a substantially improved ability to distinguish between signal and noise. This suggests that the greatest gain in signal quality is achieved is by cross-correlation and that the changes introduced by filtering are small in comparison.

A brief analysis of the frequency spectra of cross-correlations containing physiological signal and noise, and cross-correlations of noise alone indicated significant overlap. This suggests that the presence of a mfVECP signal is dependent on waveshape rather than its frequency content.

The improvements seen here are subtle. All analyses have included all 60 waveforms in the trace array and assumed that there are detectable signals present. It has been shown that this is not always the case. Further work on selected waveforms that are clearly present may show greater improvements on filtering,

The order of application of a bandpass filter and cross-correlation is important and careful attention to filter frequency response is necessary.

New methods of filtering, such as the use of wavelet filtering may provide additional improvements in the signal to noise ratio of waveforms and therefore the ease of cursor placemen. The brief investigation presented here does not indicate that significant gains will be made in attempts at distinguishing between the presence or absence of a signal, however the filters used were created for use with mfERG data and future tailoring of the algorithms to suit mfVECP data may produce more fruitful findings.

While filtering can remove sources of noise which distort the signal, and enhance our ability to detect signals, an increase in the underlying signal size would obviously have a more immediate impact on test performance. The following chapter investigates whether the method of stimulus presentation can have such an impact.

Chapter 6

Stimulus Delivery

Contents

		Page
6.0	Introduction……..	155
6.1	Methods of Stimulus Delivery……..	155
6.2	The Cathode Ray Tube …..……	157
6.3	Liquid Crystal Display Projector Delivery ……..	158
6.4	Luminance Profiles ……..	158
6.5	Stimulated Field of View ……..	160
6.6	Experiment 1 – mfVECP responses to CRT and LCD Projector Delivered Stimulation.....	162
	6.6.1 Aim ……..	162
	6.6.2 Introduction …….....	162
	6.6.3 Experiment 1a – Luminance Matching ……	162
	6.6.3.1 Methods ……	162
	6.6.3.2 Results……..	162
	6.6.4 Experiment 1b – Comparing CRT and LCD Presented Stimuli in the mfVECP ……..	166
	6.6.4.1 Methods ……..	166
	6.6.4.2 Results ….....	168
	6.6.4.3 Discussion …….	172
	6.6.4.4 Conclusion ……	172
6.7	Experiment 2 – mfVECP Field of View ……..	173
	6.7.1 Aim …….	173
	6.7.2 Methods …….....	173
	6.7.2.1 Analysis ..…….....	175
	6.7.3 Results ……..	175
	6.7.4 Discussion …….	179
6.8	Reproducibility ……..	179
6.9	Stimulus Delivery Discussion….…….. …….....	181
6.10	Stimulus Delivery Conclusion ..	184

6.0 Introduction

This chapter describes various methods of stimulus display and their impact on the mfVECP and reviews the extent of the stimulated field of view used in recently published work.

It aims to compare mfVECP responses to cathode ray tube (CRT) and Liquid Crystal Display (LCD) projector presented stimuli and to determine the optimal field of view of stimulation.

6.1 Methods of Stimulus Delivery

Multifocal electrophysiology is most commonly performed by presenting the stimulus on a cathode ray tube (CRT) monitor. Other modes of stimulus presentation have been employed in multifocal electrophysiology including LED stimulation for mfERGs (102;141).

The commercially available RetiScan^{TM} multifocal system produced by Roland Consult uses a scanning laser ophthalmoscope (SLO) to deliver the stimulus directly on to the retina (98). Virtual reality goggles or shutter goggles have been used to present stimuli dichoptically in order to reduce the time required to test both eyes (17;103-108). The LCD projector has been used extensively in this department for clinical mfERGs (64).

The relative merits of two locally available modes of stimulus delivery are compared in Table 6.1:-

CRT	LCD projector system
Becoming less readily available as LCD screens replace CRT monitors.	Projector readily available, screen custom made.
CRT monitors were readily available 10 years ago.	LCD screens are increasingly widely available.
Can present many different stimuli.	Can present many different stimuli.
Luminance and contrast can be varied.	Luminance and contrast can be varied.
Stimulus presentation rate fixed at 75Hz or manufacturer specified rate.	Stimulus presentation rate fixed at 75Hz or manufacturer specified rate.
Maximum size that can be viewed comfortably is restricted to ~ 45° of whole visual field.	A larger field of view can be stimulated.
Resolution of 640x480 pixels to 1024x768 pixels, typically.	Fixed resolution of 800x600 pixels.
Luminance profile 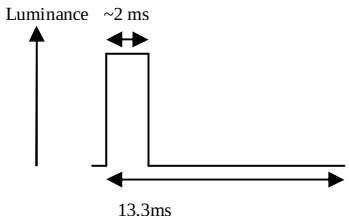	Luminance profile 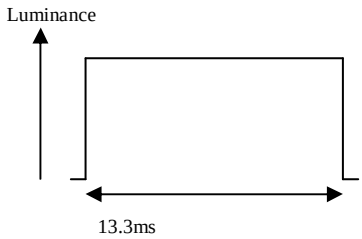

Table 6.1 *The relative merits of two locally available modes of multifocal stimulus delivery.*

6.2 The Cathode Ray Tube

Until recently the cathode ray tube or CRT monitor is the most common method of presenting the stimulus. It is now being replaced by LCD screens but has been widely used in the past.

The CRT image is formed by the incidence of an electron beam on a phosphorescent material. Electromagnetic coils deflect the beam from the left to the right of the screen for each line and from top to bottom in a raster during each frame or period of the refresh rate. Beam deflection is controlled by a time base generator in the display unit. The computer supplies synchronising pulses for the timebase generator. The brightness of the beam is controlled by the stream of pixel data which the computer supplies for each line of the raster.

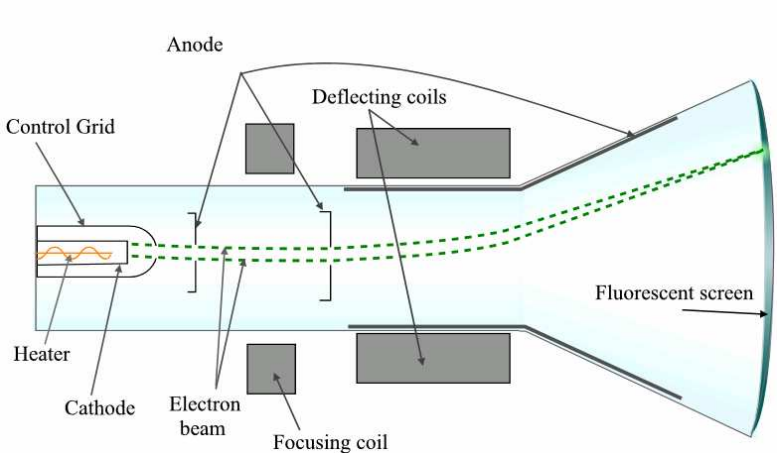

Figure 6.1 *Cathode Ray Tube (Copied from Wikipedia with permission under GNU Free Documentation License)*

A key feature of the CRT monitor is the ability to evoke responses with a high refresh rate of the monitor. This is typically 75Hz, which permits the study of the non-linear aspects of multifocal responses. The fast stimulation rate also allows a large number of averages to be acquired in a short period of time, thereby enhancing the signal to noise ratio. 75Hz translates to a frame period of 13.3ms.

6.3 Liquid Crystal Display Projector Delivery

Liquid crystals exhibit the properties of both solids and liquids and are nearly transparent. Transmitted light becomes aligned with the orientation of the constituent molecules. Applying a voltage to the liquid crystal changes the molecular orientation and hence the alignment of transmitted light. Placing polarising filters on either side of the liquid crystal means that the application or absence of an applied voltage can control whether light is transmitted or not.

LCD (liquid crystal display) projectors commonly contain three separate LCD panels, one each for the red, green, and blue components of the image signal. A halogen lamp emits light with an ideal colour temperature and a broad colour spectrum that is split by a prism. As each colour or frequency band passes through the LCD panels, individual pixels can be opened or closed to transmit or block the light, respectively. This modulation produces the image that is projected on to the screen by allowing many different shades from each colour LCD panel.

6.4 Luminance Profiles

Like the CRT, the LCD projected image is produced on a raster basis. However, the luminance of the pixel remains constant until the raster returns to it to update it with new information for the next frame of the stimulation.

Raster times are different in CRT and LCD displays and it is necessary to adjust the cross-correlation process to correct for these differences. This capacity is incorporated into the EDIU Multifocal System software.

The pulse width for a CRT system is dependent on the type of phosphor and is typically 2msec whereas the LCD projection system produces a longer pulse, which is dependent on the base period of the stimulation rate (i.e. 13.3msec for a 75Hz stimulation rate).

LCD projectors can provide higher stimulus intensity and a wider field of view.

There is a fundamental difference between the two systems, as has been illustrated by slowing the rate of stimulation during mfERG recordings (99). m-sequences are slowed by inserting filler frames. A filler frame is simply a frame in which the m-sequence does not move forward. The stimulus appears unchanged and therefore slowed. When this happens, the CRT monitor will deliver a series of pulses at 13.3ms

intervals for an extended 'ON' period, while the LCD will deliver a constant high luminance for the same duration. The mfERG response to a 2 black – 2 white filler experiment is illustrated. It shows a characteristic splitting of the main complex with the CRT stimulus due to two on-pulses. The splitting is absent from responses evoked by the LCD stimulus.

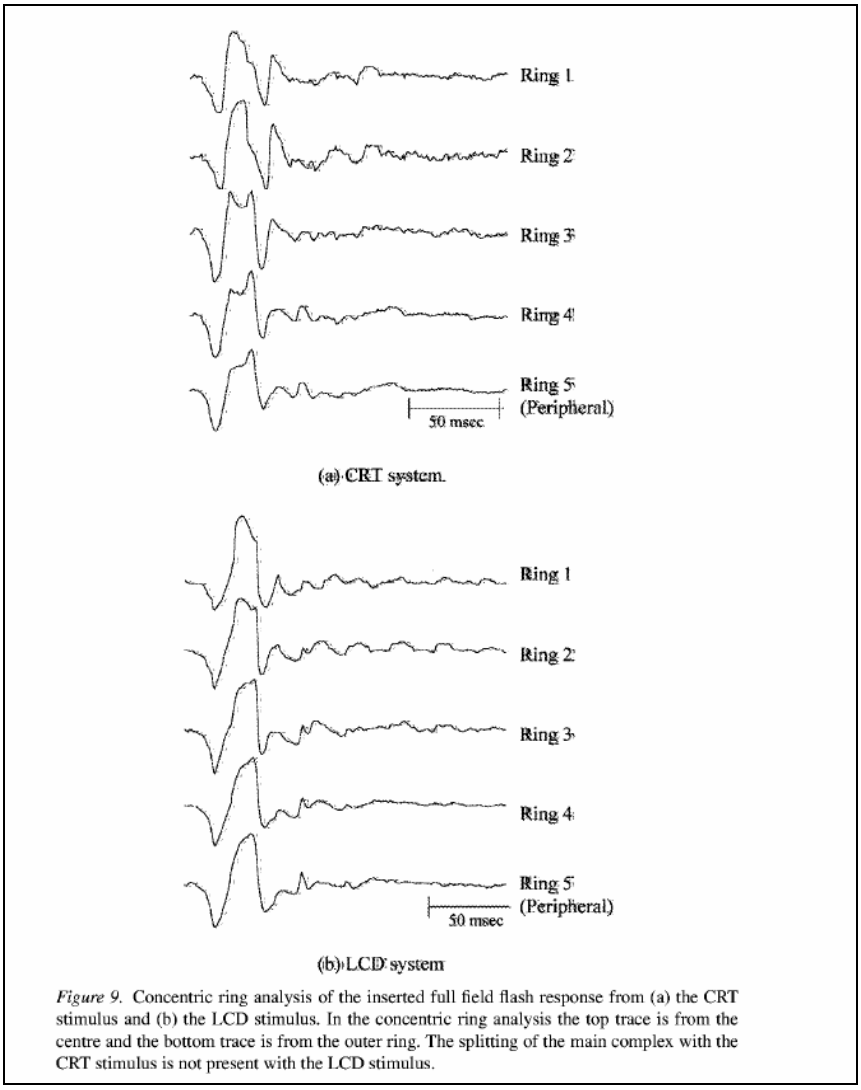

Figure 9. Concentric ring analysis of the inserted full field flash response from (a) the CRT stimulus and (b) the LCD stimulus. In the concentric ring analysis the top trace is from the centre and the bottom trace is from the outer ring. The splitting of the main complex with the CRT stimulus is not present with the LCD stimulus.

Figure 6.2 *Reproduced from Keating et al 2001 (99) with permission.*

Gawne & Woods (142) investigated the effect of CRT versus a constant luminance stimulus in primates and discovered differences in the evoked responses when pulses or flash duration was 10ms or less. While the base period of a 75Hz stimulus presentation mode is 13.3ms, the luminance profile of the CRT changes over shorter time periods. We may therefore expect to see differences in mfVECP responses based on the type of stimulus presentation method.

6.5 Stimulated Field of View

Increasing the field of view (FOV) during mfVECP recordings potentially allows us to test the function of a greater proportion of the visual field. Simultaneously maintaining the same stimulus geometry reduces the resolution of visual cortex function mapping and increases the likelihood of dipole cancellation.

Wide field stimulation has been successful used in the mfERG, where it has been shown to identify peripheral retinal toxicity in patients receiving vigabatrin for the treatment of epilepsy (60). It was concluded that the sensitivity of the standard mfERG, classed as a stimulus of less than 60° diameter of the FOV, would be unlikely to improve on the accuracy of the simple full-field flicker ERG.

It has been observed that '..the mfVECP only gives large responses to central foveal stimulation, which limits its usefulness in detailed visual field mapping. A number of factors account for the strong foveal and weak peripheral mfVECP (and VECP in general): the higher concentration of receptive fields in central foveal retina; the larger striate cortical generator area for the foveal and parafoveal projection; the posterior location and radial orientation of dipoles for central foveal stimulation. The latter factor maximises the foveal VECP, since the VECP preferentially records radial currents; the anterior and more tangential dipoles which represent peripheral stimulation produce smaller VECPs.' (11)

Despite this, current literature indicates that mfVECPs have been recorded from fields of view ranging from 6° of radius to 40.5°. Table 6.2 indicates the fields of view used by both the larger mfVECP research groups as well as those used in some smaller groups.

Field of View (radius)	Publication
16°	James AC (17)
MfVECPs recorded using close packed, scaled hexagonal regions filled with a black and white triangular pattern which was 42° by 42°. (radius 21°)	Hasegawa & Abe (143)
21.1°	Fortune B & Hood DC(109).
Hood and co-workers use a radius of 22.25°	Hood *et al* (14;19;144;145).
22°	Hoffman *et al* (120).
24° radius with the nasal step reaching 33°	Graham *et al* (68)
26°.	Graham *et al* 1999(70)
27°.	Graham *et al* 2000 (71)
The ObjectiVision^{TM} system is used with a 26° radius field of stimulation with an additional nasal step out to 32°	Goldberg *et al* (67) 2002.
26°	Martins *et al* 2004 (116) used 26° with no mention of a nasal step.
6-40.5°	Hood *et al* varied the field of view(146). This used 16 regions in the dartboard stimulus rather than 60.
8°	Wang *et al* (11)

Table 6.2 *The range of fields of view used to stimulate mfVECPs.*

6.6 Experiment 1 –mfVECP responses to CRT and LCD Projector Delivered Stimulation.

6.6.1 Aim

To compare mfVECP responses when delivered by CRT and LCD projectors.

6.6.2 Introduction

This experiment will be sub-divided. Experiment 1a describes the luminance matching of the CRT and LCD displays. Experiment 1b presents mfVECP acquisitions made using the CRT and LCD displays for stimulus delivery.

6.6.3 Experiment 1a – Luminance Matching

6.6.3.1 Methods

A high-luminance CRT monitor (Richardson Electronics, UK) was set to its highest luminance and the luminance of the LCD projection system was adjusted to match it as closely as possible. Luminance measurements were made with a regularly calibrated (147) spot photometer (Minolta LS-100, Minolta Camera Co. LTD, Japan), using the instantaneous luminance measurement setting. A mid-peripheral ring on a 40° stimulus was chosen to standardise the luminance between the two systems. A 60 hexagon mfERG flash stimulus was used to perform the luminance measurements, as the hexagons gave a larger region on to which to focus the luminance meter. The checks on the mfVECP dartboard stimulus were too small to make a measurement without partial area effects.

6.6.3.2 Results

Horizontal and vertical luminance profiles are depicted in Figures 6.3 & 6.4.

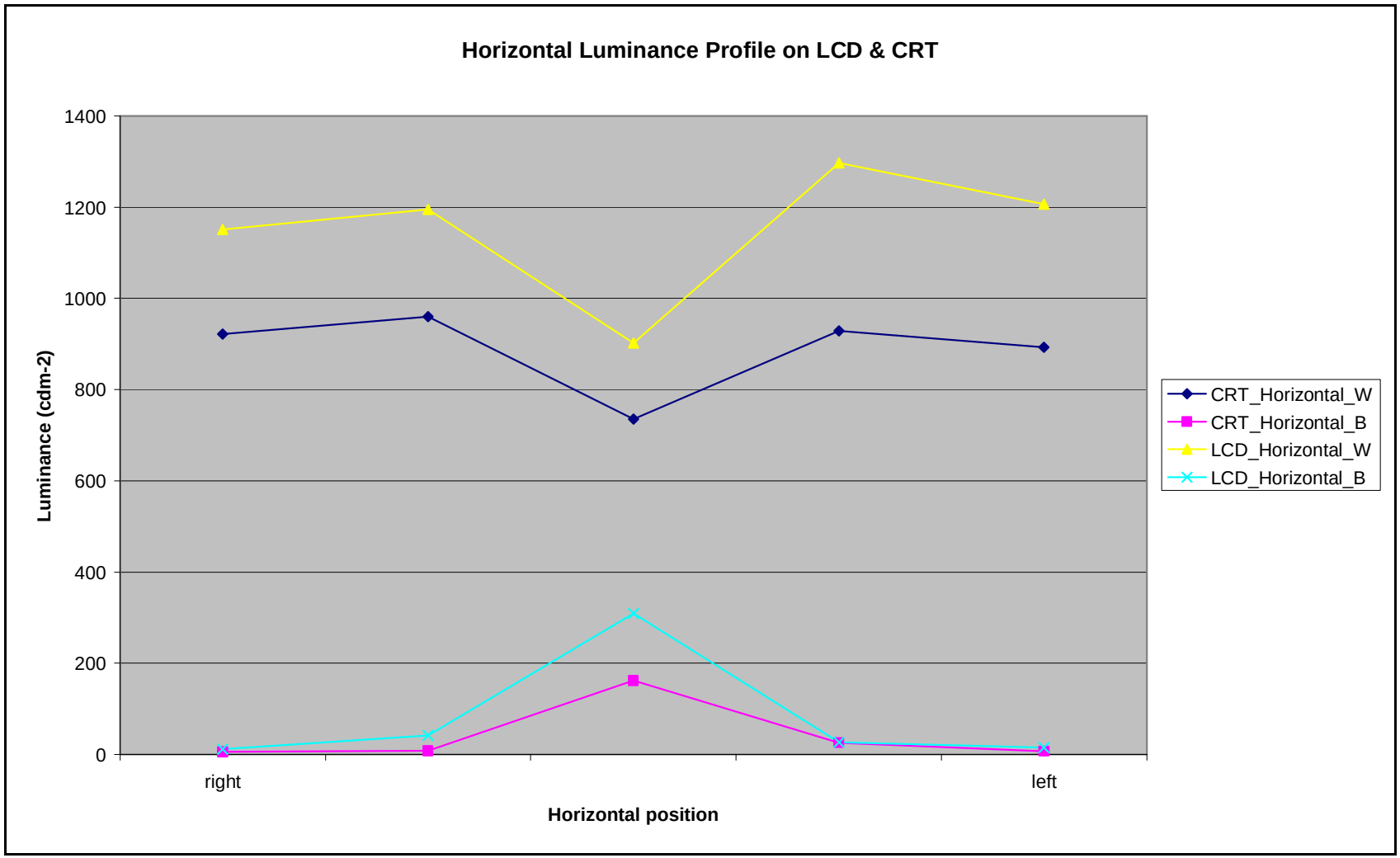

Figure 6.3 *Horizontal luminance profiles for LCD and CRT screens.*

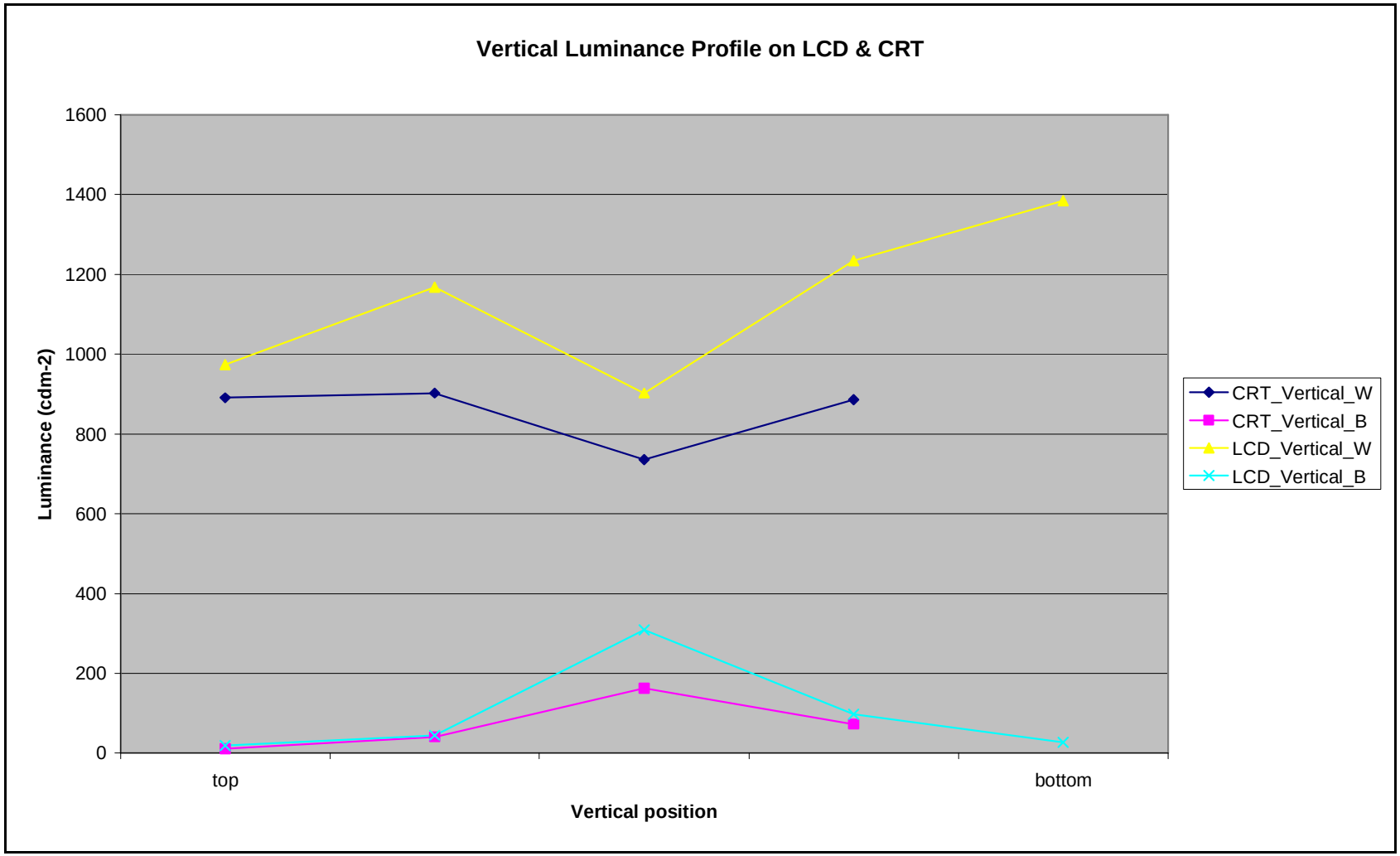

Figure 6.4 *Vertical luminance profiles for LCD and CRT screens.*

Luminance is not uniform across the whole field of view, with both the CRT and LCD projector system showing higher peripheral luminance for white regions and lower peripheral luminance for black regions.

Luminance profiles were matched as closely as possible, however they were limited by the resolution of the LCD projector settings. As a result, the LCD projector remains brighter (average white luminance = 1141cd.m^{-2}) than the CRT screen (average white luminance = 873cd.m^{-2}).

Recommended luminance levels for the mfERG are 100-200cd/m^2 for bright regions, 50-100 cd/m^2 for dark regions with a mean background luminance of 50-100 cd/m^2 (63).

The Standard for acquiring VECPs (27) suggests a minimum luminance of 80 cd/m^2 for white regions. It does not state a maximum, but does state a minimum contrast of 75% and suggests that luminance should be constant to within 30%.

Our LCD projection system showed a maximum variation of 21%, while the CRT showed a maximum variation of 16%.

CRT contrast, as calculated by Equation 6.0, varied from 99% at the periphery to 64% centrally.

LCD contrast varied between 98% at the periphery to 49% centrally.

$$Contrast = \frac{(L_{MaX} - L_{MIN})}{(L_{MaX} + L_{MIN})} \quad (30) \qquad \textbf{Equation 6.0}$$

Both systems therefore comply with the ISCEV VECP standard in terms of luminance variation, but are below the recommended contrast levels centrally. Luminance was matched as closely as possible, but the resolution with which modifications could be made prevented good agreement and left the LCD projector provided brighter stimulation.

6.6.4 Experiment 1b – Comparing CRT and LCD Presented Stimuli in the mfVECP

6.6.4.1 Methods

mfVECP responses were recorded from four normal, healthy volunteers with no known ophthalmic or neurological conditions, using the EDIU Multifocal System. Subjects were optimally refracted using their own spectacles and their pupils were not dilated. Recordings were monocular. Stimulation was provided by a 60-region dartboard pattern. Each region contained a 4x4 black and white checkerboard pattern and the size of the regions was scaled for cortical magnification.

M-sequences of length m=12, 13, 14, 15 and 16 were used to drive the pattern reversal of the stimulus regions at a rate of 75Hz. Acquisition time was approximately 1, 2, 4, 8 or 16 minutes depending on m-sequence length. This was divided into 30 second overlapping periods to allow the subject to blink and rest, in order to maintain good fixation.

mfVECPs for each m-sequence length were repeated with the stimulus presented on a CRT monitor and projected onto a screen with an LCD projector. Luminance and contrast details were reported in the previous section. In both cases, the stimulus subtended 20.5°of radius of the visual field.

Ag/AgCl electrodes were placed 4cm above the inion, 4cm left and right of the inion and 1cm below the inion on the midline. Acquired channels were Channel 0 = 4cm above the inion – 1cm below the inion, Channel 1 = 4cm left of the inion – 1cm below the inion, Channel 2 = 4cm right of the inion – 1cm below the inion and Channel 3 = 4cm left of the inion – 4cm right of the inion, similar to the montage employed by Hood *et al* (19). A reference electrode was placed at International 10-20 position F_Z and a ground electrode was placed on the temple. Electrode impedances were matched and below 5kΩ. The skin was prepared with abrasive gel and the electrodes affixed with conductive paste.

Signals were sampled at 1200Hz recorded with a 0.1 to 100Hz analogue filter and filtered through a 3-30Hz digital bandpass prior to cross-correlation.

Signal to noise ratios were calculated using the DeadM sequence characterisation of noise described in Chapter 4, and the signal window was taken as 45-150ms.

The cut-off used to identify a SNR as indicative of a detectable waveform was the 90^{th} percentile of the distribution of SNR values calculated from the noise estimations, providing a specificity of 90%.

In order for a stimulating region of the dartboard to produce a detectable waveform, it must produce a signal to noise ratio above the cut-off in at least one of the four recording channels. The maximum number of detectable waveforms from four recording electrodes is therefore 60.

6.6.4.2 **Results – Experiment 1b**

It was not possible to complete the m=12 recording for one of the four volunteers. All other recordings were successfully completed.

mfVECP responses using CRT and LCD stimulation differ.

Figure 6.5 shows Channel 0 (4cm above the inion -1cm below the inion), m=16 recordings.

Points of note include:-

- Subject JC shows clear central waveforms in the right hemifield on CRT recordings that are almost absent on LCD. This location is highlighted by arrow A.
- Subject DK shows clear waveforms on the lower left quadrant (of trace array) of the CRT response that are absent on the LCD. Indicated by arrow B.
- Subject DK – upper hemifield – third ring, counting from inside, shows small waveforms on LCD stimulation that are missing from CRT. Indicated by arrow C.
- Subject GA – there are lower field locations (just below the midline) which show waveforms on LCD but not CRT. Indicated by arrow D.
- Subject AM has trace arrays that are, in the main, very similar. However there is a peripheral region stimulating the lower field of view which evokes a response with the CRT but not the LCD.

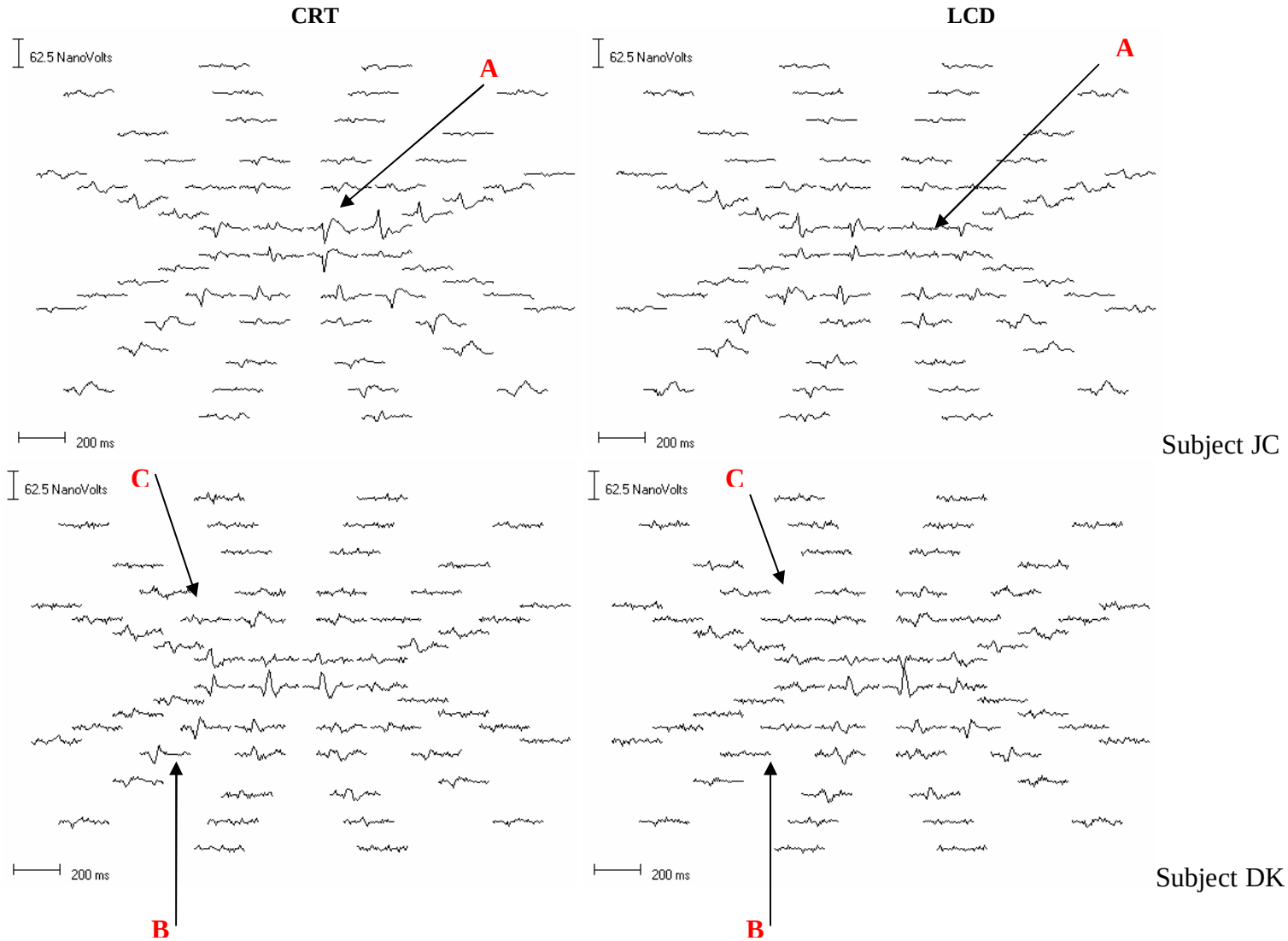
CRT
LCD
62.5 NanoVolts
A
200 ms
Subject JC
C
B
Subject DK

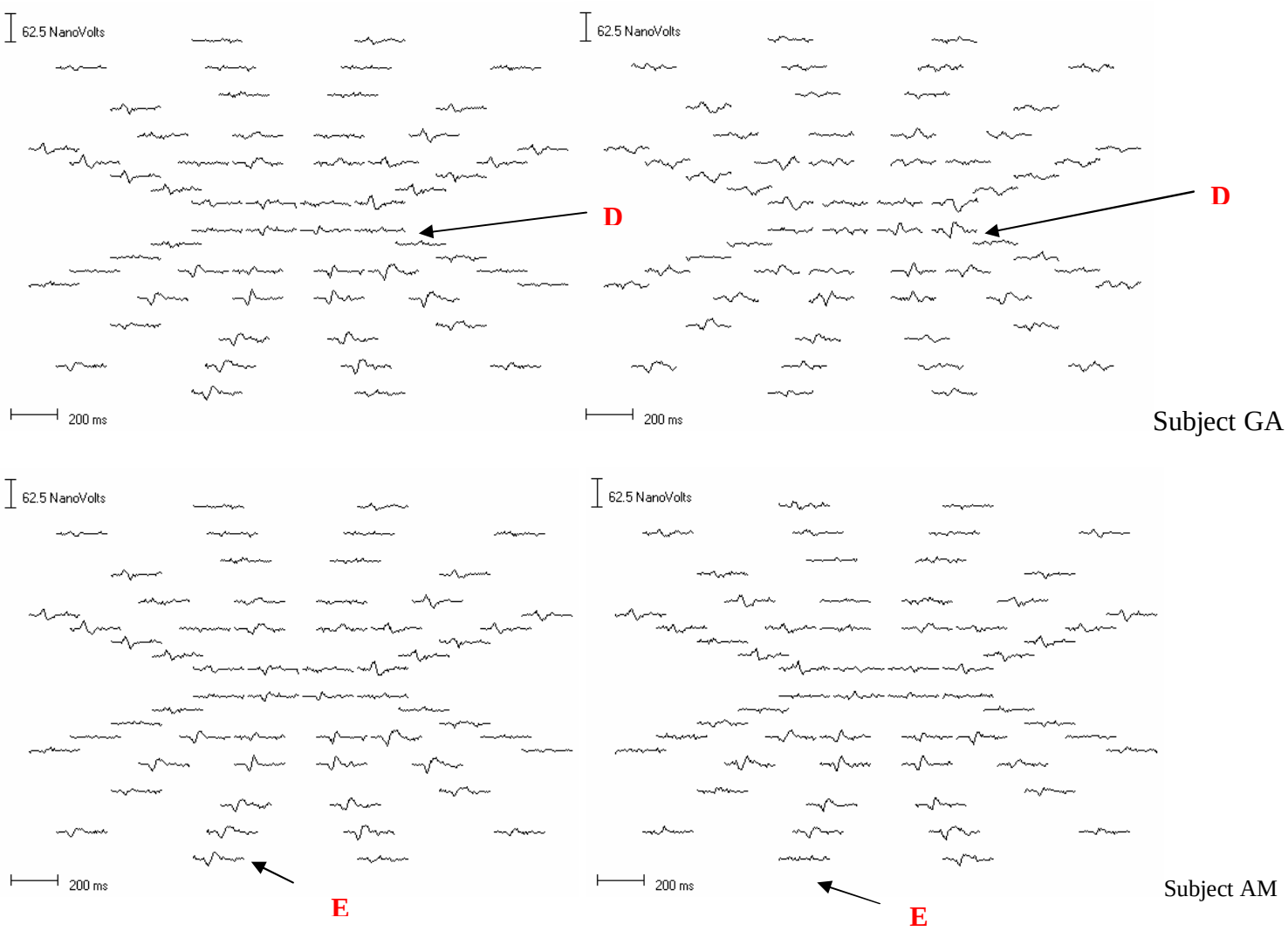

Figure 6.5 *mfVECP trace arrays from Channel 0. Data in the left hand column was acquired when the stimulus was presented via CRT, with responses to LCD stimulation on the right. Each row contains data from a different subject. m-sequence length was 16.*

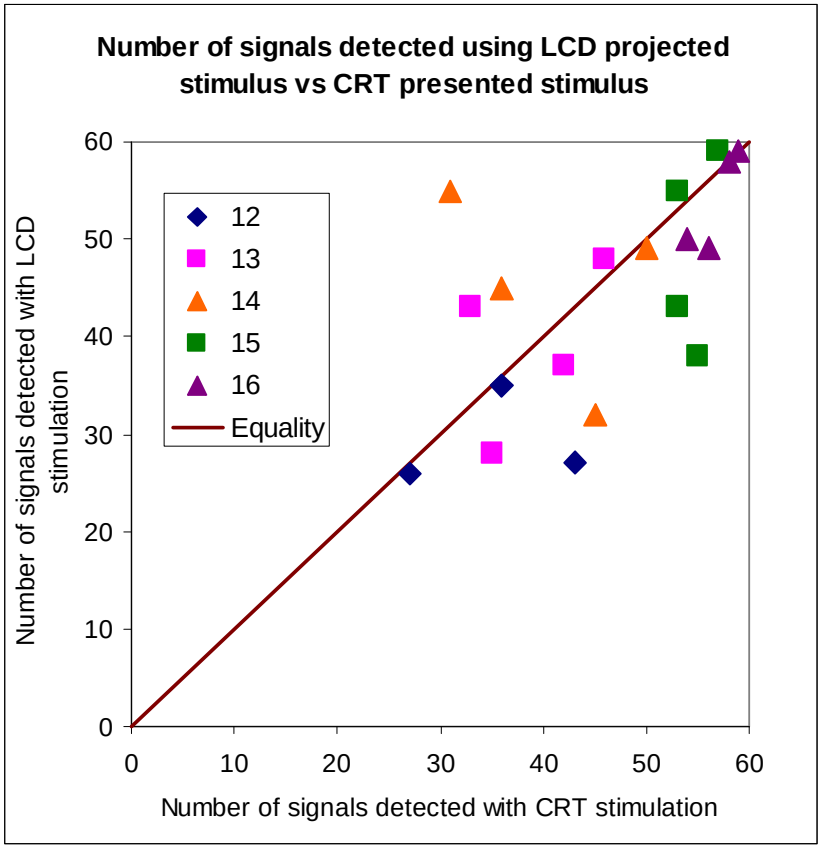

Figure 6.6 *The number of detectable waveforms achieved with LCD vs. CRT stimulation is plotted. The solid line is the line of equality. Each series of data indicates the use of a different m-sequence length. Each datapoint refers to one healthy volunteer and summarises the trace arrays from the four recording channels.*

Figure 6.6 encompasses all the data acquired in this experiment. Each data point indicates the number of waveforms that were detectable when stimulation was performed with the LCD stimulus, plotted against the number of waveforms detected when the CRT was used. The solid line indicates the line of equality. Points to the left of the line indicate better waveform detection with LCD stimulation. Points to the right indicate better performance with CRT stimulation. Each series indicates acquisitions made with a different m-sequence length.

As the m-sequence length increases, the number of detectable waveforms increases for both CRT and LCD stimulation.

There is some scatter about the line of equality, indicating that there is no clear cut answer to the question of which mode of presentation is superior. However, when m-

sequences are of length m=15 or 16 (green squares and purple triangles, respectively), the data points tend to lie to the right of the line, suggesting better performance with the CRT.

An Anderson Darling Normality Test was performed to find out whether the SNR values were normality distributed. With both datasets (CRT and LCD), the test returned a p-value of <0.001 indicating that the null hypothesis that the data are normally distributed can be rejected. Non-parametric tests were therefore used for further analysis.

The median SNR value for an m=16 recording was 1.5093 for the CRT dataset and 1.3603 for the LCD dataset.

The SNR values for each stimulus region, channel and volunteer were compared using a Wilcoxon signed rank test. It rejected the null hypothesis that the samples came from the same distribution at the p=0.01 level.

The same analysis was repeated for the m=15 recordings. This time the median SNRs were 1.2332 and 1.2256 for CRT and LCD stimulation, respectively. The Wilcoxon signed rank test was not significant at the p=0.05 level.

6.6.4.3 Discussion

The choice between using an LCD projector or CRT monitor to deliver the mfVECP stimulus makes a slight but significance difference in recordings of m-sequence length m=16, in terms of signal quality and detection.

A significant difference in SNR was not seen with m=15 recordings, possibly due to the higher noise contribution in these signals.

Beyond differences in signal amplitude or SNR, differences are identified in the presence or absence of some waveforms and the waveshape. These differences are not seen throughout the whole trace array.

6.6.4.4 Conclusion

The CRT evokes a very slightly stronger signal, there is therefore, no reason to recommend the introduction of the LCD projection system into mfVECP practice, unless there is a requirement to stimulate very large fields of view.

6.7 Experiment 2 - mfVECP Field of View

6.7.1 Aim

To determine an optimal field of view for stimulation during the recording of the mfVECP.

6.7.2 Methods

mfVECPs were recorded with stimulated fields of view of 10, 20, 30 and 40° radius.

mfVECP responses were recorded from 10 normal, healthy volunteers with no known ophthalmic or neurological conditions, using the EDIU Multifocal System. Their mean age was 34.5 years (standard deviation 12.4 , range 23-52). Subjects were optimally refracted using their own spectacles and their pupils were not dilated. Recordings were monocular and made from the right eye.

Stimulation was provided by a 60-region dartboard pattern. Each region contained a 4x4 black and white checkerboard pattern and the size of the regions was scaled for cortical magnification. The stimulus was back-projected onto a screen using an LCD projector. The stimulus subtended 10°, 20° 30° or 40° radius of the visual field. The luminance of white areas varied across the screen from 735 cdm^{-2} to 960 cdm^{-2} and black areas varied from 6 cdm^{-2} to 162 cdm^{-2}. Contrast varied from 99% peripherally to 64% at the centre of the screen.

The field of view was varied by altering the subject to screen distance.

An m=15 bit m-sequence was used to drive the pattern reversal of the stimulus regions at a rate of 75Hz. Acquisition time for each recording was approximately eight minutes, divided into 30 second overlapping periods to allow the subject to blink and rest, in order to maintain good fixation.

Data was recorded from midline bipolar channels as follows and incorporates a selection of electrode positions used by Hood *et al* (19) and Klistorner and Graham (16):

Channel 0 = 10% above the inion – 30% above the nasion, Fz.

Channel 1 = 2cm above the inion – 6cm below the inion,

Channel 2 = 2cm above the inion – 4.5cm below the inion,

Channel 3 = 4cm above the inion – the inion.

Ag/AgCl electrodes were used and impedances were matched and below 5kΩ. The skin was prepared with abrasive gel and the electrodes affixed with conductive paste. A reference electrode was placed at International 10-20 position F_Z and a ground electrode was placed on the temple.

Signals were sampled at 1200Hz recorded with a 0.1 to 100Hz analogue filter and filtered through a 3-30Hz digital bandpass prior to cross-correlation.

6.7.2.1 Analysis

SNRs were calculated using the DeadM approach to noise characterisation, described in Chapter 4. A cut-off was determined, below which a waveform was not considered detectable. The cut-off was selected to provide a specificity of 90%. The signal window was taken to be 45-150ms.

6.7.3 Results

Technical difficulties prevented completion of the protocol with one subject. Analysis is therefore based on data from n=9 subjects.

Figure 6.7 shows an example of mfVECP responses to stimulation of the four fields of view in a single subject from Channel 0 (10% of the nasion-inion distance above the inion referenced to F_z). In the top right corner, is the numbering system used to identify the regions of the stimulus and their corresponding waveform responses.

From this, several observations can be made:

- Waveform 54 in the FOV=10° recording can be seen to contribute to Waveform 59 when the FOV is expanded to 20° and the central region stimulates to a greater eccentricity.
- Waveform 32 in the FOV=30° recording can be seen at location 44 in the FOV=40° recording.
- Recognisable waveforms can be seen in some peripheral positions for recordings made with a field of view up to 30°. The most eccentric waveforms in the FOV = 40° recording do no contain clear mfVECP responses, in this individual, for this recording channel.

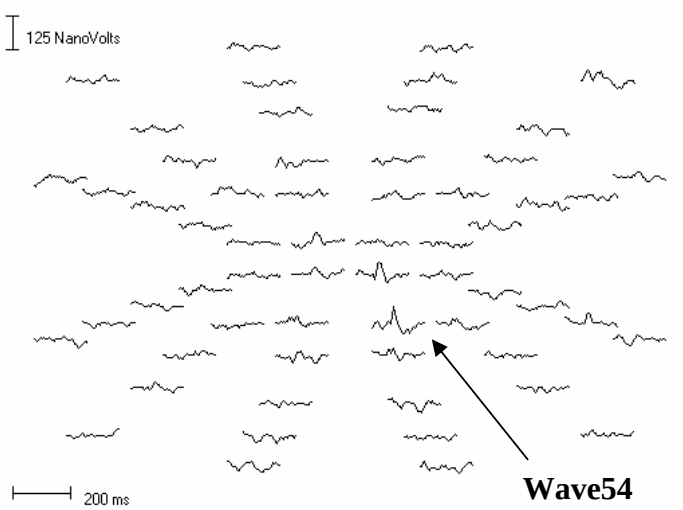

FOV Radius = 10°

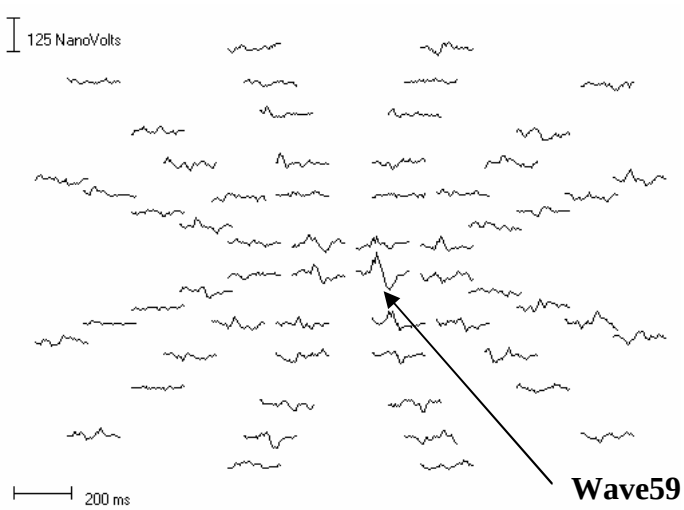

FOV Radius = 20°

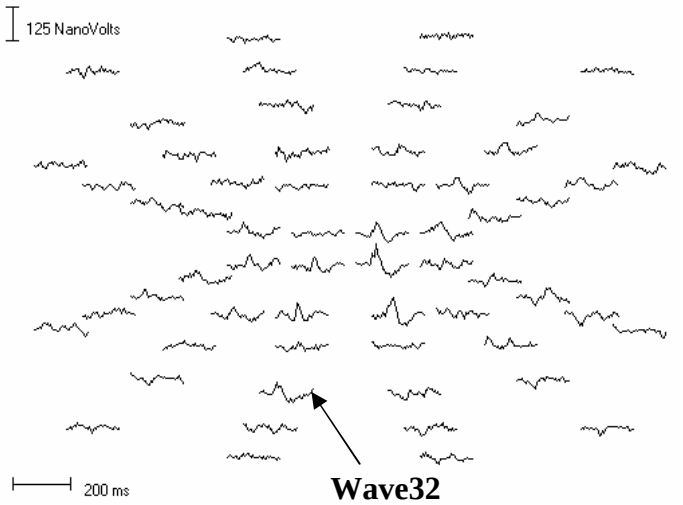

FOV Radius = 30°

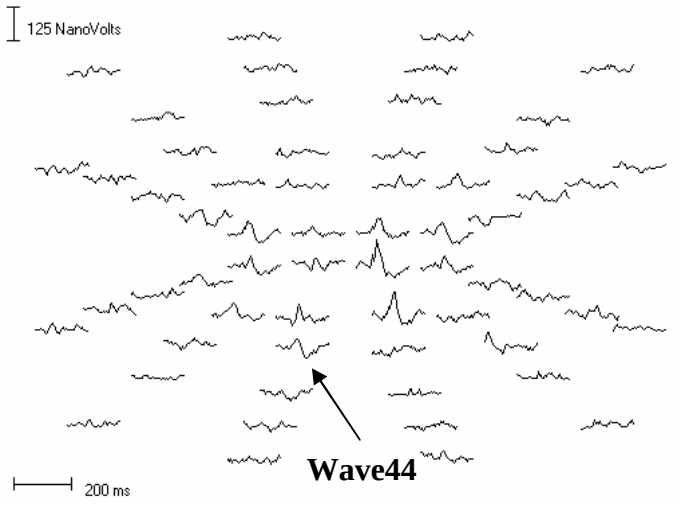

FOV Radius = 40°

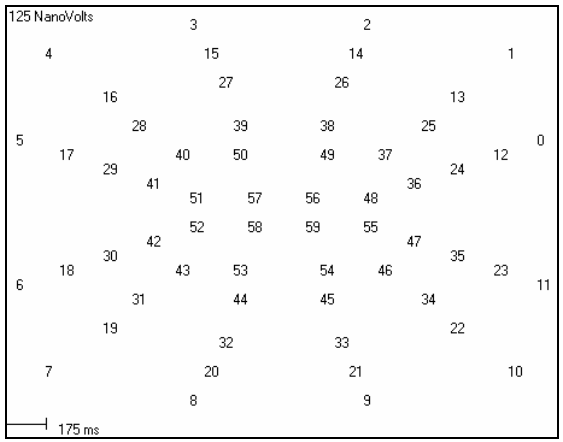

Figure 6.7 *An example of the changes seen in the trace array as the radius of the FOV was increased from 10° to 40°. All trace arrays were acquired from the same subject with Channel 0. Waveforms which appear peripherally on the small FOV recordings can be seen more centrally on larger FOV recordings, as expected. The inset in the top right corner is the numbering system used to identify the regions of the stimulus and their corresponding waveform responses.*

For the subject whose data are shown in Figure 6.7, the number of detectable waveforms seen with each FOV acquisition is shown in Table 6.3.

In this subject we see a trend towards a greater proportion of the waveforms being detectable above noise as the field of view increases. There does not appear to be any benefit to increasing the FOV from 30° to 40°.

Data for the peripheral ring indicates that Channel 0 was unable to acquire any detectable signals from the most peripheral stimulating ring.

FOV	Whole Trace Array Channel 0	Whole Trace Array All Channels	Peripheral Ring Channel 0	Peripheral Ring All Channels
10°	17 (28%)	39 (65%)	3 (25%)	5 (42%)
20°	11 (18%)	37 (62%)	3 (25%)	6 (50%)
30°	26 (43%)	49 (82%)	4 (33%)	7 (58%)
40°	26 (43%)	49 (82%)	0 (0%)	6 (50%)

Table 6.3 *The number of detectable waveforms in the trace arrays acquired with increasing field of view (FOV) is shown for a single subject. Data are presented for the whole trace array of 60 waveforms and for the peripheral ring which contains 12 waveforms.*

Figure 6.8 shows the relationship between the number of detectable waveforms from the whole trace array and the field of view of stimulation. Data are plotted for each volunteer and for the average of the volunteers. There is clearly a wide range of individual relationships, but the overall trend is for a slight increase in detection rates with increasing FOV, up to 30° of radius.

A similar plot was created for the peripheral waveforms only. A drop in detection was seen when the stimulus was increased to 40° of radius.

.

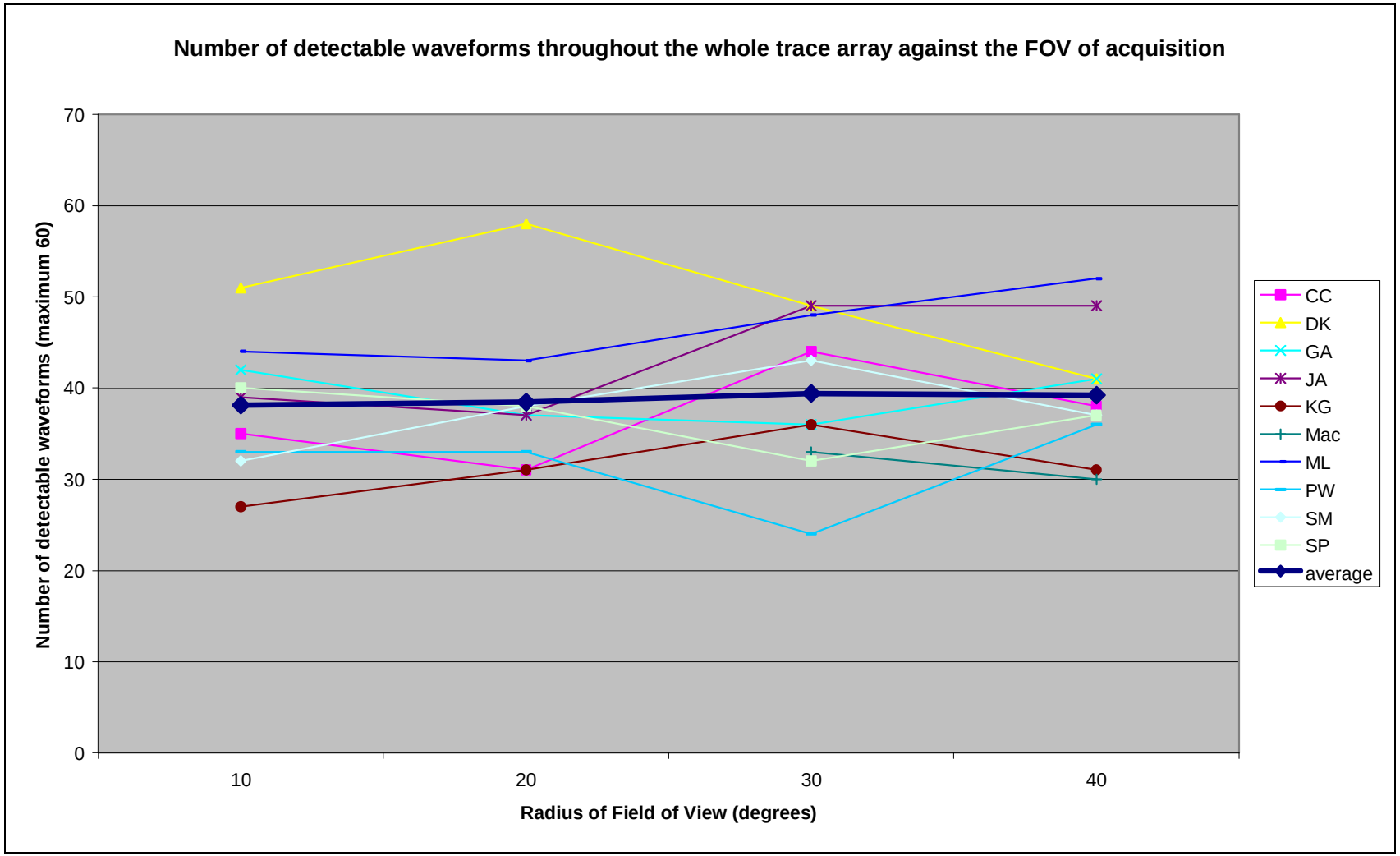

Figure 6.8 *The number of detectable waveforms in the whole trace array is plotted against the field of view of acquisition.*

6.7.4 **Discussion**

Reducing the FOV increases the local spatial resolution, but decreases the volume of visual cortex and therefore, possibly the size of signal measurable.

Data presented here suggests that there is no benefit to increasing the FOV over 30°. As the FOV increases, the area that each stimulus region stimulates increases and it is possible that dipole cancellation occurs. It is also possible that the signal from very peripheral areas is too far from the occipital pole to be reliably measured with these recording electrodes.

6.8 Reproducibility

There is a small overlap of data between the investigations of CRT and LCD stimulus presentation and the optimal FOV. Two volunteers were involved in both experiments.

Channel 0 data in the CRT vs LCD comparison was acquired from a bipolar electrode channel with the signal 1cm below the inion subtracted from that measured 4cm above the inion. The stimulus subtended 20.5° of the visual field. Using the recording made with the LCD projector delivering the stimulus, this can be compared to data acquired with Channel 3 during the FOV experiment when the FOV was 20°. Channel 3 acquired data from 4cm above the inion – the inion. The lower electrode was therefore 1cm higher in the FOV dataset than the CRT vs LCD dataset and the stimulated field of view was different by 0.5° of radius.

The waveforms are not identical, but indicate reasonable reproducibility, bearing in mind the small differences in recording parameters. This degree of similarity was seen in both subjects and is illustrated in Figure 6.9.

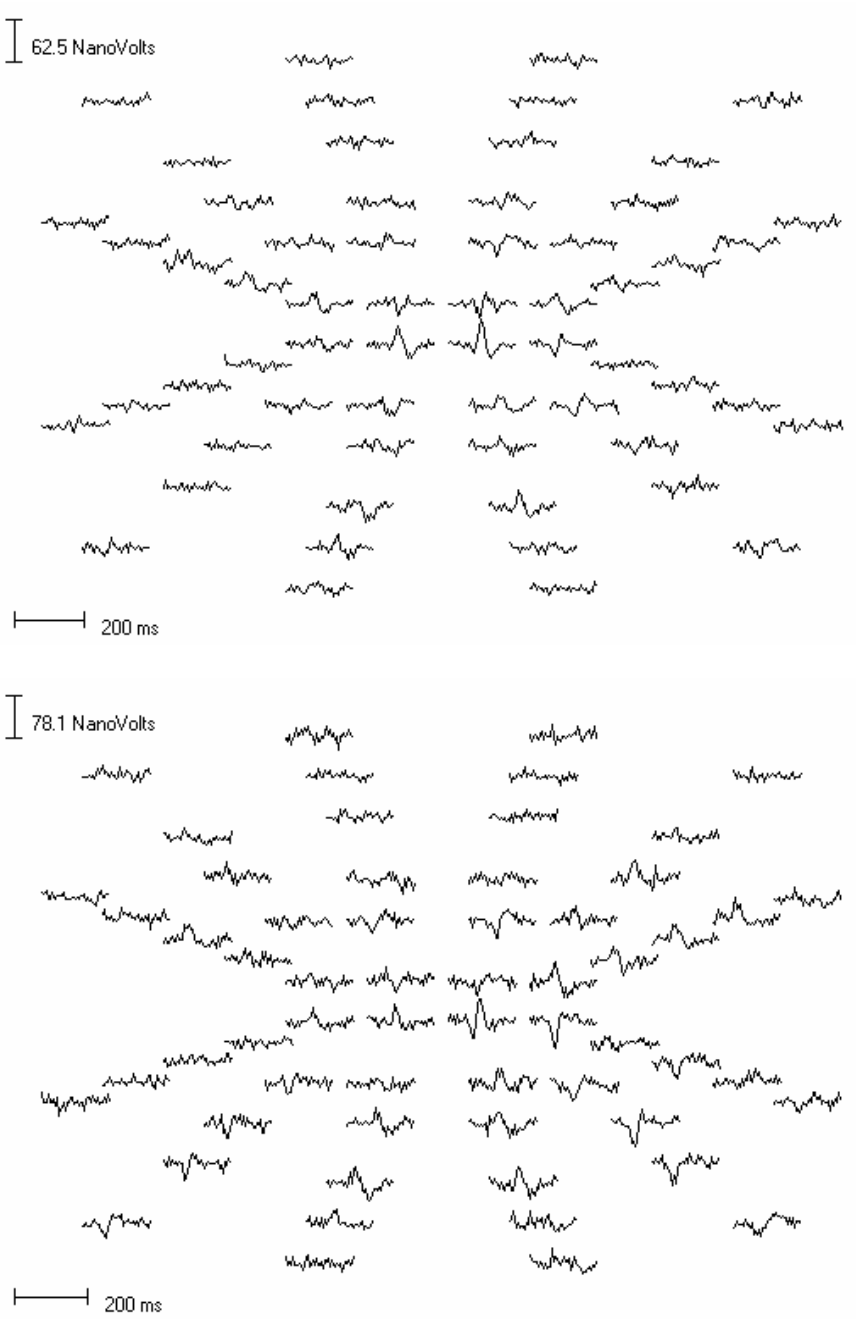

Figure 6.9 *Reproducibility of waveforms.*

Top Trace Array *Data acquired during the CRT vs LCD comparison. Recording parameters were as follows: FOV= 20.5°, bipolar recording channel, 4cm above the inion - the inion., presented via an LCD projector, 75Hz stimulation rate and an m-sequence length of m=15.*

Lower Trace Array *Data acquired during the FOV experiment. Recording parameters were as follows: FOV= 20°, bipolar recording channel, 4cm above the inion - 1cm below the inion, presented via an LCD projector, 75Hz stimulation rate and an m-sequence length of m=15.*

6.9 Stimulus Delivery Discussion

The luminance used in this experiment was higher than is commonly used elsewhere (70;129). Schimitzek & Bach (148) investigated the effect of luminance on the mfERG and found a linear increase in response density with luminance, up to 700cd.m^{-2}. They indicated subject discomfort at 700cd.m^{-2}, but that was not our experience.

The luminance and contrast of the CRT and LCD projected images were matched as closely as possible, but there remained differences between the displays and a non-uniformity across the screen in both cases, possibly arising as a result of scatter, or in the case of the CRT, of phosphor burn in the centre of the screen.

To date, luminance levels have been measured in terms of cd.s.m^{-2} for the ERG (149) and in cd.m^{-2} for the VECP(27) and the mfERG (63). The use of the time integrated unit for the ERG is advocated because flashes are recommended to be less than 5ms in duration (149) and 'temporal integration of the neuronal visual pathways is longer than the flash produced by a xenon flash tube'(147). The use of cd.m^{-2} for the VECP and mfERG is appropriate when all users employ stimulus presentation techniques that have the same luminance profile; however it may result in difficulties when new stimulation methods are used.

As discussed in the introduction, the luminance profile of a CRT screen with a 75Hz frame rate can be approximated as a 2ms square wave pulse of high luminance followed by 11.3ms of low luminance. This 'flash' duration is of the order of the duration of an ERG flash stimulus, and so it may be more consistent to use the unit of cd.s.m^{-2} for all visual electrophysiology standards.

To illustrate the impact of differing luminance profiles, consider a mfERG stimulus presented either by a CRT monitor or LCD projector system. Each hexagonal region has a 50% probability of being a 1 (high luminance) at any point in time. Over a period of 1 second (75 frames), this region will be white for 37.5 frames or 0.5sec, on average.

Assuming a nominal peak luminance of 100cd.m^{-2} for both a 75Hz CRT and a 75Hz LCD projector delivered stimulus, and idealised square wave profiles in both cases (see Table 6.1), the time integrated luminance with be:

CRT

Time integrated luminance = High luminance x time on

= High luminance x frame duration x no. of frames with a white region x fraction of frame during which luminance is high.

= 100 cd.m^{-2} x 37.5 x13.3x10-3 s x (2/13.3)

= **7.5 cd.s.m^{-2}**

LCD

Time integrated luminance = High luminance x time on

= High luminance x frame duration x no. of frames with a white region x fraction of frame during which luminance is high.

= 100 cd.m^{-2} x 37.5 x 13.3x10-3 s x (13.3/13.3)

= **50 cd.s.m^{-2}**

There is significantly more energy incident on the retina during stimulation via an LCD projector, however, the mfVECP is a response to pattern reversal rather than luminance and so we should not expect to see a significantly greater response to the higher levels of incident energy provided by the LCD projector.

Bearing in mind the variation of stimulus presentation techniques presently available, it may be worthwhile for the next revision of mfERG standards to consider recommendations, either in terms of temporally integrated luminance, or by making specific reference to luminance profiles.

In addition to the difference in incident energy, the contribution of ON and OFF responses will differ. With CRT stimulation, an ON response will be evoked at the beginning of each frame, with an OFF response being evoked 2ms later. LCD stimulation does not provide ON and OFF responses in this way, and provides contrast reversal stimulation only.

Furthermore, different LCD projectors have different luminance profiles and this may cause inter or even intra lab differences. If a new LCD projector is introduced to a laboratory, the luminance profile should be checked and compared with that of

existing LCD projectors. Where a significant difference is seen, it may be necessary to re-acquire control data.

Experiment 2 varied the FOV of stimulation, but maintained the same geometry throughout. As a result, the checksize used in each region became larger, as the FOV became larger. It is likely that refining the checksize for each region of stimulated visual cortex is important for maintaining good responses from over the FOV. Hoffman *et al* (120) investigated optimisation of the mfVECP and found an eccentricity dependent difference in the responses to pattern-onset, with larger amplitudes being seen centrally when a pattern-onset response was used, while a pattern-reversal elicited the greater responses from the periphery.

A complementary set of experiments could increase the field of view by introducing new rings to the dartboard stimulus and thus maintain the same check-size for inner rings throughout the series of acquisitions.

The FOV investigation differs from other research because the LCD stimulator was used whereas all others use CRT stimulation. This unit has had extensive experience and success with LCD stimulation when performing wide-field mfERGs, which lead us to select the LCD projection system for mfVECP acquisitions. However, it has been shown here that for mfVECP acquisitions with m-sequence length of m=16, the median SNR was slightly but significantly higher. Since the mfVECP is such a small response, all advantages in signal detection must be capitalized. CRT stimulation should therefore be the method of choice.

6.10 Stimulus Delivery Conclusion

In multifocal electrophysiology, the recovered signal quality has been shown to be better when a CRT monitor is used to deliver the stimulus rather than an LCD projector. The mfVECP is a small signal presenting challenges for signal detection and the use of a CRT monitor presented stimulus is recommended.

A range of fields of view have been stimulated during mfVECP recordings. Data presented here is the first to use a 60-region dartboard pattern to investigate the optimal field of view. It was found that signals could be recovered out to a radius of 30° of the visual field, but that the detection of waveforms beyond that was poor.

All the investigations performed in this chapter have highlighted the need for normal ranges which are specific to the precise protocol and equipment used in individual laboratories.

A small overlap in the volunteers used in the CRT vs LCD and FOV investigations allowed a brief look at reproducibility. The trace arrays show significant similarity but are not identical. There is a greater degree of variation than that seen in the data acquired in Chapter 4 with increasing m-sequence length during a single recording session. This is in keeping with the fact that the two datasets had slightly different recording parameters and were recorded during acquisition sessions separated by several months. If the mfVECP is to be used for visual field assessment in longitudinal studies, reproducibility should be investigated more thoroughly using exactly the same recording parameters on the same group of subjects on a number of occasions.

Having established the appropriate technology for presenting the mfVECP stimulus and the extent of the visual field which can usefully be investigated, there remains a wide range of parameters which are intrinsic to the stimulus and are ripe for optimisation. To name a few, these include stimulus geometry, the number of regions used, the number of checks per stimulating region, their colours, whether pattern-reversal or pattern-onset is more useful and the rate at which the pattern-reversal occurs. From this extensive list, the rate of pattern-reversal of a 60-region dartboard stimulus has been chosen as the topic of investigation in the next chapter.

Chapter 7

Rate of mfVECP Stimulus Presentation

Contents

			Page
7.0	Introduction …….		186
7.1	Aim …….		188
7.2	Methods ……..		188
	7.2.1	Analysis ……	191
7.3	Results ……		193
	7.3.1	Full Trace Arrays – Results and Discussion …	193
	7.3.2	SNR Time Window Investigation – Results and Discussion……...	197
	7.3.3	Waveforms in Detail – Results …….	199
	7.3.4	Waveforms in Detail – Discussion ……...	203
	7.3.5	ROC Comparison of Stimulation Rates – Results and Discussion …….	204
	7.3.6	Central Waveforms – Results and Discussion ..	208
	7.3.7	Overall Detection Rates – Results ……	212
	7.3.8	The Locations of Detectable Waveforms – Results ……..	214
	7.3.9	The Locations of Detectable Waveforms – Discussion …….	223
7.4	Discussion ……...		224
7.5	Future Work ……		226
7.6	Conclusion ……..		226

7.0 Introduction

Several publications have demonstrated that the rate of presentation of the visual stimulus has an impact on the size and signal to noise ratio of the recorded mfVECP. The conclusions, however, are varied.

Martins *et al* (116) discussed the impact of stimulation rate on mfVECPs performed with blue-yellow stimuli, to most effectively isolate the responses of the S cones (short wavelength sensitive cones). Stimulation rates of 75Hz and 37.5Hz were employed and the latter produced responses of greater amplitude and decreased latency. Martins compares her results to recordings reported in an ARVO poster by Balachandran (117) that were made using a black and white stimulus with a reversal frequency of 25Hz. Balachandran's data exhibited a reduction in amplitude (presumably in comparison with a standard stimulation rate of 75Hz). She goes on to suggest that the increases seen in the amplitude of the response to 37.5Hz pattern reversal of an iso-luminant blue-yellow stimulus are due to the blue-yellow pathway being a slower channel.

Fortune *et al* (109) compared conventional VECPs and summed mfVECP responses. These were found to differ in three ways; the conventional VECP shows a greater asymmetry in upper and lower field amplitudes, the implicit times of the conventional VECP is longer and a polarity reversal seen in the mfVECP is not evident in the cVECP. The same paper investigated the effect of stimulation rate, employing rates of the standard 75Hz as well as 9.4Hz and 4.7Hz. Decreasing the frequency of stimulation in five subjects resulted in significantly larger waveforms. It is suggested that this is due to changes in the state of contrast adaptation and the possible contribution of evoked response components to other stimulus attributes such as motion onset and offset. It is hypothesised that the generators of the responses to cVECP and mfVECP are different and that slowing the stimulation rate of the mfVECP shifts the balance of the generators towards those of the cVECP. It is argued that the mfVECP principally arises from V1 whereas the cVECP is more heavily influenced by extrastriate contributions.

Fortune *et al* also illustrated polarity reversal at normal stimulation rates which disappeared at slower rates. Slowing stimulation rate was shown to increase both amplitude and latency of mfVECP responses (109).

Extensive work has been performed by James AC and his colleagues (17;104;114;115;150;151). They employ a different approach to stimulation based on presenting a contrast stimulus for a single frame with an interstimulus interval between 0.4 and 0.6 seconds. Using a goggle system for stimulus delivery, contrast stimuli appeared to the right eye, left eye or both eyes. Each of the three conditions is repeated 73 times within a 109 second stimulation period and is randomly shuffled according to a uniform pseudorandom distribution. This approach has shown considerable increases in signal amplitude compared to continuous pattern reversal used in other multifocal VECP recordings. They suggest that this is due to adaptation of the response to contrast during pattern reversal.

Turning to the mfERG, Smith *et al* (152) showed that increasing LED stimulus presentation rate from 77Hz to 500Hz reduced the amplitude of the recovered signal by a factor of five. Central photoreceptors were affected to a greater degree than peripheral photoreceptors.

While a viewer cannot discern individual flashes above a given frequency (the critical-flicker-fusion frequency), this should not be considered a limitation to electrophysiological testing. Different sub-units of the visual system are capable of responding more quickly.

The frequency spectrum of an m-sequence contains a series of discrete submultiples of the presentation frequency (92;152). Therefore, the 500Hz stimulation rate described in Smith *et al* includes stimulation at 250Hz, 167Hz, 125Hz, etc.

The response to 500Hz stimulation is therefore made up of responses to lower frequencies too. In this case, only 1% is contributed by 75Hz or lower, while over 87% of the stimulus is over 125Hz. This means that there are significant contributions to frequencies over 125Hz in the multifocal photoreceptor response. These contributions cannot be fully accounted for by photoreceptors coming out of their refractory period.

7.1 Aim

The aims are to investigate the impact of stimulation rate on the mfVECP by answering the following questions:

- What changes in waveform responses are seen with different stimulation rates?
- Is the use of a SNR value calculated over a time window defined after inspection of data acquired at 75Hz appropriate when other stimulation rates result in changes in waveform latency?
- Can SNR be improved by decreasing stimulation rate?
- Does this allow differentiation of a greater proportion of waveforms from background noise?
- How are the central waveforms affected by changes in stimulation rate?
- There are some areas of the visual field from which it is difficult to obtain a mfVECP response greater than background noise. Does changing the rate of stimulation allow a better detection rate of responses to the 60 regions of the stimulus?
- If gains can be made, which parts of the visual field benefit?
- Finally, if a portion of the visual field can be shown to evoke a greater number of detectable waveforms for a specific stimulation rate, how reproducible is that finding throughout the group of normal volunteers?

7.2 Methods

mfVECP responses were recorded from 13 normal, healthy volunteers with no known ophthalmic or neurological conditions using the ActiveTwo electrode and amplifier system integrated with the EDIU Multifocal System. Full details of this system are given in Chapter 8.

Signed consent was obtained after the experimental protocol had been fully explained. Ethics approval was obtained from the West of Glasgow Local Ethics Committee.

Subjects were optimally refracted using their own spectacles and their pupils were not dilated. Recordings were monocular. Stimulation was provided by a 60-region dartboard pattern. Each region contained a 4x4 black and white checkerboard pattern and the size of the regions was scaled for cortical magnification. The stimulus was back-projected onto a screen by an LCD projector and subtended a 22° radius of the visual field. The luminance of white areas varied across the screen from 903 cdm^{-2} to 1384 cdm^{-2} and black areas varied from 12 cdm^{-2} to 309 cdm^{-2}. Contrast varied from 98% peripherally to 49% at the centre of the screen.

Each subject underwent a series of eight mfVECPs recordings. The stimulation rates were 75Hz, 37.5Hz, 25Hz, 18.75Hz & 12.5Hz using m-sequence lengths ranging from m=12 to m=15 in order to maintain reasonable recording times. Full details are given in Table 7.1. Recordings have been labelled A-H with increasing stimulation frequency and then by increasing m-sequence length.

Recording	M-sequence length (bits)	Frequency (Hz)	Time (mins)
A	13	12.5	12
B	13	18.75	8
C	13	25	6
D	12	37.5	2
E	13	37.5	4
F	13	75	2
G	14	75	4
H	15	75	8

Table 7.1 *Table showing the combination of stimulation frequency, m-sequence length and the recording time for eight mfVECP recordings, A-H.*

The stimulation rates employed allow a greater sampling of their impact on waveform responses than those presented by Martins *et al* (116), and investigate a different range of frequencies from those studied by Fortune *et al* (109).

Stimulation rates of less than 75Hz were achieved by inserting 'filler frames'. Instead of moving forward in the m-sequence every refresh period of the LCD projector, the stimulus remained unchanged for 2 frames, resulting in a stimulation rate of 37.5Hz, 3 frames (25Hz), 4 frames (18.75Hz) or 6 frames (12.5Hz).

The order of each recording was randomly varied from subject to subject, in an attempt to average out effects of fatigue.

Acquisition times were divided into 30 second overlapping periods to allow the subject to blink and rest, in order to maintain good fixation.

16 active electrodes were placed at positions indicated in Table 7.2 below.

Active Electrode No.	Position
1	F_Z
2	C_z
3	P_4
4	P_z
5	P_3
6	5% of head circumference right of PO_z
7	PO_z
8	5 % of head circumference left of PO_z
9	5% of head circumference right of O_2
10	O_2
11	O_z
12	O_1
13	5% of head circumference left of O_2
14	5% of head circumference right of the inion
15	Inion
16	5% of head circumference left of the inion
CMS	10% of head circumference left of C_z
DRL	10% of head circumference right of C_z

Table 7.2 *Active Electrode positions.*

BioSemi replaces the ground electrode used in conventional systems with two separate electrodes, the Common Mode Sense (CMS) electrode and the Driven Right Leg (DRL) electrode. These two electrodes form a feedback loop, which drives the average potential of the subject (the Common Mode voltage) as close as possible to the ADC reference voltage in the ADC-box

The CMS electrode is used as the reference for each of the 16 monopolar recording channels.

The BioSemi ActiveTwo is DC coupled and low pass filtering is performed by the ADC. This provides a very wide frequency bandwidth. Signals were sampled at 2048Hz and downsampled to 1200Hz when data was converted to a format recognizable by the EDIU Multifocal System for cross-correlation. Data was then filtered through a 3-30Hz digital bandpass prior to cross-correlation.

7.2.1 Analysis

A Delphi program was written to calculate the SNR values of the 60 waveform responses and 68 noise estimations. The DeadM method described in Chapter 4 was used. The period of 45 to 150 msec is used widely as the signal window (125).

The SNR for inactive orthogonal m-sequences was calculated. From this distribution of values, the 90^{th} percentile was calculated. Responses to active m-sequences with a SNR above this detection threshold were identified as a significant waveform.

It was observed during this analysis that in some circumstances, the waveform appeared to continue beyond the recommended window of 45 to 150msecs. As a result, SNR calculations were repeated with a longer window of 45 to 250ms. The Delphi program calculated the SNR values which were further analysed in Microsoft Excel.

A comparison of the ability of the two different time windows to distinguish between noise and signal was performed, using ROC curves.

It is worth highlighting the volume of data involved. 12 subjects each performed 8 mfVECPs. Each mfVECP produced trace arrays from 16 recording electrodes and each trace array contained 60 waveforms. In total, 12x8x16x60 = 92160 signal waveforms and 12x8x16x68 = 104448 noise estimations are available for analysis.

During the presentation of the analysis, a balance has been struck between data volume and detail. Data are presented in several formats. Analyses employing large volumes of data are counter-balanced by greater summarisation of waveform detail.

- *Full Trace Arrays* - 60 waveform trace arrays are presented for a single recording channel (A10, 10-20 position O_2) for a single subject, for each of the stimulation rates.
- *SNR Time Window Investigation* - The time window over which the SNR is calculated is investigated using a single recording channel and a single waveform from the trace array, for each of the twelve volunteers. SNR values were calculated over the periods 45-150ms and 45-250ms. Data from n=12 subjects is presented for each of the eight recordings (A-H), in an ROC analysis. ROC curves use data from a single recording channel and all 60 waveforms and 68 noise estimations from each person.
- *Waveforms in Detail* - Each subject's waveforms are presented for the eight recordings (A-H). This is restricted to a single recording channel and a single waveform from the trace array.
- *ROC Comparison of Stimulation Rates* – Data presented in the SNR Time Window Investigation is used to identify the optimal stimulation rate and m-sequence length from the recordings described in Table 7.1.
- *Central Waveform* - SNR values for each of the central waveforms have been plotted for each stimulation rate for n=12 subjects and averaged over subjects.
- *Overall Detection Rates* - Detection rates are calculated using data from all subjects and recording channels, and plotted against stimulation rate. This summarises the number of dartboard stimulating regions that result in a detectable waveform.
- *The Locations of Detectable Waveforms* - A summary of which areas of the visual field produce detectable waveforms has been created on an individual subject basis for the 12.5Hz recording. The same data averaged over the n=12 subjects is also presented.

7.3 Results

Complete datasets were recorded from 12/13 subjects. Data recorded from the remaining subject was not saved properly due to a problem with the software. Data from this subject could not therefore be used in subsequent analysis.

7.3.1 Full trace arrays – Results and Discussion

Figure 7.1(a&b) presents the full trace arrays acquired by channel A10 (position O_2) during each of the eight recordings, for a single subject.

Figure 7.1(a) shows all data acquired with an m-sequence length of m=13 for the five stimulation rates. The duration of acquisition therefore increased as stimulation rate decreased.

Figure 7.1(b) allows a comparison of three pairs trace arrays acquired at different stimulating frequencies but in the same acquisition times.

Improvements in signal quality can be seen in the form of smoother waveforms as the m-sequence length increases.

Some significant increases in signal amplitude were seen at slower stimulation rates. This is demonstrated at some waveform locations, but not all.

Although difficult to see in Figure 7.1, changes in latency were noted during this level of analysis, with a trend towards longer latencies at slower stimulation rates. In some cases, waveforms did not appear to return to baseline until well after the 45-150ms time window used for SNR value calculation was over. This is demonstrated in Figure 7.2b.

This observation prompted an investigation into whether the use of a longer time window of 45-250ms for SNR calculation would increase the SNR values of waveforms and therefore increase the number of waveforms that reach the detection threshold.

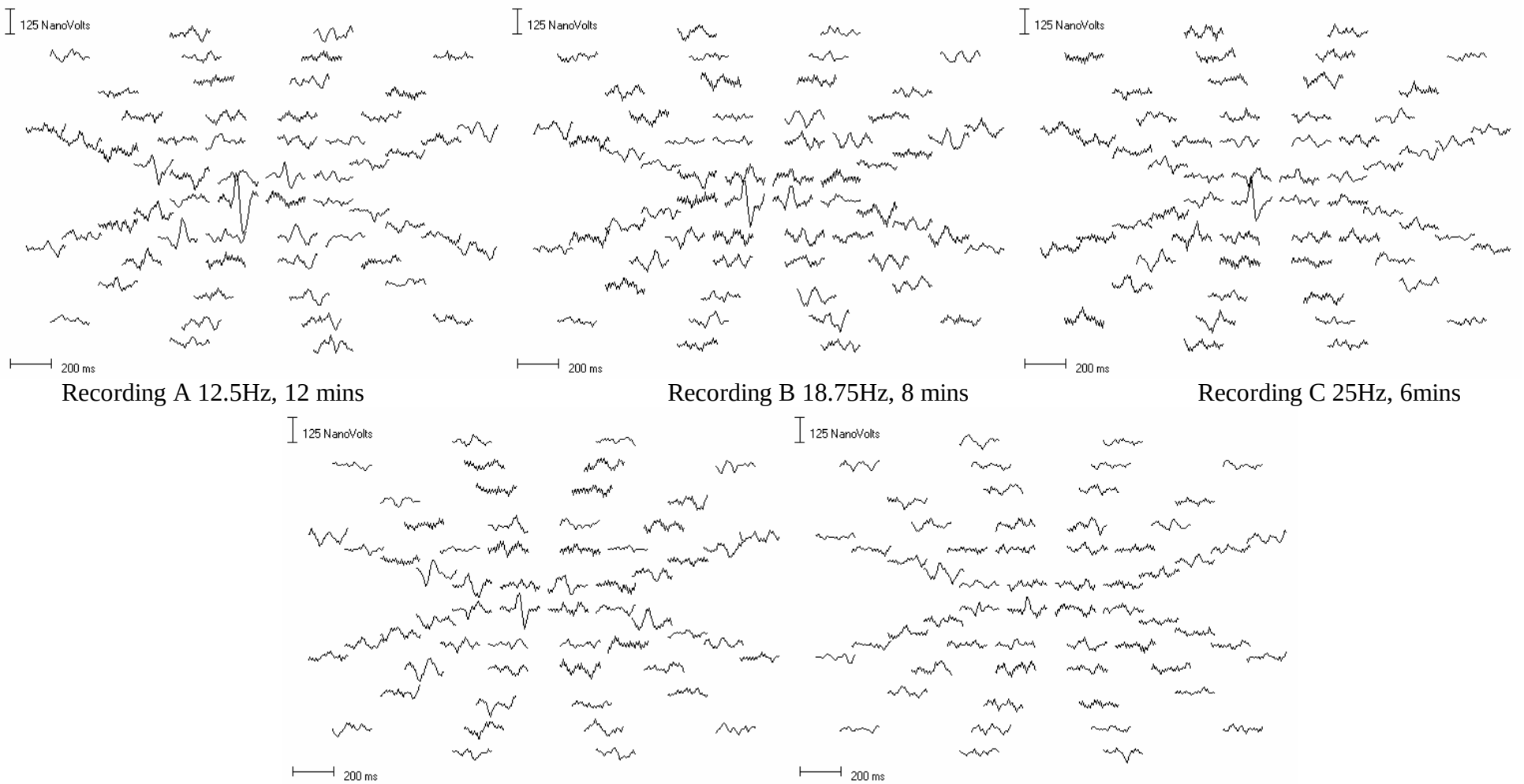

Recording A 12.5Hz, 12 mins

Recording B 18.75Hz, 8 mins

Recording C 25Hz, 6mins

Recording E 37.5Hz, 4 mins

Recording F 75Hz, 2mins

Figure 7.1(a) *Responses to stimulation at five different frequencies from a single subject. Data was acquired by Channel A10 and an m=13 bit m-sequence was used in each case. Acquisition times are noted.*

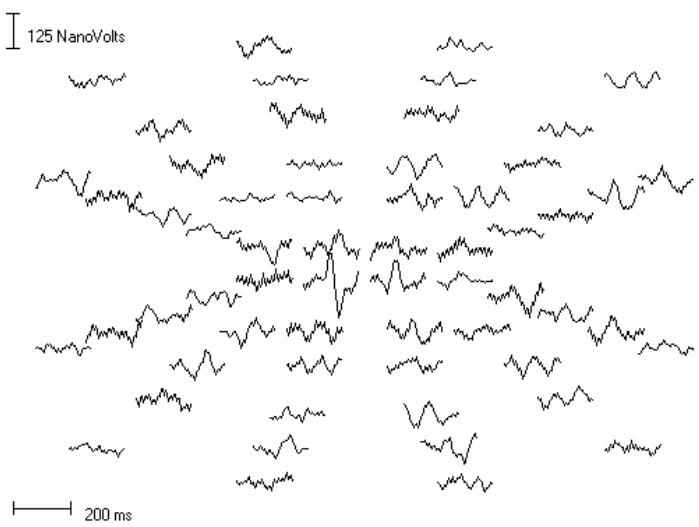

Recording B, 18.75Hz, m=13, 8mins

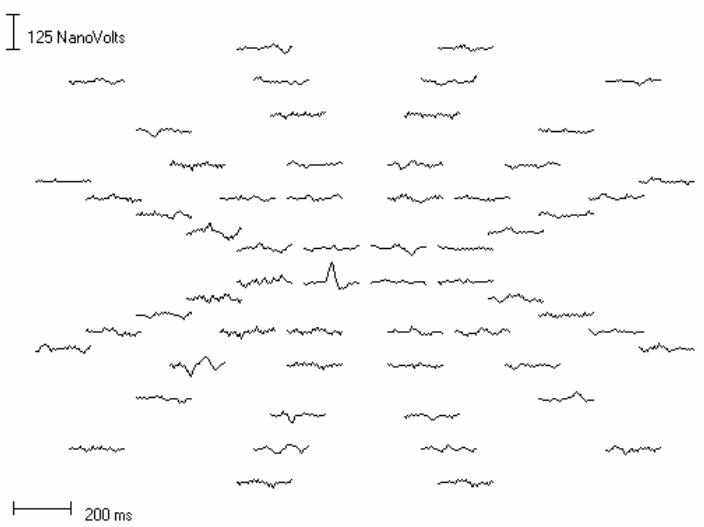

Recording H, 75Hz, m=15, 8 mins

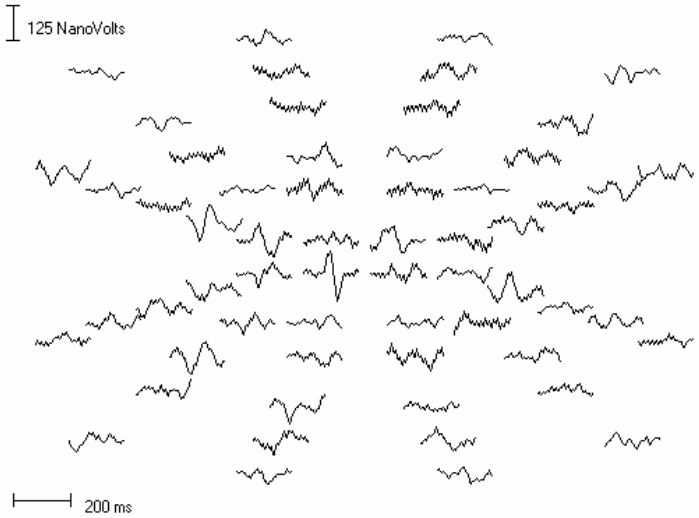

Recording E, 37.5Hz, m=13, 4 mins

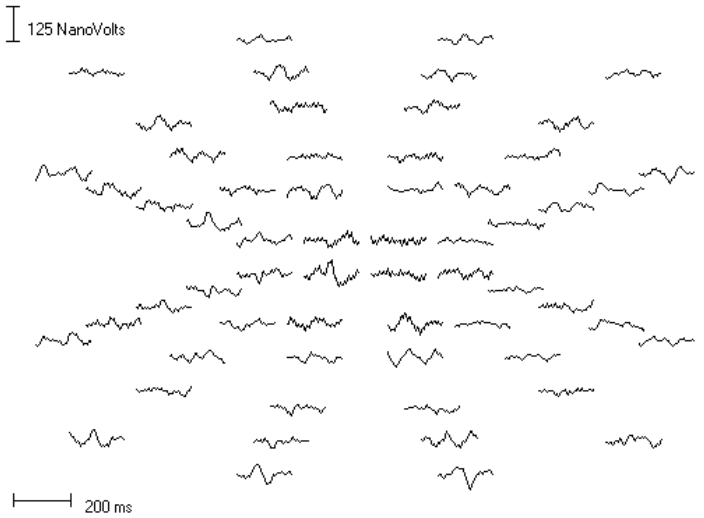

Recording G, 75Hz, m=14, 4 mins

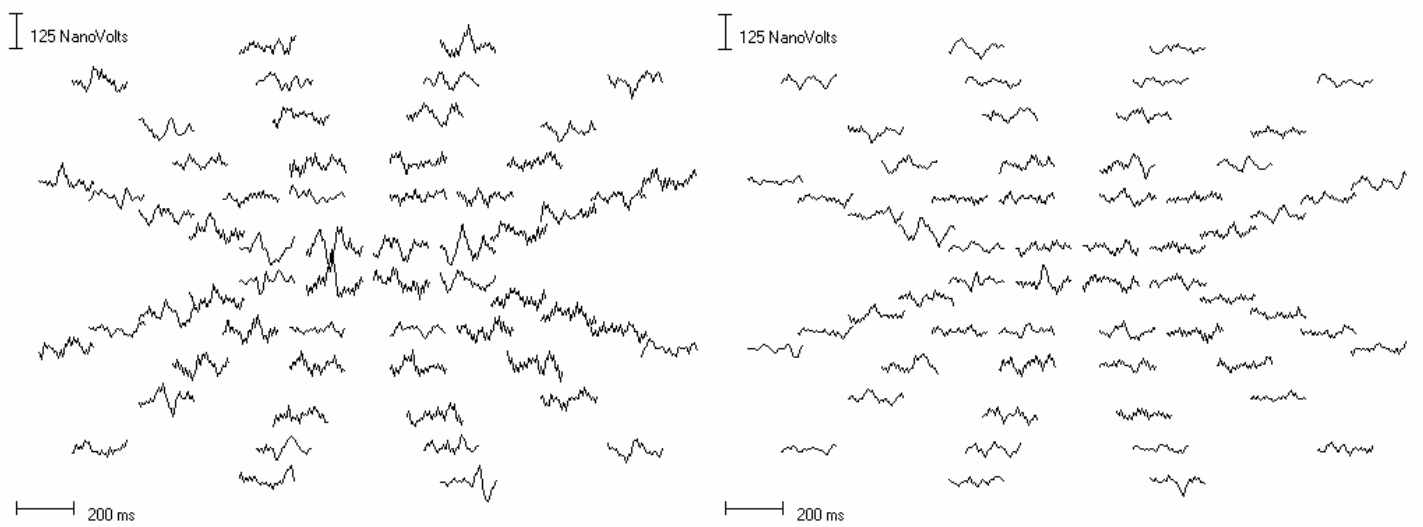

Recording D, 37.5Hz, m=12, 2mins Recording F, 75Hz, m=13, 2mins

Figure 7.1(b) *Three pairs of trace arrays are shown. In each pair, the recording time was the same, but there was a difference in the stimulation rate and m-sequence length. Data was acquired from a single subject by Channel A10.*

7.3.2 SNR Time Window Investigation – Results and Discussion

ROC curves comparing SNR values calculated using time windows 45-150ms and 45-250ms for data acquired by channel A10, from all 12 subjects, were constructed for each recording and are shown in Figure 7.2. The area under the 45-250ms time window curve (pink) was never smaller than the area under the 45-150ms curve (blue). For recordings A, B and C the area under the longer time window SNR was clearly larger.

A very small difference was seen in recordings F & G, with the longer time window showing the better results.

D, E and H showed no difference in the ROC area for the two time windows.

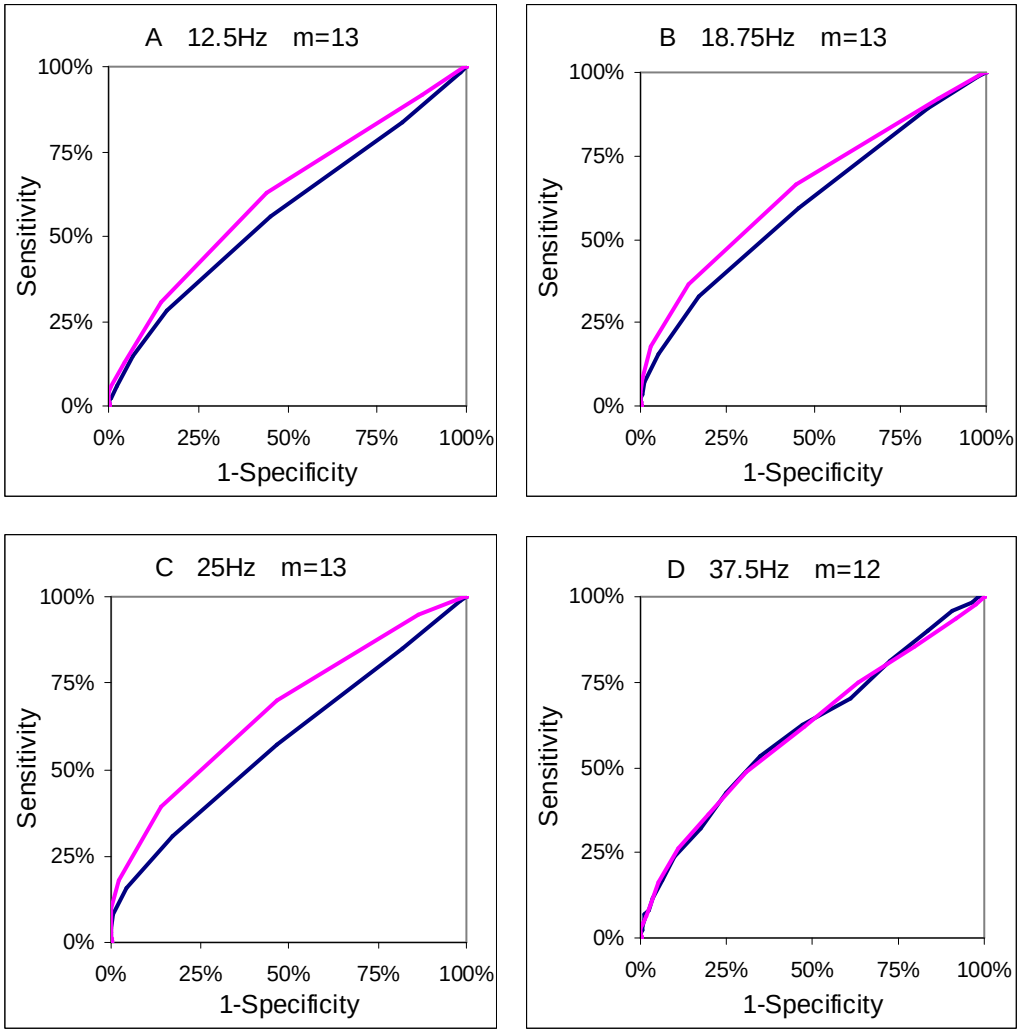

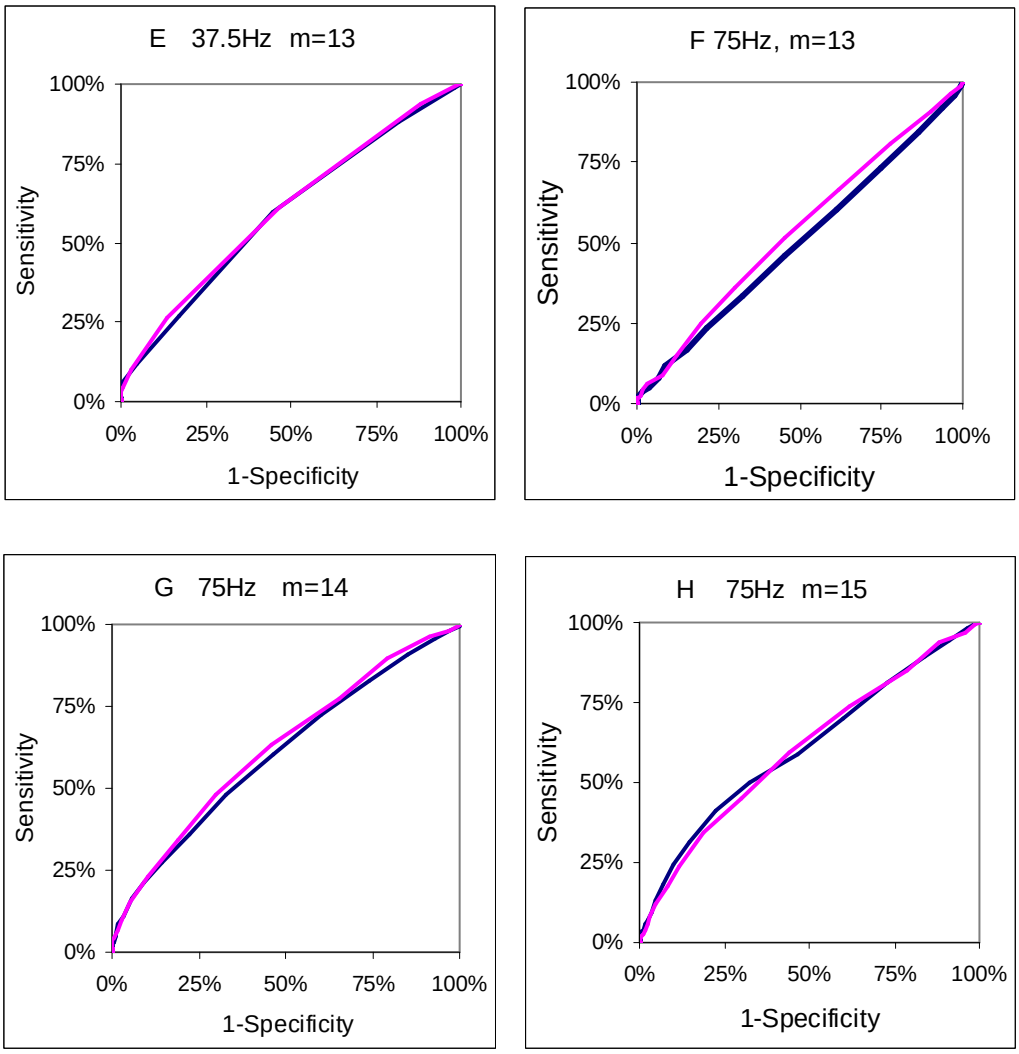

Figure 7.2 *ROC curves are presented for each of the recordings A-H (Recording A=12.5Hz m=13, B=18.75Hz m=13, C=25Hz m=13, D= 37.5Hz m=12, E=37.5Hz m=13, F=75Hz m=13, G=75Hz m=14, H=75Hz m=15). Blue and pink curves represent SNR values calculated over 45-150ms and 45-250ms, respectively. Each of the 16 curves uses 720 waveforms (60 waveforms per trace array x 12 subjects) and 816 noise estimations (68 inactive m-sequence cross-correlations x 12 subjects) acquired from recording channel A10.*

This is consistent with the observations of the preceding section, that the waveforms do not return to baseline until later than 150ms and that latencies increase as stimulation rate is decreased.

There is no evidence in the ROC curves that the use of the longer time window reduces the ability of the SNR value to detect signals. SNRs calculated over 45-250ms will therefore be used throughout the analysis in the rest of this chapter.

7.3.3 Waveforms in Detail – Results

Figure 7.3 shows the change in waveform as stimulation rate is changed. Data are shown for each of the 12 subjects and were acquired with recording channel A10 (position O_2). Every waveform is the response to stimulation from region 58 of the mfVECP stimulus. The location of this response within the waveform trace array is highlighted in Figure 7.3a

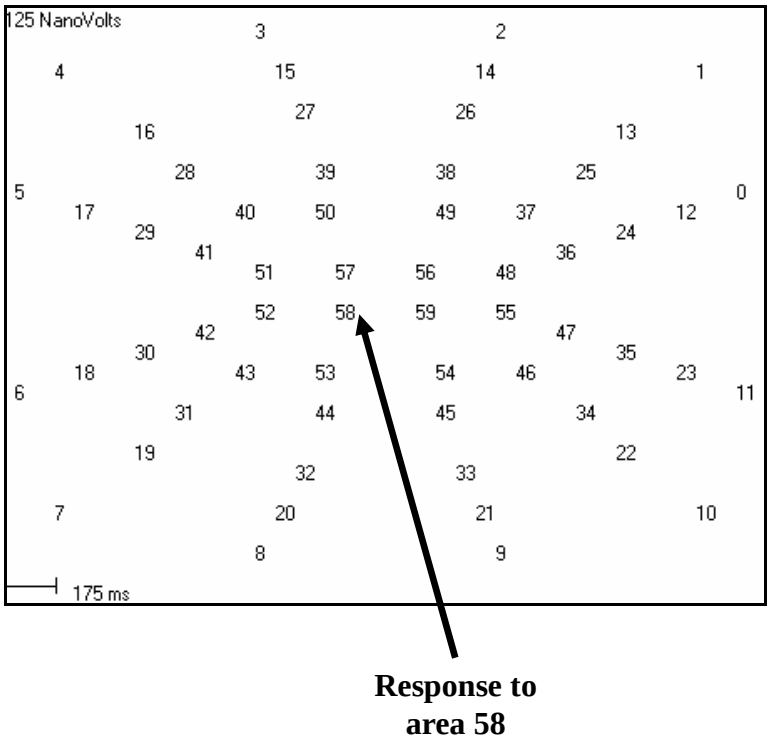

Figure 7.3a *Region 58 of the mfVECP stimulus stimulates the lower left section of the central visual field. The response to stimulation of this area appears within the waveform trace array at the location shown.*

Each subject's data contains waveforms obtained during each of the eight recordings listed in Table 7.1. The legend indicates SNR values for each waveform over the window 45-250ms.

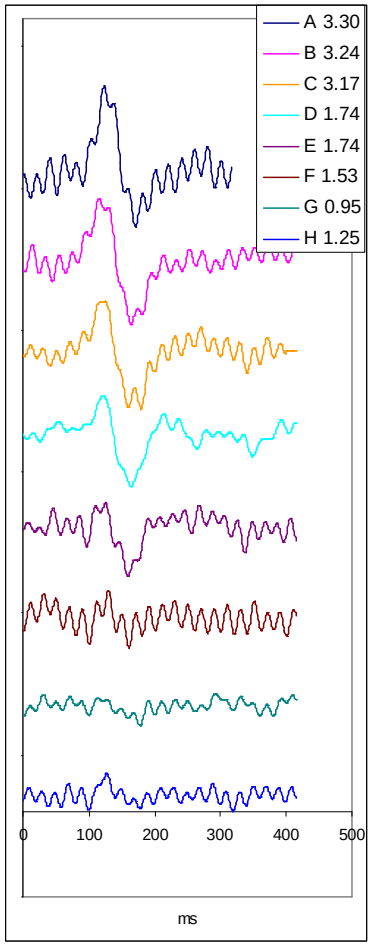
A 3.30
B 3.24
C 3.17
D 1.74
E 1.74
F 1.53
G 0.95
H 1.25
0
100
200
300
400
500
ms

AM

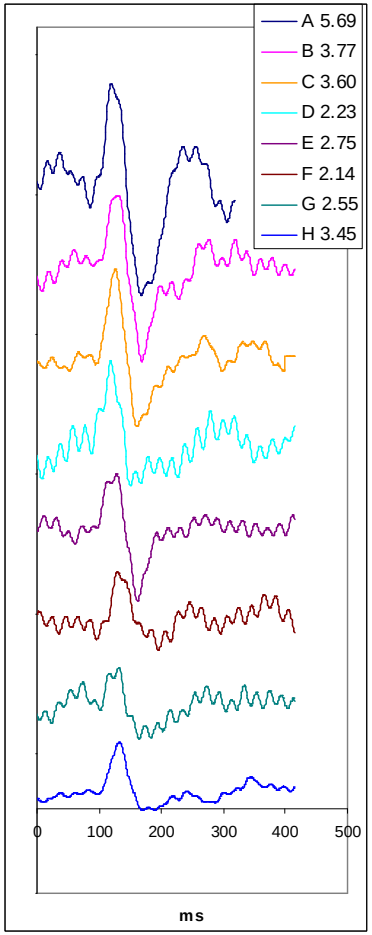
A 5.69
B 3.77
C 3.60
D 2.23
E 2.75
F 2.14
G 2.55
H 3.45
0
100
200
300
400
500
ms

CC

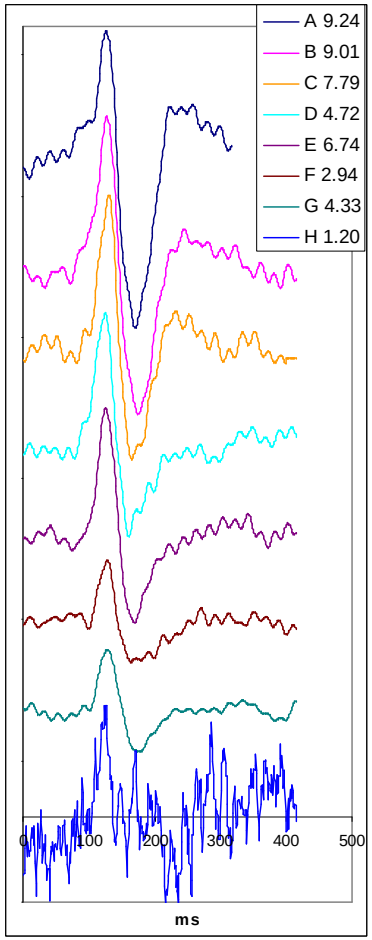
A 9.24
B 9.01
C 7.79
D 4.72
E 6.74
F 2.94
G 4.33
H 1.20
0
100
200
300
400
500
ms

DB

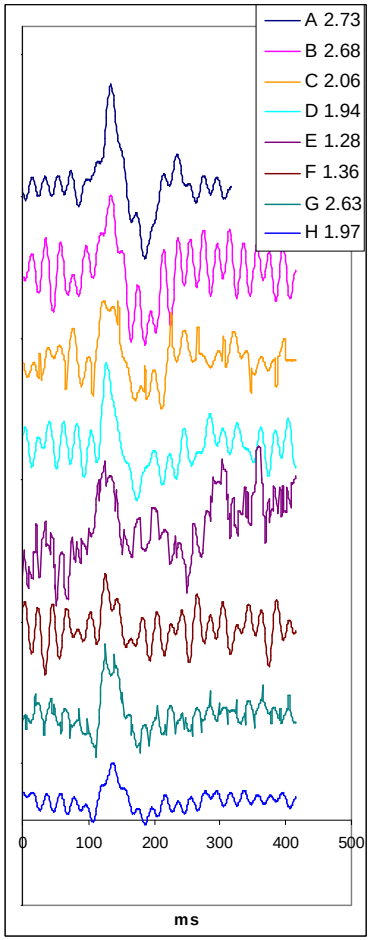
A 2.73
B 2.68
C 2.06
D 1.94
E 1.28
F 1.36
G 2.63
H 1.97
0
100
200
300
400
500
ms

DK

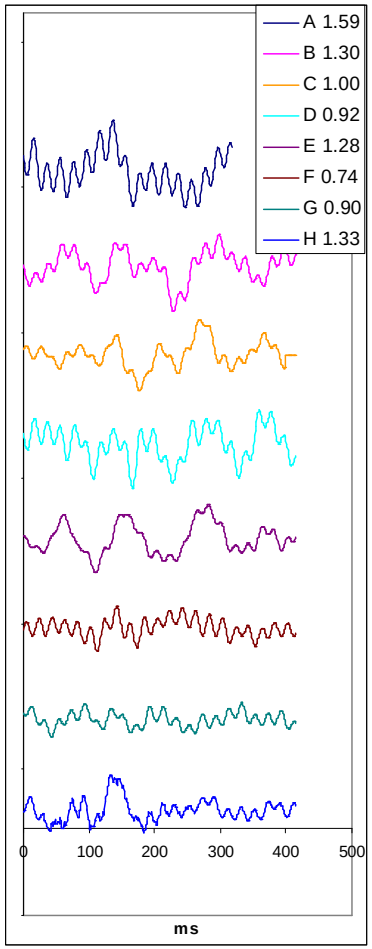
A 1.59
B 1.30
C 1.00
D 0.92
E 1.28
F 0.74
G 0.90
H 1.33
0
100
200
300
400
500
ms

DW

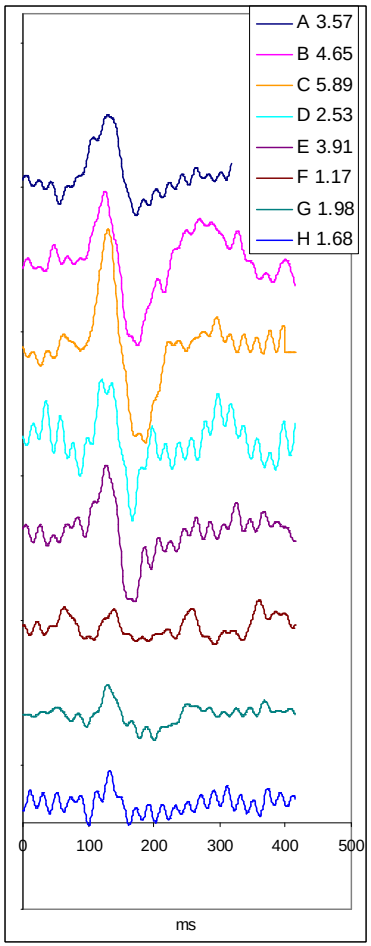
A 3.57
B 4.65
C 5.89
D 2.53
E 3.91
F 1.17
G 1.98
H 1.68
0
100
200
300
400
500
ms

FM

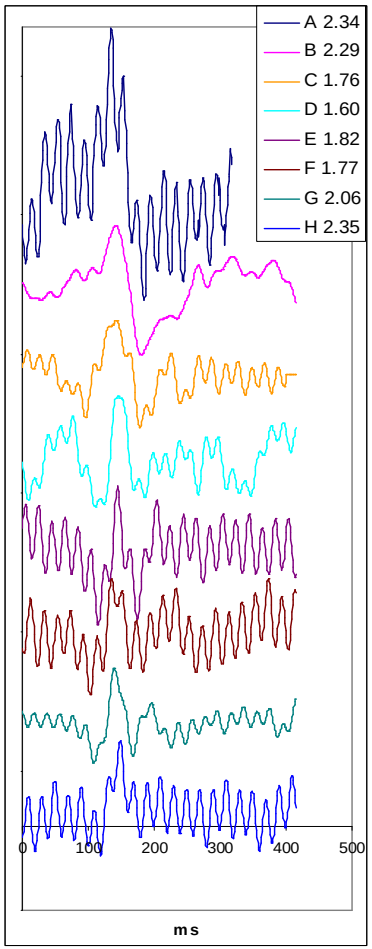
A 2.34
B 2.29
C 1.76
D 1.60
E 1.82
F 1.77
G 2.06
H 2.35
0
100
200
300
400
500
ms

JM

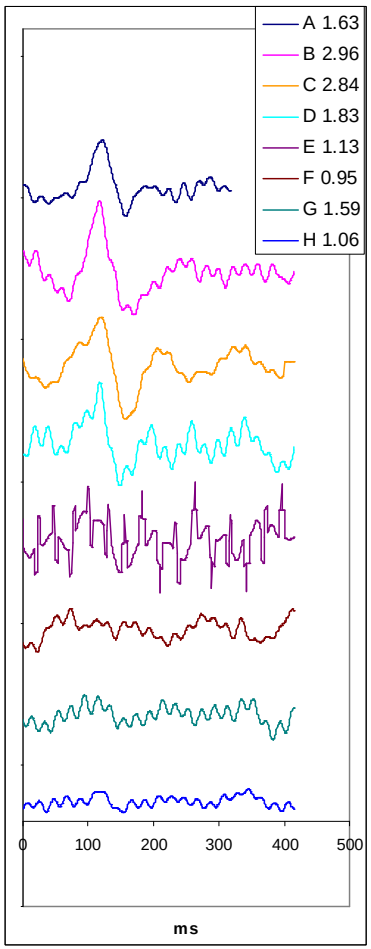
A 1.63
B 2.96
C 2.84
D 1.83
E 1.13
F 0.95
G 1.59
H 1.06
0
100
200
300
400
500
ms

ML

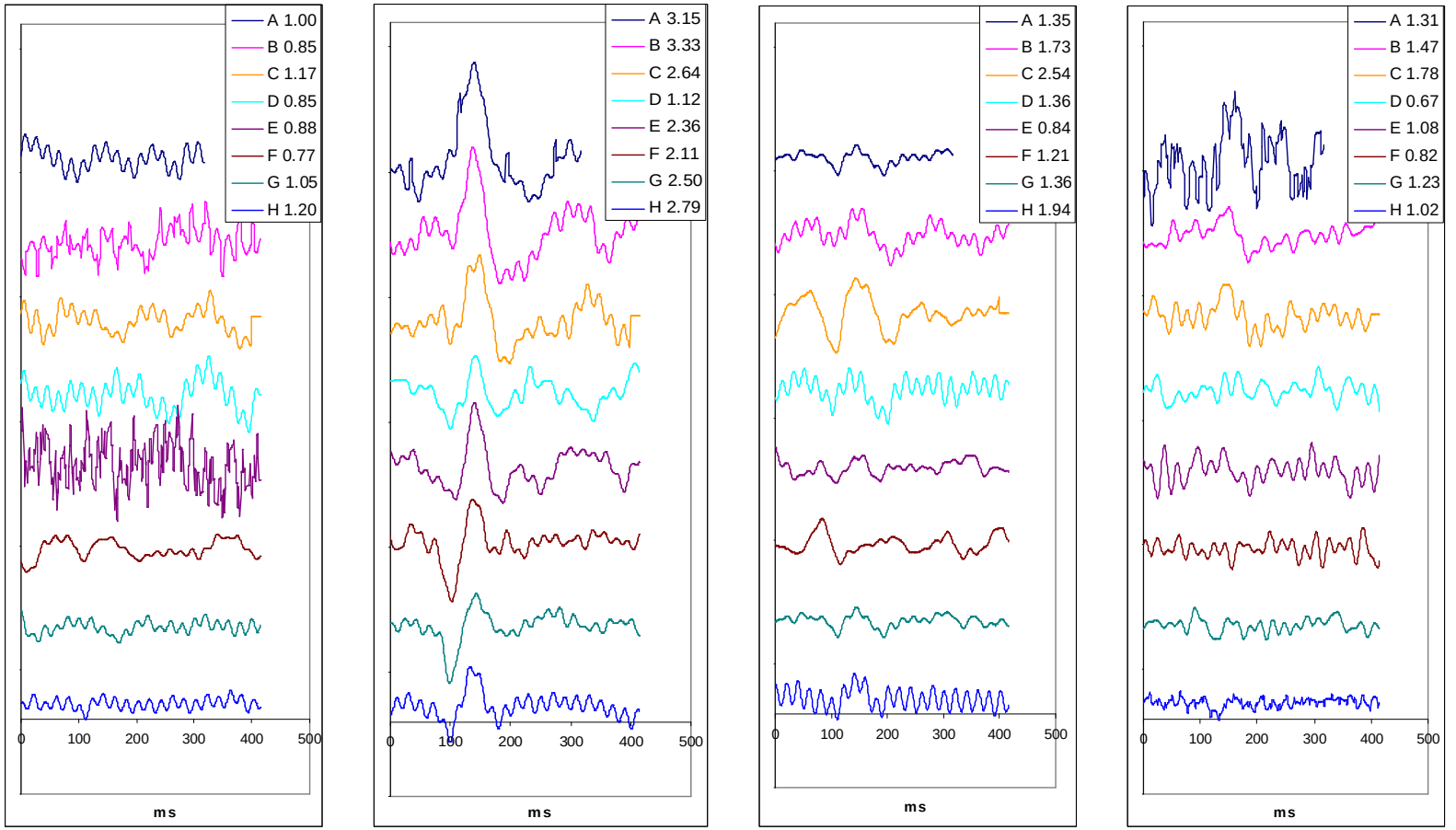

Figure 7.3b *Waveforms evoked by stimulating region 58 are shown for each recording A-H. Data was acquired by Channel A10. Stimulation rates increase from top to bottom. (Recording A=12.5Hz m=13, B=18.75Hz m=13, C=25Hz m=13, D= 37.5Hz m=12, E=37.5Hz m=13, F=75Hz m=13, G=75Hz m=14, H=75Hz m=15). The legend shows SNR values over 45-250ms. Data are presented for all 12 subjects.*

7.3.4 Waveforms in Detail - Discussion

Figure 7.3b shows considerable inter-individual variation in the waveforms. The contribution of noise also varies and in some cases is large enough to obscure the physiological response. In data from subjects DW and PG, SNR values remain below the detection threshold in all, or all but one of the depicted waveforms.

Seven subjects (CC, DB, DK, FM, JM, ML and SD) follow a similar pattern. A decrease in amplitude is seen with increasing stimulation rate and, in general, latencies are longer for the slower stimulation rates. This is partly due to the increasing prominence of a negative trough as the stimulation rate falls.

Subject SD exhibits an early negative trough at faster stimulation rates that does not appear in slower stimulated waveforms. This is not seen in the rest of this group.

6/12 subjects show an increase in SNR for each increase in m-sequence length, for the 75Hz stimulation recordings F,G and H.

Comparing recordings of the same duration, i.e. B&H (8mins) (B=18.75Hz, m=13, H = 75Hz, m=15) B gives the higher SNR in 8/12 subjects.

Similarly, E & G (4mins) (E = 37.5Hz, m=13, G = 75Hz, m=14) G shows the greater SNR in 5/12 cases.

D&F (2mins) (D=37.5Hz, m=12, F=75Hz, m=14) D shows the greater SNR in 9/12 cases, although in both cases, only approximately 50% of the waveforms presented exceeded the detection threshold.

Inspection of this data confirms that in many cases, the waveform has not returned to baseline by 150ms. This, coupled with the increase in latency at slower stimulation rates, prompted the investigation of a longer time window for calculating SNR values.

7.3.5 **ROC Comparison of Stimulation Rates – Results and Discussion**

In order to select the optimal combination of stimulation rate and m-sequence length from the recordings described in Table 7.1, ROC curves for each test were plotted.

These data are identical to that presented in the SNR Time Window Investigation, but makes use of SNR values calculated over the 45-250ms time window only. Here, ROC curves for each recording are superimposed for comparison.

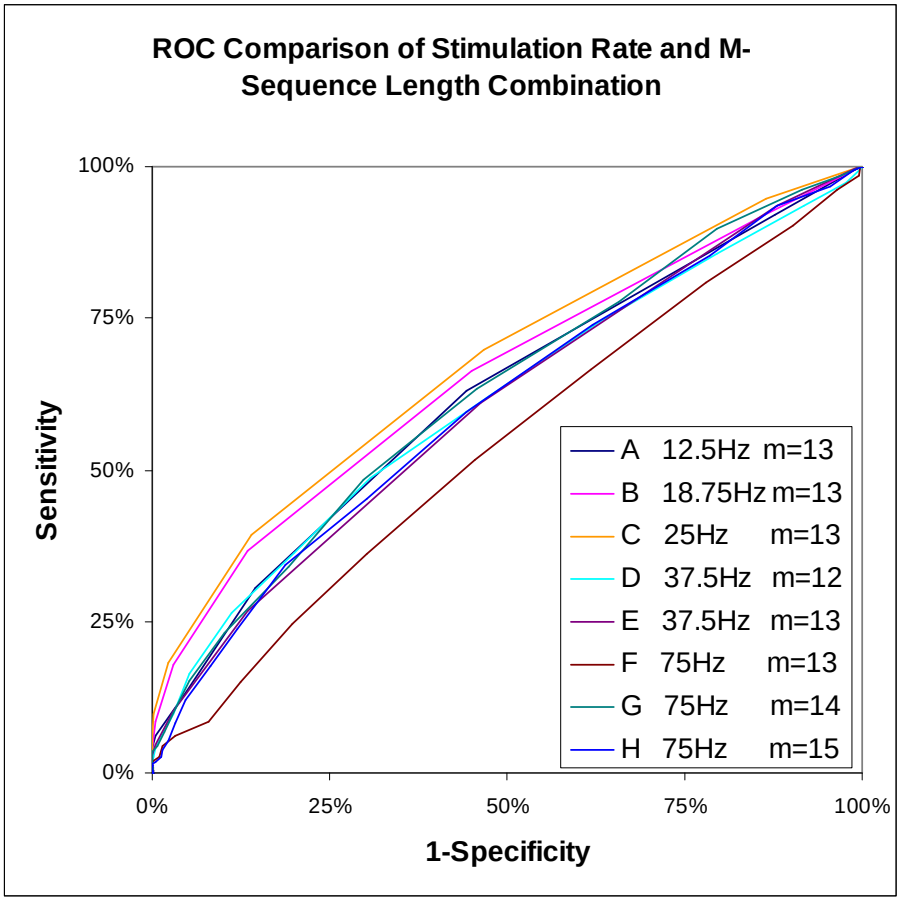

Figure 7.4 *ROC Curves for eight recordings. Data from channel A10, n=12 subjects was used in this analysis. SNR values were calculated over 45-250ms.*

The greater the area under an ROC curve, the better test performance. Figure 7.4 shows that the poorest test is test F (75Hz, m=12) which provides almost no further information than could be obtained by tossing a coin. This is perhaps not surprising since it involves only 2 minutes of recording and an m-sequence which is much shorter than those used in routine practice.

By this measure, the most robust test was recording C (25Hz, m=13), closely followed by recording B (18.75Hz, m=13).

Test performance therefore improves as the stimulation rate is decreased from 75Hz to 25Hz. No further gain is seen by reducing the stimulation rate below 25Hz. This is corroborated by the ROC curves and Figure 7.10, which is discussed later.

Differences between the remaining recordings are subtle; however it is possible to draw comparisons between recordings of different stimulation rate and m-sequence length, but the same recording time. This is particularly useful in clinical situations where the choice of m-sequence length and stimulation rate is heavily influenced by the amount of time that the patient can reasonably be expected to comply with the testing conditions. Of the eight recordings performed there are three pairs of recordings with the same recording time.

- Recordings B (18.75Hz) and H (75Hz) were both acquired in 8 minutes. Figure 7.5(a) shows a larger area underneath curve B suggesting that the slower stimulation rate and shorter m-sequence provides the more robust test.
- Recordings E (37.5Hz) and G (75Hz) were both 4 minutes long. Figure 7.5(b) shows that test G is very slightly better than test E. In this case, the faster stimulation rate is the better performer.
- Recordings D (37.5Hz) and F (75Hz) both required 2 minutes of testing time. There is good separation of these curves, seen in Figure 7.5(c), with the slower stimulation rate providing the better test.

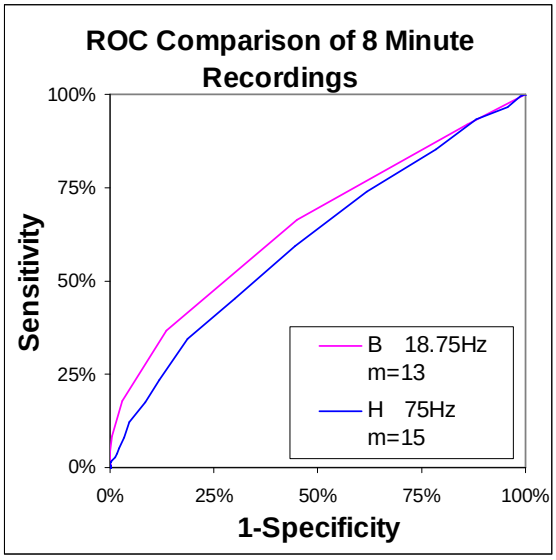

(a)

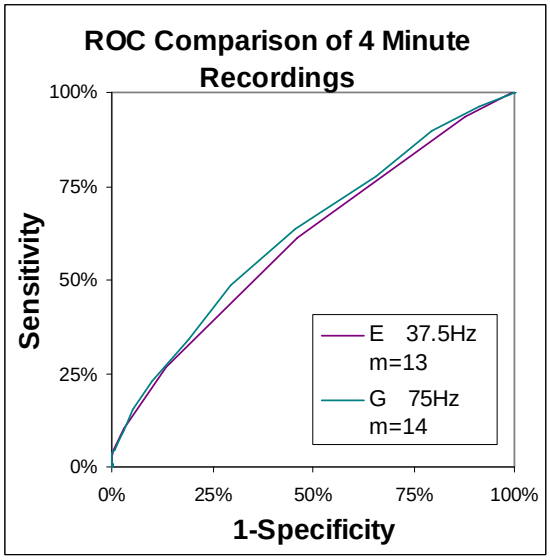

(b)

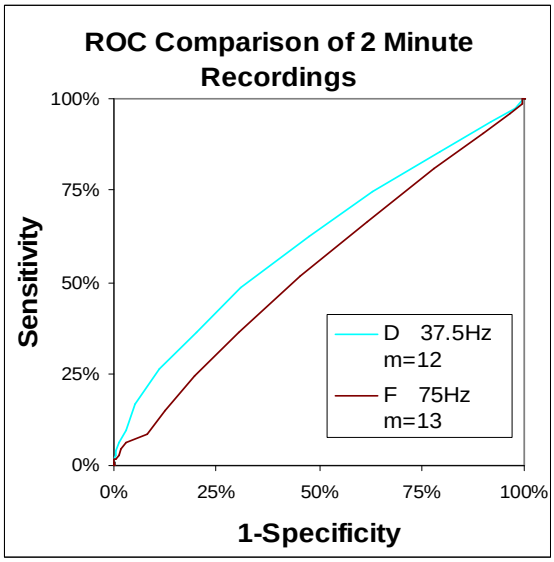

(c)

Figure 7.5 *Pairs of recordings with the same recording time are compared via ROC curves. 7.12(a) contains data from two recordings of 8 minutes duration, 7.12(b) 4 minutes duration and 7.12(c) 2 minutes duration*

Recording C (25Hz) showed the best test performance in this experiment, despite requiring only 6 minutes of recording time per eye, compared with 8 minutes required by the more standard 75Hz, m=15 recording parameters (represented by recording H). Figure 7.6 compares ROC curve for recordings C and H and shows good separation between the two. It is useful to know that acquisition time can be reduced while improving test performance.

Future experiments could investigate whether test performance improves again if stimulation rate is kept at 25Hz and the m-sequence length is increased to m=14. This would increase recording time to 12 minutes, which is significantly longer than 8 minutes. However, when viewed in terms of the results of Chapter 4 which suggested that for 75Hz recordings an m=16 recording requiring 16 minutes was worthwhile, 12 minutes may be a reasonable compromise.

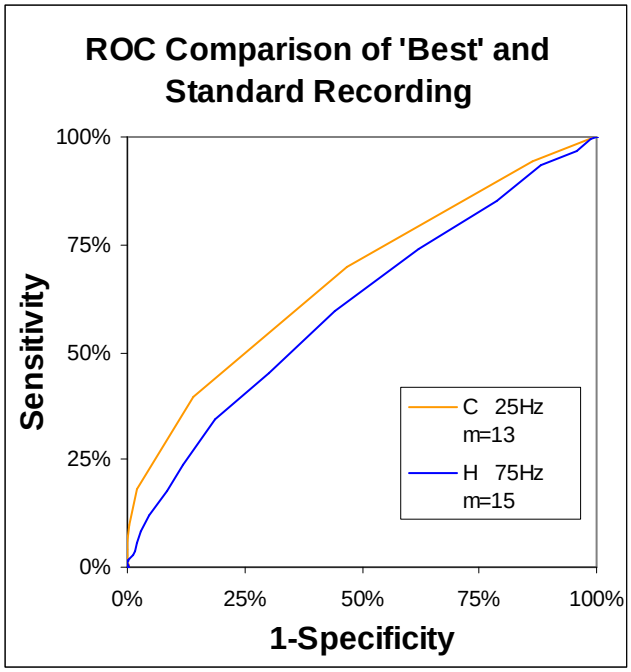

Figure 7.6 *The difference in test performance between test C, which was found to be the best performer in this experiment and test H, which uses the most commonly used combination of stimulation rate and m-sequence length (75Hz & m=15), is shown.*

7.3.6 Central Waveforms – Results and Discussion

SNR values calculated over the time window 45-250ms are plotted against stimulation rate for each subject in Figure 7.7 and 7.8. The plots illustrate data from one of the central waveforms (56 – top right, 58 – bottom left) acquired using channel A10 (position O_2).

Anderson –Darling Tests for Normality indicated a non-Normal distribution of SNR values from the 12 subjects and so non-parametric statistics are used.

The same data are presented in Figure 7.9 for all four central waveforms, but each data point is the median value from the 12 subjects. Error bars show the 95% confidence interval of the median value.

Data has been plotted for five of the eight recordings. This allows a consistent comparison of all m=13 recordings and does not confuse the plot with duplicates of the same stimulation frequency acquired with differing m-sequence lengths.

In all four central waveforms there is significant variation in the SNR values obtained from different subjects. The relationship between SNR and stimulation rate also varies however; there is an overall trend towards smaller SNR values for faster stimulation rates. The error bars suggest that differences are not statistically significant.

It is notable that the SNR values for segment 58 are far larger than the other central waveforms. This can be explained by the fact that this data was acquired from a single recording channel with the active electrode A10 at position O_2. Comparison with data acquired from electrode A12 at position O_1 (not shown) show far larger waveforms at location 59 when compared to location 58. Both channels favour the lower visual field central areas.

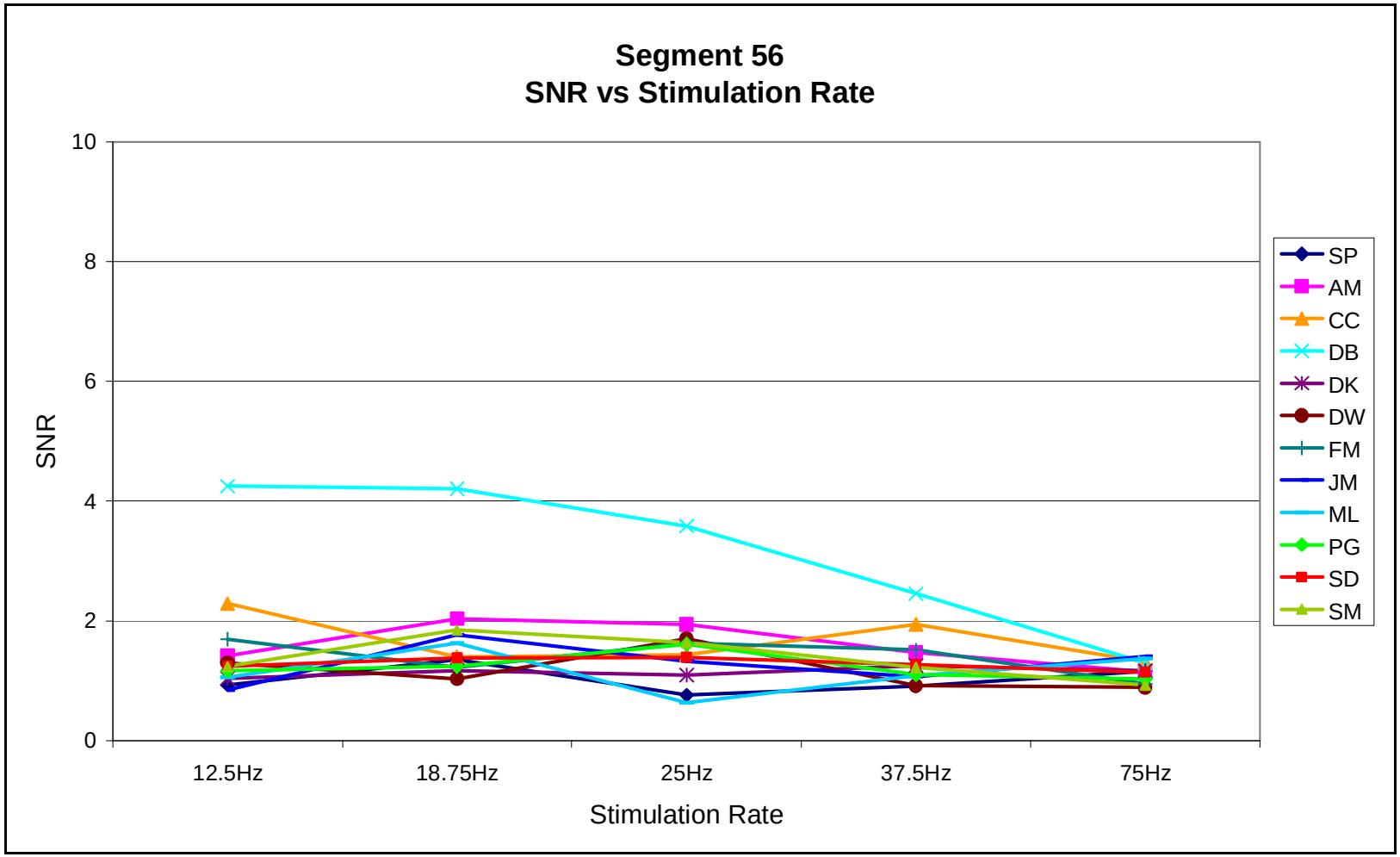

Figure 7.7 *SNR is plotted against stimulation rate for the waveform response to stimulation by region 56 (upper right central waveform in the trace array). The 12 series plot data from individual subjects. Data was acquired using channel A10 (position O_2).*

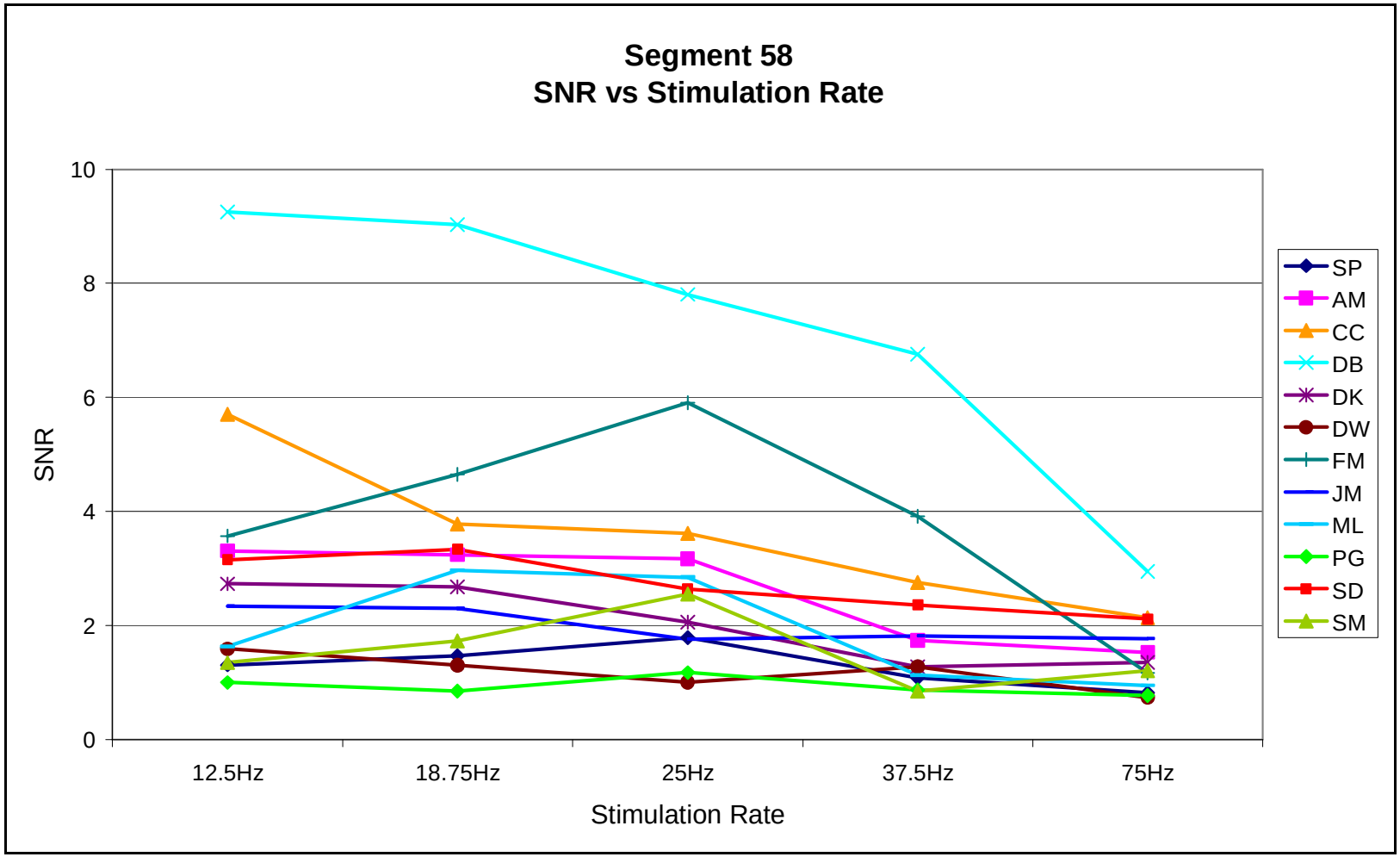

Figure 7.8 *SNR is plotted against stimulation rate for the waveform response to stimulation by region 58 (bottom left central waveform in the trace array). The 12 series plot data from individual subjects. Data was acquired using channel A10 (position O_2).*

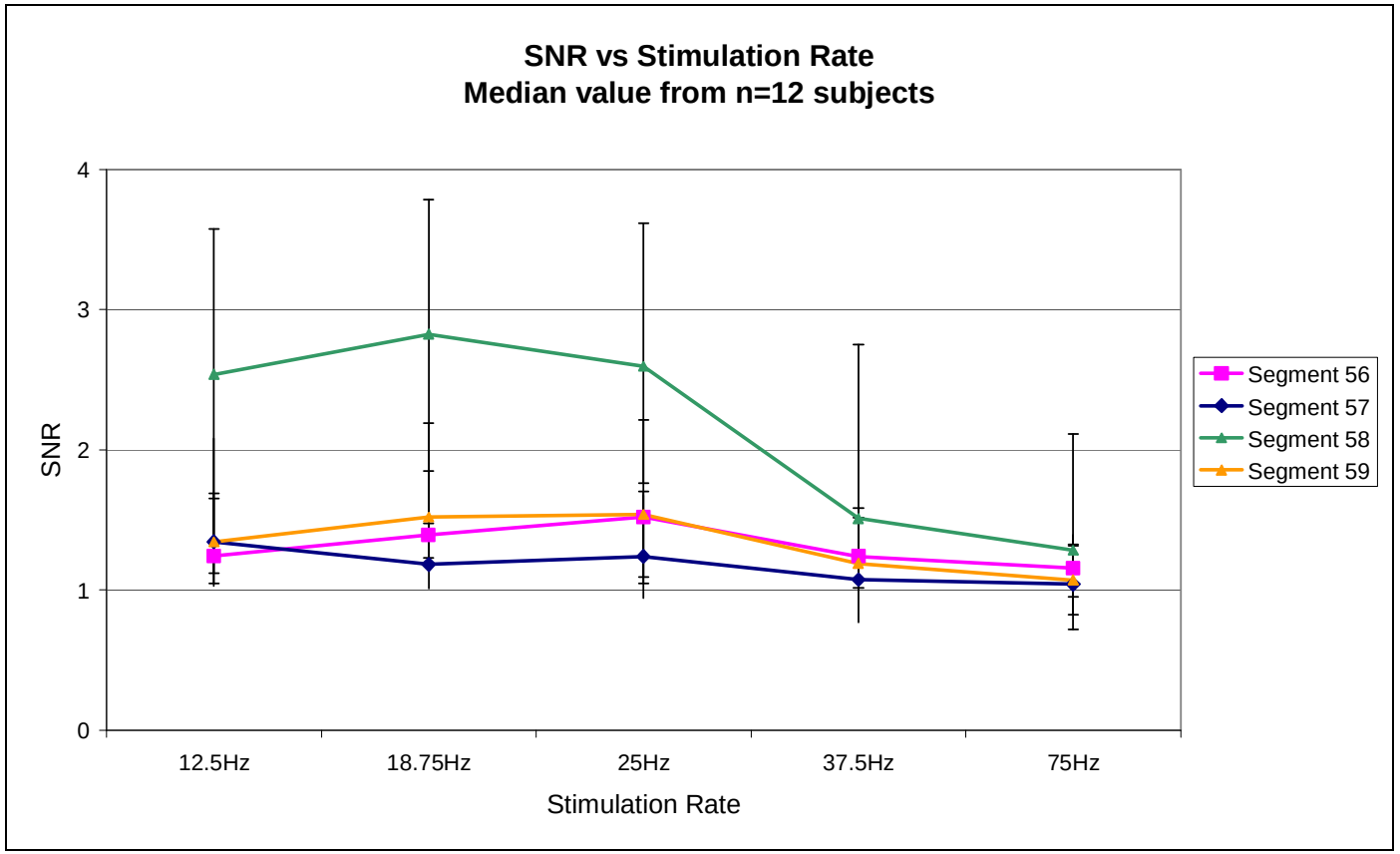

Figure 7.9 *Median SNR values are plotted against stimulation rate for the four central waveforms. This plot includes the data shown in Figures 7.4 and 7.5, but shows the median value from the n=12 subjects. Error bars show the 95% confidence interval of the median value. Data was acquired using channel A10 (position O_2).*

7.3.7 Overall Detection Rates - Results

Figure 7.10 encompasses all the data acquired using the multichannel recording system and shows the relationship between stimulation rate and the number of waveforms that exceed the detection threshold (i.e. those with a SNR value greater than the 90^{th} percentile of the distribution of SNR values of noise estimations). In order to be considered detectable, a stimulating region of the dartboard pattern had to evoke a waveform that exceeded the detection threshold for at least one of the 16 recording channels. Threshold values were calculated individually for each electrode to take into account possible differences in noise contributions.

Anderson-Darling Tests for Normality were performed on the detection rates for the 12 subjects at each stimulating frequency, and returned p values greater than 0.05. The null hypothesis that the underlying distribution is Normal should not therefore be rejected and parametric statistics can be used.

Error bars in Figure 7.10 show the 95% confidence interval of the mean. There is overlap of the 95% confidence intervals in almost every pair of stimulation rates. There is one exception which is the comparison of the 25Hz and 75Hz recordings which indicates a statistically significant increase in detection rate with the slower stimulation rate, at the $p<0.05$ level.

The highest detection rate was seen with a 25Hz stimulation rate. An average of 42/60 waveforms exceeded the detection threshold. This corresponds to a specificity of 90% and a sensitivity of 70%.

The poorest detection rate was seen with 75Hz stimulation where on average only 24 waveforms in the trace array exceeded the detection threshold. This corresponds to a specificity of 90% and a sensitivity of only 40%

.

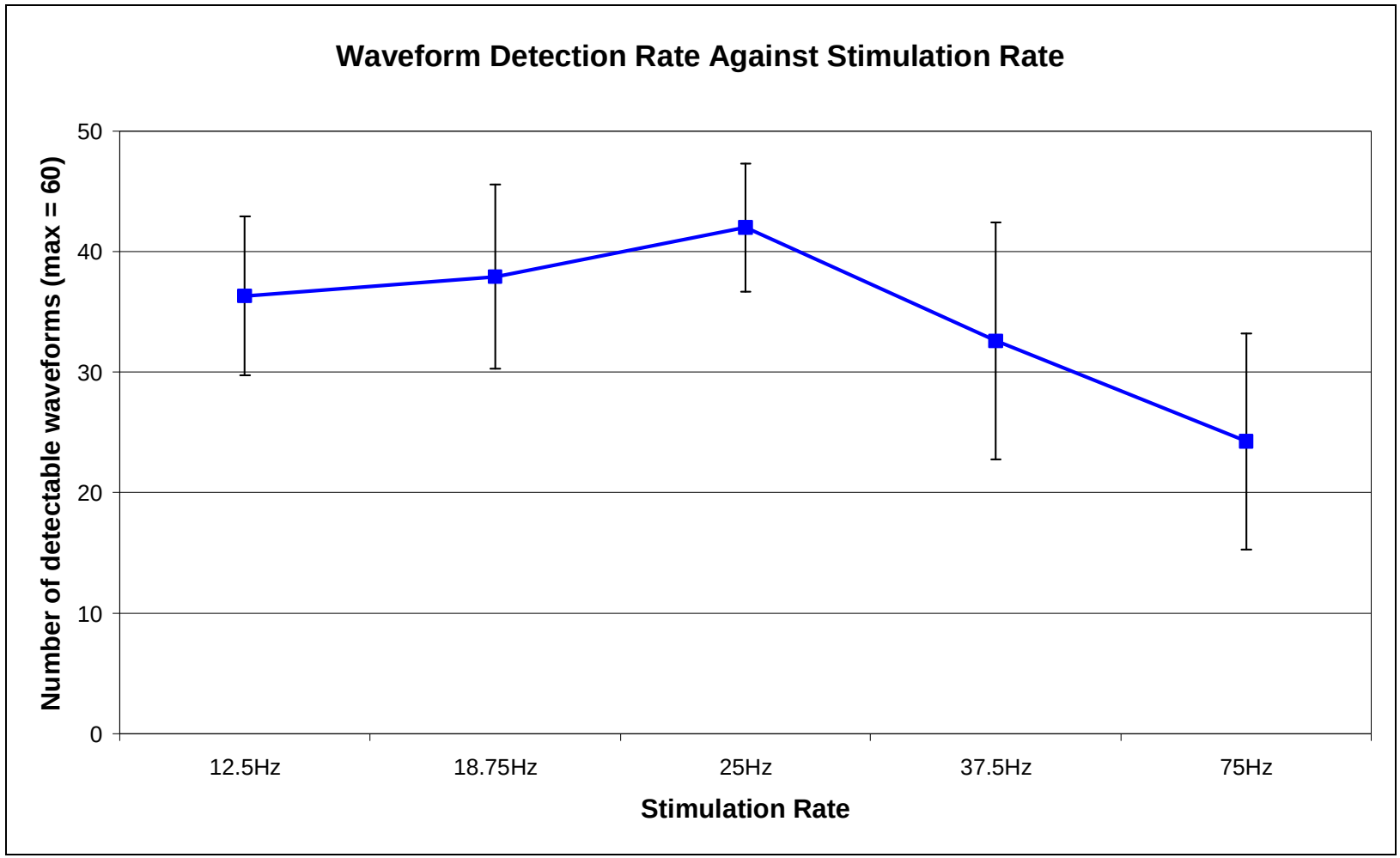

Figure 7.10 *Waveform detection rate is plotted against stimulation rate. To be detected, the SNR value had to be above the detection threshold in at least one of the 16 channels. Data are averaged over n=12 subjects. Error bars reflect the 95% confidence interval of the mean.*

7.3.8 **The Locations of Detectable Waveforms - Results**

Figure 7.11 maps the ability of the multichannel recording system to detect waveform responses to each of the stimulating regions within the mfVECP dartboard pattern when stimulation is performed at 25Hz with an m=13 bit m-sequence in an acquisition taking 6 minutes (Recording C). Detection rates in the upper field are slightly lower (68%) than the lower field (73%), but the difference is not significant at the p=0.05 level. There is no significant difference in the detection rates between the left and right hemifields.

Figure 7.12 is the same as Figure 7.11 but maps the detection rates for data acquired with 75Hz stimulation by an m=15 m-sequence, requiring 8 minutes of recording time (Recording H). Comparison of Figures 7.11 and 7.12 reveals a shift down the colour scale which reflects the falling detection rate. Again the detection rates are lower in the upper hemifield (49%) than the lower (62%). This difference is significant at the $p<0.05$ confidence level. Once again, no significant difference was seen in detection rates between the left and right hemifields.

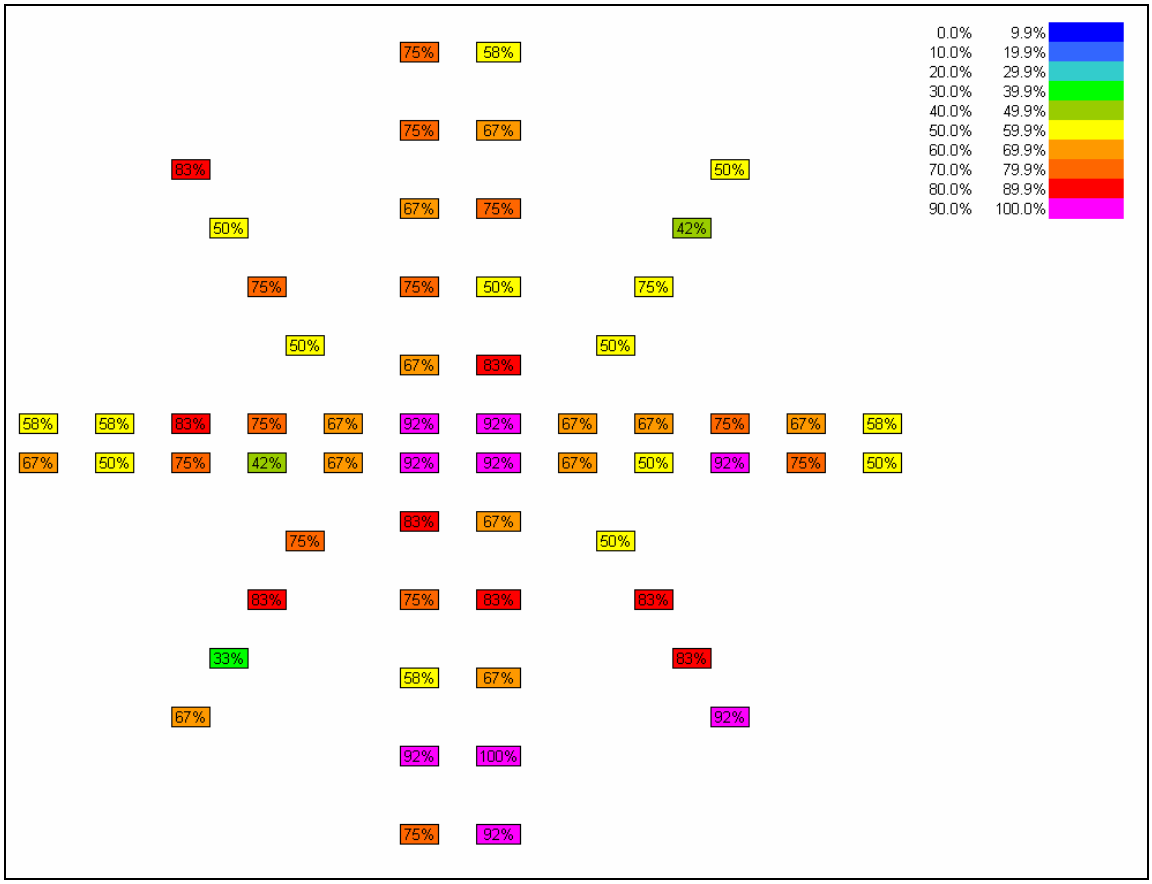

Figure 7.11 *Schematic showing how frequently waveforms in each location in the waveform trace array reach the detection threshold. For an individual waveform to be detected in any one recording, it had to reach the detection threshold in at least one of the 16 recording channels. Data from n=12 subjects was used to produce this figure, and was acquired during Recording C with a stimulation rate of 25Hz, an m-sequence length of m=13 and took 6 minutes to acquire. The colour scheme is shown in the top right-hand corner. Good detection rates are indicated by red and pink filled locations. These data are presented for the twelve subjects individually in Figure 7.14.*

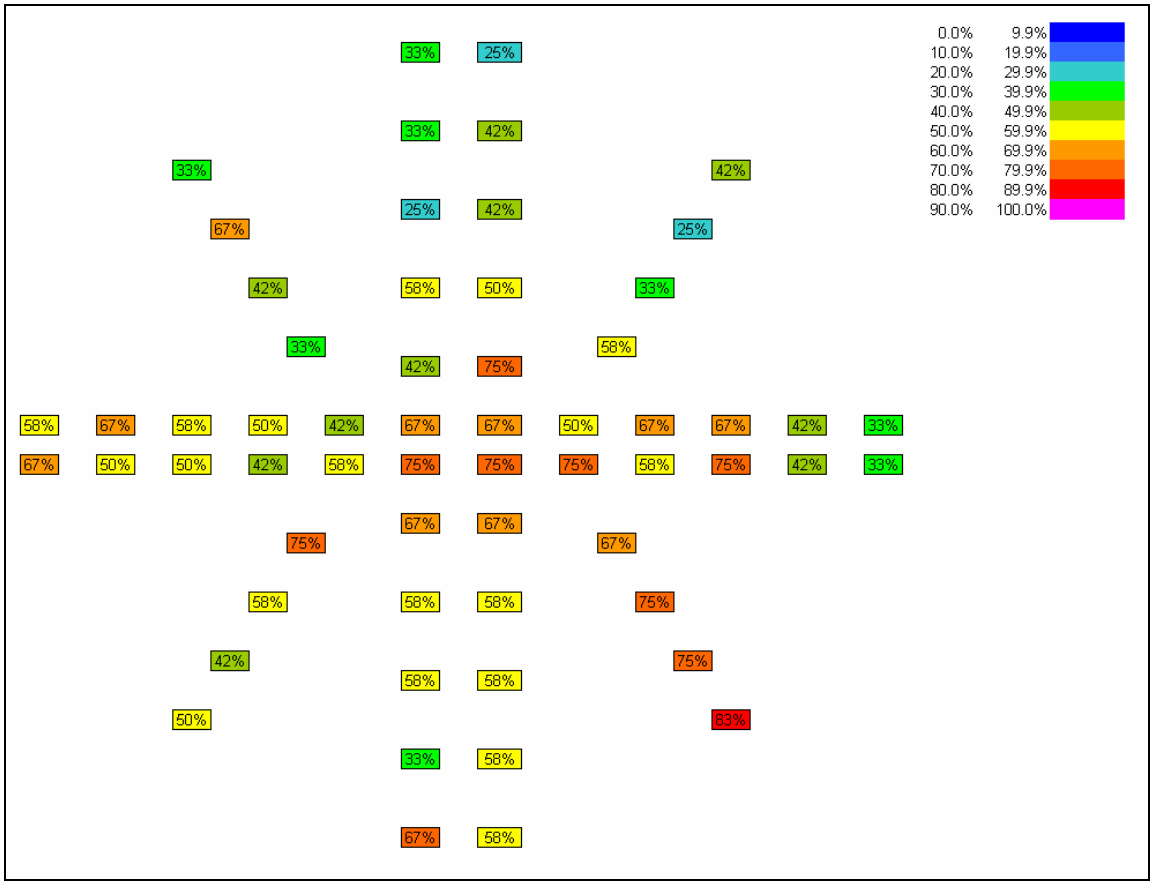

Figure 7.12 *As for Figure 7.11, this maps the detection rate of waveforms within the mfVECP trace array, but is based on Recording H (75Hz, m=15).*

Figure 7.13 shows how the detection rate changes with eccentricity for recordings C and H. There is a trend towards lower detection rates at the periphery, compared to the central waveforms. With 75Hz stimulation, this relationship is monotonically decreasing. This is not the case with 25Hz stimulation which appears to maintain higher detection rates out towards the periphery.

In general, changes in detection rate between neighbouring rings are not statistically significant (p=0.05). There are two exceptions:-

(1) the difference in the central ring and ring 2 for recording C with the central ring showing higher detection and

(2) between Rings 3 and 4 in recording C, where the more peripheral Ring 4 shows the better detection rate.

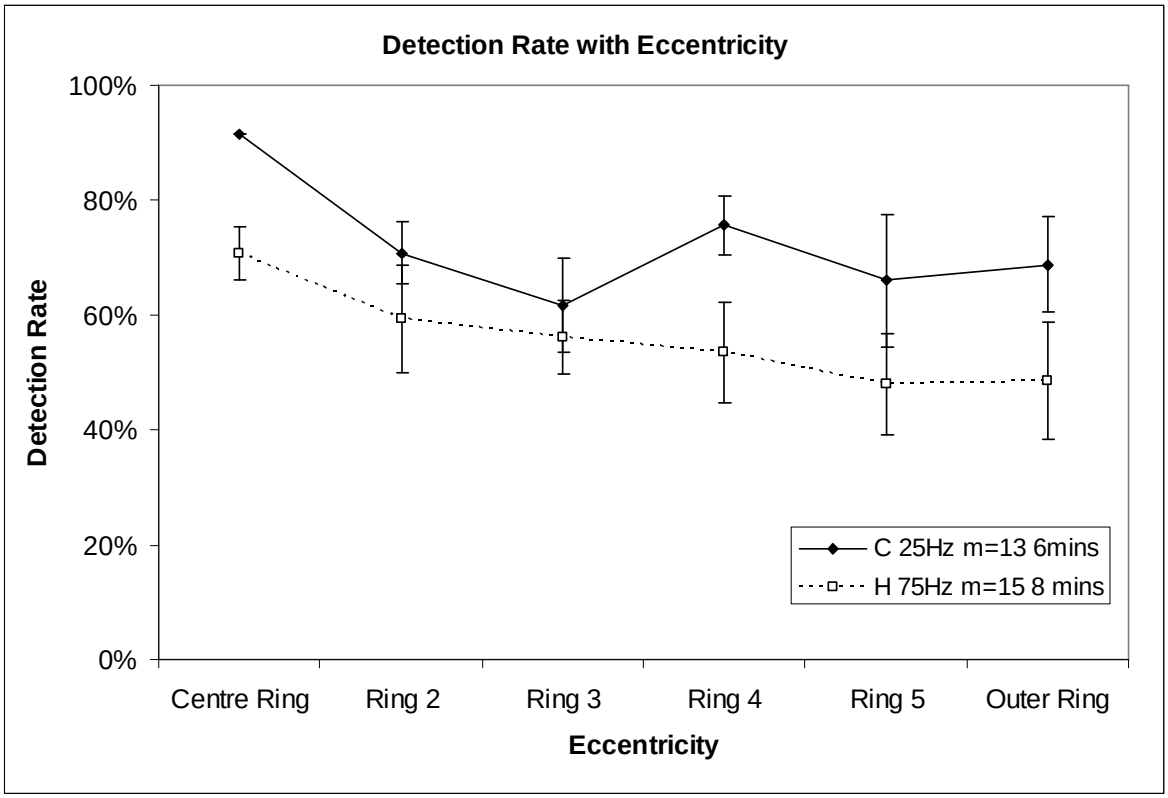

Figure 7.13 *The relationship between detection rate and eccentricity is plotted for recordings C (solid line) and H (dotted line). Error bars reflect 95% confidence intervals of the mean.*

Figure 7.14 demonstrates how consistent the pattern of detection show for Recording C (Figure 7.11), is within the 12 subjects. The colour scale is reduced to a binary system where red locations indicate that a detectable waveform was acquired by at least one of the 16 recording channels and blue indicates that no detection was possible.

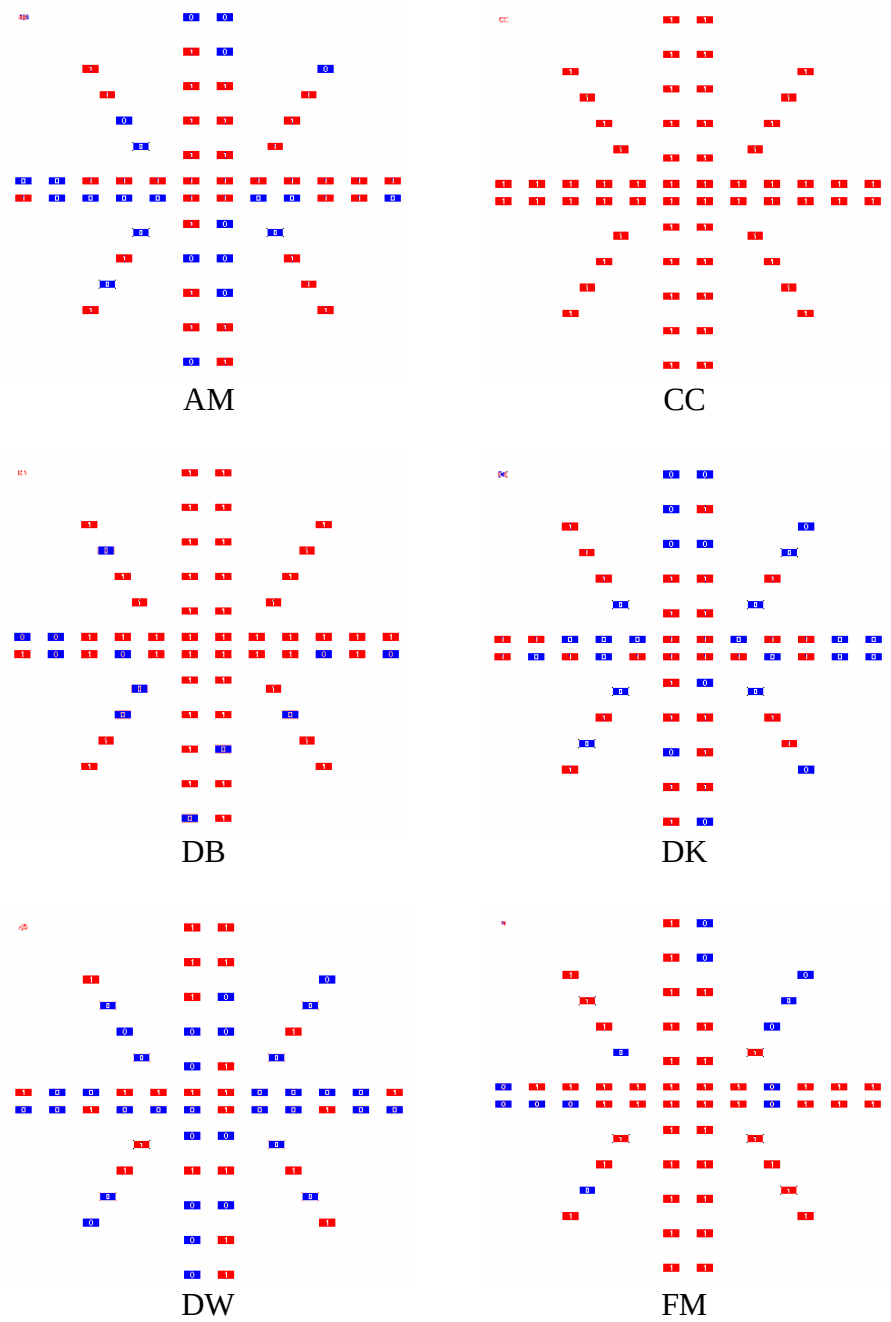

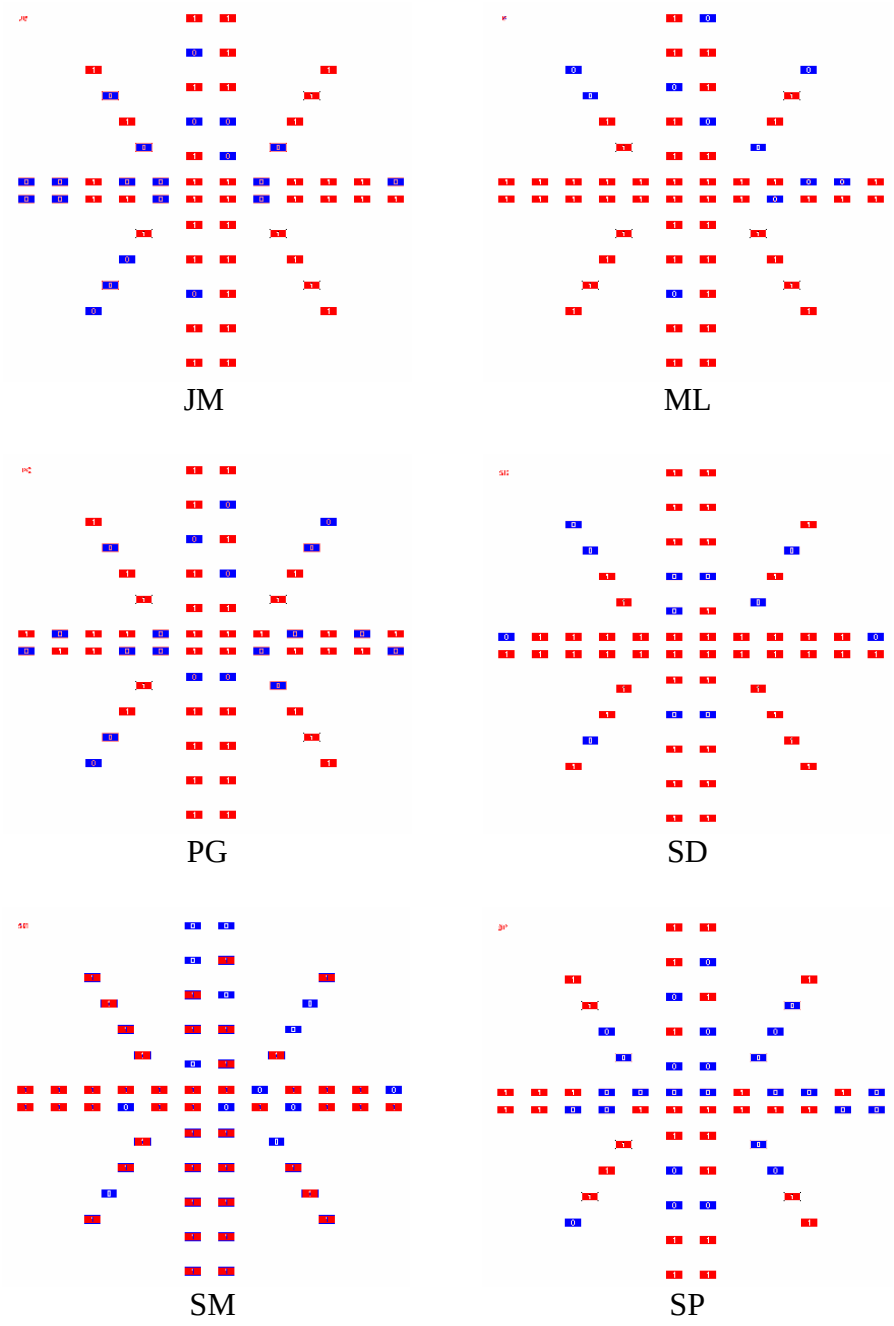

Figure 7.14 *Detectable waveforms within the mfVECP trace array are mapped. In order to be detectable, the SNR of a waveform must exceed the detection threshold in a minimum of 1 of the 16 recording channels. Red locations indicate a detected waveform. Blue locations indicate that a detectable waveform was not recovered from any of the 16 recording channels. Data presented here was acquired at 25Hz, m=13 from n=12 subjects. Individual elements depict data from each of the 12 subjects. The average of these data are shown in Figure 7.11.*

Figure 7.14 shows that:-

- There is considerable inter-individual variation in the detectable mfVECP responses.
- In general, the central 4 responses are detectable
- There is a trend towards better detection from the lower visual field and
- 100% detection was possible in one subject (CC). Trace arrays from this subject are shown in Figure 7.15.

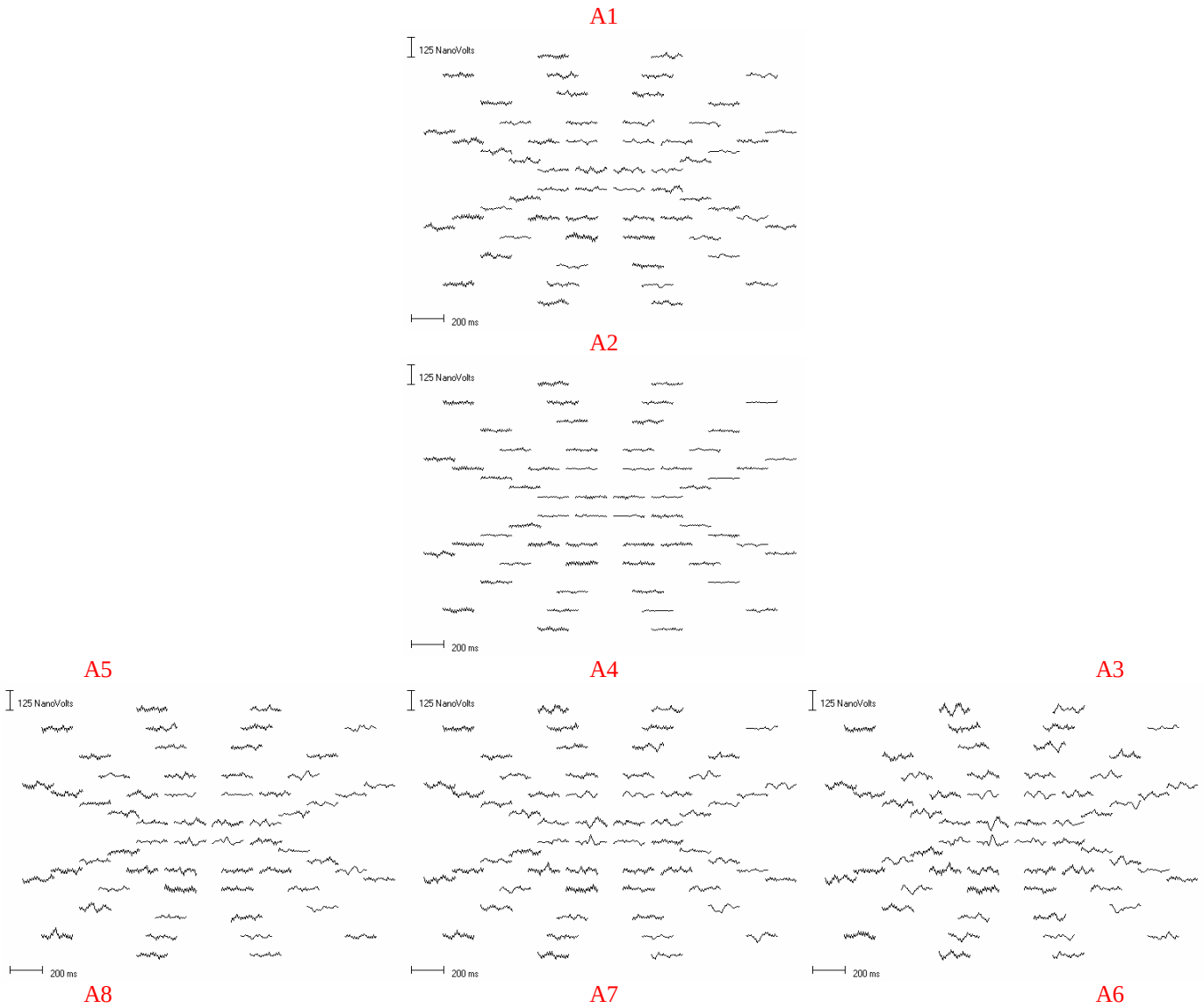
A1
125 NanoVolts
200 ms
A2
125 NanoVolts
200 ms
A5
A4
A3
125 NanoVolts
200 ms
125 NanoVolts
200 ms
125 NanoVolts
200 ms
A8
A7
A6

Figure 7.15 Trace arrays from subject CC. A detectable waveform was found in all 60 locations of the waveform array from at least one of the 16 recording electrodes

7.3.9 **The Locations of Detectable Waveforms - Discussion**

Cortical scaling of the dartboard pattern aims to allow each region to stimulate similar volumes of the visual cortex. Despite this, detection of the central waveforms was superior to that of the outer rings when both 25Hz and 75Hz stimulation were employed.

In both cases, detection of responses to stimulation of the upper visual field was poorer than that of the lower visual field. This difference was statistically significant for 75Hz stimulation ($p<0.05$), but not for 25Hz.

The detection rate showed a simple decrease with eccentricity for 75Hz stimulation. The relationship for 25Hz stimulation was slightly more complicated. Changes from ring to ring were not, in general, statistically significant, and there appeared to be a preservation of detection rates towards the periphery.

A novel finding has been shown. A 6 minute, 25Hz recording has several advantages over the more widely used 8 minute, 75Hz acquisition. Not only is the overall detection rate superior, but the degree to which the lower visual field is favoured is reduced, and the loss of detection towards the periphery of the visual field decreases when the stimulation rate is reduced. The use of 25Hz stimulation in clinical recordings is therefore highly recommended.

7.4 Discussion

The volume of data acquired in a multichannel mfVECP acquisition is considerable. It is not feasible to assess every waveform on an individual basis. While the waveforms of mfVECP recording remain variable between subjects and throughout the trace array, as evidenced in the data presented here, it is not appropriate to use simple automated means of placing cursors to determine latency and amplitude. The calculation of a SNR overcomes this to an extent. It has been shown in this chapter that slower rates of stimulation result in waveforms of longer latency and that calculating the SNR over the most commonly employed window of 45-150ms will artificially reduce the SNR and impede the detection of signals greater than noise. Automated analyses must therefore make a careful selection of the SNR time window. It has been demonstrated here that the use of a longer time window is advantageous when slower stimulation rates are used and has no negative impact on data acquired at faster stimulation rates.

Analyses presented in some of the preceding chapters have employed SNR values calculated over 45-150ms. This remains appropriate since stimulation rates were always 75Hz, a rate at which the shorter time window will not disadvantage detection rates.

In a study of mfERG waveforms and stimulation rate, Sutter (92) observes that the 'the memory of the system i.e. the duration of the kernel slices with all their induced components appears to increase when stimulation is slowed down. With a base period of 13.3ms, the mfERG kernel slices don't usually exceed 100ms. However, with a bp of 40ms induced components can often be found on the first order kernel beyond 150ms.'

In concordance with his observation, mfVECP data presented here exhibits increases in latency with slower stimulation rates.

Our findings are at odds with Martins *et al* (116), who found decreased latency with 37.5Hz stimulation compared to 75Hz. This could be attributed to methodological differences. While both experiments involved dartboard stimuli, Martins *et al* used three rings and 32 blue and yellow regions extending to a field of view of radius 26°, while a six ring, 60-region black and white stimulus, extending to a radius of 22° was used in the present experiment. Finally, the mathematics controlling pattern reversal

also differ. While single binary m-sequences were used by the EDIU Multifocal System, Martins *et al* employed the Accumap system which uses a series of short binary sequences instead.

Our results are also at odds with Martin's report of data presented by Balachandran (117), in which she indicates that black and white, 25Hz stimulated mfVECPs were reduced in amplitude – she does not specifically what she was comparing that to, but the standard 75Hz stimulation rate would be a reasonable assumption.

The findings are however in concordance with the hypothesis laid out by Fortune and Hood (109). They suggested that as the rate of stimulation slows, the mfVECP response becomes more like the conventional VECP response and that increases in signal size could be due to the activation of dipoles within the extra-striate in addition to striate cortex, whereas fast mfVECP stimulation of 75Hz is thought to evoke responses from striate cortex alone.

Improved detection rates in the upper visual field with the slower 25Hz stimulation rate could also be as a result of the recruitment of additional extrastriate areas and therefore dipoles that are more conducive to detection by the arrange of 16 monopolar electrodes used here.

Ireland *et al*(88) have investigated which m-sequences are appropriate for use in a multifocal electrophysiology – i.e. which sequences maintain orthogonality for a sufficient period of time to avoid cross-contamination of the first or second order response with higher or lower order responses. She notes that in the case of the mfVECP where the evoked potential response requires a longer time period to appear than the electroretinogram response, the cross-correlation period must be longer and there is, therefore an increased chance of cross-contamination. All m-sequences used in this experiment are orthogonal and robust to cross-contamination for a minimum of 426ms. All waveforms presented here returned to baseline well within this time frame.

Furthermore, if the stimulation rate is increased, then the cross-correlation of the physiological response must be performed over a longer window of the m-sequence, i.e. a larger number of m-sequence steps. The longer this window, the higher the chance of cross-contamination. This suggests that cross-contamination is less likely at slower stimulation rates, despite increases in waveform latency.

7.5 Future work

For practicality, several of the analyses here were restricted to a data acquired from a single recording channel. They could be repeated with the other recording channels which show good detection levels.

Only two time windows have been assessed here. Further work could include the investigation of a wider range of SNR calculation time windows.

Throughout this chapter, data trends have been reported. Statistical significance has not always been achieved; suggesting that the number of subjects tested should be increased to improve the power of the experiment. This has not been done due to limitations of time. Furthermore, the analysis of an even larger volume of data would require that the analysis process is automated to a greater extent.

Data in this chapter was presented from a significantly larger number of recording electrodes than is used in the majority of mfVECP literature. They are presented as monopolar data, as are data presented by James AC (17) who also made use of a large electrode array. While analysis presented here focussed on the monopolar data, bipolar information can be derived and may well provide further improvements in detection rate. The recording system and the use of monopolar recording electrodes is discussed in greater detail in the following chapter.

7.6 Conclusion

Reducing the stimulation rate of the pattern-reversal mfVECP results in an increase in the latency and amplitudes of responses and a late negative trough became more prominent.

The increase in latency prompted an investigation of the most appropriate time window to use for SNR calculations. This concluded that when slower stimulation rates were used, a longer time window of 45-250ms was advantageous in discriminating between true signals and data containing noise alone and that when fast stimulation rates were employed, there is no detrimental effect to using a longer time window.

Improvements in the SNR were seen at stimulation rates below the standard 75Hz. This resulted in a better test performance, as illustrated by ROC analysis, with a 25Hz stimulation rate outperforming 12, 18.75, 37.5 and 75Hz.

Changes in the SNR of central waveforms showed a trend towards increasing with decreasing stimulation rate, however the results were varied and statistical significance was not achieved.

The sensitivity of the mfVECP test can be improved by reducing the stimulating frequency from the standard rate of 75Hz to 25Hz. Further improvements in sensitivity were not seen when the stimulation rate was slowed below 25Hz.

The difference in detection rates with stimulation rate only reached statistical significance for the comparison of 75Hz and 25Hz stimulation. 25Hz stimulation for 6 minutes was superior to 8 minutes of 75Hz stimulation, despite an 8-fold decrease in the number of pattern reversals.

Detection rates are globally improved by reducing the stimulation rate from 75Hz to 25Hz. Increased detection is seen in the vast majority of response locations throughout the visual field (54/60 visual field areas). In addition, using a 25Hz stimulation rate reduces the asymmetry in signal detection in the upper and lower hemifield seen at 75Hz. Furthermore, 25Hz stimulated responses do not suffer from reduced detection rates in peripheral visual field locations to the same degree as 75Hz stimulated responses.

In short, there is much to be gained by moving from the standard stimulation rate of 75Hz and reducing it to 25Hz. Electrophysiologists can capitalise on shorter examination times, patients are required to fixate and concentrate for a shorter period of time and signal quality and test performance can be improved.

This investigation was performed using a 16-channel multifocal recording system, which provided a wealth of information. The construction and validation of this system is discussed in the next chapter.

Chapter 8

Creating A Multichannel Multifocal Electrophysiology System

Contents

		Page
8.0	Introduction …….	230
8.1	A Review of Electrode Positions used in mfVECP Acquisition ..	231
8.2	Equipment …….	234
8.2.1	EDIU Multifocal System…….....	234
8.2.2	BioSemi Systems ……	235
8.3	Synchronising mfVECP Stimulation and Data Acquisition..….	236
8.3.1	Introduction ……...	236
8.3.2	Aim …….....	236
8.3.3	Method…….....	236
8.3.4	Results…….....	237
8.3.5	Conclusion…….....	238
8.4	File Format Conversion Software …….	239
8.4.1	Introduction ……...	239
8.4.2	Aim…….....	239
8.4.3	Methods…….....	240
8.4.4	Results and Conclusion……...	241
8.5	BioSemi System Tests – ActiveOne and Large Signals……	242
8.5.1	Introduction ……..	242
8.5.2	Aim ……	242
8.5.3	Methods ……	242
8.5.4	Results ……...	245
8.5.5	Conclusion …….	246

Page

8.6 BioSemi System Tests – ActiveOne and Responses to Multifocal Stimulation …… 247
8.6.1 Aim ……..... 247
8.6.2 Method …….. 247
8.6.2.1 Sample Rate Difficulties ……..... 249
8.6.2.2 M-sequence Difficulties ……. 250
8.6.3 Results ……..... 252
8.6.3.1 Photodiode …….. 252
8.6.3.2 Normal Volunteer mfERG ……. 253
8.6.3.3 Normal Volunteer mfVECP …..... 254
8.6.4 Conclusion ……..... 255
8.7 BioSemi System Tests – ActiveTwo ……..... 256
8.7.1 Aim …… 256
8.7.2 Methods ……..…… 256
8.7.3 Results ……...…… 260
8.7.4 Conclusion …….. …… 260
8.8 Selecting Optimal Recording Locations……...……. 264
8.8.1 Introduction …… 264
8.8.2 Aims ……..…….. 264
8.8.3 Methods……..…. 264
8.8.4 Results……. 267
8.8.4.1 Individual Channels…….…… 267
8.8.4.2 Optimal Combination of Channels…….. 272
8.8.5 Discussion……... 275
8.8.5.1 Individual Channels …… 275
8.8.5.2 Optimal Combination of Channels…….. 275
8.9 Discussion ……. 278
8.10 Summary ……..... 282

8.0 Introduction

The anatomy of the visual cortex is highly convoluted and dipoles evoked within it are oriented in many different directions. The probability of detecting small responses to stimulation of small local areas of the visual field is increased if the dipoles are interrogated by a large number of scalp electrodes since there is a greater chance that a dipole will project onto the scalp in a favourable manner for detection in at least one recording channel.

The aims of the work presented in this chapter were twofold. The first was to create a multifocal electrophysiology system capable of acquiring mfVECPs from a large number of recording electrodes. Recognising that large numbers of electrodes are not necessarily attractive for routine clinical use, the second aim was provide a base of evidence acquired from normal volunteers, from which a subset of electrodes which will provide the maximum amount of information on the response of the visual cortex to stimulation of a large number of small areas of the visual field, can be selected.

The visual evoked cortical potential is conventionally recorded with between two and five electrodes. In contrast, the electroencephalogram (or EEG) makes use of a wide array of electrodes. This chapter discusses the integration of a multichannel EEG recording system with our in-house multifocal system.

The chapter begins with a literature review of the electrode placements which have been used in VECP and mfVECP recordings to date and a description of the electrophysiology acquisition systems used in the present work follows.

The integration and testing of the two electrophysiology systems is described as a series of tasks that enabled synchronisation, allowed file conversion, tested the systems' ability to record and process signals. Finally an assessment the most appropriate monopolar recording channels from 16 electrode locations.

This system was described in an ARVO 2002 abstract (153).

8.1 A Review of Electrode Positions used in mfVECP Acquisition

The electrode placements used in the conventional VECP have been standardised by ISCEV(26). This standardisation provides consistency in the recording of VECPs in different centres and allows comparison of their patient investigations and research studies.

The standard full-field VECP stimulates a large proportion of the visual field and potentials are evoked over a large volume of the visual cortex. As a result of cortical magnification, anatomy and geometry, the record is dominated by the response of the central visual field.

Cortical magnification means that the central visual field is served by a large volume of visual cortex compared to peripheral visual field (45;96;124;154). The retinotopic representation of the visual field is organised in such a way that the central visual field maps to the occipital pole while peripheral retinal areas map to cortex within the calcarine fissure (155). Peripheral responses will therefore be attenuated to a greater degree prior to measurement by surface electrodes.

Electrodes record a linear combination of signals from multiple volumes. The convoluted nature of the cortex means that the contribution of a particular volume will depend on its location and orientation within the cortex. Signal cancellation will occur at the scalp when activated volumes of cortex are geometrically opposed (12;156).

The full field VECP evokes responses from different parts of the visual field. Responses to stimulation of these local areas of the visual field are dipoles which are oriented in different ways, depending on their position within the gyri of the visual cortex. Surface electrodes measure a signal that is dependent on the distance between the dipole and the recording electrode, and the projection of the dipole onto the scalp. When a large number of local responses are simultaneously evoked, as in the full field VECP, the recorded signal is the vector sum of these contributions. Since the central visual field is represented in the occipital pole, the dipoles created by its stimulation are less attenuated than more those from more anteriorly situated areas and are optimally oriented for detection by surface electrodes, the result is a full field VECP waveform which is dominated by the central response.

Different electrode locations have been investigated by a number of investigators, including Schippers *et al* (157). An array of 14 bipolar channels was used to study the

gradient distributions and current density distributions in four subject with amblyopia and ten control subjects. Gradient maps were acquired with a number of different check sizes. The pros and cons of monopolar and bipolar channel recordings with respect to common mode rejection ratios and accuracy of recording were discussed. The common mode rejection ratio is substantially reduced in the case of subtraction of monopolar voltages compared with the direct bipolar recording. Unequal calibration and drifts of the amplifier gains by only a small percentage cause reduction of the common mode rejection ratio. Bipolar channels measure a smaller voltage. The ADC resolution can therefore be optimised over the range.

James AC (17) used a 30-electrode array when presenting the Pattern-Pulse Multifocal VEP and presented waveforms derived from monopolar data.

The mfVECP response exhibits greater inter-subject variability than the VECP.

While the positions of local gyri and sulci are very varied from one individual to the next, the position of the visual cortex within the brain, retinotopic mapping and the positions of the different visual areas V1, V2 etc remain comparatively constant.

The full-field VECP is a global, vector sum response to stimulation of a large portion of the visual field and inter-individual variation in local cortical anatomy is, to an extent, averaged out. The mfVECP however, aims to detect the behaviour of dipoles in much smaller volumes of visual cortex which are subject to greater variation in their orientation, giving rise to a greater variability in the waveform responses to stimulation of the same visual field location in different individuals. This suggests that the electrodes used for VECP acquisition may not be optimal for mfVECP acquisition and that it may in fact be useful to interrogate the visual cortex from a number of different orientations using a larger number of electrodes.

In clinical terms inter-subject variability of waveform responses makes it difficult to define a normal and abnormal response. Researchers continue to look for universally optimal recording channels.

In 1998 Klistorner, Graham and co-workers turned their attention to the electrode placement used to record the mfVECP(16;111). They found that the ISCEV recommended electrode placements favoured responses to stimulation of the lower visual field, and recommended a Bipolar Occipital Straddle (BOS) arrangement with electrodes 2cm above and below the inion that gives more uniform amplitude signals

from the entire stimulated area. They have since varied the position of the upper electrode to 3cm (76;158) and 2.5cm (123;159) above the inion. Their lower electrode has been used at 4.5cm (76;123;159) and 6cm (158) below the inion,

In previously unpublished data, mfVECPs were recorded from thirteen healthy volunteers using three bipolar channels (2cm above inion – 6cm below the inion, 2cm above the inion – 2cm below in the inion and 2cm right of the inion – 2cm left of the inion). It was found that not only did the optimal electrode channel vary from subject to subject, but that within a single subject, the responses to stimulation of different areas of the visual field were best recorded with different electrodes. This finding is in agreement with Hood and his co-workers (128), who recorded from four active electrodes and derived six recording channels. Despite increased electrode numbers, there remain visual field locations in some individuals from which it is difficult to obtain signals above the level of noise.

Most of the literature concerning electrode placement in mfVECP recording appears to have used a trial and error approach to electrode location selection, reporting their chosen optimal electrode positions.

Multichannel recordings allow us to interrogate the cortex from a larger number of locations. This gives us a greater chance of detecting small signals that may be at an inopportune orientation for detection with a smaller number of electrodes. With more electrodes there is a higher probability that an electrode will be close to a small dipole and the signal will not be attenuated before detection.

The acquisition of data from a large number of recording electrodes can inform the selection of a smaller number of channels for routine clinical use.

8.2 Equipment

The experiments described in this chapter made use of three electrophysiology acquisition systems. These are the custom-built EDIU Multifocal System described in detail in Chapter 2 and two versions of BioSemi equipment. The BioSemi and the EDIU Multifocal systems are not designed to work together. A summary of the specifications is tabulated in Table 8.1 for comparison.

	EDIU Multifocal System	BioSemi ActiveOne	BioSemi ActiveTwo
Number of recording channels available	4	48	16
File Format	.mf	.edf	.bdf
Quantisation	10-bit	16-bit	24-bit
Triggers	Integral to software acquisition.	External triggers could not control the recording of data.	An external trigger could be used to control the recording of data.
Stimulation	Software creates and controls visual stimulus.	System is not designed to deliver a visual stimulus.	System is not designed to deliver a visual stimulus.
Data processing	Software cross-correlates recorded data to recover multifocal electrophysiological responses.	Data processing is elementary and is not capable of handling cross-correlation.	Data processing is elementary and is not capable of handling cross-correlation.

Table 8.1 *Summarised Technical Details of the Recording Systems used in Developing the Multichannel Multifocal VECP.*

8.2.1 EDIU Multifocal System

The EDIU Multifocal System was described in detail in Chapter 3. It is self-contained and capable of stimulation, acquisition and data processing. In the present chapter, the stimulation and data processing functions were used and the acquisition function was provided by either the ActiveOne or ActiveTwo BioSemi systems.

8.2.2 BioSemi Systems

A 48 channel, ActiveOne BioSemi EEG amplifier was obtained. This system was selected because:

- It is capable of acquiring data from a large number of electrodes.
- It has amplification at the electrode site. Skin preparation, which is a time consuming part of subject preparation, is therefore not required.
- The resolution and dynamic range suggest that they should be suited to the size of mfVECP signals quoted in the literature (12;13;17;33;76;109;127).

BioSemi systems make use of 'active electrodes'. These perform amplification at the electrode site rather than after transmission of a small signal along a connecting wire.

The active electrode can cope with very high input impedance. By integrating the first amplifier stage with a sintered Ag-AgCl electrode, extremely low-noise measurements free of interference are possible without skin preparation. Impedance transformation occurs at the electrode and as there is very low output impedance, problems with capacitive coupling between the cable and sources of interference, as well as any artifacts induced by cable and connector movements are completely eliminated (160).

Figure 8.1 *An Active Electrode (Image taken from www.biosemi.com)*

The BioSemi systems do not control the visual stimulus, have no access to the m-sequence information and are not sufficiently sophisticated to perform cross-correlation. They can record multifocal electrophysiology but cannot perform the required data processing. The EDIU Multifocal System is capable of acquiring and cross-correlating a maximum of four data channels. Certain modifications were therefore required to integrate the two systems to allow the acquisition and cross-correlation of data from a large number of channels.

8.3 Synchronising mfVECP Stimulation and Data Acquisition

8.3.1 Introduction

The duration of standard multifocal stimulation is commonly eight minutes. In order to achieve a good response from subjects, it is necessary to divide the recording session into periods of time over which they can comfortably maintain fixation without significant movement and/or blinking. The EDIU Multifocal System delivers the stimulus in a series of 30-second segments and, when it is used to record data, data acquisition occurs only during 'stimulus on' periods. No data are recorded during rest periods. In contrast, the BioSemi system records continuously. No automated means of pausing recording during rest periods is available and so redundant physiological data are included in the data record.

Timing is critical. A mis-registration between the behaviour of the stimulus and the recorded signal will render the data useless. The cross-correlation will be shifted in time and cancellation of signal rather than recovery is anticipated.

8.3.2 Aim

To synchronise the behaviour of the mfVECP stimulus provided by the EDIU Multifocal System with the acquisition of data by the BioSemi ActiveOne.

8.3.3 Method

To create a record within the BioSemi .edf file of when the visual stimulus was active, a step-up trigger pulse was supplied at the beginning of each segment of the multifocal stimulus. Modification of both the EDIU Multifocal System software and assembly programming was necessary to achieve this. The pulse was recorded on a trigger channel in the BioSemi system. Software (Delphi 4, Borland, USA) was written to read the trigger channel in order to identify when periods of active stimulation began. Data was then taken from the BioSemi '.edf' file for 30-second intervals beginning at the start of each session. Data acquired during inactive periods was discarded by the file conversion software.

To minimise modifications to the assembly language, the trigger did not automatically step down at the end of each m-sequence segment. Instead an input from the operator was required to confirm that the segment was complete, which brought the trigger signal to a low state.

The exact duration of the m-sequence segment is known and so the period of .edf data representing stimulated physiological data can be calculated as long as the trigger step up is identified.

8.3.4 Results

It was clear during recording, via the BioSemi acquisition software (see example in Figure 8.2), that the trigger step-up pulse was created and recorded at the beginning of each m-sequence segment.

A number of tests were carried out to check that the file conversion software correctly identified the trigger step-up pulses recorded by the BioSemi system. The appearance of the step up pulses was in turn checked by visual inspection during recording. The result of one of these tests is shown below in Table 8.2. It can be seen that the file conversion software accurately identifies the trigger ON pulses. The error represented by the final two columns can be explained by the relatively poor temporal resolution of the BioSemi display software compared to that of the file conversion software.

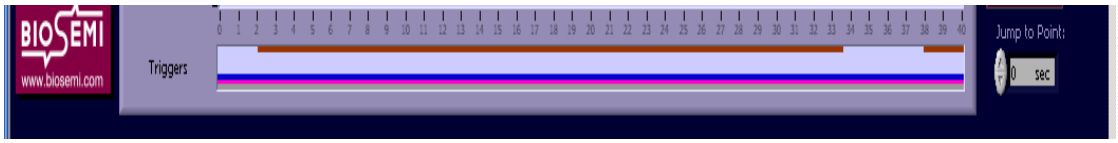

Figure 8.2 *Trigger signal as illustrated by a screenshot from the BioSemi System software. The brown line indicates the trigger status.*

Figure 8.2 above shows the trigger signal. It appears at 2 seconds, indicating the beginning of an m-sequence segment. Is disappears at 33.5 seconds. The m-sequence segment duration is 27.33seconds (this accounts for $1/8^{th}$ of a 15-bit m-sequence, while allowing overlap). The approximately 3 second delay in the trigger status returning to low is due to the delay in the operator confirming that the segment is complete. The trigger status returns to a high state at 38 seconds indicating the beginning of the second m-sequence segment.

Time of Trigger Step Up Pulse as read on BioSemi Software (seconds)	Converted into a Sample Number.	File Conversion Software identified Trigger switching On at sample number	Difference (Measured in samples)	Error (seconds)
1.6	3276.8	3357	-80.2	-0.039
3.6	7372.8	7352	20.8	0.012
5.3	10854.4	10928	-73.6	-0.036
7.3	14950.4	15045	-94.6	-0.046
8.9	18227.2	18323	-95.8	-0.047
10.7	21913.6	21908	5.6	0.003
12.3	25190.4	25104	86.4	0.042
13.7	28057.6	28070	-12.4	-0.006
15.2	31129.6	31166	-36.4	-0.018
16.6	33996.8	34126	-129.2	-0.063
18.1	37068.8	36949	119.8	0.058
19.6	40140.8	40161	-20.2	-0.010
20.9	42803.2	42735	68.2	0.033
22.6	46284.8	46298	-13.2	-0.006
23.8	48742.4	48680	62.4	0.030
25.2	51609.6	51534	75.6	0.037

Table 8.2 *Data showing that file conversion software correctly identified the trigger points.*

8.3.5 Conclusion

A method of synchronising the behaviour of the mfVECP stimulus create and delivered by the EDIU Multifocal System with the acquisition of data by the BioSemi ActiveOne has been achieved.

8.4 File Format Conversion Software

8.4.1 Introduction

The BioSemi ActiveOne system stores its data in an '.edf' file format (European Data Format) which is commonly used in commercial EEG recordings (161).

The BioSemi ActiveTwo system uses a '.bdf' file format which is very similar to the .edf format. The key difference is that it stores 24-bit data rather than 16-bit data.

The EDIU Multifocal System uses a custom designed file format known as the Multifocal File '.mf'.

.edf and .mf file structures are illustrated in Figure 8.3 and described below.

EDF Header

SR words	Channel 1	1st sec
SR words	Channel 2	1st sec
:	:	1st sec
SR words	Channel C	1st sec
SR words	Channel 1	2nd sec
SR words	Channel 2	2nd sec
:	:	2nd sec
SR words	Channel C	2nd sec
:	:	:
SR words	Channel 1	Tth sec
SR words	Channel 2	Tth sec
:	:	Tth sec
SR words	Channel C	Tth sec

MF Header

SR words	1st sec	Channel 1
SR words	2nd sec	Channel 1
SR words	:	Channel 1
SR words	Tth sec	Channel 1
SR words	1st sec	Channel 2
SR words	2nd sec	Channel 2
SR words	:	Channel 2
SR words	Tth sec	Channel 2
SR words	1st sec	Channel 3
SR words	2nd sec	Channel 3
SR words	:	Channel 3
SR words	Tth sec	Channel 3
SR words	1st sec	Channel 4
SR words	2nd sec	Channel 4
SR words	:	Channel 4
SR words	Tth sec	Channel 4

Figure 8.3 *A schematic illustration of the different structures of .mf and .edf file formats for a recording of* T *seconds' duration, recorded with a sampling rate* SR *by* C *channels.*

8.4.2 Aim

To overcome file format differences and permit data acquired by the BioSemi ActiveOne system to be cross-correlated by the EDIU Multifocal System.

8.4.3 **Methods**

Software was written using the Delphi 4 (Borland, USA) to convert .edf data into the .mf format. This allowed converted data to be read and cross-correlated using existing software. The key functional steps in the file conversion software are summarised in Figure 8.4 and are described below.

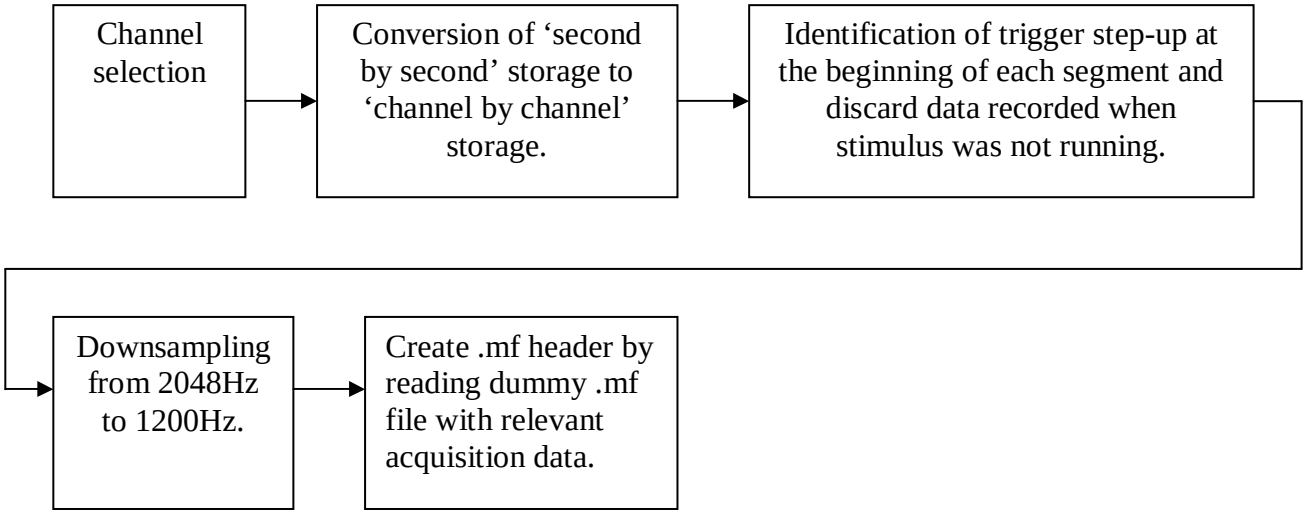

Figure 8.4 *The functional steps of the file conversion software are shown.*

- The .edf file format is designed to contain a flexible number of channels' worth of data. .mf files are structured to contain a fixed number of four. The initial step was to select four sequential channels from the .edf file that would be read and written into .mf format.

- .edf file structure records in 1 second portions. For an acquisition from *C* channels with a sampling rate of *SR* Hz, the first *C.SR* data samples will contain the first seconds' worth of data for each channel. Data for the *n*th second of acquisition from Channel *c* of *C* commences at sample number:

  $$(n\text{-}1).C.SR + c.SR \qquad \textbf{Equation 8.1}$$

  In contrast, the .mf format writes the data for each complete channel in turn. A procedure was written to read data from the .edf format and write it into .mf format.

- The BioSemi acquisition records data whether the visual stimulus is running or not. The trigger signal identifies when the stimulus is present. The .edf file

therefore contains data during which no stimulation occurs. The .mf format has no capacity for this redundant information and so it must be stripped away. A procedure that identifies trigger behaviour and removes redundant data was created. This has the advantage of ensuring that the size of the .mf file is consistent with the duration of stimulation, keeping it compatible with the cross-correlation component of the EDIU Multifocal System.

- Downsampling. The BioSemi acquires with sampling rate of 1024Hz or 2048Hz. The EDIU Multifocal System expects data acquired at 1200Hz. Data was therefore recorded at 2048Hz and down-sampled to 1200Hz. 1200Hz is selected as an integer multiple of the stimulus delivery frame rate of 75Hz and as such avoids aliasing problems. Where 2048/1200 is not an integer value, linear interpolation was used between adjacent values.
- Creating a file with a .mf header. In order to create a .mf header file, dummy multifocal files were created in the EDIU Multifocal System containing the relevant information about stimulation parameters such as m-sequence length and stimulation geometry. The file conversion software read in these header files and copied the information into a new .mf file with data acquired from the BioSemi system.

8.4.4 **Results and Conclusion**

This software was successfully written, debugged and tested on simulated data. It will be referred to as EDF2MF throughout the rest of this chapter and allows BioSemi ActiveOne data to be cross-correlated by the EDIU Multifocal System.

8.5 BioSemi System Tests – ActiveOne and Large Signals

8.5.1 Introduction

As has been discussed, mfVECP signals are small and complex. Their detection requires that several stages in the integration of two electrophysiology systems are all functioning correctly. In order to test the basic function of the BioSemi ActiveOne, large, reproducible signals whose detection is not dependent on synchronisation with the EDIU Multifocal System, were used.

8.5.2 Aim

To test whether the BioSemi equipment was functioning properly by testing it with large signals. Signals used were supplied via:

- A signal generator,
- A photodiode and
- A physiological ECG.

8.5.3 Methods

When recording systems that employ passive electrodes are tested, known signals can be applied directly to the electrode. A similar approach to testing the active electrodes used by the BioSemi System would risk damaging them. Transmission of the signal via a saline bath was a safe alternative.

The signal generator and photodiode signal were fed into a tub of saline. Recording electrodes were placed in the saline solution. The experimental set up for the photodiode recordings is shown in Figure 8.5.

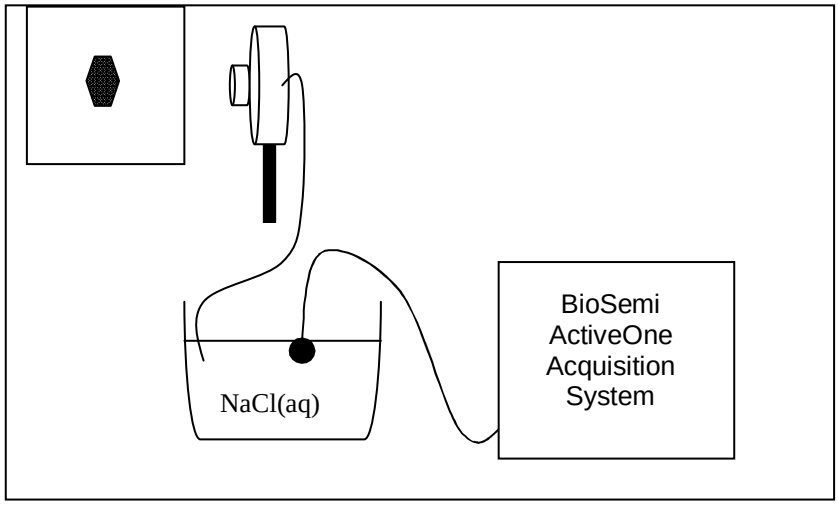

Figure 8.5 *The experimental set up used to test the multichannel acquisition system with a photodiode is shown.*

The amount by which the signal is attenuated by the saline bath was investigated by introducing a signal of known size from a signal generator. This was 5mV in size. On the BioSemi recording software, the sale indicated a signal of approx 100uV or 2% of the original signal size.

The recording electrode, the DRL (Driven Right Leg) and the CMS (Common Mode Sense) electrodes were all placed in saline solution. The DRL and CMS electrodes are necessary to provide common mode rejection. They create a loop, which drives the average electrode potential as close to the potential of the AD box reference as possible (Figure 8.6), replacing the ground electrode used in conventional systems. All electrode records are referenced to the CMS electrode. Care was taken to ensure that none of the electrodes or leads was in direct contact.

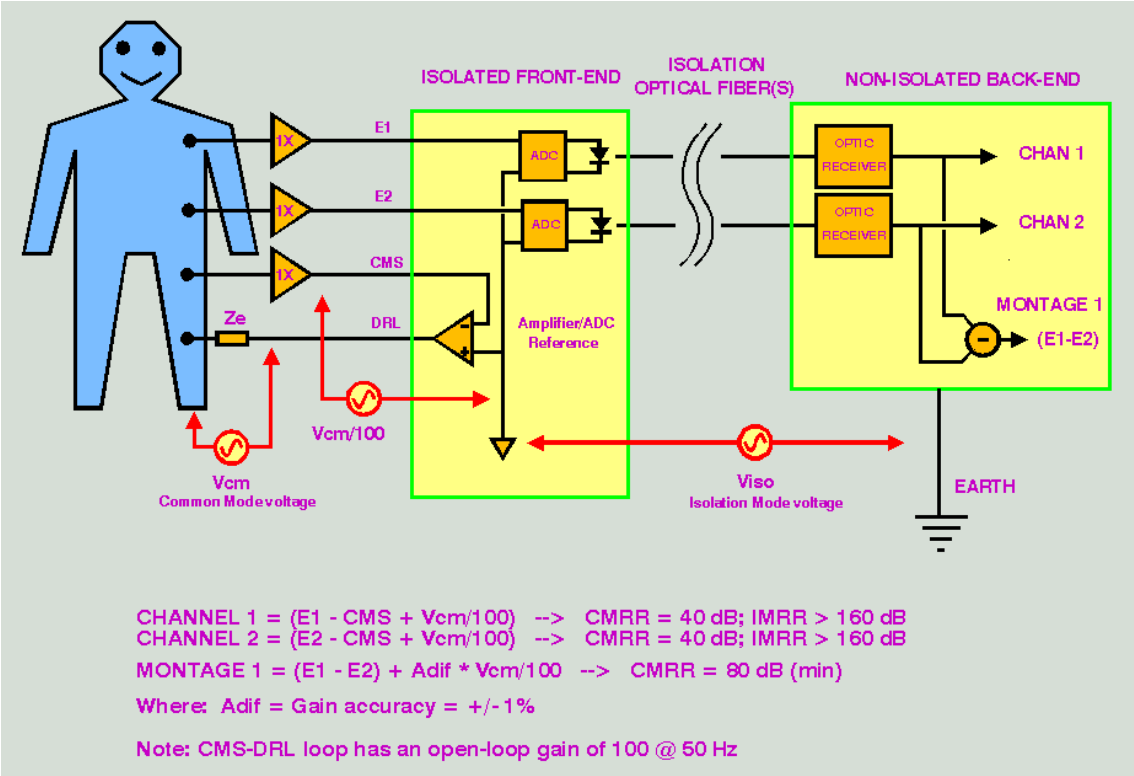

Figure 8.6 *BioSemi diagram showing how the CMS & DRL work.*

8.5.3.1 Signal Generator

Leads from a waveform simulator (Department of Clinical Physics and Bioengineering, DCPB 375) were fed into salt solution.

The normal ECG wave was selected from the variety of waveforms that the simulator can produce. An amplitude of 0.020V and a rate of 65 bpm were selected.

Each of the electrodes was placed in the solution in turn.

8.5.3.2 Photodiode

A time varying luminance profile was created using a single hexagonal region which alternated between black and white according depending on the state of an m-sequence and was projected on to a screen. The photodiode was placed in front of the stimulus and its output was fed into a bath of saline solution. A BioSemi Active Electrode was placed in the saline bath and a signal was recorded.

8.5.3.3 ECG

Physiological ECG signals were recorded simply by holding the DRL and CMS electrodes in one hand and the electrode under test in the other.

8.5.4 Results

8.5.4.1 Signal Generator

Clear waveforms were seen on each of the 48 recording channels.

8.5.4.2 Photodiode

Figure 8.7 shows two different photodiode recordings on different scales. The left hand side shows a high temporal resolution in which the approximately square wave response of the photodiode can be seen. The right shows a lower temporal resolution and illustrates the clear difference in signal when the multifocal stimulation is on (as indicated by the trigger signal – brown line) and off.

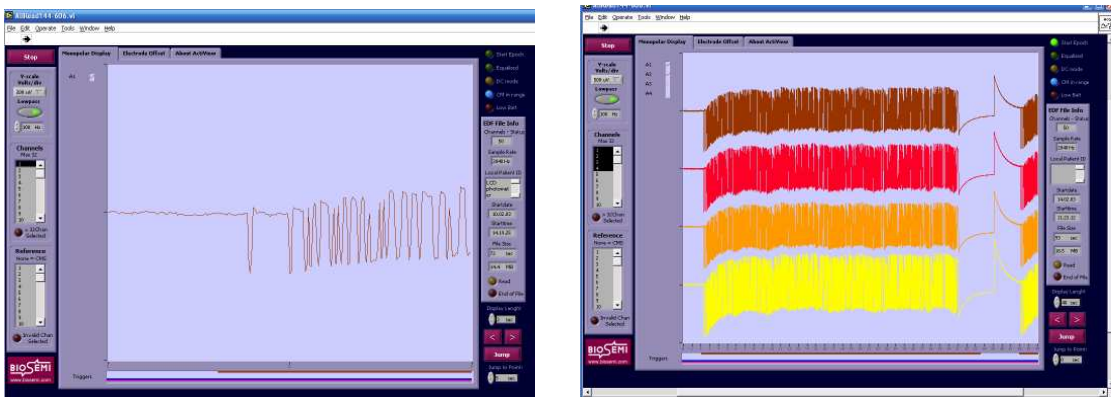

Figure 8.7 *Data recorded from the photodiode. This is a screenshot of the BioSemi file reader software. The left hand side shows a high temporal resolution record from a single electrode, while the right shows a lower temporal resolution record from four electrodes.*

8.5.4.3 ECG

Clear ECG signals were obtained and are shown in Figure 8.8. This compares well to the example ECG waveform shown in Figure 8.9 and clearly exhibits the PQRST components.

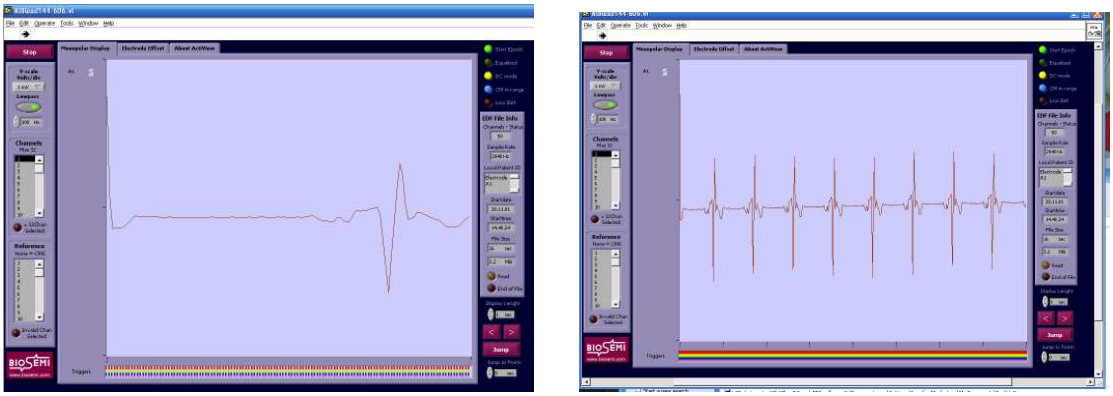

Figure 8.8 *An ECG signal shown on two different temporal scales.*

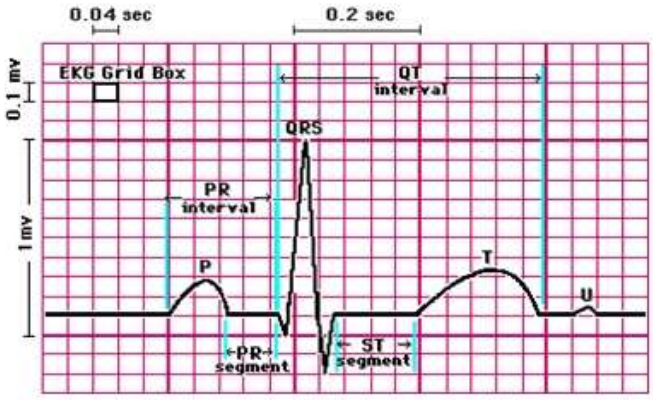

Figure 8.9 *An example ECG waveform taken from http://www.ispub.com/xml/journals/ijmt/vol2n2/ecg-fig1.jpg*

8.5.5 Conclusion

Our intended use of the BioSemi ActiveOne was non-standard and, as described in the preceding Tasks, implementation was not simple. Without any local experience of this acquisition system or the active electrodes, it was apposite to test the system with simple, large signals to ensure that representative responses were achieved prior to attempting more complex acquisitions.

Robust responses to signal generator signals, photodiode responses and ECGs were seen. It was therefore considered expedient to attempt the acquisition of more complex physiological signals.

8.6 BioSemi System Tests – ActiveOne and Responses to Multifocal Stimulation

8.6.1 Aim

To test the integration of the EDIU Multifocal System and the BioSemi ActiveOne with responses which are increasingly complex and demanding.

8.6.2 Method

A multifocal stimulus was used to evoke a response from (a) a photodiode and (b) a volunteer. Data was recorded using the BioSemi ActiveOne equipment. The format of the acquired files was converted and data was cross-correlated using the EDIU Multifocal System.

Photodiode recordings were made using the set-up described in the previous experiment. File conversion was performed using EDF2MF. Cross-correlation of newly created .mf files was performed in the EDIU Multifocal System to produce waveform array.

This was initially unsuccessful – no discernable waveforms were seen despite clear signals being seen in the .edf files. A considerable amount of time was spent debugging software to ascertain the problem. The appearance of the cross-correlated waveforms suggested that synchronisation of the stimulus behaviour and recorded data was not being achieved, resulting in cancellation of data and a noisy response. File conversion, trigger identification, dynamic range, data scaling and drift were all investigated without achieving a clear cross-correlated signal. Two problems were finally identified. The first was with the sampling rate of the BioSemi ActiveOne and the second with the presentation of the multifocal stimulus by the EDIU Multifocal System. These investigations are described in Sections 8.6.2.1 and 8.6.2.2.

With these difficulties addressed, several responses to multifocal stimulation were recorded, converted and cross-correlated. These were:

- photodiode responses to flash stimulation,

- mfERG responses measured via active electrodes placed on the skin at the outer canthus and lower eye lid,
- mfVECP responses to flash stimulation,
- mfVECP responses to a 9-region mfVECP checkerboard stimulation.

8.6.2.1 Sample Rate Difficulties

Asynchrony between the BioSemi ActiveOne sampling rate and the EDIU Multifocal Systems stimulus presentation rate was suspected. The latter has been extensively tested and verified as 75Hz, using photodiode measurements for departmental research purposes and was not investigated further here.

A modification was made to the EDIU Multifocal System to allow it to interrogate the BioSemi ActiveOne data after it had been converted using EDF2MF but before the data was cross-correlated. The modification wrote out a snapshot of 256 data samples each time the stimulating m-sequence was a +1 (high luminance).

If temporal synchrony exists between the two systems, then the first square wave (photodiode response to a liquid crystal display projector presentation of a period of high luminance) in each of the snapshots should superimpose. This was not the case.

This suggests that the sampling rate of the BioSemi ActiveOne system was not exactly the specified 2048Hz, which introduced a systematic error in the file conversion software, EDF2MF. Data are read in by selecting 27.33 seconds worth of samples from a trigger point. If the number of samples per second is not exactly as expected, then within an m-sequence segment we are sampling too much or too little of the data.

If the true sampling rate is 2048Hz, then 2048 samples contain 75 steps of the m-sequence and cross-correlation will be successful. However, if the true sampling rate is greater than 2048Hz then 2048 samples contains less than 75 steps of the m-sequence (and vice versa). This difference will mean that instead of the zero-order cross-correlation adding together responses to synchronised +1 stimulus steps and subtracting responses to synchronised –1 steps, the addition and subtraction will be averages of time delayed responses. The response will be blurred and, as observed, lost within background noise.

EDF2MF was modified to allow the user to vary the assumed sampling rate of the BioSemi ActiveOne.

It was assumed that the .edf file structure was fixed. That is, regardless of the true sampling rate, the .edf file will be structured in such a way that there are groups of 2048 consecutive samples from each channel placed side by side (Figure 8.3). The

suspected fault therefore lies with the accuracy of the BioSemi ActiveOne's clock speed.

The .edf to .mf conversion was performed with iterative changes to the assumed sample rate until the step up pulses created with each +1 step of the m-sequence were seen to align. This was achieved with a sample rate of 2133Hz.
It was verified that changing the sampling rate in this way did not introduce discontinuities to the data, by reading the data from the .edf file and writing the whole channel's data to a single stream of data. This was converted to a format readable by MS Excel, plotted and visually inspected. No discontinuities were seen.

In conclusion, it appears that the BioSemi ActiveOne has an internal clock that runs fast. The time taken to record 2048 samples was not 1 second but 0.96 seconds. This time difference prevented the immediate success of the cross-correlation process. This is unlikely to cause difficulties in conventional EEG recordings, but is crucial in the present application.

Having ascertained the actual sampling rate, the EDF2MF file conversion can account for the difference. The difference between 2048 and 2133Hz will not introduce aliasing problems since the actual BioSemi ActiveOne sampling rate is downsampled to 1200Hz for compatibility with the EDIU Multifocal System.

8.6.2.2 M-Sequence Segment Difficulties

After correcting for sampling rate errors, photodiode test data was cross-correlated in the EDIU Multifocal System. Clear photodiode responses remained elusive. The EDIU software allows the incoming data to be viewed during cross-correlation and updates a waveform trace array after cross-correlating each 30-second segments' worth of data. The first segment appeared to show promising data, but it deteriorated on each update. Oscilloscope investigations ascertained that the alterations that were made to the EDIU Multifocal System code in order to create the trigger and reset the trigger after each segment of the sequence had resulted in a bug. Instead of incrementing through the segments that create the whole multifocal file, the first segment was being repeated each time and so the whole m-sequence was not being used. This is illustrated in Figure 8.10. The cross-correlation procedure assumed that the whole m-sequence was represented. There was therefore, a mis-match between the

stimulus behaviour and the response of the photodiode resulting in cancellation of the signal. Once identified, this was simple to rectify.

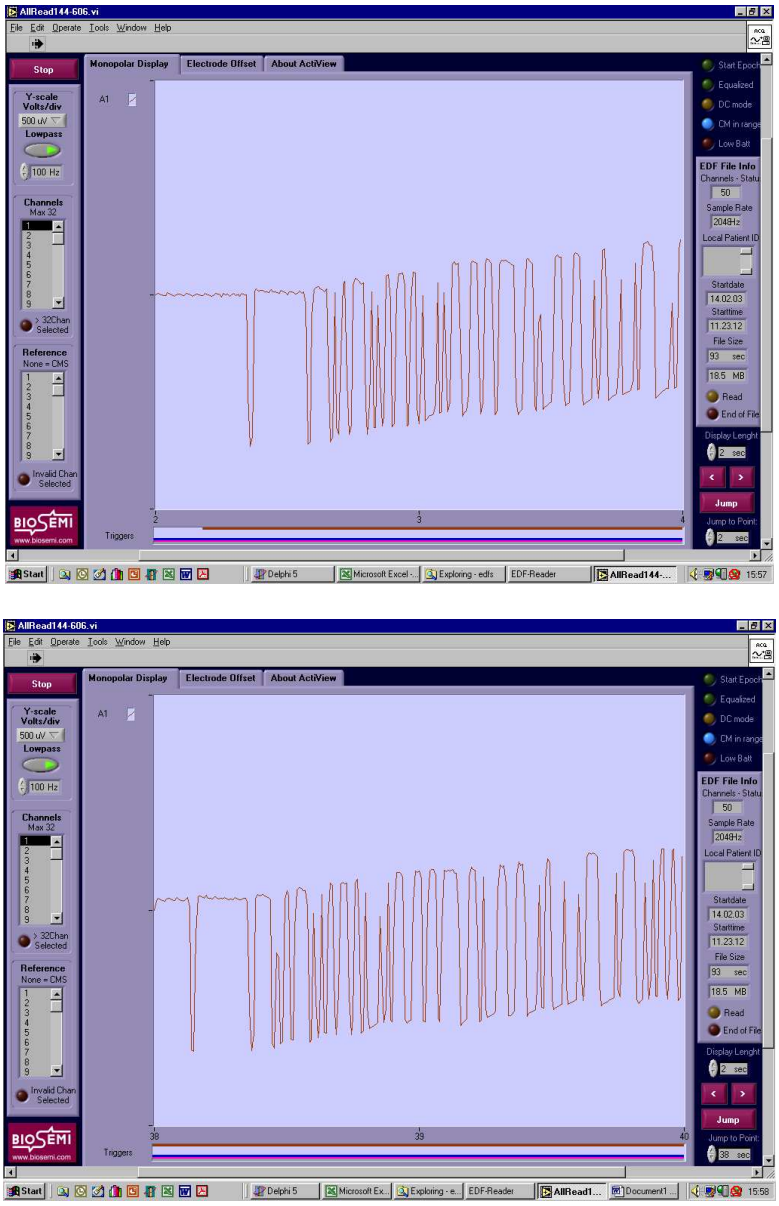

Figure 8.10 *The photodiode response to the beginning of two different 30-second segments of multifocal stimulation. The photodiode responses are very similar, suggesting that the luminance stimulation is the same in each case. This should not be the case. If stimulation increments through the whole m-sequence with each 30-second segment of stimulation, as it should, we should see a different pattern of response each time. This data highlighted a bug in the stimulation software which prevented the recovery of signals on cross-correlation.*

8.6.3 Results

8.6.3.1 Photodiode

Photodiode responses to multifocal stimulation are shown. Figure 8.11 shows the response to a hexagonal region which alternated between black and white according to an m-sequence. Figure 8.12 shows similar data. The stimulus was a seven region hexagonal pattern in this case. Stimulation was provided by an LCD projector, which provides a square wave luminance profile as shown in this trace array. The signal was passed through saline solution which accounts for the noise component.

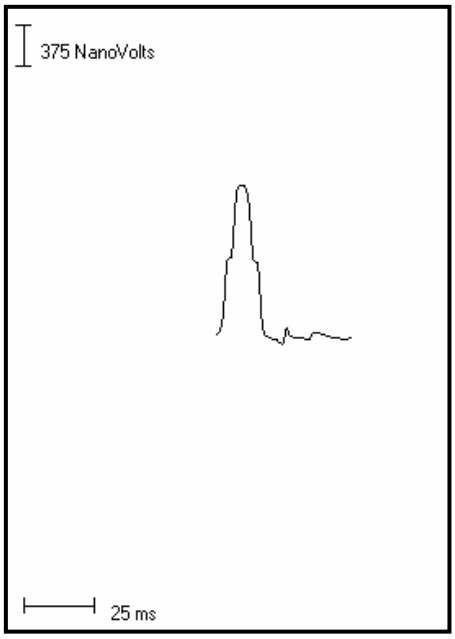

Figure 8.11 *A photodiode response recorded by BioSemi ActiveOne electrodes, converted and successfully cross-correlated. The stimulus was a single hexagonal region.*

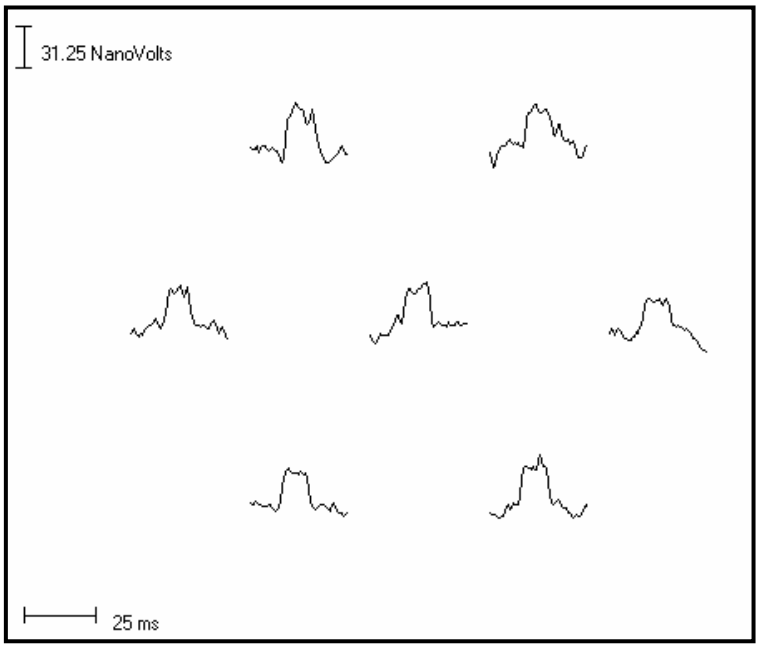

Figure 8.12 *Photodiode response recorded by BioSemi ActiveOne electrodes. Data was successfully cross-correlated. The stimulus was a seven-hexagonal-region mfERG stimulus.*

8.6.3.2 Normal Volunteer – mfERG

By placing active electrodes directly on to skin and holding them in place with micropore, it was possible to recover a mfERG response to a single flash region. A 13-bit m-sequence was used to control stimulation. A clear mfERG waveform was recovered and can be seen in Figure 8.13.

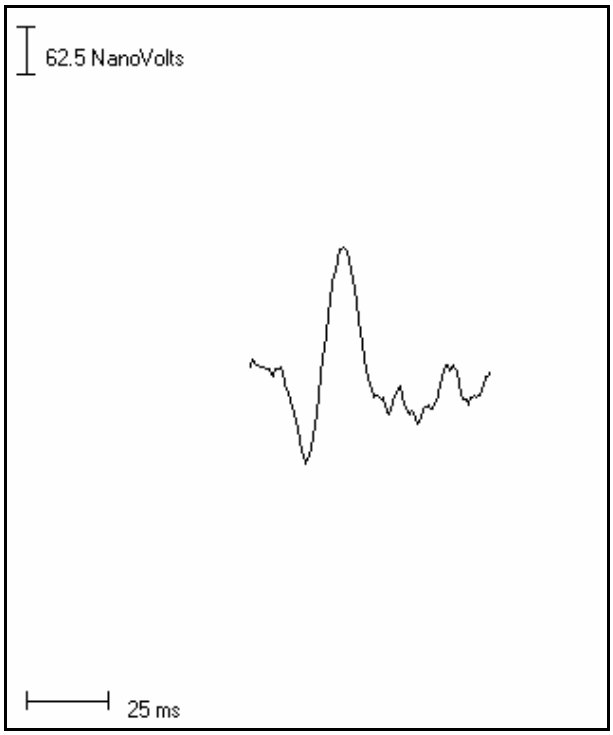

Figure 8.13 *A mfERG response to a single hexagonal flash stimulus recorded using the BioSemi ActiveOne system.*

8.6.3.3 Normal Volunteer - mfVECP

mfVECP recordings were made using a single checkerboard region reversing according to a 15-bit m-sequence. While this provides no spatial information about the visual field, it was selected to produce as large a signal as possible. Small physiological responses were successfully recovered.

The complexity of the stimulus was increased to a 9-area square checkerboard pattern. Each area contained a 4x4 checkerboard pattern. Signals were too small to recover, as can be seen in Figure 8.14.

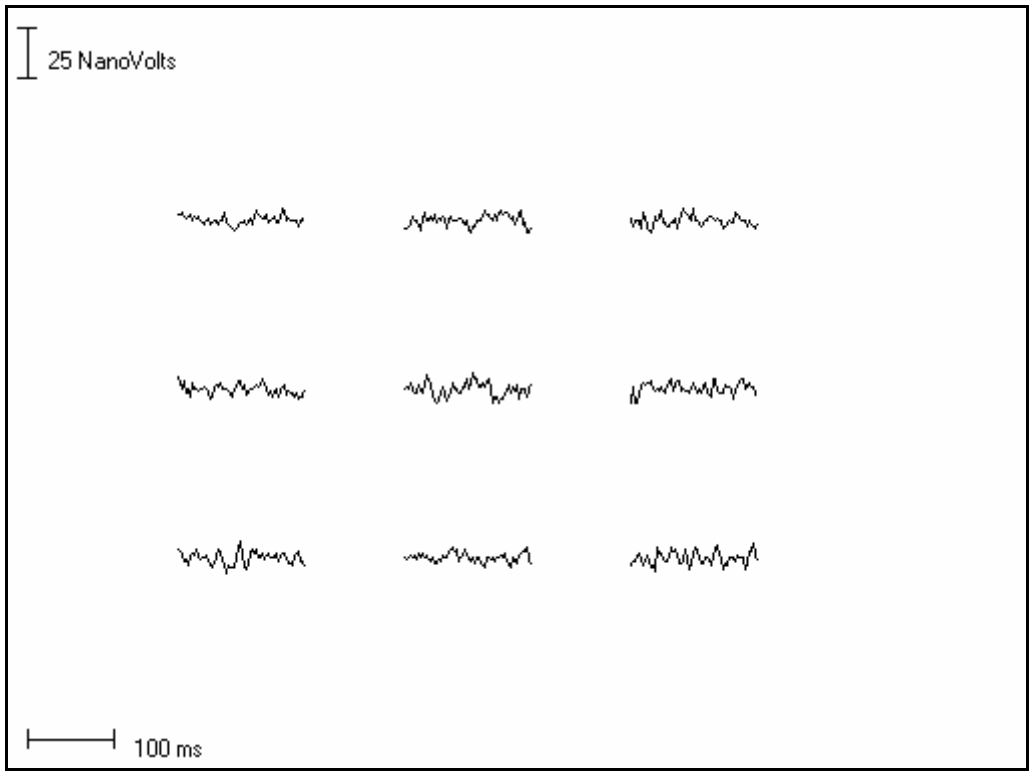

Figure 8.14 *A mfVECP response to stimulation with a square stimulus with 9 regions. Each region contained a 4x4 checkerboard pattern.*

8.6.4 Conclusion

The hardware and software of the ActiveOne and the EDIU Multifocal Systems have been successfully integrated to create a multichannel, multifocal system capable of recording multifocal electrophysiology. The resolution of the 16-bit ActiveOne ADC is sufficient to allow detection of photodiode responses to multifocal flash stimulation and mfERG sized signals. Had we encountered mfVECP signals of the magnitude reported in the literature (12;13;17;33;76;109;127) we would have been able to recover mfVECPs from the system. Our signals were significantly smaller. This is discussed further in Section 8.9.

For the size of mfVECP signals we observed, the ADC resolution was insufficient. An amplifier upgrade to the 24-bit ActiveTwo BioSemi System was obtained to allow the newly created software and system to provide extensive and detailed datasets from a group of control subjects.

8.7 BioSemi System Tests – ActiveTwo

8.7.1 Aim

To upgrade the integrated system from ActiveOne to ActiveTwo in order to provide better ADC resolution.

8.7.2 Methods

Having successfully integrated the BioSemi ActiveOne with the EDIU Multifocal System, the upgrade focussed on adapting to the differences between ActiveOne and ActiveTwo. The ActiveTwo is capable of acquiring from large numbers of electrodes. Sufficient funding was obtained to purchase 16 ActiveTwo electrodes.

8.7.2.1 Synchronising the BioSemi ActiveTwo with the EDIU Multifocal System.

A trigger can be used to start and stop saving of the data within the ActiveTwo system. If this facility were to be used, it would allow the acquired file to contain physiological data that was in response to stimulation only and to eliminate redundant data. It would require changes to the EDIU Multifocal System software and hardware code, which were considered unnecessary since the set-up described previously has been proven to work.

8.7.2.2 File Format Conversions

ActiveTwo used a different file format known as '.bdf'. This is a 24-bit version of the 16-bit .edf file format. BioSemi provided a .bdf to .edf file converter. This could be implemented at different settings that affected the balance of resolution and dynamic range.

In Chapter 7, twelve healthy normal volunteers underwent a series of eight mfVECPs with different stimulation rates. Data was recorded on the BioSemi ActiveTwo. One of the mfVECP datasets from each subject was selected at random and used to assess the appropriate range for conversion.

The .bdf file was converted to an .edf file using each of the dynamic ranges provided (1.0μV, 0.5μV, 0.25μV, 125nV, 62.5nV and 31.25nV).

A short program was written to determine whether using a high resolution conversion with a small dynamic range of 31.25nV would result in any saturation.

8.7.2.3 Testing

Tests similar to those previously described were performed.

After experiencing difficulties with the clock speed of the BioSemi ActiveOne system (Section 8.6.2.1), the sampling rate was tested using the methodology described previously. This ensured that photodiode square wave pulses in data samples taken at each +1 m-sequence step overlapped. There was no error in the ActiveTwo and an overlap was seen when a 2048Hz sampling rate was assumed by the file conversion software.

The original ActiveOne system provided 48 recording electrodes and would have allowed high spatial resolution sampling of signals from across the whole scalp. 16 active electrodes were available for acquisition with the ActiveTwo system and compromises were therefore necessary. The majority of the electrodes were placed over or near the occipital cortex, while a small number were positioned remotely from it. Positions are shown in Table 8.3 and Figure 8.15.

Active Electrode No.	Position
1	F_Z
2	C_z
3	P_4
4	P_z
5	P_3
6	5% of head circumference right of PO_z
7	PO_z
8	5 % of head circumference left of PO_z
9	5% of head circumference right of O_2
10	O_2
11	O_z
12	O_1
13	5% of head circumference left of O_2
14	5% of head circumference right of the inion
15	Inion
16	5% of head circumference left of the inion
CMS	10% of head circumference left of C_z
DRL	10% of head circumference right of C_z

Table 8.3 *Active Electrode positions.*

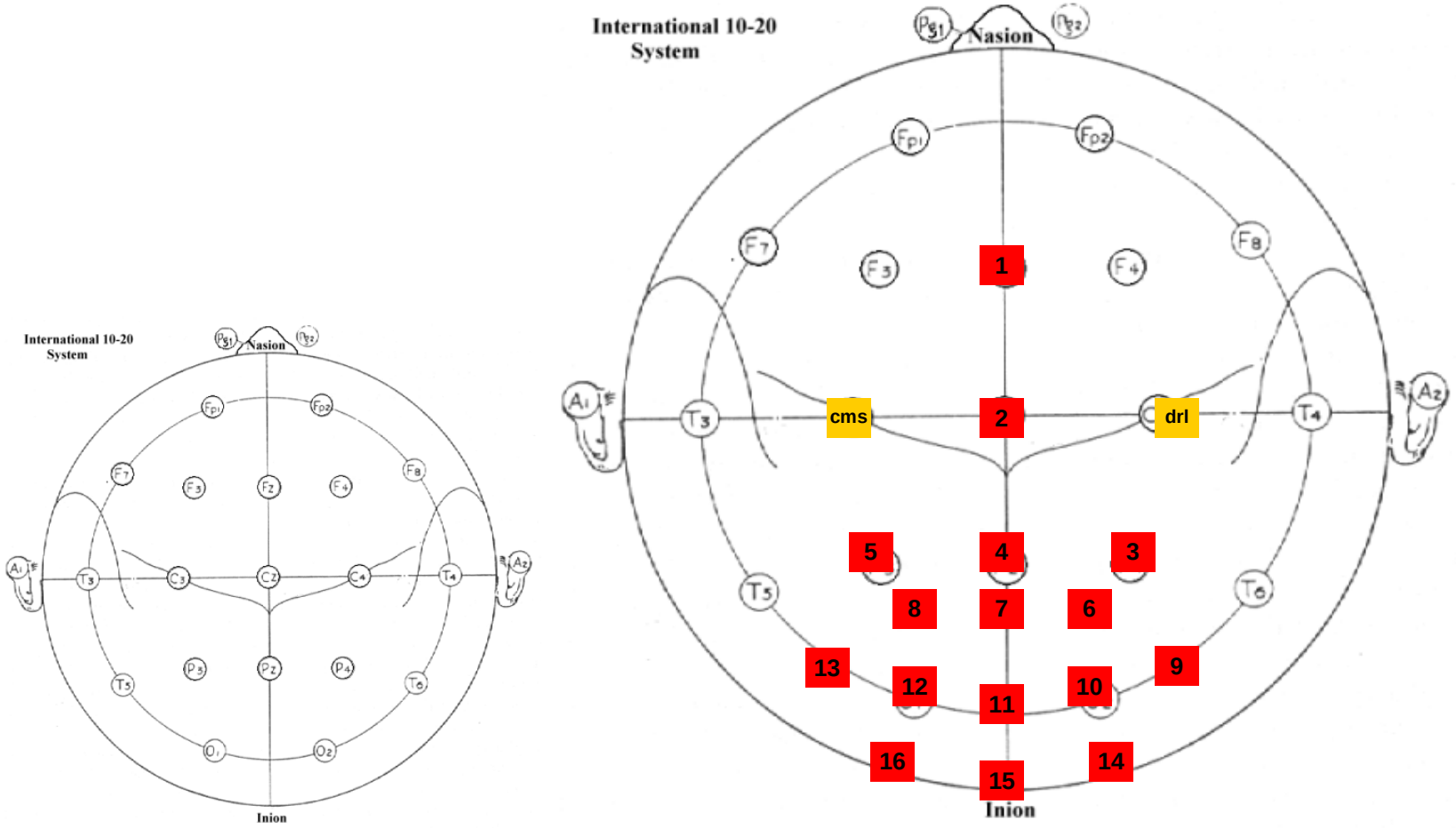

Figure 8.15 *Locations of 16 active electrodes. The left hand side shows the International 10-20 electrode placement system and the right hand side shows superimposed active electrode positions.*

8.7.3 Results

The trigger was found to behave as expected.

The specified sampling rate of 2048Hz was found to be accurate and no sampling rate correction to the EDF2MF file conversion software was necessary.

With one exception, performing the .bdf to .edf file conversion at the highest resolution with a range of 31.25nV did not result in saturation. In the exceptional case, the single channel demonstrated significant saturation. Further investigation of the raw data indicated an artefact thought to be due to an electrode becoming detached from the scalp. This channel was removed from further analyses.

The proportion of the 31.25nV range in use was, on average 6% ranging from 2% to 54%.

This was sufficient to recover the small mfVECP signals observed in this laboratory.

Figure 8.16 shows a recording from a normal volunteer acquired with channel A10 (International 10-20 position O_2). Stimulation was performed at 37.5Hz with an m=13 bit m-sequence. A 60-region dartboard stimulus subtending a radius of 28° of the visual field was used.

Figure 8.17 shows the mfVECPs acquired with all 16 recording channels from a different volunteer. Again stimulation was provided by a 60-region dartboard pattern subtending a radius of 22° of the visual field. In this example, the stimulation rate was 25Hz, m=13. It can be seen that some channels provide more useful information than others.

8.7.4 Conclusion

Integration of the BioSemi ActiveTwo with the EDIU Multifocal System was successful and together they were used to record data used to investigate the optimal rate of stimulation for mfVECP recordings (Chapter 7).

With the equipment currently available to us, we can acquire data from 16 electrodes. The system is however, capable of acquiring data from over 200 electrodes.

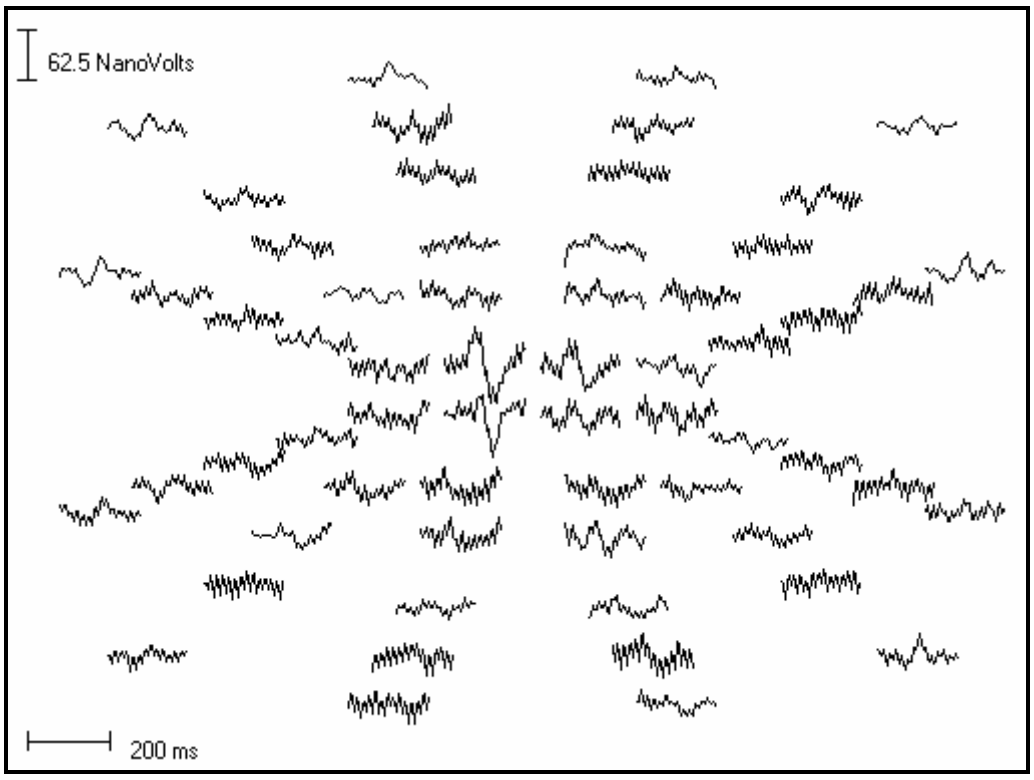

Figure 8.16 *A mfVECP recorded from a normal volunteer from the BioSemi ActiveTwo System.*

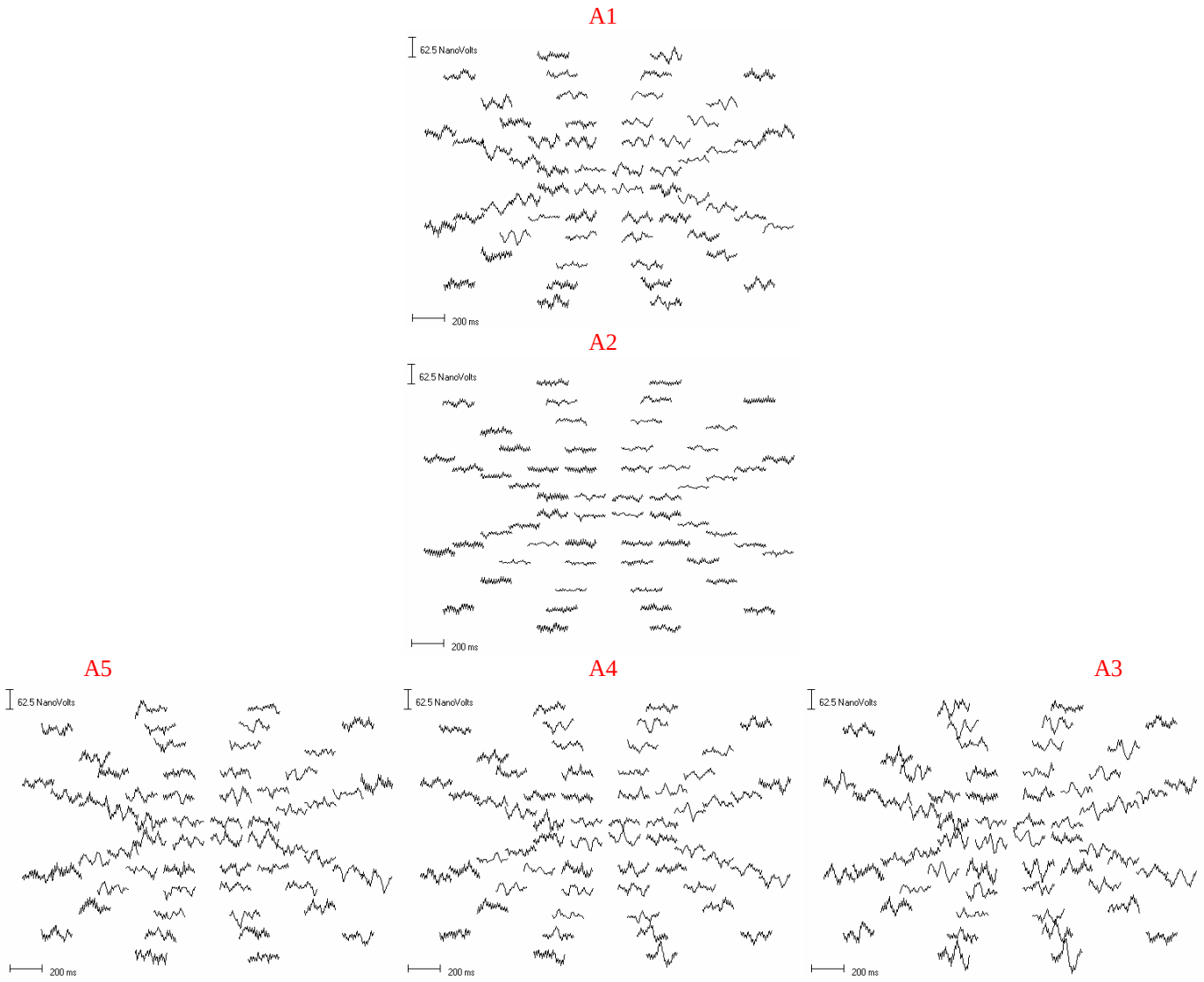
A1
62.5 NanoVolts
200 ms
A2
62.5 NanoVolts
200 ms
A5
62.5 NanoVolts
200 ms
A4
62.5 NanoVolts
200 ms
A3
62.5 NanoVolts
200 ms

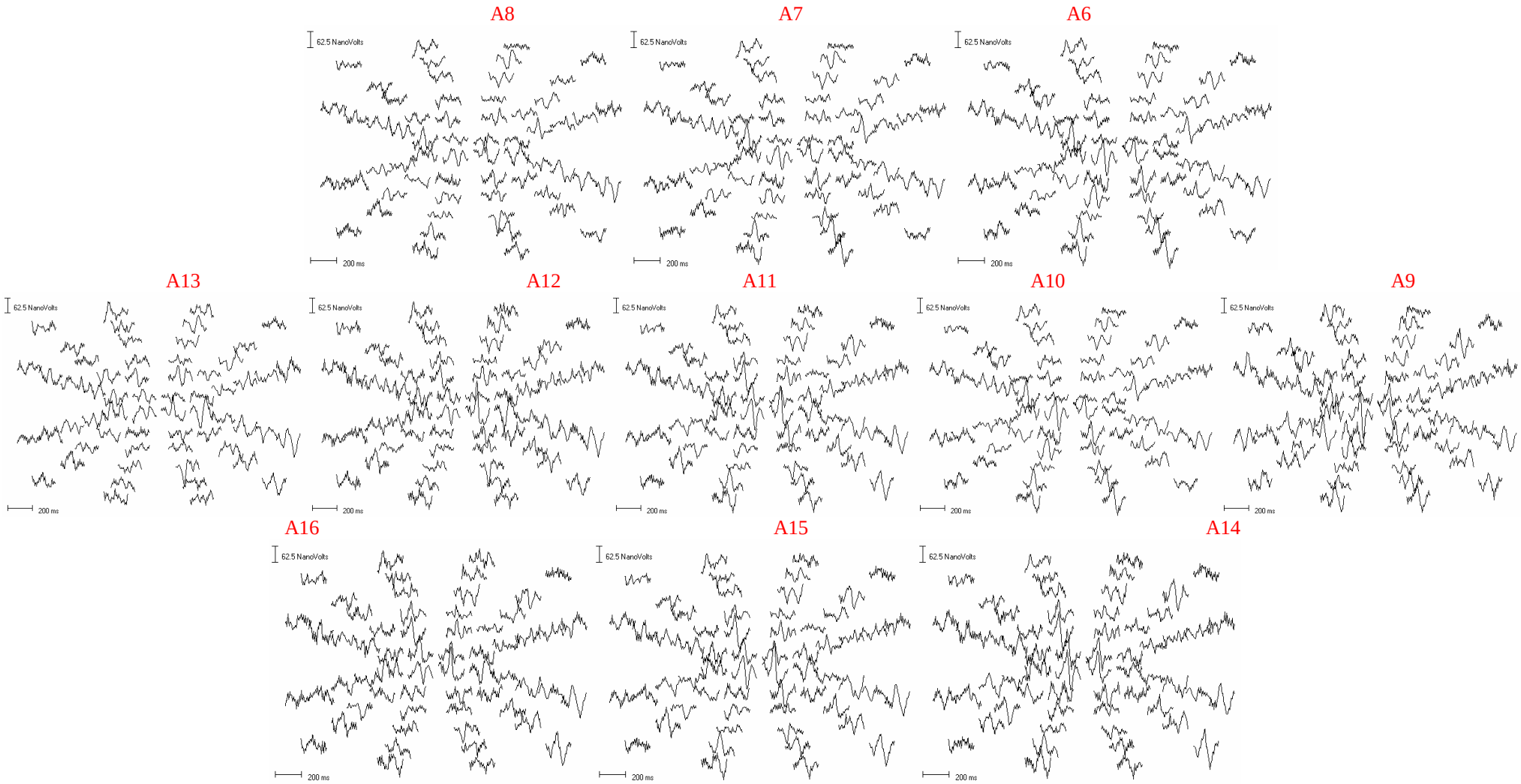

Figure 8.17 *mfVECP data acquired from 16 recording channels. Stimulation was provided by a 60-region dartboard pattern subtending a radius of 22° of the visual field. The stimulation rate was 25Hz and m-sequence length was m=13. Data was filtered through a bandpass of 3-30Hz prior to cross-correlation.*

8.8 Selecting Optimal Recording Locations

8.8.1 Introduction

Having created a system which can acquire data from 16 electrode sites, it is useful to work out which electrodes are providing us with the most useful data. It is recognised that a 16 channel acquisition may not be an attracti ve option in the clinic, particularly if active electrodes are not available and skin preparation is required.

8.8.2 Aims

To select from the 16 recording locations shown in Figure 8.15 those that most successfully obtain identifiable signals from as many of the 60 independently stimulated areas of the visual field as possible.

To select a combination of four channels which allow detection of waveforms from a maximum number of stimulated areas.

8.8.3 Methods

This investigation uses a subset of data acquired during the investigation of the optimal stimulation rate for mfVECP acquisitions, described in Chapter 7.

mfVECP responses were successfully recorded from 12 normal, healthy volunteers with no known ophthalmic or neurological conditions using the ActiveTwo electrode and amplifier system integrated with the EDIU Multifocal System.

Signed consent was obtained after the experimental protocol had been fully explained. Ethics approval was obtained from the West of Glasgow Local Ethics Committee.

Subjects were optimally refracted using their own spectacles and their pupils were not dilated. Recordings were monocular. Stimulation was provided by a 60-region dartboard pattern. Each region contained a 4x4 black and white checkerboard pattern and the size of the regions was scaled for cortical magnification. The stimulus was back-projected onto a screen by an LCD projector and subtended a 22° radius of the visual field. The luminance of white areas varied across the screen from 903 cdm^{-2} to

1384 cdm^{-2} and black areas varied from 12 cdm^{-2} to 309 cdm^{-2}. Contrast varied from 98% peripherally to 49% at the centre of the screen.

Each subject underwent a series of eight mfVECPs recordings. The stimulation rates were 75Hz, 37.5Hz, 25Hz, 18.75Hz & 12.5Hz using m-sequence lengths ranging from m=12 to m=15 in order to maintain reasonable recording times. Full details are given in Table 7.1.

Electrodes were placed as shown in Figure 8.15.

BioSemi replaces the ground electrode used in conventional systems with two separate electrodes, the Common Mode Sense (CMS) electrode and the Driven Right Leg (DRL) electrode. These two electrodes form a feedback loop, which drives the average potential of the subject (the Common Mode voltage) as close as possible to the ADC reference voltage in the ADC-box. The CMS electrode is used as the reference for each of the 16 monopolar recording channels.

The BioSemi ActiveTwo is DC coupled and low pass filtering is performed by the ADC. This provides a very wide frequency bandwidth. Signals were sampled at 2048Hz and downsampled to 1200Hz when data was converted to a format recognizable by the EDIU Multifocal System for cross-correlation. Data was then filtered through a 3-30Hz digital bandpass prior to cross-correlation.

The performance of each electrode was assessed by calculating the signal to noise ratio (SNR) of each of the 60 cross-correlated waveforms. The method of calculation is discussed in detail in Chapter 4. A window of 45-250ms was used to calculate SNR. This is different from the 45-150ms time window used in the previous chapter and is based on an observation and subsequent analysis presented in Chapter 7 (section 7.3.4). A detection rate in terms of the number of responses to each of the stimulated visual field areas was calculated. This was averaged over all eight recordings made with different stimulation rates.

Using a subset of the data acquired with a stimulation rate of 25Hz and an m-sequence length of m=13 for n=12 subjects, a selection of four electrodes was made to maximise the number of detectable waveforms in response to the 60 stimulated visual field areas.

Initial observations indicated that very little useful information was obtained from channels A1 and A2. They were therefore excluded from further investigation. All

possible combinations of a selection of four channels from the remaining 14 were assessed to optimise the number of detectable responses throughout the visual field.

8.8.4 Results

8.8.4.1 Individual Channels

From inspection of the data, it is clear that

- Channels A1 and A2 provide little useful information. This is unsurprising given their distance from the occipital pole.
- Channels A3-5 show an improvement over A1 and 2.
- Channels A6-8 are significantly better than A1-5.
- Channels A9-13 also show good trace arrays. In some subjects, the more lateral electrodes, A9 and A13 are slightly poorer.
- Channels A14-16 contain some useful information, but they are not quite as good as A10-12.

These observations were formalised in an analysis, the results of which were presented in Figures 8.18 and 8.19.

A detection threshold was defined as the 90^{th} percentile of the distributions of SNR values calculated for the un-used m-sequence cross-correlations, or noise estimations. Waveforms within the trace array exceeding the detection threshold were identified.

Analysis was performed on data acquired from 16 electrodes during all eight mfVECP acquisitions from the 12 normal, healthy volunteers.

Plots have been created for each of the electrodes, in which each stimulus region is represented. Every unit of the plot indicates the percentage of waveform responses to that region, which exceeded the detection threshold. A colour scale has been used to depict the detection rate. Unfilled or blue locations indicate a detection rate of 20% or less. Red or pink locations indicate detection rates in excess of 50%. Figure 8.19 presents such plots for all 16 recording electrodes. Data from each electrode is arranged in the pattern shown in Figures 8.15 and 8.17 and the top left insert of Figure 8.19.

Figures 8.18 and 8.19 confirm the observations listed above. It can also be seen that:

- There is better detection of responses to stimulation below the horizontal meridian compared to above.

- No single channel shows good detection of waveforms from all 60 areas of the visual field.
- The best detection rates are seen for waveform responses to stimulation of the centre of the visual field.
- The best detection rate is achieved with channel A6, which is positioned at the vertical height of PO_z and 5% of head circumference to the right of the midline.

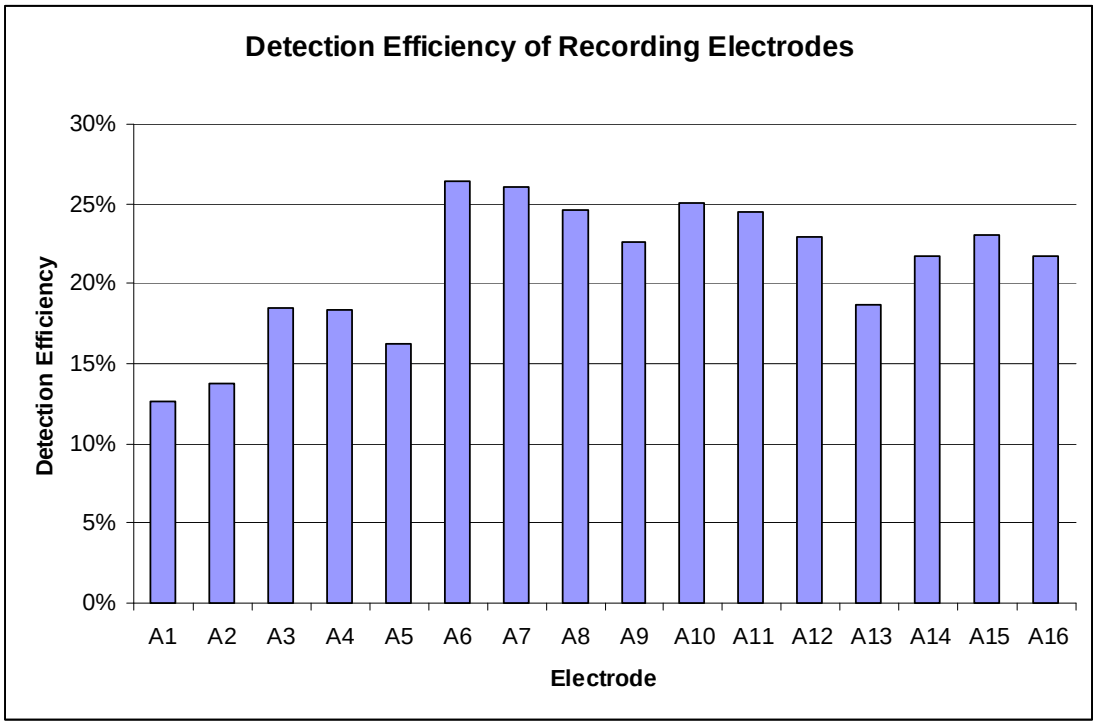

Figure 8.18 *The detection efficiency of each of the 16 recording electrodes. Data presented is an average over 60 stimulated areas over the visual field during 8 mfVECP acquisitions from each of 12 subjects.*

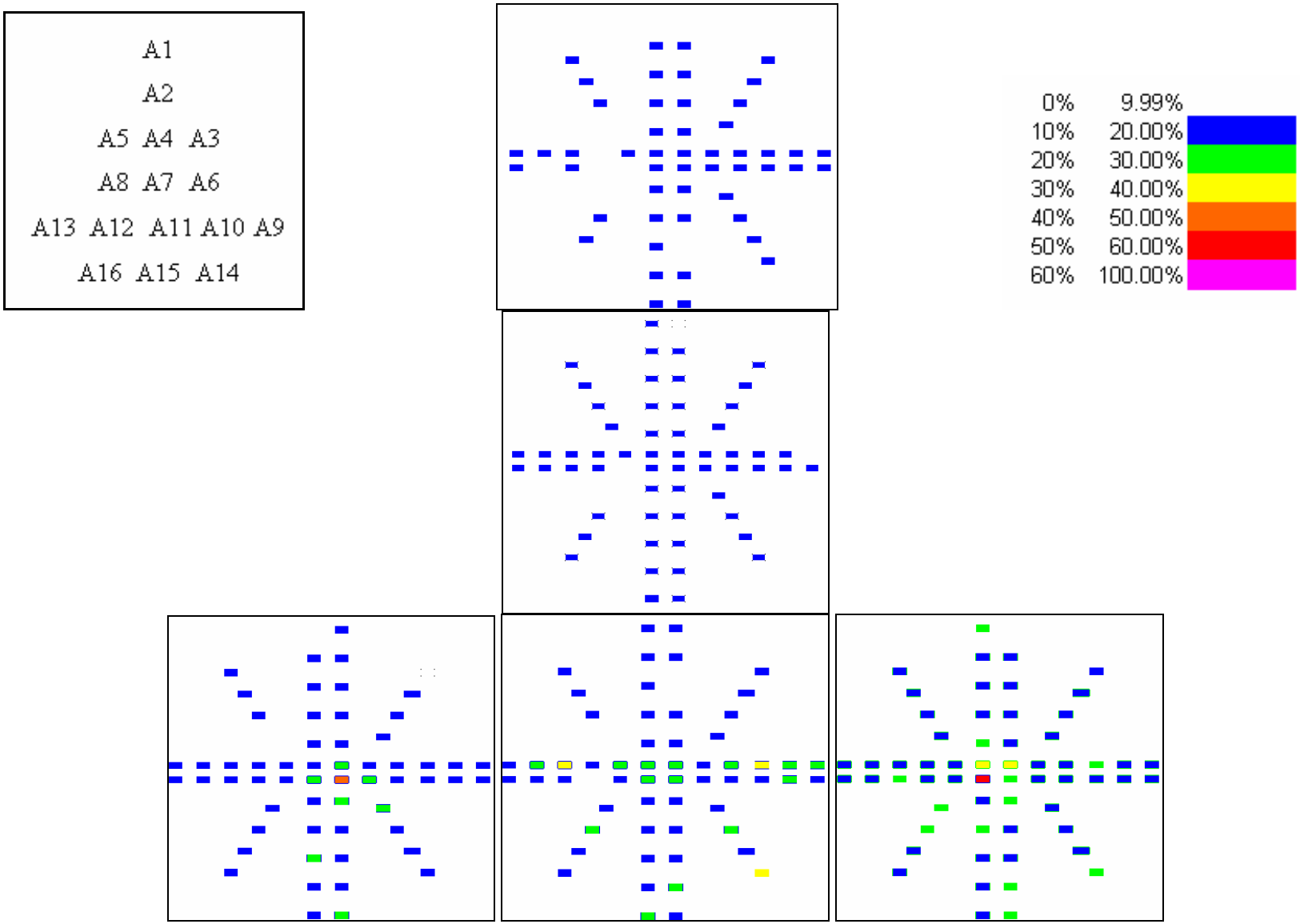
A1
A2
A5 A4 A3
A8 A7 A6
A13 A12 A11 A10 A9
A16 A15 A14
0% 9.99%
10% 20.00%
20% 30.00%
30% 40.00%
40% 50.00%
50% 60.00%
60% 100.00%

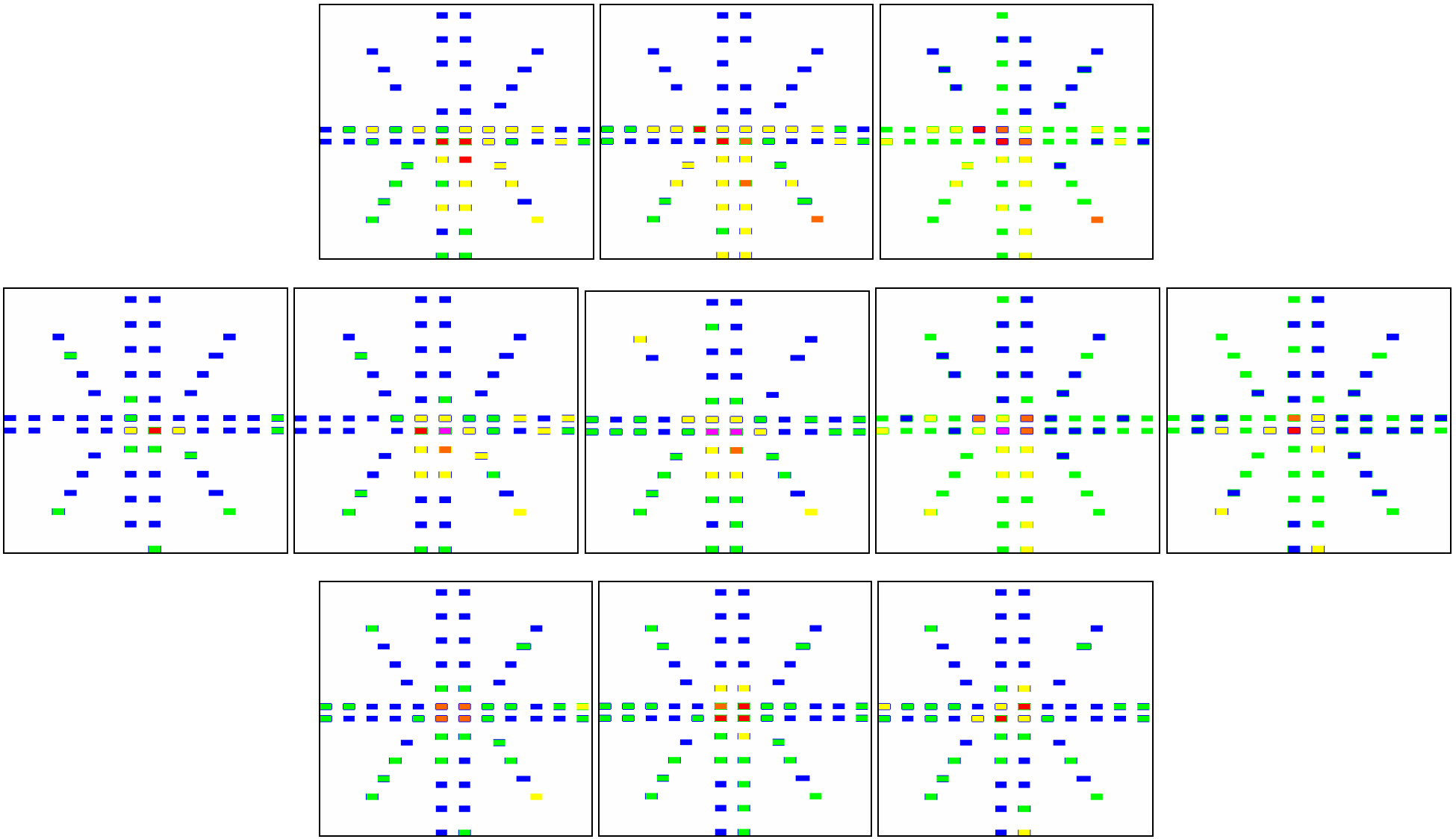

Figure 8.19 *(Previous 2 pages) Schematic showing how frequently each of the 16 recording electrodes acquires mfVECP responses that exceed the detection threshold. For each electrode, data are presented for each stimulated area of the visual field and reflects the proportion of detectable responses from a maximum of 96 (12 volunteers x 8 mfVECP recordings per volunteer). The schematic therefore summarises 92160 waveforms (60 waveforms per channel x 16 channels per recording x 8 recordings per volunteer x 12 volunteers). Data from each electrode is arranged in the pattern shown in the top left insert.*

8.8.4.2 Optimal Combination of Channels

Every possible combination of four monopolar recording channels from the 14 electrodes which were adjudged to contain useful information was assessed. The number of possible combinations, independent of order, is given by Equation 6.2 below, where r items are chosen from n.

$$\left(\frac{n}{r}\right) = nCr = \frac{n!}{r!(n-r)!} \qquad \textbf{Equation 8.2}$$

Using Equation 8.2, there are 1001 possible combinations of a choice of four electrodes from a total of 14. Selecting four from 16 increases the number of possible combinations to 1820. Based on the extent and pattern of waveform detection shown by electrodes A1 and A2 (depicted in Figure 8.17) it was not considered worthwhile to increase the computational workload of this investigation with their inclusion.

For each combination, a waveform had to be detected by a minimum of one of the four electrodes to be considered detectable. The percentage of detected waveforms was averaged over the 60 stimulated areas of the visual field for a single mfVECP recording from each of the twelve subjects.

The lowest detection rate was 42.8%, which was provided by the combination of electrodes A4, A5, A7 and A8.

The best detection rate was 57.5%, which was provided by the combination of electrodes A5, A7, A9 and A16. These are highlighted in blue in Figure 8.21.

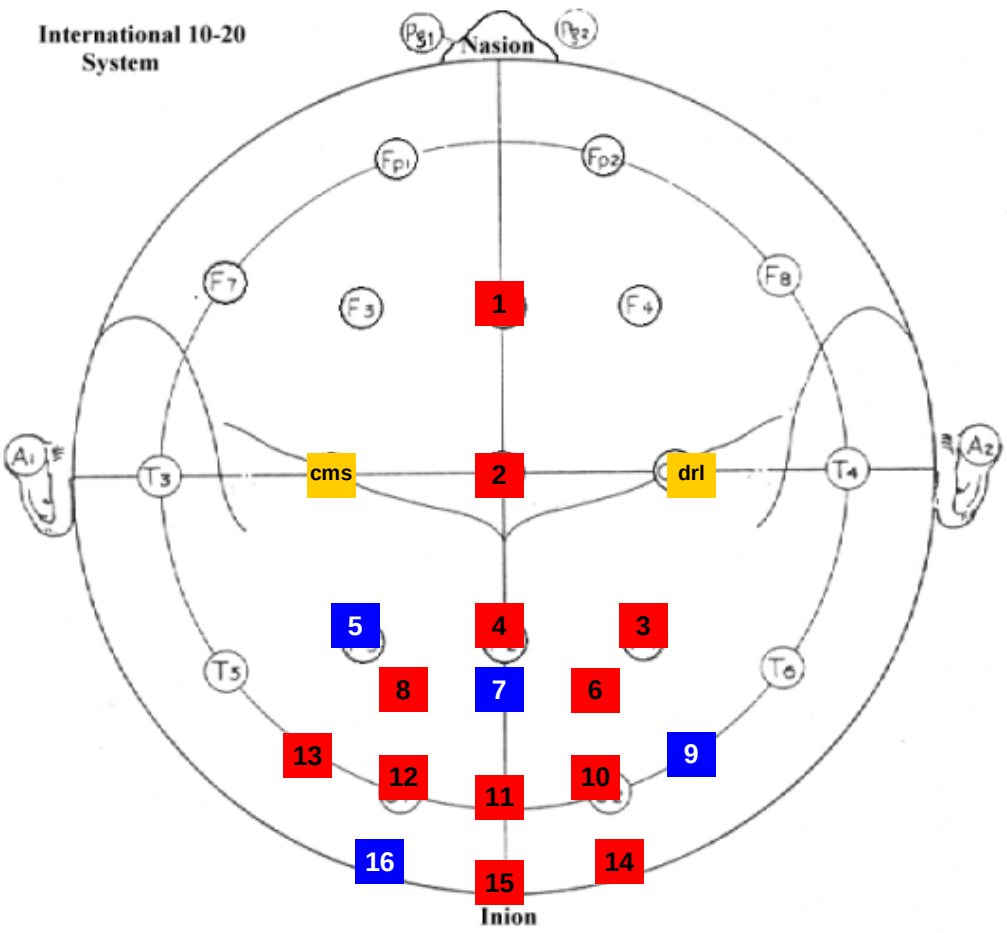

Figure 8.21 *Showing the locations of the 4 electrodes which provided the best detection performance.*

The pattern of detection using the best and worst combination of electrodes is shown in Figure 8.22. A different colour scale is used to that employed in Figure 8.19. This is because the data presented here is the combined detection rate of four complementary electrodes rather than that of single electrodes and detection rates are therefore much higher.

Improvements in detection rates are seen throughout the whole waveform trace array. The greatest improvements are seen in the detection rate of waveforms above the horizontal meridian.

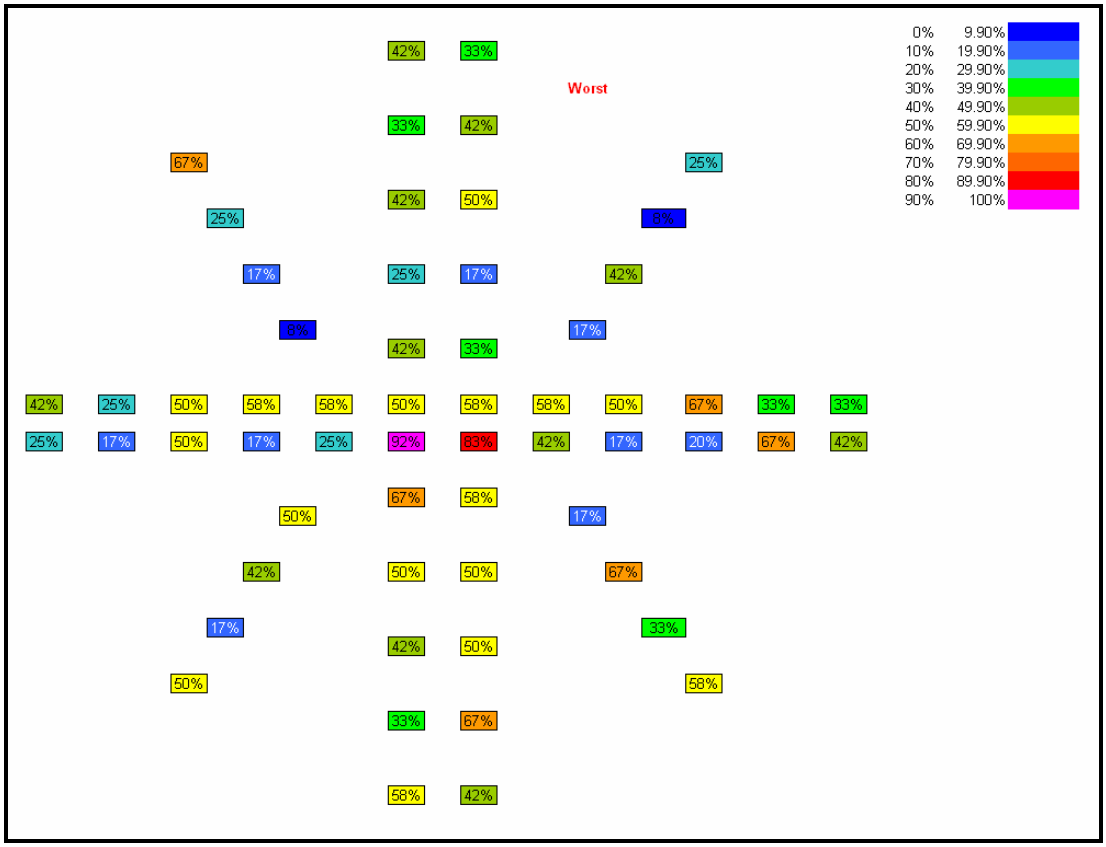

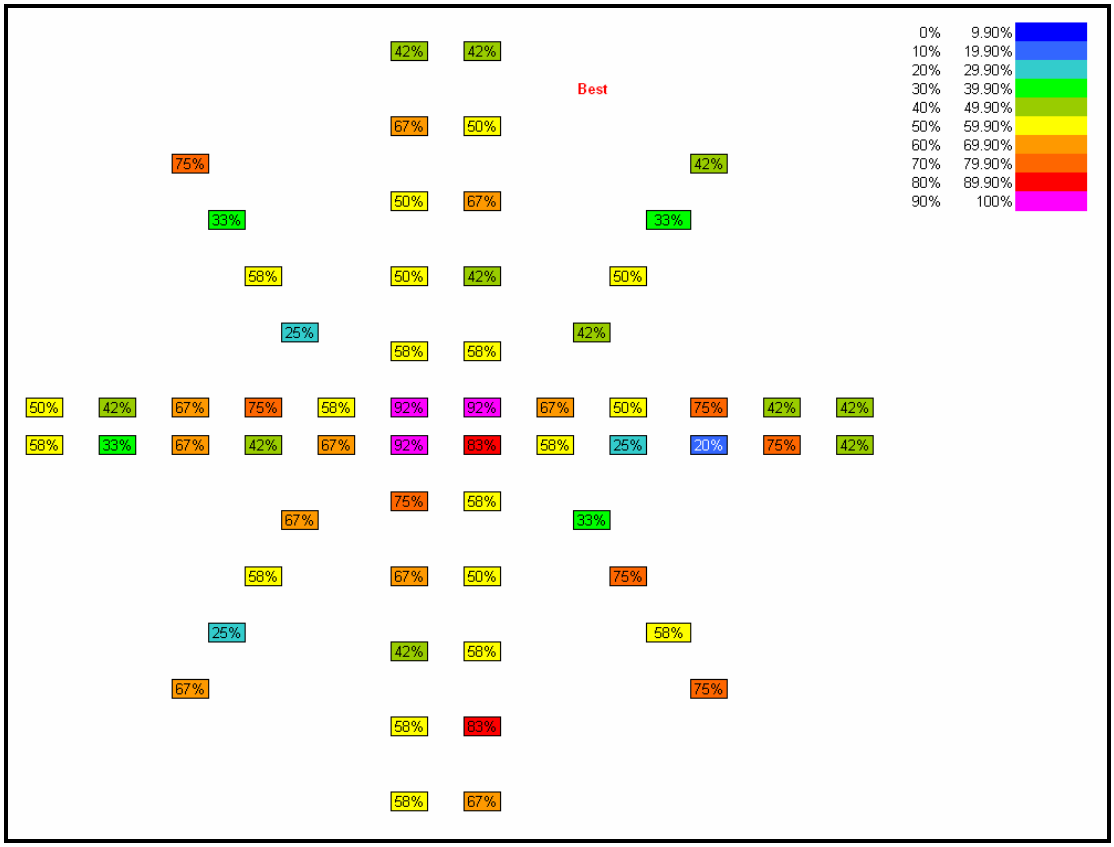

Figure 8.22 *The pattern of detection of waveforms in the trace array with the worst performing combination of four electrodes (above) and the best (below).*

8.8.5 Discussion

8.8.5.1 Individual Channels

The data presented on individual electrodes, encompasses tests performed with varying stimulation rates and m-sequence lengths and is not, therefore, a uniform dataset. However, this is a test system which is not necessarily recommended for clinical use, but for the purposes of optimisation of electrode positions and other aspects of mfVECP acquisition. It is therefore useful to know how well the electrodes perform under a variety of conditions.

Electrodes positioned over the occipital cortex detect waveforms more efficiently than those remote from it. From inspection of Figures 8.18 and 8.19, detection rates increase significantly for electrodes A6 –A16 compared to electrodes A1-5. No single electrode provides good detection of all waveforms within the trace array.

8.8.5.2 Optimal Combination of Channels

In contrast to data presented on individual recording channels, this part of the investigation used data from a single mfVECP recording for each of the twelve subjects, rather than averaging over eight recordings.

Figure 8.19 presents the individual electrode data and shows that the lower visual field is more efficiently detected by the majority of electrodes. This clear distinction is not seen in Figure 8.22 which looks at the combination of data from four recording channels. The use of a greater number of recording sites has made a significant improvement in the detection rates of waveforms from all visual field areas, due to the fact that the dipoles evoked in the visual cortex can be interrogated as four different projections onto the scalp, increasing the likelihood of at least one of the four being conducive to recording a response above the threshold of noise. The complementary nature of this data has had a particularly beneficial effect on the upper visual field.

The data presented in Figure 8.22 was acquired with a stimulation rate of 25Hz. The impact of stimulation rate is discussed in detail in Chapter 7. One of the findings is that while a standard stimulation rate of 75Hz favours the lower visual field over the upper, this disparity is not seen to the same extent when the stimulation rate is reduced to 25Hz.

Figure 8.22 shows a significant improvement in detection rates when a combination of four electrodes is used, compared to the data presented in Figure 8.19.

Combinations of four electrodes were assessed. Four electrodes are a manageable number to use in the clinical situation, regardless of electrode type. When active electrodes are used, there is no need for skin preparation and so there is little disadvantage to either the patient or the test operator in using more acquisition electrodes. Each additional channel will, however, increase the quantity of data to be stored, processed and interpreted. Further automation of data processing is required to make this a manageable, routine task.

Using four channels, the maximum detection rate was found to be 57.5%. The combination of a greater number of channels may increase this value.

The optimal combination of channels was found to be A5, A7, A9 and A16. In International 10-20 terms these can be described as positions P_3, PO_z, 5% of head circumference right of O_2 and 5% of head circumference left of the inion. This represents an electrode from each horizontal row of the 16 electrode array, and electrodes from opposite sides of the occipital cortex. The combination therefore detects the widest possible variety of projections of stimulated dipoles on to the surface of the scalp.

When different combinations of electrodes were considered, improvements in detection rates were gradual. To illustrate, there were 37 combinations of four electrodes which gave a detection rate of 55% or greater, not all of which exhibited the left sided bias of the A5, A7, A9 and A16 combination. The distribution of the electrodes at different horizontal positions and on different sides of the scalp is however, a feature in all 37 cases. The first 12 cases are shown in Figure 8.23.

It seems likely that a repetition of this analysis with a different dataset could result in a different optimal combination, but that the pattern of distribution above, below and on either side of the inion is unlikely to change.

Specific electrode locations cannot therefore be recommended from this analysis, but the pattern of having electrodes on either hemisphere and distributed at different vertical heights is consistent throughout the best twelve combinations. These features are also seen in electrode placements used by research groups headed by Hood and Klistorner and Graham, in their bipolar recording channels.

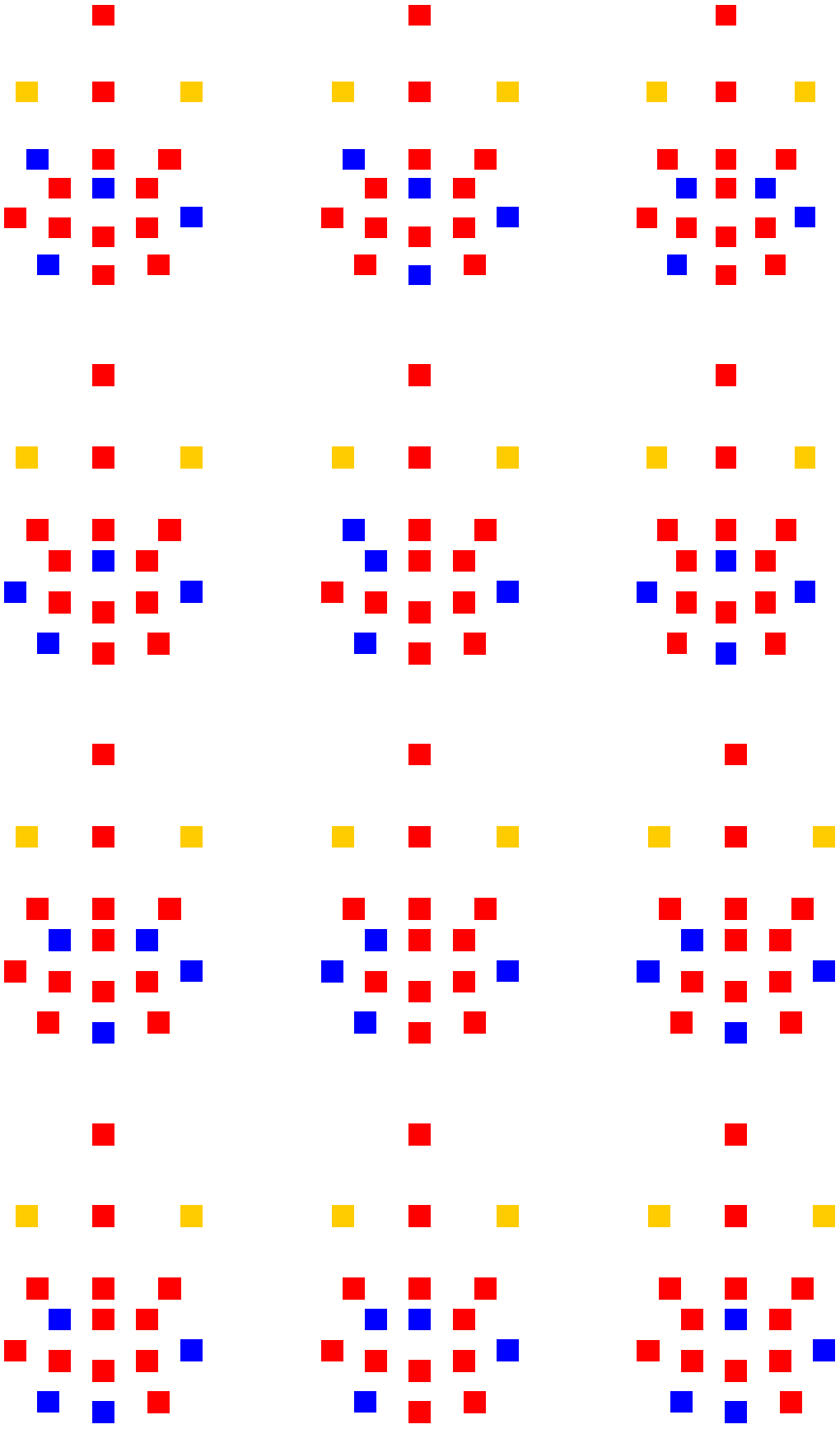

Figure 8.23 *The first 12 best combinations of four electrodes. Each unit of the diagram is a copy of the overlay of electrode positions in Figure 8.21.*

8.9 Discussion

Data acquired by the BioSemi system is written to file in a monopolar format, with each electrode referenced to the Common Mode Sense electrode. Monopolar data is therefore more accessible than bipolar channel data.

The use of monopolar recording channels referenced to the average potential of the subject (See Section 8.5.3) with electrodes in the locations described in Figure 8.15 and Table 8.3) is very similar to that used by James in his multichannel investigation of the Pattern-Pulse Multifocal VEP (17). In his study, electrodes were placed at the inion and above, as is the case here, and monopolar data were presented. In that study data was presented dichoptically via a shutter goggle system to a FOV of 16° of radius preventing a meaningful comparison of his data with that presented here.

Those investigators who use a smaller number of recording channels in mfVECP acquisitions tend to use bipolar recording channels.

In a wide range of studies, Hood and his colleagues acquire from three bipolar channels with electrodes placed 4cm above the inion and on the inion along the midline, and 4cm right and left of the midline at a height of 1cm above the inion (14;14;15;19;125;136;162) and go on to derive a further three bipolar channels by subtraction. Klistorner, Graham and their colleagues have used electrodes 4cm either side of the inion a further two electrodes placed on the midline at a variety of heights above and below the inion (76;77;111;123;158;159;163).

With the multichannel multifocal system created here, it is possible to create bipolar data by subtracting the data files from one another either prior to or after cross-correlation. This could provide 240 possible bipolar data channels from 16 recording electrodes.

A brief comparison of BioSemi acquired data has been performed by creating bipolar data from electrode placements close to those used in the acquisition from the EDIU multifocal system with Ag/AgCl electrodes in bipolar recording channels in earlier chapters. Those recording channels were chosen as examples of those used by other authors.

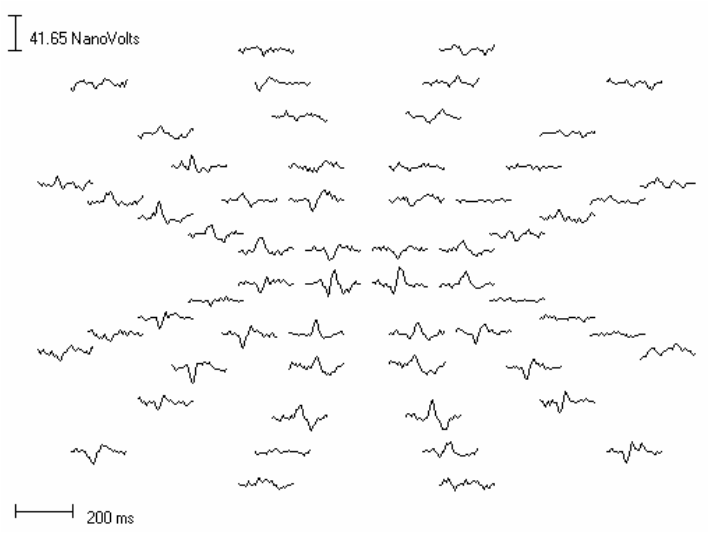

(a)

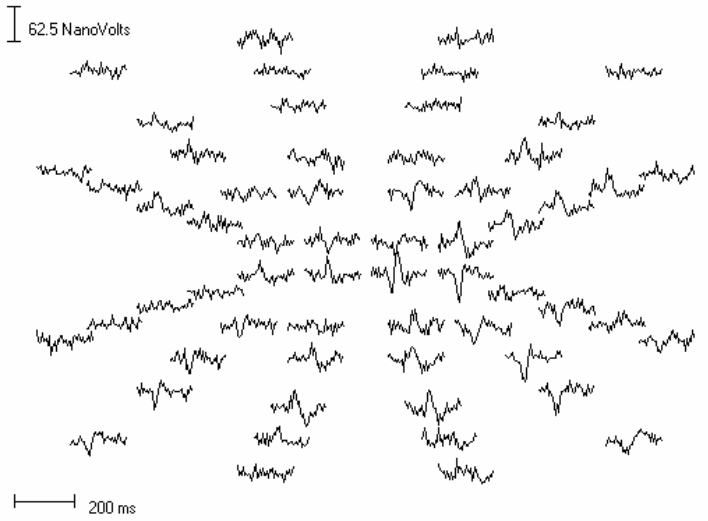

(b)

Figure 8.20 *The top row (a) shows bipolar data derived from the BioSemi Multifocal Multichannel Acquisition system. The bottom row (b&c) is data acquired from the same subject with the EDIU Multifocal system and Ag/AgCl electrodes. In all cases, stimulation was 75Hz, an m=15 bit m-sequence was used and stimulation was presented by an LCD projector. Differences exist in the FOV of stimulation and exact electrode positions. These were as follows: (a) FOV = 22°, electrodes POz – inion (approx 4.5cm above the inion – the inion), (b) FOV = 20°, electrodes 4cm above the inion – the inion and (c) FOV = 20.5°, electrodes 4cm above the inion – the inion.*

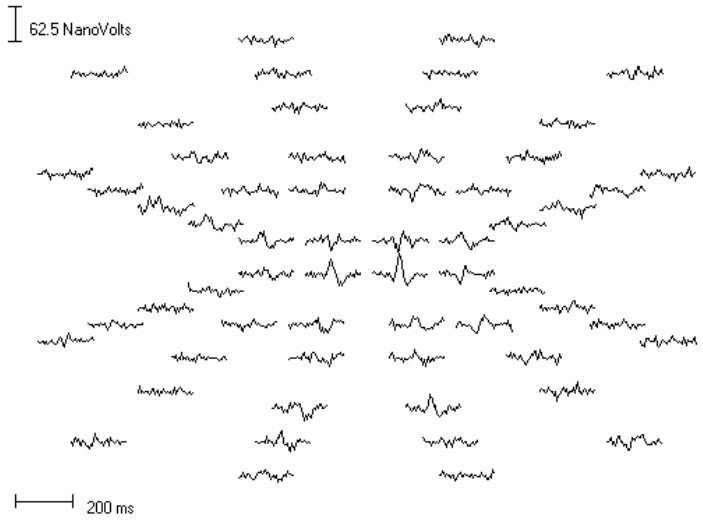

(c)

.

Figure 8.20 shows a comparison of bipolar data derived by subtraction of monopolar data acquired with the BioSemi multichannel multifocal system and data recorded from bipolar channels by the EDIU Multifocal System. Trace arrays show similar but not identical responses. Greater agreement could be achieved with an exact replication of all recording parameters such as FOV, precise electrode locations and the type of electrode used. Waveshape shows good agreement in many trace array locations, as does latency. Differences are seen in amplitude due to differences in sensitivity and amplification of the two acquisition systems.

It is not possible to do a direct comparison of our data to published trace arrays from the work of Hood, Klistorner and Graham and their research groups because of their technique of selecting the best data from a selection of recording channels. Furthermore, Klistorner & Graham's work uses channels with electrodes placed below the inion, an area of the scalp which was not sampled with our 16-electrode array on this occasion. We do not therefore have truly comparable data. The software required to make and present such a selection is not available for the present work, but would undoubtedly be a useful addition to the EDIU software in the future.

Further work on a direct comparison would be instructive. The multichannel multifocal system that has been created is fully capable of performing such a comparison and providing a wealth of information about a great number of bipolar recording channels.

Following the approach of James (17), monopolar data has been presented. It is further analysed in the following section, with the aim of selecting a group of four of the 16 monopolar recording channels which can provides the greatest amount of useful information about responses to stimulation of all areas of the visual field. This was performed in recognition of the fact that large electrode arrays may not be considered attractive for routine clinical protocols.

Investigation into the appropriate resolution for file format conversion showed that the smallest dynamic range with, correspondingly, the highest resolution accommodated the mfVECP data comfortably. This highlights the fact that the signals being recorded in this laboratory are particularly small. Signals recorded by other laboratories have been reported as much larger (12;13;17;33;76;109;127). This may be due to the use of an LCD projector to create the stimulus.

The LCD projector was selected for use in this series of experiments because the department has extensive clinical and research experience of its use. LCD stimulation has been shown to evoke robust mfERGs due to its high luminance, the wide FOV it can provide and the low levels of electromagnetic interference it creates. The differences between CRT and LCD stimulation in the mfVECP are discussed in detail in Chapter 5. The equipment available for use in this study was therefore designed for mfERG rather than mfVECP acquisition. In light of the findings of Chapter 5, repeating the experiments described here with CRT stimulation would be appropriate and may provide larger responses.

The hardware and software of the EDIU Multifocal and BioSemi Systems are not designed to work together. Integration has been successfully achieved for research use, but the software control of acquisition and the file conversions required do not as yet make it a user-friendly system for routine clinical use.

Future modifications of the EDIU multifocal system could include the ability to cope with a larger number of channels of data, making the processing of multichannel data simpler to manage.

.

8.10 Summary

The multichannel acquisition capabilities of the BioSemi ActiveOne and ActiveTwo systems have been successfully integrated with the stimulus presentation and data processing functions of the EDIU Multifocal system, resulting in a research tool that can simultaneously record mfVECPs from 16 electrode locations without the need to use skin preparation.

The experiments in this chapter describe the evolution of a multichannel system capable of recording simple physiological and non-physiological signals to one that can receive trigger input from complex, time critical visual stimuli and allow responses to multifocal stimulation to be cross-correlated. The final step of increasing the system resolution permitted the recovery of small mfVECP signals. A series of problems were identified and solved along the way.

Optimal monopolar recording channels have been determined. A combination of four electrodes positioned above, below and to the right and left of the occipital pole was shown to interrogate the evoked dipoles within the occipital cortex most efficiently.

This is a very powerful system that can acquire a very large quantity of data has been developed. We were restricted to a mere 16 electrodes, but by calculating data from bipolar recording channels, post acquisition, it would be possible to provide 240 bipolar data channels. The BioSemi ActiveTwo is capable of acquiring data from as many as 200 electrodes, which theoretically could provide data from 19900 bipolar channels, allowing interrogation of the visual cortex from an incredibly large number of orientations.

A larger number of electrodes would allow a greater sampling of the positions below the inion and would permit a direct comparison of all recording channels currently being used in the literature.

This could be used to provide a very thorough investigation of where to place electrodes for robust, routine clinical use. While four has been selected as a practical number of electrodes to be used clinically, it is worth noting that the use of active electrodes and the lack of skin preparation required with this system means that the routine acquisition of data from a larger number of channels could be tolerated well by patients and visual electrophysiologists alike.

Chapter 9

Conclusions and Further Work

Contents

		Page
9.0	Overview……	284
9.1	Quantifying Multifocal Signal Quality …….....	285
9.2	Filter Bandwidth ... ……...	287
9.3	Stimulus Delivery ……	289
9.4	Rate of mfVECP Stimulus Presentation ……	290
9.5	Multichannel, Multifocal Recording System and Investigation of Electrode Placement ……	292
9.6	Conclusion …….	293

9.0 Overview

The multifocal visual evoked cortical potential is an exciting development in multifocal electrophysiology and objective field testing. Achieving clear, unambiguous waveforms is, however, technically challenging. This thesis tackled a number of areas in which there is potential for improving performance.

The issues investigated were:

- Whether a novel method of SNR calculation could improve the ability to distinguish between true signals and traces containing noise alone.
- What is the most appropriate bandpass filter to use with mfVECP data?
- Whether mfVECP stimulation should be presented on a CRT monitor or by an LCD projector.
- What is the most effective stimulation rate?
- What are the most appropriate recording channels ?

9.1 Quantifying Multifocal Signal Quality

Optimising the mfVECP requires the acquisition and analysis of substantial quantities of data. Automated methods of waveform characterisation are therefore necessary.

A novel method of calculating the signal to noise ratio in multifocal electrophysiology recordings has been presented which employs orthogonal m-sequences that are not used to control regions of the stimulus. The method is referred to as the Dead M-sequence or Dead-M SNR.

The Dead-M approach allows the creation of a number of noise estimates providing a group of waveforms which are unrelated to the response of the visual cortex to multifocal stimulation. This permits receiver operating characteristic (ROC) curve analysis to test the performance of the mfVECP test under different conditions.

The Dead-M SNR has been compared to one of the most widely used methods of mfVECP SNR calculation (Delayed Time Window, DTW) and found to give comparable results. The Dead-M SNR values of cross-correlations of the physiological response with unused orthogonal m-sequences returns a distribution of SNR values which is more tightly distributed than those achieved using the DTW. This creates a small improvement in the ability to distinguish between noise and signal. mfVECP test performance can therefore be improved, albeit slightly, by the use of the DeadM SNR value calculation method.

Having illustrated the advantages of the Dead-M SNR, it was put into practise with robust mfERG signals. A small, statistically significant improvement in signal quality is demonstrated when data are acquired using gold foil electrodes instead of DTL electrodes. While this is an interesting finding in its own right, it shows that the Dead-M SNR is a useful metric not only with mfVECP data but also with more robust mfERG data.

A final test of the Dead-M SNR metric was performed by using it to quantify the improvements in signal quality of mfVECP data with increasing m-sequence length. The Dead-M SNR increased with each increment of the m-sequence as expected, but failed to reach the maximum theoretical improvement. This is likely explained by a real reduction in the size of the visual evoked responses as acquisition time increases and a genuine absence of responses in some recording channels to the behaviour of dipoles evoked at disadvantageous orientations within the visual cortex which will

remain undetectable, rather than an anomaly in the behaviour of the Dead-M SNR metric. The SNR of mfVECP responses is low and the increments seen with increasing m-sequence length support the use of as long an m-sequence length as can be tolerated.

mfVECP trace arrays obtained with different m-sequence lengths showed good agreement in amplitude, latency and waveshape despite obvious differences in the level of superimposed noise, indicating good reproducibility. Reasonable reproducibility was seen with later experiments with similar but not precisely reproduced recording parameters. Further work should include an assessment of reproducibility based on exact repetitions of all recording parameters.

Other methods of SNR value calculation have been presented (125;129;158) and the Dead-M SNR metric could usefully be compared with them.

Later experiments presented within this thesis noted increased latencies, raising the question of what is the most appropriate window over which to calculate a SNR value. A time window of 45-250ms was compared against a frequently used window of 45-150ms. Under specific experimental conditions, there was a benefit to using the longer time window.

If future experimental work results in further increases in latency or major changes in waveshape, it would be worthwhile to reconsider the time window used for SNR value calculations.

9.2 Filter Bandwidth

A detailed study of the most appropriate bandpass filter to apply to mfVECP data was carried out. Recent literature reports the use of a variety of filters (17;19;123;128;138;139), but little information is given to support the selections made.

The use of noise estimations based on cross-correlations of the raw data with unused, orthogonal m-sequences allows ROC analysis to tease out the difference between improvements in SNR and improvements in mfVECP test performance. It was shown that the frequency spectra of noise estimations and waveforms containing both signal and noise were very similar and that filtering therefore has an impact on both. While filtering can increase the SNR of waveforms within the trace array, it also increases the SNR of noise estimations. As a result, improvements in test performance are not as great as might be hoped from inspection of the signal SNR data alone.

Filtering with a bandpass of 3 to 20Hz after cross-correlation has been performed showed the best performance and maximised the SNR of waveforms within the trace array.

It is increasingly simple to apply post-acquisition, post-cross-correlation filters to improve data appearance and SNR. Continued acquisition of data with a relatively wide hardware bandpass filter, with the removal of unwanted frequencies post-acquisition, is therefore recommended. The results of the present study would suggest that a default post cross-correlation filter of 3 to 20Hz should be used, but an experienced reporter should be able to tailor filtering for individual recordings, since noise contributions are not constant.

This investigation looked at only two types of filter, the Kaiser and a first order Bessel filter. There are a wide range of other filters available which may show further improvements. At a simple level, the investigations performed here could be extended to include comparisons with the impact of higher order Bessel filters, or other filter designs such as the Butterworth. As noted in Chapter 5, more sophisticated methods of data filtering are being introduced and are increasingly simple to apply. Wavelet filtering is one example which could provide further benefit. While Smart filtering was not particularly successful in the brief investigation described in Chapter 5, if

written specifically to work with mfVECP data, it could provide additional advantages.

9.3 Stimulus Delivery

The technology used to deliver visual stimulation has been discussed and a comparison of the use of a CRT monitor and an LCD projection system was investigated.

In the mfVECP, the recovered signal quality is better when a CRT monitor is used to deliver the stimulus rather than an LCD projector. Since the mfVECP is a small signal presenting challenges for signal detection, the use of a CRT monitor presented stimulus is recommended over an LCD projector.

This comparison looked at LCD projectors and CRT screens. While this was an appropriate comparison when the experiments were performed, there have been developments in VDU technology which means that LCD screens are now far more widely available than CRT screens. As such future work could usefully look at aspects of the LCD screen stimulus delivery which may have an impact on response topography and signal quality.

A range of fields of view were stimulated during mfVECP recordings. Data presented here is the first to use the most commonly used 60-region dartboard pattern to investigate the optimal field of view. It was found that signals could be recovered out to a radius of 30° of the visual field, but that the detection of waveforms beyond that was poor.

Field of view investigations employed midline recording channels. It is possible that differently oriented channels could improve detection rates from very peripheral areas.

The field of view of stimulation was varied, while the same geometry was maintained throughout. As a result, the checksize used in each region became larger, as the field of view increased became larger. A complementary set of experiments could increase the field of view by introducing new rings to the dartboard stimulus and thus maintain the same check-size for inner rings throughout the series of acquisitions.

9.4 Rate of mfVECP Stimulus Presentation

mfVECP stimulation is most frequently performed at 75Hz. However there is evidence that slower stimulation rates may result in more robust responses (17;104;109;114-116;150). A group of 12 healthy volunteers therefore underwent mfVECP testing at frequencies of 12.5Hz, 18.75Hz, 25Hz, 37.5Hz and 75Hz.

It was found that sensitivity of the mfVECP test can be improved by reducing the stimulating frequency from the standard rate of 75Hz to 25Hz. Further improvements in sensitivity were not seen when the stimulation rate was slowed below 25Hz.

These improvements were accompanied by changes in the form, amplitude and timing of the waveform. As the stimulation rate was decreased, latencies were seen to increase, amplitudes increased and a late negative trough became more prominent.

The difference in detection rates with stimulation rate reached statistical significance for the comparison of 75Hz and 25Hz stimulation. 25Hz stimulation for 6 minutes was superior to 8 minutes of 75Hz stimulation, despite an 8-fold decrease in the number of pattern reversals. In a situation where signal quality can be poor and clinical subjects cannot always tolerate long testing protocols, this is a particularly interesting finding.

Subtle advantages were seen in the balance of signal detection in the upper and lower hemifields and the maintenance of detection rates from peripheral visual field locations when 25Hz stimulation was employed. This suggests that the slower stimulation rate evokes responses from different parts of the visual cortex and could include a greater contribution from extra-striate cortex.

Future experiments could investigate whether test performance improves further if the stimulation rate is kept at 25Hz and the m-sequence length is increased to m=14. This would increase recording time to 12 minutes, which is significantly longer than 8 minutes. However, when viewed in terms of the results of Chapter 4 which suggested that for 75Hz recordings an m=16 recording requiring 16 minutes was worthwhile or the work of Hood and co-workers who regularly perform two runs of an m=15bit m-sequence at 75Hz requiring 16 minutes (14;125;146;162), 12 minutes may be a reasonable compromise.

The stimulation frequencies employed here were limited by the necessity of using integer fractions of 75Hz. Additional improvements may be seen with other frequencies close to 25Hz.

This work provides a sound basis for changing the standard stimulating parameters from 75Hz using an m=15 bit m-sequence to 25Hz with an m=13 bit m-sequence.

9.5 Multichannel, Multifocal Recording System and Investigation of Electrode Placement

The multichannel acquisition capabilities of an EEG recording system were successfully integrated with the stimulus presentation and data processing functions of the EDIU Multifocal system, resulting in a research tool that can simultaneously record mfVECPs from at least 16 electrode locations without the need to use skin preparation.

The experiments in this chapter described the evolution of a multichannel system capable of recording simple physiological and non-physiological signals to one that can receive trigger input from complex, time-critical visual stimuli and allow responses to multifocal stimulation to be cross-correlated.

The system was used with 16 recording electrodes but is capable of simultaneously recording data from many more. The ISCEV standard for conventional VECPs (27) uses monopolar recording channels and this thesis focussed the acquired data in a monopolar format. Bipolar channels can be simply calculated by subtraction and are a natural progression for future investigations. When recording from a large number of electrodes, there are a very large number of pairs of electrodes from which bipolar data can be derived. This would permit the interrogation of the visual cortex from a very large number of orientations which will increase the probability of evoked dipoles within the convolutions of the cortex being detectable.

Optimal monopolar recording channels electrode positions have been determined. A combination of four electrodes positioned above, below and to the right and left of the occipital pole was shown to interrogate the evoked dipoles within the occipital cortex most efficiently. A significant volume of data was acquired in the presented experiments. This could be analysed further and may highlight the fact that different combinations of electrode positions are optimal under different stimulating parameters, such as stimulation frequency.

Dipole source localisation is another direction which could be taken. It could test the hypothesis that the mfVECP is generated within the striate cortex when 75Hz stimulation is used and that there is a greater contribution from non-striate areas when slower stimulation rates are used.

9.6 Conclusion

The ability of the mfVECP to identify physiological responses to stimulation of independent areas of the visual field has been assessed. Performance has been shown to improve when the presence or absence of a waveform is determined by a novel SNR metric, when data is filtered post-acquisition through a 3-20Hz bandpass after cross-correlation and when a CRT is used to deliver the stimulus rather than an LCD projection system. The field of view of stimulation can usefully be extended to a radius of 30° when a 60-region dartboard pattern is employed. Performance can be enhanced at the same time as acquisition time is reduced by 25%, by the use of a 25Hz rate of stimulation instead of the frequently employed rate of 75Hz.

A multi-channel multifocal system was created and used to demonstrate that a combination of electrodes above, below and to the right and left of the occipital pole produced the best response detection rate. This will be an invaluable tool in future investigations of the optimal bipolar recording channels for acquisition of mfVECP data and will allow interrogation of the visual cortex from a very large number of orientations.

Reference List

(1) Holmes G, Lister WT. Disturbances of Vision from Cerebral Lesions, with Special Reference to the Cortical Representation of the Macula. Brain 1916; 39:34-73.

(2) Warnking J, Dojat M, Guerin-Dugue A, Delon-Martin C, Olympieff S, Richard N et al. fMRI retinotopic mapping--step by step. Neuroimage 2002; 17(4):1665-1683.

(3) Engel SA, Glover GH, Wandell BA. Retinotopic organization in human visual cortex and the spatial precision of functional MRI. Cereb Cortex 1997; 7(2):181-192.

(4) Slotnick SD, Yantis S. Efficient acquisition of human retinotopic maps. Hum Brain Mapp 2003; 18(1):22-29.

(5) Fox PT, Miezin FM, Allman JM, Van Essen DC, Raichle ME. Retinotopic organization of human visual cortex mapped with positron-emission tomography. J Neurosci 1987; 7(3):913-922.

(6) Endo S, Toyama H, Kimura Y, Ishii K, Senda M, Kiyosawa M et al. Mapping visual field with positron emission tomography by mathematical modeling of the retinotopic organization in the calcarine cortex. IEEE Trans Med Imaging 1997; 16(3):252-260.

(7) Shipp S, Watson JD, Frackowiak RS, Zeki S. Retinotopic maps in human prestriate visual cortex: the demarcation of areas V2 and V3. Neuroimage 1995; 2(2):125-132.

(8) Nishiyama T, Ohde H, Haruta Y, Mashima Y, Oguchi Y. Multifocal magnetoencephalogram applied to objective visual field analysis. Jpn J Ophthalmol 2004; 48(2):115-122.

(9) Owaki T, Takeda T. A study of relationship between multifocal VEF responses and binocular disparity. Neurol Clin Neurophysiol 2004; 2004:107.

(10) Tabuchi H, Yokoyama T, Shimogawara M, Shiraki K, Nagasaka E, Miki T. Study of the visual evoked magnetic field with the m-sequence technique. Invest Ophthalmol Vis Sci 2002; 43(6):2045-2054.

(11) Wang L, Barber C, Kakigi R, Kaneoke Y, Okusa T, Wen Y. A first comparison of the human multifocal visual evoked magnetic field and visual evoked potential. Neurosci Lett 2001; 315(1-2):13-16.

(12) Baseler HA, Sutter EE, Klein SA, Carney T. The topography of visual evoked response properties across the visual field. Electroencephalogr Clin Neurophysiol 1994; 90:65-81.

(13) Baseler HA, Sutter EE. M and P components of the VEP and their visual field distribution. Vision Res 1997; 37:675-690.

(14) Hood DC, Greenstein VC, Odel JG, Zhang X, Ritch R, Liebmann JM et al. Visual field defects and multifocal visual evoked potentials: evidence of a linear relationship. Arch Ophthalmol 2002; 120(12):1672-1681.

(15) Hood DC, Odel JG, Winn BJ. The multifocal visual evoked potential. J Neuroophthalmol 2003; 23(4):279-289.

(16) Klistorner AI, Graham SL, Grigg JR, Billson FA. Electrode position and the multi-focal visual-evoked potential: role in objective visual field assessment. Aust N Z J Ophthalmol 1998; 26 Suppl 1:S91-S94.

(17) James AC. The pattern-pulse multifocal visual evoked potential. Invest Ophthalmol Vis Sci 2003; 44(2):879-890.

(18) McFadzean RM, Condon BC, Barr DB. Functional magnetic resonance imaging in the visual system. J Neuroophthalmol 1999; 19(3):186-200.

(19) Hood DC, Greenstein VC. Multifocal VEP and ganglion cell damage: applications and limitations for the study of glaucoma. Prog Retin Eye Res 2003; 22(2):201-251.

(20) Aine CJ, Supek S, George JS, Ranken D, Lewine J, Sanders J et al. Retinotopic organization of human visual cortex: departures from the classical model. Cereb Cortex 1996; 6(3):354-361.

(21) Braddick OJ, O'Brien JM, Wattam-Bell J, Atkinson J, Hartley T, Turner R. Brain areas sensitive to coherent visual motion. Perception 2001; 30(1):61-72.

(22) Desimone R, Schein SJ, Moran J, Ungerleider LG. Contour, color and shape analysis beyond the striate cortex. Vision Res 1985; 25(3):441-452.

(23) Moran J, Desimone R. Selective attention gates visual processing in the extrastriate cortex. Science 1985; 229(4715):782-784.

(24) Henson DB, Morris EJ. Effect of uncorrected refractive errors upon central visual field testing. Ophthalmic Physiol Opt 1993; 13(4):339-343.

(25) Wall M. What's new in perimetry. J Neuroophthalmol 2004; 24(1):46-55.

(26) Harding GF, Odom JV, Spileers W, Spekreijse H. Standard for visual evoked potentials 1995. The International Society for Clinical Electrophysiology of Vision. Vision Res 1996; 36(21):3567-3572.

(27) Odom JV, Bach M, Barber C, Brigell M, Marmor MF, Tormene AP et al. Visual evoked potentials standard (2004). Doc Ophthalmol 2004; 108(2):115-123.

(28) Tyler CW, Apkarian P, Levi DM, Nakayama K. Rapid assessment of visual function: an electronic sweep technique for the pattern visual evoked potential. Invest Ophthalmol Vis Sci 1979; 18(7):703-713.

(29) Bach M, Maurer JP, Wolf ME. Visual evoked potential-based acuity assessment in normal vision, artificially degraded vision, and in patients. Br J Ophthalmol 2008; 92(3):396-403.

(30) Spehlmann R. Evoked Potential Primer: Visual, Auditory and Somatosensory Evoked Potentials in Clinical Diagnosis. Butterworth Publishers, 1985.

(31) Hoffmann MB, Seufert PS, Bach M. Simulated nystagmus suppresses pattern-reversal but not pattern-onset visual evoked potentials. Clin Neurophysiol 2004; 115(11):2659-2665.

(32) Saunders KJ, Brown G, McCulloch DL. Pattern-onset visual evoked potentials: more useful than reversal for patients with nystagmus. Doc Ophthalmol 1997; 94(3):265-274.

(33) Hood DC, Zhang X, Greenstein VC, Kangovi S, Odel JG, Liebmann JM et al. An interocular comparison of the multifocal VEP: a possible technique for detecting local damage to the optic nerve. Invest Ophthalmol Vis Sci 2000; 41(6):1580-1587.

(34) Hennerici M, Wenzel D, Freund HJ. The comparison of small-size rectangle and checkerboard stimulation for the evaluation of delayed visual evoked responses in patients suspected of multiple sclerosis. Brain 1977; 100 Pt 1:119-136.

(35) Rossini PM, Pirchio M, Sollazzo D, Caltagirone C. Foveal versus peripheral retinal responses: a new analysis for early diagnosis of multiple sclerosis. Electroencephalogr Clin Neurophysiol 1979; 47(5):515-531.

(36) Halliday AM, Michael WF. Changes in pattern-evoked responses in man associated with the vertical and horizontal meridians of the visual field. J Physiol 1970; 208(2):499-513.

(37) Bradnam MS, Montgomery DM, Evans AL, Keating D, McClure EA, Damato BE et al. Objective detection of hemifield and quadrantic field defects by visual evoked cortical potentials. Br J Ophthalmol 1996; 80(4):297-303.

(38) Jeffreys DA, Smith AT. The polarity inversion of scalp potentials evoked by upper and lower half-field stimulus patterns: latency or surface distribution differences? Electroencephalogr Clin Neurophysiol 1979; 46(4):409-415.

(39) Lesevre N. Chronotopographical analysis of the human evoked potential in relation to the visual field (data from normal individuals and hemianopic patients). Ann N Y Acad Sci 1982; 388:156-182.

(40) Skrandies W, Lehman D. Spatial Principle Components of Multichannel Maps Evoked by Lateral Visual Half-Field Stimuli. Electroencephalogr Clin Neurophysiol 1982; 54:662-667.

(41) Ossenblok P, Spekreijse H. The extrastriate generators of the EP to checkerboard onset. A source localization approach. Electroencephalogr Clin Neurophysiol 1991; 80(3):181-193.

(42) Lesevre N, Joseph JP. Modifications of the pattern-evoked potential (PEP) in relation to the stimulated part of the visual field (clues for the most probable origin of each component). Electroencephalogr Clin Neurophysiol 1979; 47(2):183-203.

(43) Butler SR, Georgiou GA, Glass A, Hancox RJ, Hopper JM, Smith KR. Cortical generators of the CI component of the pattern-onset visual evoked potential. Electroencephalogr Clin Neurophysiol 1987; 68(4):256-267.

(44) Cohn NB, Kircher J, Emmerson RY, Dustman RE. Pattern reversal evoked potentials: age, sex and hemispheric asymmetry. Electroencephalogr Clin Neurophysiol 1985; 62(6):399-405.

(45) Howe JW, Mitchell KW. Visual evoked cortical potential to paracentral retinal stimulation in chronic glaucoma, ocular hypertension, and an age-matched group of normals. Doc Ophthalmol 1986; 63(1):37-44.

(46) Sutter EE, Tran D. The field topography of ERG components in man--I. The photopic luminance response. Vision Res 1992; 32:433-446.

(47) Hood DC, Holopigian K, Greenstein V, Seiple W, Li J, Sutter EE et al. Assessment of local retinal function in patients with retinitis pigmentosa using the multi-focal ERG technique. Vision Res 1998; 38:163-179.

(48) Dolan FM, Parks S, Hammer H, Keating D. The wide field multifocal electroretinogram reveals retinal dysfunction in early retinitis pigmentosa. Br J Ophthalmol 2002; 86(4):480-481.

(49) Dolan FM, Parks S, Keating D, Dutton GN, Evans AL. Multifocal electroretinographic features of central retinal vein occlusion. Invest Ophthalmol Vis Sci 2003; 44(11):4954-4959.

(50) Dolan FM, Parks S, Keating D, Dutton GN, Evans AL. Multifocal electroretinographic features of central retinal vein occlusion. Invest Ophthalmol Vis Sci 2003; 44(11):4954-4959.

(51) Dolan FM, Parks S, Keating D, Dutton GN. Wide field multifocal and standard full field electroretinographic features of hemi retinal vein occlusion. Doc Ophthalmol 2006; 112(1):43-52.

(52) Dolan FM, Parks S, Keating D, Dutton GN. Wide field multifocal and standard full field electroretinographic features of hemi retinal vein occlusion. Doc Ophthalmol 2006; 112(1):43-52.

(53) Hvarfner C, Andreasson S, Larsson J. Multifocal electroretinography and fluorescein angiography in retinal vein occlusion. Retina 2006; 26(3):292-296.

(54) Hood DC. Assessing retinal function with the multifocal technique. Prog Retin Eye Res 2000; 19(5):607-646.

(55) Stiefelmeyer S, Neubauer AS, Berninger T, Arden GB, Rudolph G. The multifocal pattern electroretinogram in glaucoma. Vision Res 2004; 44(1):103-112.

(56) Bearse MA, Jr., Adams AJ, Han Y, Schneck ME, Ng J, Bronson-Castain K et al. A multifocal electroretinogram model predicting the development of diabetic retinopathy. Prog Retin Eye Res 2006; 25(5):425-448.

(57) Palmowski AM, Sutter EE, Bearse MA, Jr., Fung W. Mapping of retinal function in diabetic retinopathy using the multifocal electroretinogram. Invest Ophthalmol Vis Sci 1997; 38(12):2586-2596.

(58) Maia-Lopes S, Silva ED, Silva MF, Reis A, Faria P, Castelo-Branco M. Evidence of widespread retinal dysfunction in patients with stargardt disease and morphologically unaffected carrier relatives. Invest Ophthalmol Vis Sci 2008; 49(3):1191-1199.

(59) Kretschmann U, Seeliger MW, Ruether K, Usui T, Apfelstedt-Sylla E, Zrenner E. Multifocal electroretinography in patients with Stargardt's macular dystrophy. Br J Ophthalmol 1998; 82(3):267-275.

(60) McDonagh J, Grierson DJ, Keating D, Parks S. The wide field multifocal ERG reveals a retinal defect caused by vigabatrin toxicity. Br J Ophthalmol 2001; 85(1):119-120.

(61) McDonagh J, Stephen LJ, Dolan FM, Parks S, Dutton GN, Kelly K et al. Peripheral retinal dysfunction in patients taking vigabatrin. Neurology 2003; 61(12):1690-1694.

(62) Chisholm JA, Williams G, Spence E, Parks S, Keating D, Gavin M et al. Retinal toxicity during pegylated alpha-interferon therapy for chronic hepatitis C: a multifocal electroretinogram investigation. Aliment Pharmacol Ther 2005; 21(6):723-732.

(63) Marmor MF, Hood DC, Keating D, Kondo M, Seeliger MW, Miyake Y. Guidelines for basic multifocal electroretinography (mfERG). Doc Ophthalmol 2003; 106(2):105-115.

(64) Parks S, Keating D, Evans AL. The Wide Field Multifocal ERG: a review of 2115 investigations. Invest Ophthalmol Vis Sci 2002; 43:S1794.

(65) Rodarte C, Hood DC, Yang EB, Grippo T, Greenstein VC, Liebmann JM et al. The effects of glaucoma on the latency of the multifocal visual evoked potential. Br J Ophthalmol 2006.

(66) Balachandran C, Graham SL, Klistorner A, Goldberg I. Comparison of objective diagnostic tests in glaucoma: Heidelberg retinal tomography and multifocal visual evoked potentials. J Glaucoma 2006; 15(2):110-116.

(67) Goldberg I, Graham SL, Klistorner AI. Multifocal objective perimetry in the detection of glaucomatous field loss. Am J Ophthalmol 2002; 133(1):29-39.

(68) Graham SL, Klistorner AI, Goldberg I. Clinical application of objective perimetry using multifocal visual evoked potentials in glaucoma practice. Arch Ophthalmol 2005; 123(6):729-739.

(69) Graham SL, Klistorner A. Electrophysiology: a review of signal origins and applications to investigating glaucoma. Aust N Z J Ophthalmol 1998; 26(1):71-85.

(70) Graham SL, Klistorner A, Grigg JR, Billson FA. Objective perimetry in glaucoma: recent advances with multifocal stimuli. Surv Ophthalmol 1999; 43 Suppl 1:S199-S209.

(71) Graham SL, Klistorner AI, Grigg JR, Billson FA. Objective VEP perimetry in glaucoma: asymmetry analysis to identify early deficits. J Glaucoma 2000; 9(1):10-19.

(72) Graham SL, Klistorner A. The diagnostic significance of the multifocal pattern visual evoked potential in glaucoma. Curr Opin Ophthalmol 1999; 10(2):140-146.

(73) Hood DC, Zhang X. Multifocal ERG and VEP responses and visual fields: comparing disease-related changes. Doc Ophthalmol 2000; 100(2-3):115-137.

(74) Hood DC. Objective measurement of visual function in glaucoma. Curr Opin Ophthalmol 2003; 14(2):78-82.

(75) Kanadani FN, Hood DC, Grippo TM, Wangsupadilok B, Harizman N, Greenstein VC et al. Structural and Functional Assessment of the Macular Region in Patients with Glaucoma. Br J Ophthalmol 2006.

(76) Klistorner A, Graham SL. Objective perimetry in glaucoma. Ophthalmology 2000; 107(12):2283-2299.

(77) Klistorner AI, Graham SL. Early magnocellular loss in glaucoma demonstrated using the pseudorandomly stimulated flash visual evoked potential. J Glaucoma 1999; 8(2):140-148.

(78) Klistorner AI, Graham SL, Martins A. Multifocal pattern electroretinogram does not demonstrate localised field defects in glaucoma. Doc Ophthalmol 2000; 100(2-3):155-165.

(79) Klistorner AI, Graham SL. Multifocal pattern VEP perimetry: analysis of sectoral waveforms. Doc Ophthalmol 1999; 98(2):183-196.

(80) Thienprasiddhi P, Greenstein VC, Chu DH, Xu L, Liebmann JM, Ritch R et al. Detecting Early Functional Damage in Glaucoma Suspect and Ocular Hypertensive Patients With the Multifocal VEP Technique. J Glaucoma 2006; 15(4):321-327.

(81) Thienprasiddhi P, Greenstein VC, Chen CS, Liebmann JM, Ritch R, Hood DC. Multifocal visual evoked potential responses in glaucoma patients with unilateral hemifield defects. Am J Ophthalmol 2003; 136(1):34-40.

(82) Zhang X, Hood DC. Increasing the sensitivity of the multifocal visual evoked potential (mfVEP) technique: incorporating information from higher order kernels using a principal component analysis method. Doc Ophthalmol 2004; 108(3):211-222.

(83) Fraser C, Klistorner A, Graham S, Garrick R, Billson F, Grigg J. Multifocal visual evoked potential latency analysis: predicting progression to multiple sclerosis. Arch Neurol 2006; 63(6):847-850.

(84) Fraser CL, Klistorner A, Graham SL, Garrick R, Billson FA, Grigg JR. Multifocal visual evoked potential analysis of inflammatory or demyelinating optic neuritis. Ophthalmology 2006; 113(2):323.

(85) Hood DC, Odel JG, Zhang X. Tracking the recovery of local optic nerve function after optic neuritis: a multifocal VEP study. Invest Ophthalmol Vis Sci 2000; 41(12):4032-4038.

(86) Pakrou N, Casson R, Kaines A, Selva D. Multifocal objective perimetry compared with Humphrey full-threshold perimetry in patients with optic neuritis. Clin Experiment Ophthalmol 2006; 34(6):562-567.

(87) Zhang W, Zhao K. Multifocal VEP difference between early- and late-onset strabismus amblyopia. Doc Ophthalmol 2005; 110(2-3):173-180.

(88) Ireland JM, Keating D, Hoggar SG, Parks S. Identification of appropriate primitive polynomials to avoid cross-contamination in multifocal electroretinogram responses. Med Biol Eng Comput 2002; 40(4):471-478.

(89) Al Yousuf N, Parks S, Dhillon B, Keating D. Acute zonal occult outer retinopathy. Br J Ophthalmol 2000; 84(1):118-119.

(90) Keating D, Parks S. Multifocal Techniques. In: Heckenlively JR, Arden GB, Nusinowitz S, Holder GE, Bach M, editors. Principles and Practice of Clinical Electrophysiology of Vision. MIT Press, 2006.

(91) Sutter EE. The Fast m-Transform: A Fast Computation of Cross-Correlations with Binary m-Sequences. Siamese Journal of Computing 1991; 20(4):686-694.

(92) Sutter E. The interpretation of multifocal binary kernels. Doc Ophthalmol 2000; 100(2-3):49-75.

(93) Sutter EE. Imaging visual function with the multifocal m-sequence technique. Vision Res 2001; 41(10-11):1241-1255.

(94) Sutter EE. The brain response interface: communication through visually-induced electrical brain responses. Journal of Microcomputer Applications 1992; 15:31-45.

(95) Collins AD, Sawhney BB. Pseudorandom binary sequence stimulation applied to the visual evoked response. Normative data and a comparative study with pattern and flash stimulation. Doc Ophthalmol 1993; 83(2):163-173.

(96) Horton JC, Hoyt WF. The representation of the visual field in human striate cortex. A revision of the classic Holmes map. Arch Ophthalmol 1991; 109(6):816-824.

(97) Keating D, Parks S, Evans AL, Williamson TH, Elliott AT, Jay JL. The effect of filter bandwidth on the multifocal electroretinogram. Doc Ophthalmol 1996; 92(4):291-300.

(98) Keating D, Parks S, Evans A. Technical aspects of multifocal ERG recording. Doc Ophthalmol 2000; 100(2-3):77-98.

(99) Keating D, Parks S, Malloch C, Evans A. A comparison of CRT and digital stimulus delivery methods in the multifocal ERG. Doc Ophthalmol 2001; 102(2):95-114.

(100) Parks S, Keating D, Williamson TH, Evans AL, Elliott AT, Jay JL. Functional imaging of the retina using the multifocal electroretinograph: a control study. Br J Ophthalmol 1996; 80(9):831-834.

(101) Parks S, Keating D, Evans AL, Williamson TH, Jay JL, Elliott AT. Comparison of repeatability of the multifocal electroretinogram and Humphrey perimeter. Doc Ophthalmol 1996; 92(4):281-289.

(102) Keating D, Parks S, Smith D, Evans A. The multifocal ERG: unmasked by selective cross-correlation. Vision Res 2002; 42(27):2959-2968.

(103) Arvind H, Klistorner A, Graham SL, Grigg JR. Multifocal Visual Evoked Responses to Dichoptic Stimulation Using Virtual Reality Goggles: Multifocal VER to Dichoptic Stimulation. Doc Ophthalmol 2006.

(104) James AC, Ruseckaite R, Maddess T. Effect of temporal sparseness and dichoptic presentation on multifocal visual evoked potentials. Vis Neurosci 2005; 22(1):45-54.

(105) Maddess T, James AC, Bowman EA. Contrast response of temporally sparse dichoptic multifocal visual evoked potentials. Vis Neurosci 2005; 22(2):153-162.

(106) Ruseckaite R, Maddess T, Danta G, James AC. Frequency doubling illusion VEPs and automated perimetry in multiple sclerosis. Doc Ophthalmol 2006.

(107) Ruseckaite R, Maddess T, Danta G, Lueck CJ, James AC. Sparse multifocal stimuli for the detection of multiple sclerosis. Ann Neurol 2005; 57(6):904-913.

(108) Maddess T, James AC, Ruseckaite R, Bowman EA. Hierarchical decomposition of dichoptic multifocal visual evoked potentials. Vis Neurosci 2006; 23(5):703-712.

(109) Fortune B, Hood DC. Conventional pattern-reversal VEPs are not equivalent to summed multifocal VEPs. Invest Ophthalmol Vis Sci 2003; 44(3):1364-1375.

(110) Stensaas SS, Eddington DK, Dobelle WH. The topography and variability of the primary visual cortex in man. J Neurosurg 1974; 40(6):747-755.

(111) Klistorner AI, Graham SL, Grigg JR, Billson FA. Multifocal topographic visual evoked potential: improving objective detection of local visual field defects. Invest Ophthalmol Vis Sci 1998; 39(6):937-950.

(112) Martins A, Klistorner A, Graham S, Billson F. Effect of fixation tasks on multifocal visual evoked potentials. Clin Experiment Ophthalmol 2005; 33(5):499-504.

(113) Greenstein V, Thienprasiddhi P, Ritch R, Liebmann JM, Hood DC. A Method for Comparing Electrophysiological, Psychophysical and Structural Measures of Glaucomatous Damage. Arch Ophthalmol 2004; 122:1276-1284.

(114) James AC, Maddess T, Bowman E. Effect of Presentation Rate and Pulse Duration on the Pattern-pulse Multifocal Visual Evoked Potential (PPMVEP). Invest Ophthalmol.Vis.Sci. 44, E-abstract 4114. 2003.
Ref Type: Abstract

(115) James AC, Winkles N, Maddess T. Comparison of Contrast Reversing and Pattern-Pulse Stimulation for Multifocal Visual Evoked Potential Analysis. Invest Ophthalmol.Vis.Sci. 45, E- abstract 5485. 2004.
Ref Type: Abstract

(116) Martins A, Klistorner A, Graham S, Billson F. Effect of check size and stimulation rate on blue-yellow multifocal visual evoked potentials. Clin Experiment Ophthalmol 2004; 32(3):270-274.

(117) Balachandran C, Martins A, Klistorner A, Graham SL. Comparison of Isoluminant Blue/yellow Multifocal Visual Evoked Potential (m-VEP) with Black/white m-VEP. Invest Ophthalmol.Vis.Sci. Poster B24. 2003.
Ref Type: Abstract

(118) Regan D, Spekreijse H. Evoked potentials in vision research 1961-86. Vision Res 1986; 26(9):1461-1480.

(119) Halliday AM, McDonald WI, Mushin J. Delayed visual evoked response in optic neuritis. Lancet 1972; 1(7758):982-985.

(120) Hoffmann MB, Straube S, Bach M. Pattern-onset stimulation boosts central multifocal VEP responses. J Vis 2003; 3(6):432-439.

(121) Palmowski AM, Berninger T, Allgayer R, Andrielis H, Heinemann-Vernaleken B, Rudolph G. Effects of refractive blur on the multifocal electroretinogram. Doc Ophthalmol 1999; 99(1):41-54.

(122) Pieh C, Hoffmann MB, Bach M. The influence of defocus on multifocal visual evoked potentials. Graefes Arch Clin Exp Ophthalmol 2005; 243(1):38-42.

(123) Klistorner AI, Graham SL. Electroencephalogram-based scaling of multifocal visual evoked potentials: effect on intersubject amplitude variability. Invest Ophthalmol Vis Sci 2001; 42(9):2145-2152.

(124) Slotnick SD, Klein SA, Carney T, Sutter EE. Electrophysiological estimate of human cortical magnification. Clin Neurophysiol 2001 Jul ;112 (7):1349 -56 2001; 112:1349-1356.

(125) Zhang X, Hood DC, Chen CS, Hong JE. A signal-to-noise analysis of multifocal VEP responses: an objective definition for poor records. Doc Ophthalmol 2002; 104(3):287-302.

(126) Gerth C, Delahunt PB, Crognale MA, Werner JS. Topography of the chromatic pattern-onset VEP. J Vis 2003; 3(2):171-182.

(127) Hood DC. Electrophysiologic imaging of retinal and optic nerve damage: the multifocal technique. Ophthalmol Clin North Am 2004; 17(1):69-88.

(128) Hood DC, Zhang X, Hong JE, Chen CS. Quantifying the benefits of additional channels of multifocal VEP recording. Doc Ophthalmol 2002; 104(3):303-320.

(129) Klistorner AI, Graham SL. Effect of eccentricity on pattern-pulse multifocal VEP. Doc Ophthalmol 2005; 110(2-3):209-218.

(130) Hagan RP, Fisher AC, Brown MC. Examination of un-used m-sequences in multifocal recordings to estimate noise level. Briscev Abstracts , Poster P9. 2007.
Ref Type: Abstract

(131) Barber C. Electrodes and the recording of the human electroretinogram (ERG). Int J Psychophysiol 1994; 16(2-3):131-136.

(132) Mohidin N, Yap MK, Jacobs RJ. The repeatability and variability of the multifocal electroretinogram for four different electrodes. Ophthalmic Physiol Opt 1997; 17(6):530-535.

(133) Chisholm JA, Williams G, Spence E, Parks S, Keating D, Gavin M et al. Retinal toxicity during pegylated alpha-interferon therapy for chronic hepatitis C: a multifocal electroretinogram investigation. Aliment Pharmacol Ther 2005; 21(6):723-732.

(134) Bland M. *An Introduction to Medical Statistics*. Third Edition ed. New York: Oxford University Press, 2000.

(135) Horowitz P, Hill W. The Art of Electronics. Second ed. Cambridge: Cambridge University Press, 1989.

(136) Hood DC, Yu AL, Zhang X, Albrecht J, Jagle H, Sharpe LT. The multifocal visual evoked potential and cone-isolating stimuli: implications for L- to M-cone ratios and normalization. J Vis 2002; 2(2):178-189.

(137) Chen JY, Hood DC, Odel JG, Behrens MM. The effects of retinal abnormalities on the multifocal visual evoked potential. Invest Ophthalmol Vis Sci 2006; 47(10):4378-4385.

(138) Martins A, Balachandran C, Klistorner AI, Graham SL, Billson FA. Effect of pupil size on multifocal pattern visual evoked potentials. Clin Experiment Ophthalmol 2003; 31(4):354-356.

(139) Chan HL, Tam WK, Chen CL, Ng NC. The detection of small simulated field defects using multifocal VEPs. Ophthalmic Physiol Opt 2003; 23(3):205-212.

(140) Dudgeon SM, Keating D, Parks S. Multimodal Imaging With the Combined SLO/OCT and Micro–Multifocal ERG. Investigative Ophthalmology and Vision Science 47, E-abstract 3317. 2006.
Ref Type: Abstract

(141) Leifert D, Todorova MG, Prunte C, Palmowski-Wolfe AM. LED-generated multifocal ERG on- and off-responses in complete congenital stationary night blindness -- a case report. Doc Ophthalmol 2005; 111(1):1-6.

(142) Gawne TJ, Woods JM. Video-rate and continuous visual stimuli do not produce equivalent response timings in visual cortical neurons. Vis Neurosci 2003; 20(5):495-500.

(143) Hasegawa S, Abe H. Mapping of glaucomatous visual field defects by multifocal VEPs. Invest Ophthalmol Vis Sci 2001; 42(13):3341-3348.

(144) Hood DC, Thienprasiddhi P, Greenstein VC, Winn BJ, Ohri N, Liebmann JM et al. Detecting early to mild glaucomatous damage: a comparison of the multifocal VEP and automated perimetry. Invest Ophthalmol Vis Sci 2004; 45(2):492-498.

(145) Hood DC, Zhang X, Winn BJ. Detecting glaucomatous damage with multifocal visual evoked potentials: how can a monocular test work? J Glaucoma 2003; 12(1):3-15.

(146) Hood DC, Ghadiali Q, Zhang JC, Graham NV, Wolfson SS, Zhang X. Contrast-response functions for multifocal visual evoked potentials: a test of a model relating V1 activity to multifocal visual evoked potentials activity. J Vis 2006; 6(5):580-593.

(147) Brigell M, Bach M, Barber C, Moskowitz A, Robson J. Guidelines for calibration of stimulus and recording parameters used in clinical electrophysiology of vision. Doc Ophthalmol 2003; 107(2):185-193.

(148) Schimitzek T, Bach M. The influence of luminance on the multifocal ERG. Doc Ophthalmol 2006; 113(3):187-192.

(149) Marmor MF, Holder GE, Seeliger MW, Yamamoto S. Standard for clinical electroretinography (2004 update). Doc Ophthalmol 2004; 108(2):107-114.

(150) James AC, Maddess T, Goh XL, Winkles N. Spatially sparse pattern-pulse stimulation enhances multifocal visual evoked potential analysis. Invest Ophthalmol.Vis.Sci. 46, E-abstract 3602. 2005.
Ref Type: Abstract

(151) Maddess T, James AC, Bowman EA. Contrast Responses of Dichoptic Multifocal Visual Evoked Potential Responses to Contrast Reversing and Temporally Sparse Stimuli. Invest Ophthalmol.Vis.Sci. 45, E-abstract 3501. 2004.
Ref Type: Abstract

(152) Smith DC, Keating D, Parks S, Evans AL. An instrument to investigate temporal processing mechanisms with the multifocal ERG. J Med Eng Technol 2002; 26(4):147-151.

(153) Chisholm JA, Parks S, Keating D, Evans AL. A Multi-channel Multifocal VECP System. Invest Ophthalmol.Vis.Sci. 43, E-abstract 4741. 2005.
Ref Type: Abstract

(154) Rovamo J, Virsu V. An estimation and application of the human cortical magnification factor. Exp Brain Res 1979; 37(3):495-510.

(155) Engel SA, Rumelhart DE, Wandell BA, Lee AT, Glover GH, Chichilnisky EJ et al. fMRI of human visual cortex. Nature 1994; 369(6481):525.

(156) Brusa A, Mortimer C, Jones SJ. Clinical evaluation of VEPs to interleaved checkerboard reversal stimulation of central, hemi- and peripheral fields. Electroencephalogr Clin Neurophysiol 1995; 96(6):485-494.

(157) Schippers V, Silny J, Rau G, Teping C. Results with multichannel topographical bipolar recordings of the visual evoked potential in normals and amblyopes. Doc Ophthalmol 1990; 76(1):91-101.

(158) Klistorner AI, Graham SL, Grigg J, Balachandran C. Objective perimetry using the multifocal visual evoked potential in central visual pathway lesions. Br J Ophthalmol 2005; 89(6):739-744.

(159) Klistorner A, Graham SL. Intertest variability of mfVEP amplitude: reducing its effect on the interpretation of sequential tests. Doc Ophthalmol 2005; 111(3):159-167.

(160) Active Electrodes. 16-5-2007.
Ref Type: Internet Communication

(161) Kemp B, Varri A, Rosa AC, Nielsen KD, Gade J. A simple format for exchange of digitized polygraphic recordings. Electroencephalogr Clin Neurophysiol 1992; 82(5):391-393.

(162) Hood DC, Zhang X, Rodarte C, Yang EB, Ohri N, Fortune B et al. Determining abnormal interocular latencies of multifocal visual evoked potentials. Doc Ophthalmol 2004; 109(2):177-187.

(163) Balachandran C, Klistorner AI, Graham SL. Effect of stimulus check size on multifocal visual evoked potentials. Doc Ophthalmol 2003; 106(2):183-188.